Sustainability optimization of the thermo-biochemical pathway for the production of second-generation ethanol

Dissertation

for the purpose of obtaining the degree of doctor

at Delft University of Technology

by the authority of the Rector Magnificus,

prof. dr. ir. T.H.J.J. van der Hagen

chair of the Board of Doctorates

to be defended publicly on

Tuesday 15 December 2020 at 15:00 o' clock

by

Elisa MAGALHÃES DE MEDEIROS

engenheira química, Universidade Estadual de Campinas, Brazil

born in Rio de Janeiro, Brazil

This dissertation has been approved by the promotors.

Composition of the doctoral committee:

Rector Magnificus	chairperson
Prof.dr.ir. H.J. Noorman	Delft University of Technology, promotor
Prof.dr. R. Maciel Filho	University of Campinas, Brazil, promotor
Dr. J.A. Posada Duque	Delft University of Technology, co-promotor

Independent members:

Prof.dr.ir. A.A. Kiss	Delft University of Technology
Prof.dr.ir. C.A. Ramirez Ramirez	Delft University of Technology
Prof.dr.ir. E. Zondervan	University of Twente
Dr. A. Pinto Mariano	University of Campinas, Brazil
Prof.dr.ir. W. de Jong	Delft University of Technology, reserve member

Table of Contents

Summary

Renewable energy plays a key role in the fight to reduce greenhouse gas emissions while providing for human well-being and economic development. However, despite environmental benefits in terms of carbon sequestration, largely promoted biorenewable resources such as sugarcane and corn starch, so-called 1st generation (1G) feedstocks, are associated with other types of social and environmental issues that highly contradict the notion of sustainability, such as the food versus fuel conflict and the contribution to impacts such as deforestation, soil degradation, loss of biodiversity and contamination of water resources. As reaction to these issues, a lot of effort has been put into the development of technologies to extract and convert useful energy from non-food crops and agro-industrial residues, such as sugarcane bagasse, corn stover, and wheat straw. These now called 2nd generation (2G) feedstocks offer an extra challenge since fermentable sugars are not readily available; nonetheless, myriad technologies have been (and are being) developed to convert 2G materials into fuels and chemicals, with perhaps the most representative product being ethanol, a widely employed engine fuel and gasoline additive.

2G or cellulosic ethanol can be produced via biochemical pathways, thermochemical pathways, or a third option that combines aspects of the other two, commonly called the thermo-biochemical, or hybrid, pathway. The latter is the focus of this thesis, which explores this pathway via process modeling, simulations, (multi-objective) optimization, and other strategies applied in order to determine which process choices and conditions lead to the best performance in terms of main sustainability aspects. While the thermochemical process of gasification enables the nearly full conversion of biomass without the need for complex and expensive stages of pretreatment and hydrolysis, the subsequent biological conversion (fermentation) of syngas might offer several advantages when compared to the traditional catalytic conversion, e.g. higher flexibility of H_2:CO ratios and tolerance to gas contaminants . Although certain challenges may drawback the commercial competitiveness of syngas fermentation, such as the low productivity when compared to heterotrophic fermentation, intelligent

choices of process integration and design parameters could substantially enhance the performance of the process.

In **Chapter 1**, a general introduction is given about this pathway, and the motivation and specific goals of this research are laid out. The scope of the project is narrowed down to one specific configuration of this pathway, which comprises the indirectly-heated gasification of biomass residues to produce syngas, its further conversion to ethanol via autotrophic fermentation with acetogenic bacteria, and ethanol purification using distillation and molecular sieves when anhydrous ethanol is the desired product. The main goal of this thesis is to find out which design parameters and process conditions lead to the best performance in terms of simultaneous and often conflicting aspects related to sustainability, i.e. profitability, environmental impact (specifically, carbon footprint) and energy efficiency. For this the process had to be investigated as a whole and also individually for its main units. The specific goals included the process design, the construction of mathematical models and simulations, the evaluation of alternatives for energy recovery, impact analysis, the development of a multi-objective sustainability optimization framework, and the implementation of strategies to reduce the complexity of the optimization problems. These goals are addressed in Chapters 2 through 5.

Chapter 2 presents a preliminary economic assessment of this route, which is performed after developing the process design and simulation of one possible configuration tuned to be energy self-sufficient. Apart from the aforementioned process units, this configuration also includes heat recovery/integration and electricity production. To enable the simulation, several assumptions had to be made with regard to conversions, yields and product selectivity, which were based on data available in the literature. This chapter also gives a more detailed literature review of the process and current research gaps. Our analysis suggests a poor economic performance in comparison with 1G ethanol, but the results of minimum ethanol selling price (MESP), energy efficiency and product yield are comparable to other 2G technologies such as gasification followed by mixed alcohol synthesis, simultaneous saccharification & fermentation, and hydrolysis followed by fermentation.

Syngas fermentation is further explored in **Chapter 3**, which presents a dynamic model for this process in a continuous stirred-tank reactor. The biological

conversion of syngas using acetogens is a fairly young technology with the potential to offer advantages such as gas composition flexibility, but it also presents challenges due to the low solubility of the gaseous substrates, the formation of undesired acetate and slow uptake of substrate by the cells. Although models for this process are still scarce in the literature, they are necessary to evaluate the effects of operating conditions, gain understanding of the process and ultimately optimize it. The model developed here takes into account the mass transfer of substrate and products between the gas and liquid phases, the consumption of CO, H_2 and CO_2 by the cells, inhibition by products and substrate, cell growth and death, and acetic acid re-assimilation occurring under low pH. The set of unknown parameters used in the system of differential-algebraic equations was estimated using experimental data from three articles available in the literature, encompassing distinct experimental conditions. The different types of parameters and input variables were discussed in this chapter, as well as their interactions and impacts on the outcomes of the bioreactor. Finally, the model was used to evaluate the effects of syngas composition and conduct an optimization of this unit. The main contributions of this chapter are the dynamic model itself and the estimation of the kinetic parameter set, but some of the model predictions can be highlighted: (i) it was observed that the sensitivity of the kinetic parameters on the outcomes of the reactor is dependent on the operating conditions; (ii) ethanol productivity and CO conversion are conflicting targets when CO-rich gas is used, but higher conversions can be maintained if the H_2 content is increased; (iii) the maximum productivity with full CO conversion is predicted to occur with a feed gas containing approximately 55% CO and 45% H_2.

The biokinetic model developed in **Chapter 3** was then incorporated into a fluid dynamic model of a bubble column reactor, which is presented in **Chapter 4**. This model considers spatial distribution of the state variables, instead of homogeneity. Therefore, the concentrations of CO, H_2, CO_2, ethanol and acetic acid vary with height in the gas and liquid phases, as well as the gas velocity, the volumetric gas-liquid mass transfer coefficient k_La and the gas hold-up. This model was then used to predict the reactor output at steady-state for a sub-system comprising the bioreactor fed with fresh syngas and recycled gas, distillation, ethanol dehydration, and water recycle from the distillation bottoms to the bioreactor. To facilitate the optimization of this sub-system, which involves a large number of computationally expensive objective function evaluations, surrogate

models were employed in the optimization framework, instead of the original models. These are artificial neural networks that were trained and validated with data produced with the original bubble column models and Aspen simulations of the distillation columns. The optimization was then conducted with multi-objective genetic algorithm for three combinations of targets related to capital investment, minimum selling price, energy efficiency and productivity. Apart from an analysis of trade-offs and optimal values of distinct decision variables, this chapter also discusses the impacts of the mass transfer coefficient k_La and an overview of strategies to enhance it, as it was observed that higher k_La values can lead to a significant improvement of the global performance.

After starting this research with a view of the whole process (**Chapter 2**), then concentrating our efforts towards the development of models for one of its units (**Chapters 3 and 4**), and on the development of strategies for sustainability optimization (demonstrated in **Chapter 4** for a sub-system of the process), **Chapter 5** zooms out again to a view of the whole, now equipped with the tools developed in the previous chapters. In **Chapter 5**, the sub-system comprising the bioreactor and downstream stages is integrated into a framework for optimization of the whole process from biomass residues to ethanol. For this work a new model was also developed for the indirectly-heated gasifier. The models of different units were combined in one framework with embedded calculations of economic parameters, heat and power consumption and production, CO_2 equivalent emissions, water consumption and other performance indicators that are re-calculated as the input variables are changed. We discuss the effects of these variables on the global outcomes as well as their interactions and correlations between responses of different categories. Finally, the system was optimized with respect to three simultaneous objectives: minimum ethanol selling price, energy efficiency and carbon footprint. The optimal trade-offs were discussed for two cases (sugarcane bagasse and wood residues), along with an analysis about the trends of the decision variables at the Pareto-optimal solutions and an estimation of uncertainties. According to the results, the key variables defining the trade-offs are the temperature in the gasification bed, the fraction of biomass added to the combustion bed of the gasifier, and the ratio between the volumetric flow rate of fresh syngas at the inlet of the bioreactor and the volume of liquid in the bioreactor.

Finally, **Chapter 6** presents an overview of the results and the strategies presented for sustainability optimization, which involve the use of techniques such as surrogate modeling with machine learning, principal component analysis for reduction of the objective function space, and multi-objective genetic algorithm. These strategies were applied specifically for one configuration of the thermo-biochemical route, but could be extended to other technological routes and different processes and products. The limitations of our work are also summarized in this chapter, along with our view on opportunities for future research in this field. The results of this thesis cannot be used to affirm that the thermo-biochemical route is economically viable or sustainable today, but they do indicate good performance in terms of energy efficiency and carbon footprint, which are expected to bring also economic revenues in the years to come.

Resumo

As energias renováveis desempenham um papel fundamental nos esforços para reduzir as emissões de gases de efeito estufa e ao mesmo tempo prover recursos para o bem-estar humano e desenvolvimento econômico. Entretanto, apesar de benefícios ambientais quanto ao sequestro de carbono, certas fontes biorenováveis populares, como a cana-de-açúcar e o amido de milho, chamadas de matérias-primas de primeira geração (1G), estão também associadas a outros tipos de problemas sociais e ambientais que contradizem fortemente o conceito de sustentabilidade. Por exemplo, como o dilema combustíveis versus alimentos, e a contribuição a impactos como desflorestamento, degradação do solo, perda de biodiversidade e contaminação de recursos aquáticos. Como reação a esses problemas, muito se tem investido no desenvolvimento de tecnologias para extrair e converter energia útil de biomassas não-comestíveis e resíduos agroindustriais, como o bagaço de cana e a palha de milho e de trigo. O uso dessas matérias-primas, agora chamadas de 2ª geração (2G), oferece um desafio a mais pois os açúcares fermentescíveis são de difícil acesso; ainda assim, diversas tecnologias já foram ou estão sendo desenvolvidas para converter materiais 2G em combustíveis e produtos químicos, sendo um dos mais representativos o etanol, usado como combustível em carros de motor flex e aditivo para a gasolina.

Etanol 2G, ou celulósico, pode ser produzido por rotas bioquímicas, termoquímicas, ou por uma terceira opção que combina aspectos das outras duas, comumente chamada de rota termo-bioquímica, ou rota híbrida. Esta última é o foco desta tese, que a explora por meio de modelagem, simulações, otimização (multi-objetivo), e outras estratégias aplicadas de forma a determinar quais escolhas e condições de processo levam ao melhor resultado em termos de sustentabilidade. Enquanto o processo termoquímico de gaseificação permite a conversão quase completa da biomassa sem a necessidade de etapas complexas e caras de pré-tratamento e hidrólise, a subsequente conversão biológica (fermentação) do syngas pode oferecer algumas vantagens quanto comparada à tradicional conversão catalítica, e.g. maior flexibilidade na proporção H_2:CO e maior tolerância a contaminantes presentes no gás. Embora alguns desafios ainda atrapalhem a competitividade do processo de fermentação do syngas, como a

baixa produtividade em comparação à fermentação heterotrófica, escolhas inteligentes de integração, condições de processo e parâmetros de projeto poderiam melhorar significativamente o seu desempenho.

O **Capítulo 1** desta tese apresenta uma introdução geral a essa rota, assim como a motivação e os objetivos específicos desta pesquisa. O escopo do projeto é limitado a uma configuração específica da rota termo-bioquímica, compreendendo uma etapa de gaseificação indireta de resíduos de biomassa para produzir syngas, sua subsequente conversão a etanol via fermentação autotrófica com bactérias acetogênicas, e a purificação do etanol empregando destilação e peneiras moleculares quando etanol anidro é o produto desejado. O objetivo principal desta tese é determinar os parâmetros de projeto e condições de processo que levam ao melhor desempenho com relação a aspectos simultâneos e comumente conflitantes ligados a sustentabilidade, i.e. lucro, impacto ambiental (especificamente, pegada de carbono) e eficiência energética. Para isso o processo foi estudado como um todo e também individualmente para suas unidades principais. Os objetivos específicos incluíram o design do processo, a construção de modelos matemáticos e simulações computacionais, a avaliação de alternativas para recuperação de energia, análise de impactos, o desenvolvimento de uma framework para otimização multi-objetivo de sustentabilidade, e a implementação de estratégias para reduzir a complexidade dos problemas de otimização. Esses objetivos são abordados nos Capítulos 2 a 5.

O **Capítulo 2** apresenta uma análise econômica preliminar dessa rota, feita após o projeto conceitual do processo e a simulação de uma configuração possível ajustada para ser energeticamente auto-suficiente. Além das unidades de processo citadas previamente, essa configuração inclui também recuperação e integração energética, bem como produção de eletricidade. Diversas hipóteses foram feitas relacionadas a conversões, rendimentos e seletividade de produtos, sendo estas baseadas em informações disponíveis na literatura. Esse capítulo fornece também uma revisão mais detalhada sobre o processo e as lacunas de pesquisa. Nossa análise sugere um desempenho econômico baixo em comparação com o etanol 1G, mas os resultados de preço mínimo de venda (MESP - minimum ethanol selling price), eficiência energética e rendimento de produto são comparáveis a outras tecnologias 2G como gaseificação seguida de síntese catalítica de álcoois, sacarificação e fermentação simultâneas, e hidrólise da biomassa seguida de fermentação.

A fermentação de syngas é explorada em maior detalhe no Capítulo 3, que apresenta um modelo dinâmico desse processo e um reator perfeitamente agitado (CSTR). A conversão biológica do syngas empregando bactérias acetogênicas é uma tecnologia nova com o potencial de oferecer vantagens como maior flexibilidade na composição do gás, mas apresenta também alguns desafios devido à baixa solubilidade do substrato gasoso, à formação paralela de acetato não-desejado e ao uptake restrito de substrato pelas células. Embora ainda seja difícil encontrar modelos matemáticos desse processo, eles são necessários para avaliar os efeitos das condições operacionais, ganhar entendimento do processo, e por fim otimizá-lo. O modelo desenvolvido aqui considera a transferência de massa de substrato e produtos entre as fases gás e líquido, o consumo celular de CO, H_2 e CO_2, a inibição celular causada por produtos e substrato, crescimento e morte das células, e re-assimilação de ácido acético sob baixo pH. O conjunto de parâmetros desconhecidos utilizados no sistema de equações diferenciais e algébricas foi estimado a partir de dados experimentais retirados de três artigos científicos, que abrangem diferentes condições experimentais. Os tipos de parâmetros e variáveis de input são discutidos nesse capítulo, assim como as suas interações e impactos nos resultados do biorreator. Por fim, o modelo foi usado para avaliar os efeitos da composição do syngas e conduzir uma otimização dessa unidade. As principais contribuição desse capítulo são o próprio modelo dinâmico e a estimação do conjunto de parâmetros cinéticos, mas certas predições do modelo podem ser enfatizadas: (i) observou-se que a sensibilidade dos parâmetros cinéticos depende também das condições operacionais; (ii) a produtividade de etanol e a conversão de CO representam objetivos conflitantes quando o gás de alimentação é rico em CO, mas conversões maiores podem ser mantidas quando aumenta-se o teor de H_2 no gás; (iii) a produtividade máxima com conversão total de CO é esperada com um gás de alimentação contendo aproximadamente 55% CO e 45% H_2.

O modelo bio-cinético desenvolvido no **Capítulo 3** foi então incorporado no modelo dinâmico de uma reator de coluna de bolhas, apresentado no **Capítulo 4**. Este modelo considera distribuição espacial das variáveis de estado, em vez de homogeneidade. Portanto, as concentrações de CO, H_2, CO_2, etanol e ácido acético nas fases gás e líquido variam com a altura na coluna, assim como a velocidade superficial do gás, o coeficiente volumétrico de transferência de massa gás-líquido k_La, e hold-up de gás. O modelo foi usado então para calcular a saída do reator em

estado estacionário, dentro de um sub-sistema compreendendo o biorreator alimentado com syngas fresco e reciclado, destilação, desidratação do etanol, e reciclo de água do fundo das colunas de destilação para o biorreator. Para facilitar a otimização desse sub-sistema, que envolve calcular as funções objetivo repetidas vezes, um procedimento caro computacionalmente, modelos substitutos mais rápidos foram empregados no lugar dos modelos originais. Esses são, por exemplo, redes neurais que foram treinadas e validadas com dados gerados pelos modelos originais da coluna de bolhas e pelas simulações em Aspen das colunas de destilação. A otimização foi então programada com algoritmo genético multi-objetivo para três combinações de objetivos relacionados ao investimento, ao preço mínimo de venda MESP, à eficiência energética e à produtividade. Além da análise de trade-offs e dos valores ótimos das diversas variáveis de decisão, esse capítulo discute também os impactos do coeficiente de transferência de massa $k_L a$ e fornece uma visão geral das estratégias para melhorar esse número, já que se observou um aumento significativo do desempenho global do processo quando são considerados valores mais altos de $k_L a$.

Após começar esta pesquisa com uma visão do processo como um todo (**Capítulo 2**), e depois concentrar nossos esforços no desenvolvimento de modelos para uma de suas unidades específicas (**Capítulos 3** e **4**), bem como no desenvolvimento de estratégias para a otimização de sustentabilidade (demonstrada no **Capítulo 4** para um sub-sistema do processo), no **Capítulo 5** nós voltamos novamente a uma visão do todo, agora equipados com as ferramentas desenvolvidas nos capítulos anteriores. No **Capítulo 5**, o sub-sistema consistindo no biorreator e etapas downstream é integrado à framework de otimização do processo completo a partir de resíduos de biomassa até etanol. Para esse trabalho um novo modelo foi desenvolvido para o gaseificador indireto, sendo este detalhado no Capítulo 5. Os modelos referentes às diferentes unidades foram combinados em uma framework contendo os cálculos de parâmetros econômicos, consumo de energia (calor e eletricidade), emissões de CO_2 equivalente, consumo de água e outros indicadores de desempenho relacionados a sustentabilidade, que são recalculados a cada mudança nas variáveis de entrada. São discutidos os efeitos dessas variáveis nos resultados globais assim como suas interações e correlações entre respostas de categorias distintas. Por fim, o sistema foi otimizado com relação a três objetivos simultâneos: preço mínimo de venda (MESP), eficiência energética e pegada de

carbono. Os trade-offs ótimos foram discutidos para dois casos (bagaço de cana e resíduos de madeira), junto com uma análise a respeito das tendências observadas para as variáveis de decisão nas soluções Pareto-ótimas, e uma discussão sobre as incertezas nos resultados. De acordo com os resultados, as principais variáveis que definem os trade-offs são a temperatura no leito de gaseificação, a fração de biomassa adicionada ao leito de combustão do gaseificador, e a razão entre a vazão volumétrica de syngas fresco na entrada do biorreator e o volume de líquido no mesmo.

Para concluir, o **Capítulo 6** apresenta uma visão geral dos resultados e das estratégias utilizadas para a otimização de sustentabilidade, que envolvem o uso de técnicas como machine learning para geração de modelos substitutos, análise de componentes principais para redução do espaço de funções objetivo, e algoritmo genético multi-objetivo. Essas estratégias foram aplicadas especificamente para uma configuração dentro da rota termo-bioquímica, mas poderiam também ser estendidas a outras rotas tecnológicas, processos e produtos. Nesse capítulo são discutidas também as limitações deste trabalho, assim como oportunidades para pesquisas futuras dentro deste campo. Os resultados desta tese não podem ser usados para afirmar que a rota termo-bioquímica é economicamente viável ou ainda sustentável, porém eles indicam um desempenho favorável em termos de eficiência energética e pegada de carbono.

Samenvatting

(Translated by Britte Bouchaut; Reviewed by Henk Noorman)

Hernieuwbare energie speelt een sleutelrol in de strijd om de uitstoot van broeikasgassen te verminderen en zorgt tegelijkertijd voor menselijk welzijn en economische ontwikkeling. Ondanks milieuvoordelen van koolstofvastlegging worden breed aanbevolen biologisch hernieuwbare hulpbronnen zoals suikerriet en maïszetmeel, zogenaamde 1^e generatie (1G) grondstoffen, geassocieerd met sociale- en milieukwesties die sterk in tegenspraak zijn met het begrip duurzaamheid, zoals het voedsel-brandstofconflict en de bijdrage aan effecten zoals ontbossing, bodemaantasting, verlies van biodiversiteit en vervuiling van watervoorraden. Als reactie op deze problemen is er veel energie gestoken in de ontwikkeling van technologieën om nuttige energie uit niet-voedingsgewassen en agro-industriële reststromen, zoals suikerrietbagasse, maïsstengels en tarwestro te halen en om te zetten. Deze zogenaamde 2^e generatie (2G) grondstoffen bieden een extra uitdaging omdat fermenteerbare suikers niet direct beschikbaar zijn; desalniettemin zijn (en worden) talloze technologieën ontwikkeld om 2G-grondstoffen om te zetten in brandstoffen en chemicaliën, met ethanol als het meest toegepaste product, een veelgebruikt motorbrandstof- en benzineadditief.

2G- of cellulose-ethanol kan worden geproduceerd via biochemische- of thermochemische routes, of via een derde optie die de aspecten van de eerdere twee combineert - ook wel de thermo-biochemische of hybride route genoemd. Deze laatste is de focus van dit proefschrift, dat deze weg verkent via procesmodellering, simulaties, (multi-objectieve) optimalisatie en andere toegepaste strategieën om te bepalen welke proceskeuzes en voorwaarden leiden tot de beste prestaties van de belangrijkste duurzaamheidsaspecten. Terwijl het thermochemische vergassingsproces de bijna volledige omzetting van biomassa mogelijk maakt zonder de noodzaak van complexe en dure stadia van voorbehandeling en hydrolyse, zou de daaropvolgende biologische omzetting (fermentatie) van syngas verschillende voordelen kunnen bieden in vergelijking met de traditionele katalytische omzetting, b.v. hogere flexibiliteit van H_2:CO-

verhoudingen en tolerantie voor gasverontreinigingen. Hoewel bepaalde uitdagingen het commerciële concurrentievermogen van de syngasfermentatie kunnen aantasten, zoals een lagere productiviteit in vergelijking met heterotrofe fermentatie, zouden intelligente keuzes van procesintegratie en ontwerpparameters de prestatie van het proces aanzienlijk kunnen verbeteren.

In **Hoofdstuk 1** wordt een algemene inleiding gegeven over dit traject en worden de motivatie en specifieke doelen van dit onderzoek uiteengezet. Het toepassingsgebied van het project is beperkt tot één specifieke configuratie van deze route die bestaat uit de indirect verwarmde vergassing van biomassaresiduen om syngas te produceren, de verdere omzetting in ethanol via autotrofe fermentatie met acetogene bacteriën, en ethanolzuivering met behulp van destillatie en moleculaire zeven wanneer watervrije ethanol het gewenste product is. Het voornaamste doel van dit proefschrift is om erachter te komen welke ontwerpparameters en procescondities leiden tot de beste prestaties betreffende gelijktijdige en vaak tegenstrijdige aspecten qua duurzaamheid, d.w.z. winstgevendheid, milieu-impact (carbon footprint) en energie-efficiëntie. Hiervoor moest het proces als geheel worden onderzocht, en ook de hoofdeenheden afzonderlijk. De specifieke doelen omvatten het procesontwerp, de constructie van wiskundige modellen en simulaties, de evaluatie van alternatieven voor energieterugwinning, impactanalyse, de ontwikkeling van een multi-objectief duurzaamheidsoptimalisatiekader en de implementatie van strategieën om de complexiteit van de problemen omtrent optimalisatie te verminderen. Deze doelen komen aan de orde in de Hoofdstukken 2 tot en met 5.

Hoofdstuk 2 presenteert een voorlopige economische beoordeling van deze route die wordt uitgevoerd na het ontwikkelen van het procesontwerp en de simulatie van één mogelijke configuratie die is afgestemd op energie-onafhankelijkheid. Afgezien van de bovengenoemde proceseenheden omvat deze configuratie ook warmteterugwinning / integratie en elektriciteitsproductie. Om de simulatie mogelijk te maken moesten er verschillende aannames worden gedaan van conversies, opbrengsten en productselectiviteit die waren gebaseerd op in de literatuur beschikbare gegevens. Dit hoofdstuk geeft ook een meer gedetailleerd literatuuroverzicht van het proces en de huidige onderzoekshiaten. Onze analyse suggereert slechte economische prestaties in vergelijking met 1G-ethanol, maar de resultaten van de minimale ethanolverkoopprijs (MESP), energie-efficiëntie en productopbrengst zijn vergelijkbaar met andere 2G-

technologieën zoals vergassing gevolgd door gemengde alcoholsynthese, gelijktijdige versuikering en fermentatie, en hydrolyse gevolgd door fermentatie.

De fermentatie van syngas wordt verder onderzocht in **Hoofdstuk 3**, dat een dynamisch model voor dit proces presenteert in een continu geroerde tankreactor. De biologische conversie van syngas met behulp van acetogenen is een vrij jonge technologie die voordelen kan bieden zoals flexibiliteit van de gassamenstelling. Maar het levert ook uitdagingen op vanwege de lage oplosbaarheid van de gasvormige substraten, de vorming van ongewenst acetaat en de langzame opname van substraat door de cellen. Hoewel modellen voor dit proces in de literatuur nog schaars zijn, zijn ze nodig om de effecten van bedrijfsomstandigheden te evalueren, inzicht te krijgen in het proces en uiteindelijk te optimaliseren. Het hier ontwikkelde model houdt rekening met de massaoverdracht van substraat en producten tussen de gas- en vloeistoffase, het verbruik van CO, H_2 en CO_2 door de cellen, remming door producten en substraat, celgroei en dood, en herassimilatie van azijnzuur wat optreedt bij een lage pH. De onbekende parameters in het systeem van differentiaal-algebraïsche vergelijkingen zijn geschat met behulp van experimentele gegevens uit drie artikelen die beschikbaar zijn in de literatuur en die verschillende experimentele omstandigheden omvatten. In dit hoofdstuk worden de verschillende soorten parameters en inputvariabelen besproken, evenals hun interacties en effecten op de uitkomsten van de bioreactor. Ten slotte wordt het model gebruikt om de effecten van syngas-samenstelling te evalueren en een optimalisatie van deze eenheid uit te voeren. De belangrijkste bijdragen van dit hoofdstuk zijn het dynamische model zelf en de schatting van de kinetische parameterset, maar enkele van de modelvoorspellingen kunnen benadrukt worden: (i) er werd waargenomen dat de gevoeligheid van de kinetische parameters voor de uitkomsten van de reactor afhankelijk zijn van de bedrijfsomstandigheden; (ii) ethanolproductiviteit en CO-omzetting zijn tegenstrijdige doelen wanneer CO-rijk gas wordt gebruikt, maar hogere omzettingen kunnen worden gehandhaafd als het H_2-gehalte wordt verhoogd; (iii) voorspeld wordt dat de maximale productiviteit bij volledige CO-omzetting optreedt met een voedingsgas dat ongeveer 55% CO en 45% H_2 bevat.

Het in **Hoofdstuk 3** ontwikkelde biokinetische model wordt vervolgens opgenomen in een vloeistofdynamisch model van een bellenkolomreactor, dat in **Hoofdstuk 4** wordt gepresenteerd. Dit model beschouwt de ruimtelijke verdeling

van de toestandsvariabelen in plaats van homogeniteit. Daarom variëren de concentraties CO, H_2, CO_2, ethanol en azijnzuur met de hoogte in de gas- en vloeistoffase, evenals de gassnelheid, de volumetrische gas-vloeistofmassaoverdrachtscoëfficiënt kLa en de gasophoping. Dit model wordt vervolgens gebruikt om de reactoroutput bij steady-state te voorspellen voor een subsysteem bestaande uit de bioreactor die wordt gevoed met vers syngas en gerecycled gas, destillatie, dehydratatie van ethanol en recirculatie van water afkomstig van de destillatiebodems naar de bioreactor. Om de optimalisatie van dit subsysteem, dat een groot aantal computationeel dure objectieve functie-evaluaties omvat, te vergemakkelijken worden surrogaatmodellen gebruikt in het optimalisatiekader in plaats van de originele modellen. Dit zijn kunstmatige neurale netwerken die zijn getraind en gevalideerd met gegevens die zijn geproduceerd met de originele bellenkolommodellen en Aspen-simulaties van de destillatiekolommen. De optimalisatie wordt vervolgens uitgevoerd met een multi-objectief genetisch algoritme voor drie combinaties van doelen met betrekking tot kapitaalinvestering, minimale verkoopprijs, energie-efficiëntie en productiviteit. Afgezien van een analyse van afwegingen en optimale waarden van verschillende beslissingsvariabelen bespreekt dit hoofdstuk ook de effecten van de massaoverdrachtscoëfficiënt kLa en een overzicht van strategieën om deze te verbeteren, aangezien hogere kLa-waarden kunnen leiden tot een significante verbetering van de wereldwijde prestaties.

Na het starten van dit onderzoek met het oog op het hele proces (**Hoofdstuk 2**), hebben we onze inspanningen geconcentreerd op de ontwikkeling van modellen voor een van zijn eenheden (**Hoofdstukken 3 en 4**) en op de ontwikkeling van strategieën voor optimalisatie van duurzaamheid (aangetoond in **Hoofdstuk 4** voor een subsysteem van het proces). Daarna zoomt **Hoofdstuk 5** opnieuw uit naar een overzicht van het geheel, nu uitgerust met de gereedschappen die in de vorige hoofdstukken zijn ontwikkeld. In **Hoofdstuk 5** is het subsysteem met de bioreactor en de stroomafwaartse stadia geïntegreerd in een raamwerk voor optimalisatie van het hele proces van biomassa-residuen tot ethanol. Voor dit hoofdstuk is ook een nieuw model ontwikkeld voor de indirect verwarmde vergasser. De modellen van verschillende units worden gecombineerd in één raamwerk met ingebedde berekeningen van economische parameters, warmte- en energieverbruik en productie, CO_2-equivalente emissies, waterverbruik en andere prestatie-indicatoren die opnieuw worden berekend als de

inputvariabelen wijzigen. We bespreken de effecten van deze variabelen op de globale resultaten, evenals hun interacties en correlaties tussen reacties uit de verschillende categorieën. Ten slotte is het systeem geoptimaliseerd met drie gelijktijdige doelstellingen: minimale verkoopprijs voor ethanol, energie-efficiëntie en ecologische voetafdruk. De optimale afwegingen worden besproken voor twee gevallen (suikerrietbagasse en houtresten), samen met een analyse van de trends van de beslissingsvariabelen bij de Pareto-optimale oplossingen en een schatting van onzekerheden. Volgens de resultaten zijn de belangrijkste variabelen die de afwegingen bepalen de temperatuur in het vergassingsbed, de fractie biomassa die aan het verbrandingsbed van de vergasser wordt toegevoegd en de verhouding tussen het volumetrische debiet van vers syngas bij de inlaat van de bioreactor en het vloeistofvolume in de bioreactor.

Ten slotte geeft **Hoofdstuk 6** een overzicht van de resultaten en de strategieën die worden voorgesteld voor optimalisatie van duurzaamheid, waarbij technieken als surrogaatmodellering met machine learning, analyse van hoofdcomponenten voor het verminderen van de objectieve functieruimte en een multi-objectief genetisch algoritme worden gebruikt. Deze strategieën worden specifiek toegepast voor één configuratie van de thermo-biochemische route, maar kunnen worden uitgebreid tot andere technologische routes en verschillende processen en producten. De beperkingen van ons werk worden ook samengevat in dit hoofdstuk, samen met onze kijk op mogelijkheden voor toekomstig onderzoek op dit gebied. De resultaten van dit proefschrift kunnen niet worden gebruikt om te bevestigen dat de thermo-biochemische route tegenwoordig economisch levensvatbaar of duurzaam is, maar ze duiden wel op goede prestaties op het gebied van energie-efficiëntie en CO_2-voetafdruk, die naar verwachting in de komende jaren ook economische inkomsten zullen opleveren.

Chapter 1

General Introduction

"*Let man then contemplate the whole of nature in her full and grand majesty, and turn his vision from the low objects which surround him. Let him gaze on that brilliant light, set like an eternal lamp to illumine the universe; let the earth appear to him a point in comparison with the vast circle described by the sun; and let him wonder at the fact that this vast circle is itself but a very fine point in comparison with that described by the stars in their revolution round the firmament. But if our view be arrested there, let our imagination pass beyond; it will sooner exhaust the power of conception than nature that of supplying material for conception.*"

Blaise Pascal, Pensées

1.1. Introduction and Motivation

In 2019, the word of the year chosen by Collins Dictionary was, not surprisingly, *climate strike*, in reference to the numerous protests and demonstrations about climate change that swept the globe throughout the year. A similar message of concern had been conveyed the year before with the word choice *single-use*, referring to disposable plastic that quickly turns into trash. These two issues, climate change and waste, are behind another buzzword that is certain to make word of the year anytime soon: *bioeconomy*. (If not bioeconomy, then certainly circular economy or green economy will.) "The art of bringing value to the valueless", as well defined in the Biofuels Digest (Lane, 2019), bioeconomy tackles not only CO_2 emissions, but also pollution, waste management and energy security. Put simply, bioeconomy promotes the use of biomass as the main raw material for the production of energy, transportation fuels, chemicals and plastics, thus replacing fossil resources and giving rise to biorefineries, as opposed to oil refineries.

Within the vast domain of bioeconomy, this thesis is focused on one of its staples: bioethanol, a renewable, clean-burning and high-octane liquid fuel commonly used as additive for gasoline or as pure fuel in flexible-fuel cars. Fuel blends of different ethanol levels are widely used in the world and perceived as a way to reduce dependency on petrol and cut carbon emissions in the transportation sector. As of 2020, nearly all of the commercialized ethanol is produced from 1st-generation (1G) feedstocks, i.e. food crops such as sugarcane in Brazil and corn in the US. However, despite the reduction of fossil-derived CO_2 emissions, the rapid expansion of biofuels since the early 2000's has raised not only the ethical food-versus-fuel debate, but other environmental concerns related to issues such as soil degradation, biodiversity loss, and the increased use of fertilizers contributing to eutrophication and emissions of nitrous oxide, a strong greenhouse gas (GHG) (Goldemberg et al, 2008). In order to extenuate these impacts and increase the sustainability of biofuels, research efforts from both academia and industry have been put into the development and implementation of technologies based on the use of non-food resources, also called 2nd-generation (2G) feedstocks, e.g. agricultural waste such as sugarcane bagasse and corn stover, and non-food crops such as switchgrass. Lignocellulosic biomass (such as the abovementioned examples) is often used as synonym for 2G feedstocks, although 2G refers more broadly to any carbonaceous material that is not a food crop, thus also

encompassing other types of waste such as municipal solid waste (MSW) and industrial off-gas (e.g. basic oxygen furnace (BOF) gas from steel mills).

Pathways for the production of fuels from lignocellulosic biomass are essentially two: the biochemical pathway comprising pretreatment and enzymatic or acid hydrolysis of biomass followed by fermentation of sugars to ethanol; and the thermochemical pathway comprising biomass gasification and the following conversion of the produced synthesis gas (syngas) to ethanol and other products. The conversion of syngas to liquid fuels and chemicals can proceed with chemical catalysts (catalytic route) or microbial catalysts (fermentation). Research and development on the production of fuels and chemicals from lignocellulosic biomass have been concentrated on the fully-biochemical route (i.e. pretreatment and enzymatic and/or acid hydrolysis followed by fermentation of sugars), a fact associated with a long familiarity of the fermentation industry with hydrolysis of starch to obtain glucose (Brown, 2010). Like starch, cellulose is also a polymer of glucose; however, it is not only more recalcitrant than the former, but the fact that it is entrenched in a matrix of lignin makes such process even more complex and difficult to manage. In this aspect, thermochemical routes offer a significant advantage since gasification is able to convert nearly all biomass components, including recalcitrant lignin, to syngas. Furthermore, other non-lignocellulosic residues, such as non-recycled plastics that are present in MSW, might also be converted via gasification (GBB, 2013). Syngas is a mixture consisting primarily of CO and H_2 and has long been considered an important building block in the catalytic conversion to liquid fuels and chemicals such as methanol, formaldehyde, acetic acid and olefins (Subramani and Gangwal, 2008).

The so-called thermo-biochemical, or hybrid, pathway couples the thermochemical conversion of biomass to syngas with the biological conversion of syngas to fuels and chemicals using acetogenic bacteria. The pathway has attracted companies and scientists due to the potential advantages its constituent steps offer when compared to the other pathways. In more specific terms, while the first step (thermochemical conversion) dismisses the complex stage of obtaining sugars from lignocellulosic biomass, besides admitting a wide variety of feedstocks, the second step (biochemical conversion) is believed to offer several advantages over catalytic conversion of syngas, such as higher specificity, higher yields, lower energy costs due to operation under mild conditions, and higher resistance to poisoning (Klasson et al., 1991). Nonetheless, this is still a new route that has not been fully explored. For example, not only is there a need for research

on the biological conversion of syngas (e.g. with the design of reactors that enhance the mass transfer coefficient), but the integrated process must be improved as a whole, starting with appropriate gasification conditions to produce syngas with favorable composition for the fermentation, to the design of energy-efficient separation processes and the evaluation of power cycles using syngas that is generated in the process. It is also worth noting that despite high expectations and promising results of ethanol yield and selectivity announced by the leading gas fermentation company, LanzaTech, the scientific publications regarding this technology indicate a number of research gaps: limited understanding of microbial physiology aspects related to product selectivity (i.e. acid or alcohol formation) and cell inhibition by products, substrate and other components (e.g. syngas contaminants); inconsistent reports of growth rate, selectivity and yields; few papers about nutrient medium optimization; limited modeling, simulation and optimization studies. The latter were the targets of this research project.

Only a few works have investigated the performance of this route with regard to sustainability goals (for example, through techno-economic assessment and Life Cycle Assessment), such as Benalcázar et al. (2017), Pardo-Planas et al. (2017) and Roy et al. (2015). However, although they contribute meaningful results to the field, process conditions are mostly fixed or evaluated through univariate sensitivity analysis, and optimizations studies have not been conducted. Though the original goal of our research was to perform a classic early stage sustainability assessment (i.e. techno-economic assessment plus life cycle analysis), the project evolved instead into the pursuit, development and application of strategies to optimize sustainability within this route. This being a novel, not fully understood and commercialized technology, one of our goals was to find out which actions, process improvements and process conditions lead to the best performance in terms of the specific aspects of sustainability considered here, namely: economic viability, environmental impact (specifically, carbon footprint) and energy efficiency. Efficient methodologies for sustainability optimization are still scarce in the literature, as the integration of processes and the evaluation and optimization of multiple (and conflicting) objectives entail a high computational cost (Gonzalez-Garay and Guillen-Gosalbez, 2018), therefore in this work we also aimed at identifying, developing and implementing strategies in this domain.

Chapters 2 through 5 of this thesis are presented in the structure of research articles, the first three of which have already been published in peer-review

journals. To avoid redundancy and repetition, a deeper literature review is left for the introduction sections of these articles.

1.2. Objectives and Structure of this Thesis

This thesis started as an investigation into the sustainability of the gasification-fermentation route for ethanol production from biomass waste. The question was not exactly "is this commercially viable?" and "is this sustainable?", but instead: how can this process be designed to optimize its performance in terms of three values: profitability, energy efficiency, and environmental impact? A disclaimer must be made: throughout this thesis we take the liberty of referring to this goal as *sustainability optimization*, although a few simplifications are made: first, the social domain (one of the pillars of sustainability) is excluded from our models and assessments, as this work focuses on the industrial stage of the production chain and not on upstream stages where social impacts mostly occur; moreover, the only environmental impacts addressed here are CO_2 emissions and water footprint. Although many other indicators exist to account for environmental impacts, such as abiotic depletion potential, acidification and eutrophication potential, human and environmental toxicity potential, among others, we must keep in mind that each added indicator increases the dimension of the multi-objective optimization problem that is the ultimate goal of this work. The choice of carbon and water footprint was due to two main reasons: first, these are direct results from our models, dismissing therefore the use of multiplication factors that are dependent on the different LCA methods available and that would bring an extra layer of uncertainty to our results; secondly, results from LCA studies in the literature suggest a significant degree of correlation between indicators, with several of them being directly related to CO_2 emissions or fossil fuel consumption. For example, in the work by Capaz et al. (2020), which evaluated distinct technological routes with regard to 8 environmental indicators, a tendency can be observed in the ranking of these technologies according to different indicators, although trade-offs were also observed among these environmental impacts. Another example is the work by Lasvaux et al. (2016), who conducted a detailed statistical analysis on the correlations between LCA environmental indicators and concluded that the set of indicators can be simplified to ease the decision making process without causing any loss of information. To summarize, this thesis does not tackle the whole concept of sustainability, but this term is used throughout the text when referring to the combination of economic, environmental and energetic indicators explored in this work.

It's also important to clarify that we do not intend to compare the "sustainability score" of this pathway with other technological routes, since such "score" is highly dependent on the process design, operating conditions and, just as relevant, the assumptions considered for the models and assessments.

In order to achieve the aforementioned main goal, the objectives below were defined, motivated by the identified knowledge gaps, and are addressed in the chapters of this thesis.

1.2.1. Preliminary assessment of economic viability for a possible configuration of the thermo-biochemical route

The literature review on syngas fermentation revealed a limited number of studies about techno-economic assessment, modeling and optimization of thermo-biochemical routes, as well as divergent results among the existing publications and often incomplete or unclear presentation of the assumptions considered. As starting point for this research project, we aimed at identifying the challenges, prospects and literature gaps surrounding this technology, and developing the process design and simulation for a energy self-sufficient plant comprising biomass gasification, syngas fermentation, heat recovery, power production and ethanol distillation. With this we also intended to deliver a first estimate of economic viability and energy efficiency for this process. This goal was fulfilled with our publication de Medeiros et al. (2017), presented in Chapter 2 of this thesis.

1.2.2. Modeling of syngas fermentation in a continuous stirred-tank reactor

In order to predict the outcomes of the syngas bioreactor as function of its design and operating parameters, a mathematical model was needed to describe this process. Our next goal was therefore to build a dynamic model of a continuous stirred-tank reactor (CSTR) taking into account multiple input variables and the simultaneous phenomena of gas-liquid mass transfer, cell growth and death, and chemical reactions. We aimed at estimating the kinetic parameters needed in the model using experimental data from publications, obtained under different conditions and modes of operation, and it was also our goal to investigate the effects of these parameters and the model input variables (e.g. reactor dilution rate) on the main response variables (e.g. ethanol concentration and selectivity, syngas conversion). Since there were no previous studies in the field of syngas fermentation contemplating parameter estimation, statistical treatment and

sensitivity analysis of both process conditions and kinetic parameters, our publication de Medeiros et al. (2019a), presented in Chapter 3, was designed to fulfill this gap.

1.2.3. Modeling of syngas fermentation in a bubble column reactor

Following the development of the CSTR model, our goal was to expand this model to that of a bubble column reactor (BCR), which would also account for the concentration gradients of substrate and products along the column. Ultimately this is the model to be used in our sustainability optimization framework. Our publications de Medeiros et al. (2020), presented in Chapter 4, and de Medeiros et al. (2019b) lay out this model and represent our contribution to the field of syngas fermentation modeling.

1.2.4. Modeling of indirectly-heated gasification of biomass

For the preliminary assessment mentioned in Sec. 1.2.1, the gasifier was simulated with an equilibrium model; the rationale behind this choice, as well as its limitations, are laid out in Chapter 2. However, to increase the accuracy of our results, one of our goals was to develop a robust model for this process without neglecting the deviations from equilibrium that occur in real operation. Theoretical and experimental articles about different gasification technologies are not hard to find, but while many optimization works involving this process make use of equilibrium models, published kinetic models are often difficult to reproduce or unsuitable due to their high degree of complexity, very limited range of values for the input variables and high specificity with regard to the experimental set-up and conditions used. Although a detailed kinetic model was not part of our research scope, we wished to build a new model for a dual-fluidized bed gasifier which incorporates previously reported correlations for syngas and char yields in an optimization routine to regulate the amounts of excess air and additional fuel needed to maintain the desired temperatures. This model is thoroughly explained in Chapter 5.

1.2.5. Development of surrogate models (artificial neural networks)

Additionally to the investigation of technologies and construction of models, one of our goals was to develop and implement strategies to support the sustainability optimization framework. Multi-objective optimization problems are more challenging to solve than one objective, especially when highly non-linear

functions are present – as is the case here and in a variety of real-world problems. Many works about optimization make use of short-cut models to enable the use of linear or non-linear programming methods, and when multiple objectives are involved these are often reduced to one through some type of weighting method. Metaheuristic methods, such as the genetic algorithm (GA) employed in our work, are convenient for this kind of complex problem but also entail a high computational cost due to the large number of objective function evaluations per iteration. Therefore we looked for an alternative to the approach of connecting the Aspen simulation to the metaheuristic optimization solver, which not only can be very slow but is also subjected to issues with non-convergence of the simulation. Our proposition is not to use short-cut models, but instead to gather sets of data obtained with detailed models (as mentioned in Sections 1.2.2-4) and use these to fit surrogate models that will be used to speed-up the optimization procedure. For these surrogate or reduced models we chose the application of artificial neural networks (ANN's) due to their capability to handle highly non-linear data. One of the goals of our project was therefore to generate data for these ANN's, train them and implement them in the sustainability optimization framework. This is demonstrated in Chapter 4 (de Medeiros et al., 2020) and Chapter 5, where the ANN's were applied for two types of intricate models: the BCR model (differential-algebraic equation system) and Aspen simulations (nonlinear system of MESH equations – material-equilibrium-summation-enthalpy – that define the distillation process).

1.2.6. Evaluation of energy recovery and energy self-sufficiency within thermo-biochemical routes

Energy efficiency is a pivotal indicator of the performance of a process, therefore one of our goals was to explore the possibilities of energy recovery through heat integration and power production. While in our preliminary assessment (see Sec. 1.2.1 and Chapter 2) the process design targeted an energy self-sufficient plant configuration, we also wished to analyze the trade-off between energy self-sufficiency and product (ethanol) yield. This is investigated and discussed in Chapter 5.

1.2.7. Computation of capital and operating costs, energy efficiency and carbon footprint

As mentioned previously, these are the main sustainability indicators considered in this work. The implementation of calculations for these responses in the optimization framework was therefore an essential goal of this project. The methods used, assumptions and results are presented in Chapters 2, 4 and 5.

1.2.8. Development of multi-objective optimization frameworks for optimization of sustainability goals and evaluation of Pareto-optimal solutions

The last goal is a combination of previous goals: the developed models and algorithms are incorporated in the final framework where optimization methods are applied to minimize the defined objective functions. This is done separately for a sub-system comprising the steps of fermentation and distillation and later for the whole process. The idea was to first test and demonstrate the proposed strategies with a smaller system. As there were no previous publications of the kind in the field of syngas fermentation, our publication de Medeiros et al. (2020), presented in Chapter 4, filled this literature gap. Subsequently the stages of gasification and energy recovery were added to the framework, thereby making it complete for the achievement of our main goal. As part of the sustainability optimization we also include the analysis of effects and correlations between distinct input variables, as well as between the objective functions, and an interpretation of the Pareto-optimal solutions. This goal is addressed in Chapter 5 of this thesis.

References

Benalcázar, E.A., Deynoot, B.G., Noorman, H., Osseweijer, P., Posada, J.A., 2017. Production of bulk chemicals from lignocellulosic biomass via thermochemical conversion and syngas fermentation: a comparative techno-economic and environmental assessment of different site-specific supply chain configurations. Biofuels, Bioprod. Bioref. 11, 861–886.

Brown, R.C., 2010. Biomass refineries based on hybrid thermochemical-biological processing – an overview. In: Biorefineries – Industrial Processes and Products, Status Quo and Future Directions. Edited by Birgit Kamm, Patrick R. Gruber, Michael Kamm. WILEY-VCH GmbH & Co. KGaA, Weinheim.

Capaz, R.S., de Medeiros, E.M., Falco, D.G., Seabra, J.E.A., Osseweijer, P., Posada, J.A., 2020. Environmental trade-offs of renewable jet fuels in Brazil: beyond the carbon footprint. Sci. Total Environ. 714, 136696.

de Medeiros, E.M., Posada, J.A., Noorman, H., Osseweijer, P., Maciel Filho, R., 2017. Hydrous bioethanol production from sugarcane bagasse via energy self-sufficient gasification-fermentation hybrid route: simulation and financial analysis. Journal of Cleaner Production 168, 1625-1635.

de Medeiros, E.M., Posada, J.A., Noorman, H., Maciel Filho, R., 2019a. Dynamic modeling of syngas fermentation in a continuous stirred-tank reactor: multi-response parameter estimation and process optimization. Biotechnology and Bioengineering 116, 2473–2487.

de Medeiros, E.M., Posada, J.A., Noorman, H., Maciel Filho, R., 2019b. Modeling and multi-objective optimization of syngas fermentation in a bubble column reactor. In: A.A. Kiss, E. Zondervan, R. Lakerveld, L. Ozkan (Eds.). Computer Aided Chemical Engineering, Volume 46: 29th European Symposium on Computer Aided Process Engineering (p.p. 1531-1536).

de Medeiros, E.M., Noorman, H., Maciel Filho, R., Posada, J.A., 2020. Production of ethanol fuel via syngas fermentation: optimization of economic performance and energy efficiency. Chemical Engineering Science: X 5, 100056.

Goldemberg, J., Coelho, S.T., Guardabassi, P., 2008. The sustainability of ethanol production from sugarcane. Energ. Policy 36, 2086–2097.

Gonzales-Garay, A., Guillen-Gosalbez, G., 2018. SUSCAPE: A framework for the optimal design of SUStainable ChemicAl ProcEsses incorporating data envelopment analysis. Chem. Eng. Res. Des. 2018, 245–264.

GBB, 2013. Gasification of non-recycled plastics from municipal solid waste in the United States. Gershman, Brickner and Bratton, Inc. Prepared for The American Chemistry Council.

Klasson, K.T., Ackerson, C.M.D., Clausen, E.C., Gaddy, J.L., 1991. Bioreactor design for synthesis gas fermentation. Fuel 70, 605 – 614.

Lane, 2019. Letter from Europe: The Bioeconomy's Journey to Yes through the Valley of No. https://www.biofuelsdigest.com/bdigest/2019/06/24/letter-from- europe-the-bioeconomys-journey-to-yes-through-the-valley-of-no/, accessed on 14/03/2020.

Lasvaux, S., Achim, F., Garat, P., Peuportier, B., Chevalier, J., Habert, G., 2016. Correlation of Life Cycle Impact Assessment methods (LCIA) and indicators for construction materials: What matters? Ecological Indicators 67, 174 – 182.

Pardo-Planas, O., Atiyeh, H.K., Phillips, J.R., Aichele, C.P., Mohammad, S., 2017. Process simulation of ethanol production from biomass gasification and syngas fermentation. Bioresour. Technol. 245, 925–932.

Roy, P., Dutta, A., Deen, B., 2015. Greenhouse gas emissions and production cost of ethanol produced from biosyngas fermentation process. Bioresour. Technol. 192, 185–191.

Subramani, V., Gangwal, S.K., 2008. A review of recent literature to search for an efficient catalytic process for the conversion of syngas to ethanol. Energy & Fuels 22, 814 – 839.

Chapter 2

Hydrous bioethanol production from sugarcane bagasse via energy self-sufficient gasification-fermentation hybrid route: simulation and financial analysis

"Ylla: Yll...do you ever wonder if there are beings living on the third planet?
Yll: The third planet is incapable of supporting life. Our scientists have said there is far too much oxygen...
Ylla: ... oxygen...
Yll: oxygen in the atmosphere.
Ylla: But wouldn't it be fascinating if there were people?"

Ray Bradbury, The Martian Chronicles

2.1. Introduction

Hydrous bioethanol (E100), a solution of ethanol and water near the azeotrope composition (93 – 95 wt% ethanol), is largely used in Brazil as a biofuel in flexible-fuel light vehicles. Due to its cost competitiveness with gasoline and growing public concern over issues of environmental and energy security, E100 production and sales have increased at fast rates, a trend which is expected to continue. In 2015, for example, E100 consumption saw a 37.5% increase compared to the previous year, accounting for more than 17.8 billion liters consumed nationwide (UNICA, 2016). In Brazil, the widespread commercialization of E100 reflects the well-established industry built on mature 1st-generation technology for sugarcane production, extraction, fermentation and ethanol distillation. However, while the use of bioethanol as substitute (or additive) for gasoline may effectively reduce the emissions of fossil-originated carbon dioxide, the massive expansion of sugarcane and other crops may result in significant environmental impacts, such as soil degradation, contamination of aquatic systems and eutrophication due to use of fertilizers and herbicides, and emissions of nitrous oxide (a strong greenhouse gas), also associated to the use of fertilizers (Souza et al., 2015). In this context, efforts to minimize environmental damage and increase sustainability indices in biofuels and biobased products sectors have boosted scientific research on 2nd-generation technology, i.e. the conversion of lignocellulosic biomass (Cheali et al., 2015) or wastes (Férnandez-Dacosta et al., 2015) to biofuels and biochemicals.

Traditionally, two main platforms are considered for the conversion of lignocellulose to ethanol, namely: i) a biochemical platform comprising biomass pre-treatment, hydrolysis and sugars fermentation; and ii) a thermochemical platform comprising biomass gasification and syngas conversion to ethanol. The latter conversion can be accomplished via two distinct pathways: a high-pressure, metal-based catalytic conversion, which characterizes a thermochemical-catalytic process (usually called simply the thermochemical route); and a biological conversion (i.e. fermentation), characterizing a thermochemical-biochemical (hybrid) process. Although less popular than the other pathways, the so-called hybrid pathway has received growing attention in the past years, both inside and outside academic circles. For example, Lanzatech, one of the companies seeking to commercialize the fermentation of syngas or waste gas from steel production, has been attracting special media attention (Lane, 2015).

Ethanol can be produced by strictly anaerobic, mostly mesophilic, bacteria that are capable of autotrophically converting CO, CO_2 and H_2 according to Eqs. (2.1) and (2.2) as result of the Wood-Ljungdahl metabolic pathway (Vega et al., 1989). This process has been reported to offer several advantages over catalytic conversion, such as higher yields, higher reaction specificity, lower energy requirements, syngas composition flexibility and higher resistance to contaminants (Klasson et al., 1992). Furthermore, gasification of biomass is feedstock-flexible and capable of utilizing all biomass components, including lignin, while dismissing complex pre-treatment and avoiding the use of expensive enzyme cocktails (Shen et al., 2015). Notwithstanding these potential advantages, syngas fermentation is still at an early stage of technological development compared to other conversion routes and therefore requires improvements and better understanding of several processing aspects. For example, there are several open issues regarding unsettled parameters, such as: (i) threshold resistance of microorganisms to syngas contaminants; (ii) optimal conditions and bioreactor design for ethanol production; and (iii) optimal integration between gasification, syngas fermentation and distillation; among others.

$$6CO + 3H_2 \rightarrow C_2H_5OH + 4CO_2 \qquad\qquad (2.1)$$

$$2CO_2 + 6H_2 \rightarrow C_2H_5OH + 3H_2O \qquad\qquad (2.2)$$

Despite the increasing number of publications regarding syngas fermentation, only a few articles have presented techno-economic or environmental assessments of integrated processes based on this technology. Piccolo and Bezzo (2009) performed process design, heat integration and economic assessment to evaluate the feasibility of a hybrid route in comparison with enzymatic hydrolysis followed by fermentation, finding the latter to be more financially attractive. Wei et al. (2009), using a black-box system model based on literature data, concluded that, from a process engineering perspective, the hybrid gasification-fermentation route would be less feasible than both hydrolysis followed by sugars fermentation and gasification followed by chemical synthesis. Moreover, an optimization study delivered by Martín and Grossmann (2011) regarding technological routes for lignocellulosic ethanol production via gasification demonstrated chemical synthesis to be a better choice for syngas conversion than syngas fermentation, although the authors also reported promising results of production costs. In contrast, Wagner and Kaltschmitt (2012), using process simulation in Aspen Plus

to compare the three types of pathway, found gasification followed by syngas fermentation to be the most energy efficient process. More recently, Roy et al. (2015) evaluated the production cost and greenhouse gas emissions for four scenarios using the hybrid route for ethanol production and arrived at promising results, especially if untreated feedstock is used. Besides these examples, the production of other products through syngas fermentation has also been assessed by Choi et al. (2010), who demonstrated the viability of producing polyhydroxyalkanoate (PHA) and H_2 through this route.

In this study, a process design has been proposed for the production of hydrous ethanol (E100) from sugarcane bagasse using gasification and syngas fermentation in an energy self-sufficient plant. For this purpose, literature data and engineering skills have been combined in the development of a predictive model for further assessments. Unsettled issues, e.g. concerning effects of syngas contaminants on biological productivity, have been simplified but are explicitly addressed in the text. Important issues such as water consumption, carbon conversion, energy production and efficient concentration of highly dilute ethanol were addressed. A complete and integrated process flowsheet – from biomass residues to syngas, and from syngas to E100 and power –was designed and simulated in Aspen Plus using Hierarchy blocks to separate the different units in the process. Furthermore, a financial model was built to estimate the capital expenditure (CAPEX) and the operating expenditures (OPEX), and to probabilistically estimate the minimum ethanol selling price (MESP) via Monte Carlo simulation.

2.2. Methodology

The approach is based on quantitative results generated by professional process simulators using up-to-date literature information on biomass gasification and syngas fermentation with acetogenic bacteria. The separation flowsheet adopts rigorously modeled multiple-effect distillation to cut heat consumption.

2.2.1. Process Design and Simulation

The commercial software Aspen Plus was used to simulate the conceptual integrated process for E100 production from sugarcane bagasse via the hybrid route: biomass gasification and syngas fermentation. The plant capacity is assumed to be 624 dry metric tons of bagasse per day, which is a compatible figure

considering a medium scale sugarcane processing plant of roughly 1.7 million metric tons of sugarcane per harvest.

Material and energy balances were calculated for the proposed process flow diagram (PFD) in Aspen Plus environment from user-specified inlet streams, unit operations and additional subroutines. Aspen PFDs are available in Appendix A in the Supplementary Material. A simplified block flow diagram of the process is depicted in Fig. 2.1, with the respective Aspen PFD in Fig. A1-1 (Appendix A1). The following sections (2.2.1.1 to 2.2.1.5) provide specific details on the simulation methodology applied for each unit. When relevant, block models and stream/block names are parenthesized to facilitate their identification in the Aspen PFDs. It is recommended that the reader follows the text with the flowsheets at hand for easier comprehension.
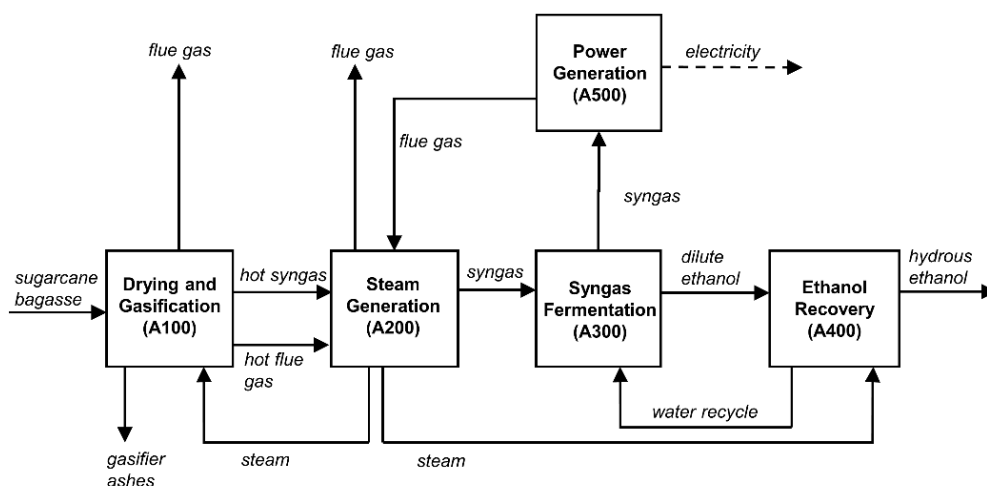
Figure 2.1. Simplified block flow Diagram of E100 production from sugarcane bagasse via gasification and syngas fermentation.

2.2.1.1. Gasification Unit (A100)

The Gasification Unit (Fig. A1-2, Appendix A1) comprises the following unit operations: biomass feed handling and drying; indirectly-heated gasification in dual circulating fluidized bed; and cyclone removal of particulates. This type of gasifier consists of two separate, interconnected, beds, through which hot bed material circulates and transfers heat between different zones. In the gasification

zone (GZ) bed, steam is added as sole gasifying agent, while in the combustion zone (CZ) bed, air is added as combustion agent. With this configuration, high quality syngas, with higher concentration of H_2 and no dilution in N_2, can be produced. The simulation assumes no energy losses and achievement of equilibrium conditions, and thermodynamic properties are calculated using the Redlich-Kwong-Soave equation of state (RKS-EOS).

In this unit, wet sugarcane bagasse (stream LCM-IN) is fed with a mass flow rate of 52,000 kg/h and a moisture content of 50 wt%, which is then reduced to 10 wt% in a rotary dryer using hot flue gases from the combustion of a fraction of the char that is formed during the pyrolysis reactions that take place in the gasifier. The RYield block RD simulates drying of moisture with hot gases, while the cyclone separator RD-CYC separates gas and solid phases after drying. Biomass is modeled in Aspen Plus as a non-conventional component characterized by the component attributes specified in Table 2.1. Proximate and ultimate analyses were obtained from the simulation of a sugarcane processing plant as described by Bonomi et al. (2011). The higher heating value (HHV) was calculated using the correlation formulated by Parikh et al. (2005). Since non-conventional components do not participate in phase and chemical equilibrium calculations, an RYield reactor model (block DCMP) is firstly used to decompose biomass into its constituent elements (C, H_2, O_2, N_2, Cl, S, H_2O) to enable the subsequent calculations. Although this stage of decomposition (not to be confused with pyrolysis) is not observed in reality, it configures an effective resource to quantitatively simulate operations with heterogeneous solids (Aspen Technology, 2011) such as biomass gasification (Ramzan et al., 2011), and its enthalpy change must be accounted for in the heat balance.

The gasifier itself consists of two fluidized beds with circulation of bed material (olivine) which is responsible for heat transfer between the CZ and the GZ. Pre-heated air at 130°C is fed into the CZ (RStoic model), where char is burned to provide heat for the endothermic gasification reactions. The separator S-1 represents the separation of the char fraction that is used for combustion. The GZ (RGibbs model) is fed with biomass and saturated steam (STM-GSF) which acts as gasifying agent at 2.5 bar (127.5 °C). The steam-to-biomass ratio (STBR), defined here as the mass ratio of steam plus biomass moisture to dry biomass, is 0.34, a value which was chosen inside the typical range of 0.2 – 2, with a preference for lower values due to lower energy consumption (Silva and Rouboa, 2014). The

temperatures in the GZ and the CZ are assumed to be 950°C and 1000°C, respectively, which is consistent with operating ranges reported for this type of gasifier (Brown, 2011; Worley and Yale, 2012). The gas then passes through a cyclone (CYC) to remove particulates. Although the simulation neglects tar formation, the economic evaluation assumes that the gasifier module represents both a gasifier and a tar reformer which catalytically converts hydrocarbons into CO and H_2, thereby approaching equilibrium conditions. As a matter of fact, it is a reasonable approximation to assume equilibrium composition at the tar reformer outlet since the catalyst shows significant water-gas-shift (WGS) activity (Dutta et al., 2011).

Syngas compositions and yields are strongly affected by a number of parameters, such as biomass composition and size, gasifier temperature and STBR (Puig-Arnavat et al., 2010). In order to avoid modeling unnecessary complex kinetics related to the large number of reactions taking place during gasification and reforming in this preliminary conceptual design, the gasifier model adopts a multi-reaction equilibrium approach with considerations of operating conditions that would in fact favor the achievement of equilibrium (i.e. very high temperature and use of tar reforming catalysts). This is a common approach for gasifier models reported in the literature (Baratieri et al., 2008; Esmaili et al., 2016; Van der Heijden and Ptasinski, 2012). Although complete equilibrium conditions are unlikely in real operations, equilibrium models are very important to the design of chemical processes, as they set limiting operation performances. As a notable example, distillation columns and sour gas absorbers with aqueous ethanolamines are commonly sized using equilibrium approach models, but rarely operate at strict equilibrium conditions. In the same way, it is evident that the equilibrium approach simplifies the gasifier model, but it does not undermine significantly the integrated process, given the high temperature conditions which accelerate kinetics driving the real reactor performance to near equilibrium. Taking into account that the final goal of this work is an overall assessment that considers several concomitant sources of uncertainty within a Monte Carlo framework, it is reasonable to consider that the relaxation brought by modeling the gasification step with multi-reaction chemical equilibrium is not sufficient to compromise the final results and/or our conclusions.

Table 2.1. Sugarcane Bagasse Component Attributes

Ultimate Analysis (wt%, daf)						Proximate Analysis (wt%, db)				HHV (db)
C	H	O	N	Cl	S	FC	VM	Ash	Moisture	(MJ.kg^{-1})
46.96	5.72	44.05	0.27	0.02	0.04	18.00	79.06	2.94	50.00	18.5

daf: dry-ash-free basis; db: dry basis; FC: fixed carbon; VM: volatile material

2.2.1.2. Steam Generation Unit (A200)

The heat exchanger network in A200 (Fig. A1-3, Appendix A1) consists of five heat exchangers (E-1 to E-5) producing process steam by cooling of hot gases. Two categories of steam are produced in this unit: (i) 2.5 bar saturated steam, used as utility and gasifying agent; and (ii) 10 bar saturated steam, used as utility. The hot inlet gases are: (i) syngas from A100 (H-SYNGAS); (ii) hot flue gas from the CZ in A100 (H-GAS-1); and (iii) hot exhaust from the gas turbine in A500 (H-GAS-3). The liquid streams W2B-1 and W10B-1 are the steam utilities return as saturated liquid, while WGSF-1 is a fresh water stream directed for the production of steam for the gasification unit.

Heat from syngas is recovered until it reaches a temperature of 73°C. The cooling water (CW) then continues with heat removal until 60°C, which is assumed to be the syngas inlet temperature at the Venturi scrubber (VS). The scrubbing water (W-VS) is specified with a flow rate to provide a liquid to gas volumetric ratio (L/G) of 1 L/m3, according to Dutta et al. (2011). The W-VS is maintained inside a closed loop with makeup and purge of approximately 8% of the recirculating flow rate. The liquid purge (WW-1) is sent to off-site wastewater treatment. The cold syngas, leaving the scrubber at a temperature of 54°C, is sent to fermentation in A300.

2.2.1.3. Syngas Fermentation Unit (A300)

A300 (Fig. A1-4, Appendix A1) consists essentially of a bioreactor, a microfiltration system for cell separation and a CO_2 scrubber for recovery of ethanol vapors from the fermenter off-gas. In this unit, A300, the property method NRTL-HOC was used due to the highly non-ideal mixture containing ethanol, water and acetic acid, which dimerizes in the vapor phase. Henry's Law was used as ideality model for reference state calculations of the light gases CO, CO_2 and H_2 in the aqueous phase.

Several types of bioreactor have been reported for syngas fermentation with different operating modes (continuous, batch or semibatch), for example: stirred tank (Klasson et al., 1991), bubble column (Rajagopalan et al., 2002), trickle bed (Klasson et al., 1991), hollow fiber membrane (Shen et al., 2014a) and monolithic biofilm reactors (Shen et al., 2014b). The process herein represented is based on a model that considers the experimental data reported by Gaddy et al. (2007) for syngas fermentation in a continuous agitated tank with water and cell recycle. Vapor-Liquid Equilibrium between the contacting phases in the fermenter is described by two blocks: (i) a stoichiometric reactor (FM) which simulates the fermentation reactions; and (ii) a flash separator (S-1) which properly separates the off-gas (OGAS-1) and the liquid phase broth (BRTH-1). The bioreactor is kept at 37°C by chilled water entering at 15°C and leaving at 25°C. Two heat exchangers (E-1 and E-2) are used to cool the reactor liquid inlet which is composed mostly of recycle water from distillation.

Experimental results of continuous and steady state syngas fermentation using the strain *Clostridium ljungdahlii* with water and cell recycle were retrieved from the US Patent 7,285,402 B2, Example 15 (Gaddy et al., 2007). Although other authors have reported low ratios of ethanol to acetate in the broth (Richter et al., 2013; Younesi et al., 2005), Gaddy et al. (2007) reported high productivities of ethanol with nearly zero acetate production when using water and cell recycle. According to the authors, recycling the water from distillation which contains small amounts of acetate is an effective measure to enhance ethanol production, as acetate inhibition is promoted after it reaches concentration levels between 3 g/L and 5 g/L, hence leading to zero net acetate production and more carbon conversion to ethanol.

In order to simplify the model and enable its construction in Aspen environment, the following assumptions are considered: (i) by recycling aqueous broth with dilute acetic acid after distillation, there is no net acetic acid production due to the establishment of equilibrium between ethanol and acetic acid, hence acetic acid concentration in the reactor remains constant and the only reactions occurring are represented by Eqs. (2.1) and (2.2); (ii) concentration of cells remains approximately constant at 3 g/L with 100% cell recycle after separation by microfiltration (MF), therefore it is assumed that carbon consumed for cell production and maintenance is negligible; (iii) conversions of 90% of CO and 60% of H_2 are achieved; (iv) Liquid Retention Time (LRT) ≈ 23 h (volume of liquid in

the reactor divided by liquid volumetric flow rate); and (v) Gas Retention Time (GRT) ≈ 12 min (volume of liquid in the reactor divided by inlet gas volumetric flow rate).

Applying these assumptions, broth concentrations around 23 g/L of ethanol, 6 g/L of acetic acid and 3 g/L of cells should be achieved (Gaddy et al., 2007). The total volume required for fermentation is directly obtained from the choice of GRT and the syngas flow rate, which is a known result from the upstream flowsheet. The assumption of negligible biomass production is supported by the fact that ethanol formation is usually not associated with growth in the Wood/Ljungdahl pathway (Richter et al., 2013). The CO_2 scrubber (block S) is modeled in Aspen as an absorption (RadFrac) column using sufficient water feed to recover roughly 95% of ethanol vapors. The scrubber gas outlet, containing unreacted CO and H_2, is sent to the gas turbine in the Power Generation Unit (A500).

2.2.1.4. Ethanol Distillation Unit (A400)

With approximately 2 wt% of ethanol, the broth obtained from syngas fermentation is highly diluted compared to the broth from sugars fermentation, leading to an even more energy intensive recovery by distillation. Nevertheless, given the state of the art of separation technologies, distillation remains as the best alternative at hand and this evaluation can serve as baseline for future investigations on other separation processes. The Aspen PFD of A400 is shown in Fig. A1-5 (Appendix A1), while Fig. 2.2 illustrates the distillation configuration considered.

In order to reduce energy consumption, heat integration is proposed in a pre-concentration step (Fig. 2.2) where three similar towers, T-1, T-2 and T-3, operating at different pressures are used in an arrangement of multiple-effect distillation (MED) to concentrate ethanol up to about 15 wt%, after which it is sent to a fourth atmospheric column (T-4) where hydrous ethanol at 93 wt% is obtained as distillate.

Heat integration of distillation columns using multiple-effect technique seeks to reduce energy consumption by linking the condenser of a higher pressure column to the reboiler of a lower pressure column (Linnhoff et al., 1983). Many configurations of MED systems have been studied based on different combinations of number of effects, column pressures and feed-splitting, among

other factors (Chiang and Luyben, 1983; Henley and Seader, 1981; Wankat, 1993). As Chiang and Luyben (1983) remarked, such MED systems and other energy-saving configurations were seldom used in the past when energy costs were low, since savings would easily be offset by higher capital costs. However, in the past decades, the increase in energy costs at a much faster rate than equipment costs has drawn attention to energy-saving schemes such as MED, especially for application in large-scale processes. Recently, for example, Dias et al. (2011) and Palacios-Bereche et al. (2015) evaluated the use of double-effect distillation in the production process of 1st -generation ethanol from sugarcane, with one of the columns operating under vacuum. Similarly, Martín and Grossmann (2011), studying routes for the production of lignocellulosic ethanol, proposed a triple-effect distillation arrangement with the first two columns under vacuum.

In the present study, vacuum distillation columns were avoided due to higher costs and more complex control of cascaded vacuum systems, besides the need for larger column diameters. Therefore, the proposed MED scheme uses distillation columns operating at 6 bar, 3 bar and 1 bar, with respective reflux ratios of 0.20, 0.26 and 0.05 in molar basis. The three MED columns have 20 stages each, while T-4 has 45 stages and a reflux ratio of 4.6. In the MED, the split fractions and reflux ratios were adjusted so as to match the condenser duty of T-1 with the reboiler duty of T-2, and the condenser duty of T-2 with the reboiler duty of T-3. In order to spare CW and reduce heat demand in T-4, tower T-3 has a partial condenser with vapor distillate only, while T-1 and T-2 produce saturated liquid distillates. The three distillates are mixed and fed to T-4. Any ethanol dragged with CO_2 in the vapor streams from the partial condensers in T-1, T-2 and T-4 is recovered and recycled after cooling of vapors to 35°C.

Pinch Analysis was done inside Hierarchy block A400 in order to design an effective heat exchanger network (E-1 to E-9 in Fig. A1-5, Appendix A1) capable of recovering heat from hot streams and minimizing utility usage to pre-heat feed streams. Distillation bottoms consist mainly of water with small amounts (<1 wt.%) of acetic acid, which are recycled to the bioreactor. RadFrac model was used for all columns, with VLE modeling via method NRTL-HOC.
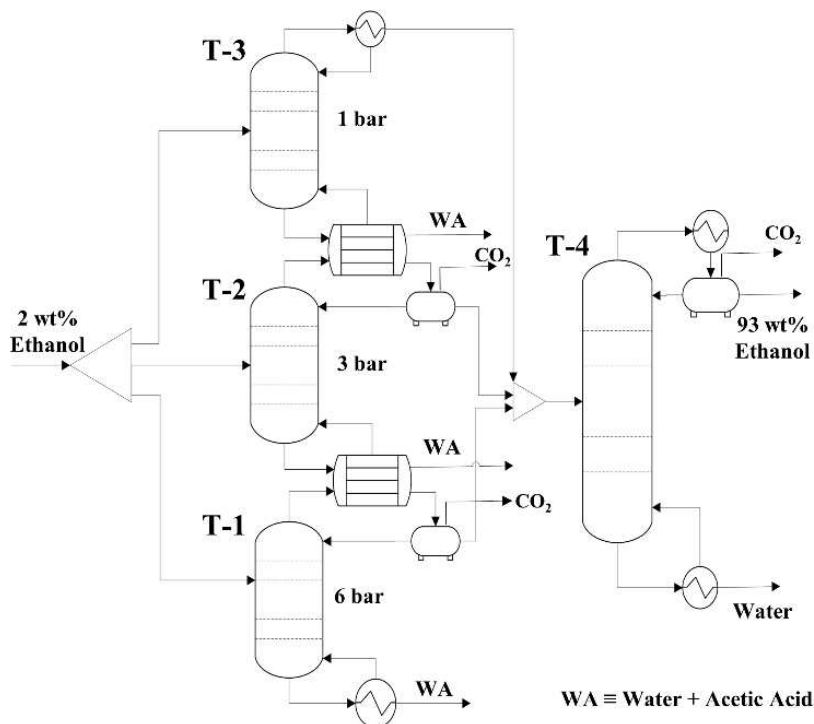
Figure 2.2. Configuration of distillation columns for recovery of E100.

2.2.1.5. Power Generation Unit (A500)

A500 (Fig. A1-6, Appendix A1) was designed as a combined Brayton/Rankine cycle due to the high efficiency associated with this cycle, reaching up to 60% (Bass et al., 2011). The gas turbine fuel is the off-gas from the bioreactor containing unconverted CO and H_2. CO_2 produced in fermentation reactions is also present at high concentration, but its separation would be too costly and therefore it is not considered here. Although the presence of CO_2 in the gas fuel will decrease its heating value, hence the power output, it has been reported that the dilution of syngas with nonflammable gases such as N_2 and CO_2 does not affect significantly the combustion efficiency, the temperature at the nozzle, or the combustion stability (Lee et al., 2012). On the other hand, adding diluents is an effective way of controlling and adjusting NOx emissions, due to the observed logarithmic relation between diluent heat capacity (mass flow rate multiplied by constant pressure heat capacity) and NOx reduction per unit power (Lee et al., 2012). The simulation of the gas turbine was based on the SGT-300 gas turbine by Siemens (Siemens AG, 2009). A pressure ratio of 14 was set in the stage of air compression

(C-2) and a slightly higher ratio, i.e. 14.2, was used in the compression of fuel gas (C-1). The air flow rate was set so that the exhaust gas would achieve a temperature of 545°C at the turbine outlet, implying a temperature at the expander inlet, after combustion, of around 1050°C. This is in agreement with other reports of gas turbine temperature profiles (e.g. Wärtsilä (2016) reports temperatures between 1200°C and 1400°C at the expander inlet). The hot flue gas from the gas turbine is split in two streams: (i) H-GAS-3 is sent to A200 for steam generation; and (ii) FG-E1 is sent to the boiler E-1 in the Rankine Cycle. All machines – compressors, gas turbine, steam turbine and pump – operate with adiabatic efficiency of 85%. The total output power generated in A500 is represented by the dotted line stream EE-T.

2.2.2. Financial Analysis

The simulation results were used to create a financial model capable of predicting the Net Present Value (NPV) according to ethanol selling price. The model was then used to estimate the minimum ethanol selling price (MESP) for the production profile obtained in the designed process, that is, the ethanol selling price for NPV break-even (NPV = 0), assuming an Internal Rate of Return IRR = 10% (Aden et al., 2002).

The platform used for model construction was the MS Excel program CAPCOST, conceived and made available by Turton et al. (2008). CAPCOST estimates capital cost through a module costing technique and uses programmed functions to perform Cash Flow Analysis and Monte Carlo simulations. In this study the investment assumptions are based on the grassroots cost, i.e. the cost of building a completely new plant on a new land. Main assumptions for the financial analysis are summarized in Table 2. The base year is 2015, therefore the prices were adjusted to a CEPCI (Chemical Engineering Plant Cost Index) of 542.8, as published for November 2015 (Chemical Engineering, 2016).

CAPEX, or the total capital investment, is obtained by summing up the grassroots cost, the land cost and the working capital. OPEX includes: (i) direct (variable) production costs (DPC), such as raw materials, labor and maintenance; (ii) fixed production costs (FPC), such as property taxes and insurance; and (iii) general expenses (GE), such as R&D and distribution. The assumptions considered for OPEX calculation were based on the common ranges reported by Peter and Timmerhaus (1991) and are presented in Table A1-1 (Appendix A1).

Table 2.2. Main Assumptions for Financial Evaluation

Project life	20 years
Construction period	2 years
Hours per operating year	8328
Taxation rate	35%
Annual interest rate	10%
Salvage value	0
Depreciation method	Straight line
Cost of land	US$1,250,000
Working capital (Turton et al., 2008)	$0.1(C_{RM} + FCI_L + C_{OL})$
Cost of operating labor	*10% OPEX*

C_{RM}: Cost of raw materials; FCI_L: fixed capital investment excluding land purchase; C_{OL}: cost of operating labor.

2.2.2.1. Purchase Cost of Equipment (PCE) Estimation

CAPCOST has a set of built-in equations to estimate PCE inside given ranges of operation (Turton et al., 2008). When operational capacity is found to be outside the allowed range for equations, one can consider extrapolation by the six-tenths-factor rule in Eq. 3 (Peters and Timmerhaus, 1991). PCE for the following types of equipment were calculated directly on CAPCOST: compressors, steam turbine, electric drives, heat exchangers, blowers, pumps (with drives), distillation and absorption towers, fermenters, and gas turbine. Sizes (or capacities) for the equipment were obtained from results of material and energy balances calculated in Aspen.

To estimate the capital cost of the bioreactors, the vessels were assumed to have 975 m³, with 80% of working capacity and operation under atmospheric pressure at the top of the vessel. The total volume of fermentation, calculated as explained in Sec. 2.1.3, was then used to find the required number of vessels. It is worth mentioning that, although fermentation stirred-tanks in the industry today have between 100 – 500 m³ of capacity, the maximum practical volume is expected to be in the range of 800 – 1500 m³ (Moulijn et al., 2013). According to Humbird and Fei (2016), who simulated the oxygen transfer rate for different liquid volumes, increasing the vessel size up to 1000 m³ would not affect significantly the cost of gas supply, as the power required for a given gas transfer rate would increase approximately linearly with the liquid volume. However, the authors do point out a practical and economic limit of 1000 m³ per vessel.

For equipment costs that were not available in the CAPCOST database, other references were consulted and prices were adjusted to proper year and capacity. For such cases, the sources and results are detailed in Tables A1-4 (gasification unit), A1-5 (microfiltration) and A1-6 (cooling tower) of Appendix A1. Assumptions considered for the water chiller are also listed in Appendix A1 (Table A1-3).

$$\cos t \text{ at capacity } A = \cos t \text{ at capacity } B \times \left(capacity\ A/capacity\ B \right)^{0.6} \quad (2.3)$$

2.2.2.2. Costs of Raw Materials (CRM), Wastewater Treatment (CWT) and Utilities (CUT)

Sugarcane bagasse is the most relevant raw material, accounting for nearly 90% of total CRM. For the base evaluation, it is assumed that its delivered cost is 38 US$ per dry metric ton (Jacques, 2016). Other raw materials costs were retrieved from elsewhere and adjusted to the year 2015 (see Table A1-7, Appendix A1): gasifier bed material (Dutta et al., 2011), tar reformer catalyst (Dutta et al., 2011), CW tower antifouling chemicals (Turton et al., 2008) and process water (Dutta et al., 2011). Wastewater treatment, required for liquid purges, is assumed to cost 0.06 US$/m³ of wastewater based on the cost of tertiary treatment suggested in (Turton et al., 2008) updated to 2015 price. Waste disposal of gasifier ashes is assumed to cost 36 US$ per metric ton (Turton et al., 2008).

The utilities used in the process include: 2.5 bar steam, 10 bar steam, electricity, cooling water (30°C – 40°C) and chilled water (15°C – 25°C). All utilities are produced inside the plant, i.e. CUT = 0, and the consumption rates (including electricity from pumps and compressors, cooling water, and heating) were calculated directly in Aspen simulations, excepting the fermenter stirring, which was assumed to demand 0.45 kW per cubic meter of liquid (Heinzle et al., 2006).

2.2.2.3. Monte Carlo Simulation (MCS)

After building the base financial model, Monte Carlo simulations were performed to account for uncertainties in the economic evaluation. MCS works by repeatedly calculating an objective function after randomly sampling input parameter values out of specified probability distributions. In this study, the Net Present Value (NPV) was selected as the objective function and the uncertain input parameters were chosen to be the fixed capital investment FCIL (excluding land purchase

cost) and the cost of raw materials (CRM). Since the factorial estimate of capital cost used in this study is usually associated with an accuracy of ±30% (Peters and Timmerhaus, 1991), FCIL was put to vary within this range. The cost of raw materials, as defined in Sec. 2.2.2, was chosen to vary within a range of ±70%. MCS was specifically used to find the probability of obtaining non-negative NPV, assuming the aforementioned uncertainties, under different ethanol selling prices.

2.3. Results and Discussion

2.3.1. Simulation

Design choices presented in Sec. 2.2 resulted in a production capacity of 71,000 m^3/year of E100, corresponding to approximately 0.33 m^3 per dry metric ton of feedstock. Table 2.3 presents a comparison with other studies regarding ethanol yield and LHV-based energy efficiency (η_{LHV}) , i.e. the ratio between LHV in ethanol product and LHV in the dry feedstock. Given that the process was designed to achieve energy self-sufficiency, electricity production in the Combined Cycle (A500) was only slightly above the total requirement of the plant, reaching 1,280 kWh/ m^3, or 50 kWh/ m^3 of electricity surplus.

Table 2.3. Comparison of main results with other works

	This study	Dutta et al., 2011	Porzio et al., 2012	Wei et al., 2009	Wei et al., 2009
Route	TB	TC	B (SSCF)	B (HF)	TB
Feedstock	Sugarcane bagasse	Pine chips	Poplar	Hardwood chips	Hardwood chips
Ethanol yield (m^3 per dry metric ton)	0.330	0.318	0.303-0.316	0.205	0.324
η_{LHV} (%)	38	40	35-37	24	37

TB: thermochemical-biochemical; TC: thermochemical-catalytic; B: biochemical; SSCF: simultaneous saccharification co-fermentation; HF: hydrolysis and fermentation.

Carbon conversion from biomass to ethanol was found to be just below 30%, a similar result to the one reported by Humbird et al. (2011) for the conceptual design of biochemical conversion of corn stover to ethanol. Although the feedstocks and other parameters are different, this result is an example refuting the common argument that thermochemical routes are inherently more carbon efficient due to full utilization of biomass components in the gasifier. Although

carbon from biomass can be fully consumed in gasification, it is not necessarily all converted to syngas, as part of it might be sacrificed for energy generation in combustion reactions. While high carbon to syngas conversions of 95 – 99% can be achieved in directly-heated (partial-oxidation) fluidized gasifiers, indirectly-heated systems like the one considered here usually achieve lower conversions of 60 – 75%, in return of producing better quality syngas (Brown, 2011). Indeed, in the present study, only about 60% of carbon conversion to syngas was achieved, with the remaining carbon leaving as CO_2. Nonetheless, there is indisputable advantage in indirect heating systems in comparison with direct systems that would require air or pure oxygen. If air is used, then the syngas will be highly diluted with N_2, causing the fugacities of CO and H_2 in the gas phase to be lower and therefore seriously hindering the fermentation step due to the reduction of the mass transfer rates of these compounds. On the other hand, using O_2 would require the insertion of an Air Separation Unit (ASU), which is an expensive process in terms of energy and cost, both capital and operating types (Bhattacharya et al., 2012).

Table 2.4 shows the syngas composition at the fermenter inlet, as well as the broth and the gas composition at the outlet. As explained in Sec. 2.1.1, a generic model of gasifier using the equilibrium approach under equilibrium-favoring conditions was preferred instead of adopting the results of a specific gasification plant. Nevertheless, the results herein presented are comparable to empirical results of steam gasification obtained elsewhere under similar temperature conditions: for example, Nipattummakul et al. (2011) reported the following syngas approximate (molar) composition for steam gasification of oil palm empty fruit branches between 900°C and 1000°C: 50% H_2, 25-30% CO, 14-19% CO_2. Moreover, the results are similar to those presented by NREL (Dutta et al., 2011) via simulation: 40.3% H_2, 9.4% CO_2, 32.3% CO, 16.2% H_2O, 1.5% CH_4.

The syngas composition calculated in the present study also contains small amounts of contaminants: 2 ppm NH_3, 196 ppm H_2S, 91 ppm HCl, 5 ppm COS. However, the model does not take into account the influence of these compounds on process variables such as pH and osmolarity or on the metabolism of the microorganisms. It is assumed that such levels of impurities are not enough to affect fermentation performance, damage the equipment or significantly alter the process in general. Although there is still a need for further research regarding tolerance limits to contaminants, there is evidence that syngas impurities such as

HCN could achieve levels at which the process is potentially burdened (Lane, 2014). Other contaminants, such as H_2S and COS, were found insignificant unless at much higher concentrations (Vega et al., 1990).

Syngas fermentation does not require a specific H_2/CO ratio or the absence of CO_2 (Spath and Dayton, 2003), therefore the gas is assumed to be fed to the fermenter without any prior step of water-gas shift or CO_2 abatement for adjustment of composition. Yet, it is clear from Eqs. (2.1)-(2.2) that the gas composition is an important project parameter as it affects the availability of carbon (provided by CO or CO_2) and electrons (provided by H_2 or CO) for the microbial metabolism. For example, in the absence of H_2, the theoretical (i.e. maximum) carbon yield to ethanol (Y_{th}) will be 1/3, with the remaining carbon being oxidized to CO_2, according to Eq. (2.4) (Phillips et al., 1994). In the presence of H_2 and with H_2:CO ≤ 2, Yth is predicted from Eq. (2.5), which is easily deduced from Eqs. (2.1)-(2.2). Furthermore, the presence of CO_2 in the substrate has been reported to increase product formation, although CO is consumed preferably (Heiskanen et al., 2007). In this case, it can be shown from Eqs. (2.1)-(2.2) that Y_{th} is calculated from Eq. (2.6). In all cases, it is evident from the equations that higher yields are obtainable when H_2 is provided with the gas. For the present design, the syngas composition presented in Table 2.4 would lead to a theoretical carbon yield of 0.68, while the actual carbon yield was obtained as 0.48. For comparison, other authors have reported carbon yields for different syngas molar compositions, such as: 0.24 for substrate containing 20% CO, 5% H_2, 15% CO_2 and 60% N_2 (Shen et al., 2014a); 0.28 for substrate containing 60% CO, 35% H_2 and 5% CO_2 (Richter et al., 2013).

$$CO + H_2O \xrightarrow{CODH} CO_2 + 2H^+ + 2e^- \qquad (2.4)$$
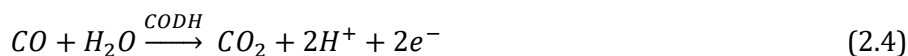
Where CODH ≡ carbon monoxide dehydrogenase.

$$Y_{th} = \frac{1}{3}\left(1 + \frac{x_{H_2}}{x_{CO}}\right) \quad [mol\ C\ /\ mol\ C] \qquad (2.5)$$

$$Y_{th} = \frac{x_{CO} + x_{H_2}}{3(x_{CO} + x_{CO_2})} \quad [mol\ C\ /\ mol\ C] \qquad (2.6)$$

With concern to broth composition, simulation results are consistent with the experimental values reported in the reference used here as base for modeling, i.e.

23 g/L ethanol, 6 g/L acetate, 3 g/L cells (Gaddy et al., 2007), which is a good indication that the present model has performed well. The total volume required for fermentation would imply the use of nine fermentation vessels of 975 m^3 for the assumptions considered in this study.

Table 2.4. Composition of Syngas Substrate, Fermenter Off-Gas and Broth Outlet (wet basis)

	Syngas (mol %)	Off-gas (mol %)		Broth (wt%)
CO	26.3	6.4	C_2H_5OH	2.0
H_2	48.5	46.9	H_3CCOOH	0.5
CO_2	10.4	39.5	cells	0.3
H_2O	14.6	6.3	H_2O	97.2

Regarding water consumption, the process would require a freshwater usage of 11.6 m^3/m^3 E100, of which 82% are due to blowdown, windage and evaporative losses in the CW tower. An estimated range of 1.9 – 6 m^3/m^3 has been reported for lignocellulosic ethanol production (Aden, 2007). Since the present design considers water to be the main carrier of cooling, a first attempt on process improvement would be to include air-cooled heat exchangers whenever possible, for example in the condenser of the distillation tower. This could significantly reduce freshwater consumption, as shown by Martín et al. (2011). One should keep in mind, however, that air-cooling efficiency would be fairly compromised in tropical climate regions such as Brazil.

Energy requirements in the distillation unit (A400) were found to be 8,700 MJ/m^3 with the use of multiple-effect distillation as pre-concentration step. This is lower than the estimated 10,500 MJ/m^3 by Piccolo and Bezzo (2007) for a 2.4 wt% broth obtained via the thermochemical-biochemical route, and higher than the range of 4,400 – 6,400 MJ/m^3 estimated in the same reference for three types of fully-biochemical routes, where the ethanol concentration in the broth is also higher, expected to be around 5 wt% (Hamelinck et al., 2005).

The requirements for the distillation towers, i.e. heating (Qr) and cooling (Qc), are depicted in Fig. 2.3, as a temperature-enthalpy flow diagram. The shaded areas indicate the distillation towers, of which T-1, T-2 and T-3 are heat integrated in the multiple-effect stack, and T-4 delivers the hydrous ethanol product. Fig. 2.3 evidences the reduction of external heat requirements accomplished with the

MED system, which is effectively close to 1/3 of the total reboiler duty of the three pre-concentration columns. Vertical dotted lines indicate clearly the perfect matching of the reboiler with condenser duties between T-1 (6 bar) and T-2 (3 bar), and between T-2 and T-3 (1 bar). Fig. 2.3 also suggests the possibility of improving heat integration in the pre-concentration step by including in the MED stack a fourth column that could be positioned between T-2 and T-3, reducing the pre-concentration heat load by roughly 25%. It is also observable that T-4 has a low energy requirement, which is to some extent due to the fact that one of the feed streams, the distillate from T-3, is provided in the vapor phase. On the other hand, T-4 has a high requirement of CW due to the same reason.
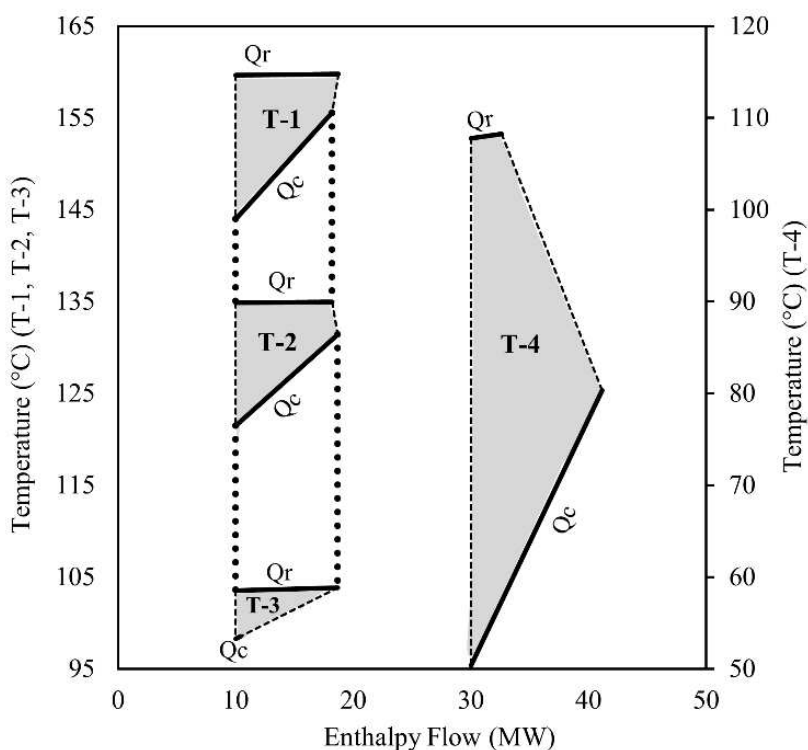
Figure 2.3. Temperature enthalpy diagram for the distillation columns. The x-axis represents enthalpy flow changes.

2.3.2. Financial Analysis

Table 2.5 summarizes the main economic results of the base model. CAPEX or the total capital investment, is consistent with other estimates for 2nd generation plants when considering the annual capacity, as presented in Fig. 2.4. An equivalent annual cost associated with CAPEX is also presented in Table 2.5. The OPEX is an important fraction of the MESP, as it makes up about 59% of costs and accounts to roughly twice the costs related to CAPEX (i.e. the return on investment (ROI) and depreciation). The minimum net profit represents the ROI associated with the MESP.

TB: thermochemical-biochemical; B: biochemical; HW-PT: hot water pretreatment; DA-PT: dilute acid pretreatment; TC: thermochemical-catalytic
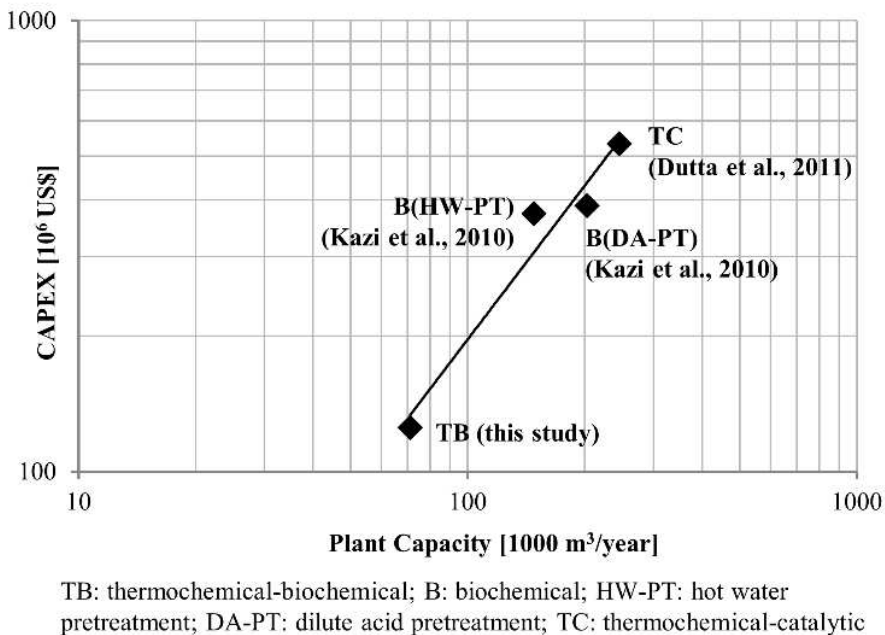
Figure 2.4. Comparison of CAPEX estimate with other studies. CAPEX results from other works were adjusted to 2015 prices.

The overall contributions to MESP are depicted in Fig. 2.5 and a comparison with other works is presented in Fig. 2.6. Sugarcane bagasse is responsible for about 16% of the MESP, which is relatively low when compared to the feedstock contributions presented in Fig. 2.6 for other studies. However, it is worth noting that these results consider other feedstocks, namely woody biomass and corn stover. Another report for 2nd-generation biochemical plants using sugarcane residues has shown that, similar to the present study, feedstock costs are

estimated to make up about 20% of costs (Jacques, 2016). Cheali et al. (2016) have shown that biomass conversion to ethanol through thermochemical-catalytic routes can indeed be advantageous over biochemical conversion depending on the characteristics of the feedstock (lignin and overall carbon content), despite the usually higher investments. For the assessment of four different scenarios varying the types of feedstock (poplar wood or corn stover) and conversion pathways (biochemical or thermochemical-catalytic), they found that feedstock costs contributed from 59 to 62.4%, with MESP ranging from $500/m^3 to $560/m^3, which is considerably lower than the result presented here. In a study on thermochemical-biochemical routes for bioethanol production from miscanthus, Roy et al. (2015) predicted ethanol production costs ranging from $780/m^3 to $900/m^3, however the results presented are not sufficient for further comparisons. An attractive picture was estimated by Martín and Grossmann (2011), with production costs ranging between $0.84/gal ($222/m^3) and $1.07/gal ($283/m^3), however, besides significant differences in their process flowsheet, their model makes several optimistic assumptions, particularly affecting separation costs, such as broth composition of 5 wt% of ethanol (or even 15 wt% in some scenarios), constant ethanol-water relative volatility of 2.2 and Fenske equation design in the distillation columns.

Table 2.5. Main Economic Results (2016)

Grassroots cost	US$111.5 million
Plant *CAPEX*	US$125.15 million (US$14.7 million per year)
Plant *OPEX* [2]	US$29.6 million per year (417 US$/m^3)
Minimum net profit	US$9.7 million per year (136 US$/m^3)
Minimum ethanol selling price	706 US$/m^3

[1] Includes: costs of raw materials and waste treatment; labor costs; maintenance and repair; operating supplies; laboratory charges; patents and royalties; property taxes and insurance; plant overheads; administration; distribution and selling; and R&D.

The current market price of E100, around $450/m^3 (UNICA, 2016), is considerably lower than the predicted MESP in Table 2.5. Nevertheless, the results are comparable to predictions for other lignocellulosic ethanol processes, such as the ones presented in Fig. 2.6, and to the MESP estimated for existing biochemical-based plants: $2.2/gal $580/ m^3) for Raizen, $3.3/gal ($870/ m^3) for DuPont and $4.6/gal ($1220/ m^3) for Abengoa (Jacques, 2016). Since those studies consider anhydrous ethanol, the results are expected to be slightly lower in the present

study, which considers hydrous ethanol (dehydration by molecular sieves should contribute to operating costs with roughly $0.05/kg (Cardona et al., 2010)).

MESP: 710 US$/m³
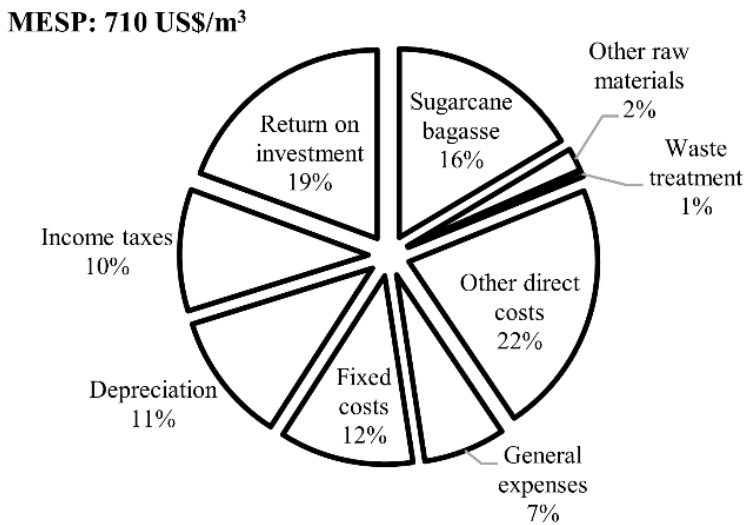
Figure 2.5. Composition of MESP.

Fig. 2.7 depicts the NPV cumulative probability curves obtained from MCS. The curves – from left to right – are relative to the values of the ethanol selling price for which the probability of achieving non-negative NPV is 20%, 40%, 60%, 80% and 100%. Non-negative NPV means the project has greater chances of being profitable than non-profitable. One could affirm, then, that the current process design would very likely attain profit for E100 selling prices above US$780/ m³, even if the grassroots cost were found to be 30% higher than the base case and the raw materials were 70% more costly. At the other extreme, selling prices below US$680/ m³ are less likely to provide positive results, but would still be feasible if optimistic conditions were to be achieved, with low values of feedstock price and capital investment.
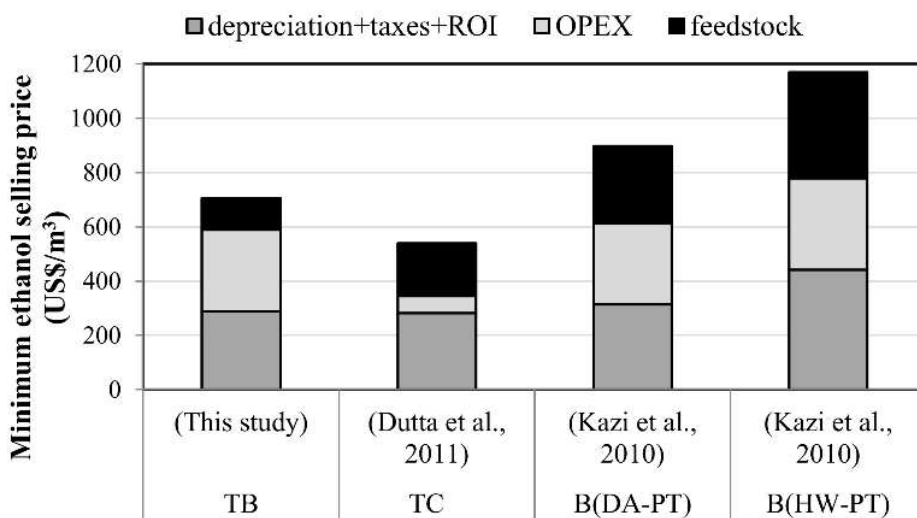
TB: thermochemical-biochemical; TC: thermochemical-catalytic; B: biochemical; DA-PT: dilute acid pre-treatment; HW-PT: hot water pre-treatment.

Figure 2.6. Comparison of MESP composition with other studies. Feedstock cost is presented separately from other OPEX costs.
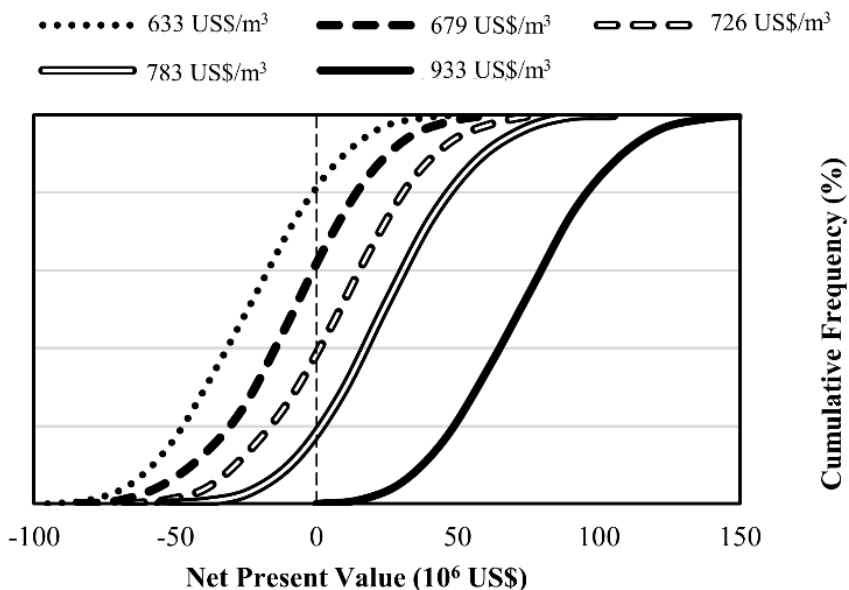
Figure 2.7. NPV cumulative frequency distribution according to ethanol selling price. Curves show the probabilities of achieving non-negative NPV: 20% (dotted line); 40% (filled dashed line); 60% (unfilled dashed line); 80% (unfilled solid line); 100% (filled solid line).

2.4. Conclusions

This study presented a conceptual process design for the production of hydrous ethanol from sugarcane bagasse employing the so-called hybrid route based on gasification and syngas fermentation technology. The model is comprised of five distinct units that are integrated in a self-sufficient process in terms of energy (heat and power) and environment. Several steps of the process model are simplified due to a lack of reliable empirical data, for example, the model does not describe the effects of syngas contaminants on fermentation performance. In the same context, it is noteworthy that results of conversion, titer and yields in fermentation could vary significantly as observed with the high level of discrepancy among results reported in the literature. Hence, financial results could be substantially different if fermentation conditions diverged from the considerations made in this study. Nevertheless, the presented model has demonstrated to be a useful resource for the evaluation of technological potential of this route in comparison with other second generation technologies.

Simulation results indicate the potential to achieve energy self-sufficiency with an ethanol yield of 0.33 m^3 per metric ton of dry sugarcane bagasse, considering a production plant with annual capacity of 71,000 m^3. The financial analysis predicted the base case MESP to be 706 US\$/m^3. When considering uncertainties in the fixed capital investment and in the total cost of raw materials, the MESP ranges from 633 US\$/m^3 to 933 US\$/m^3, from low (20%) to high (100%) probability of achieving non-negative NPV. Even though the predicted ethanol selling prices are higher than the current market price of hydrous ethanol, the results demonstrate comparative potential for competitiveness in relation to other lignocellulosic ethanol technologies. Nonetheless, additional research is needed at different stages of the process to better understand and improve the technology, especially with regard to optimal conditions and reactor design for syngas fermentation, syngas cleaning requirements and efficient energy integration.

References

Aden, A., Ruth, M., Ibsen, K., Jechura, J., Neeves, K., Sheehan, J., Wallace, B., Montague, L., Slayton, A., Lukas, J., 2002. Lignocellulosic Biomass to Ethanol Process Design and Economics Utilizing Co-Current Dilute Acid Prehydrolysis and Enzymatic Hydrolysis for Corn Stover, Report NREL/TP-510-32438. National Renewable Energy Laboratory (NREL). Golden, Colorado.

Aden, A., 2007. Water usage for current and future ethanol production. Southwest Hydrol. 6, 22 – 23.

Aspen Technology, 2011. Aspen Plus - Getting Started Modeling Processes with Solids.

Baratieri, M., Baggio, P., Fiori, L., Grigiante, M., 2008. Biomass as an energy source: Thermodynamic constraints on the performance of the conversion process. Bioresour. Technol. 99, 7063–7073. doi:10.1016/j.biortech.2008.01.006

Bass, R.J., Malalasekera, W., Willmot, P., Versteeg, H.K., 2011. The impact of variable demand upon the performance of a combined cycle gas turbine (CCGT) power plant. Energy 36, 1956–1965. doi:10.1016/j.energy.2010.09.020

Bhattacharya, A., Bhattacharya, A., Datta, A., 2012. Modeling of hydrogen production process from biomass using oxygen blown gasification. Int. J. Hydrogen Energy 37, 18782–18790. doi:10.1016/j.ijhydene.2012.09.131

Bonomi, A., Pinto, A., Charles, M., Farias De Jesus, D., Coutinho, H., Franco, J., Cunha, M.P., Oliveira De, M., Dias, S., Ferreira, M., Otávio, C., Paulo, C., Mantelatto, E., Maciel, R., Tassia, F., Junqueira, L., 2011. Technological Assessment Program (PAT) - The Virtual Sugarcane Biorefinery (VSB). Report. Brazilian Bioethanol Science and Technology Laboratory (CTBE), Brazilian Center for Research in Energy and Materials (CNPEM), São Paulo, Brazil.

Brown, R.C., 2011. Thermochemical Processing of Biomass: Conversion into Fuels, Chemicals and Power, Thermochemical Processing of Biomass: Conversion into Fuels, Chemicals and Power. doi:10.1002/9781119990840

Cardona, C.A., Sanchez, O.J., Gutierrez, L.F., 2010. Process synthesis for fuel ethanol production. CRC Press, Florida, USA.

Cheali, P., Posada, J.A., Gernaey, K.V., Sin, G., 2015. Upgrading of lignocellulosic biorefinery to value-added chemicals: Sustainability and economics of bioethanol-derivatives. Biomass and Bioenergy 75, 282–300. doi:10.1016/j.biombioe.2015.02.030

Cheali, P., Posada, J.A., Gernaey, K.V., Sin, G., 2016. Economic risk analysis and critical comparison of optimal biorefinery concepts. Biofuels, Bioprod. Bioref. 10, 435–445. doi:10.1002/bbb.1654

Chemical Engineering Magazine, 2016. Issue of March 2016.

Chiang, T.-P., Luyben, W.L., 1983. Comparison of Energy Consumption in Five Heat-Integrated Distillation Configurations. Ind. Eng. Chem. Process Des. Dev. 22, 175–179.

Choi, D.W., Chipman, D.C., Bents, S.C., Brown, R.C., 2010. A techno-economic analysis of polyhydroxyalkanoate and hydrogen production from syngas fermentation of gasified biomass. Appl. Biochem. Biotechnol. 160, 1032–1046. doi:10.1007/s12010-009-8560-9

Dias, M.O.S., Modesto, M., Ensinas, A. V., Nebra, S.A., Filho, R.M., Rossell, C.E. V, 2011. Improving bioethanol production from sugarcane: Evaluation of distillation, thermal integration and cogeneration systems. Energy 36, 3691–3703. doi:10.1016/j.energy.2010.09.024

Dutta, A., Talmadge, M., Hensley, J., Worley, M., Dudgeon, D., Barton, D., Groenendijk, P., Ferrari, D., Stears, B., Searcy, E.M., Wright, C.T., Hess, J.R., 2011. Process design and economics for conversion of lignocellulosic biomass to ethanol. Report NREL/TP-5100-51400. National Renewable Energy Laboratory (NREL), Golden, Colorado.

Esmaili, E., Mostafavi, E., Mahinpey, N., 2016. Economic assessment of integrated coal gasification combined cycle with sorbent CO_2 capture. Appl. Energy 169, 341–352. doi:10.1016/j.apenergy.2016.02.035

Fernández-Dacosta, C., Posada, J.A., Kleerebezem, R., Cuellar, M.C., Ramirez, A., 2015. Microbial community-based polyhydroxyalkanoates (PHAs) production from wastewater: Techno-economic analysis and ex-ante environmental assessment. Bioresour. Technol. 185, 368–377. doi:10.1016/j.biortech.2015.03.025

Gaddy, J.L., Arora, D.K., Ko, C.-W., Phillips, J.R., Basu, R., Wikstrom, C. V., Clausen, E.C., 2007. Methods for increasing the production of ethanol from microbial fermentation. US 7,285,402 B2.

Hamelinck, C.N., Van Hooijdonk, G., Faaij, A.P.C., 2005. Ethanol from lignocellulosic biomass: Techno-economic performance in short-, middle- and long-term. Biomass and Bioenergy 28, 384–410. doi:10.1016/j.biombioe.2004.09.002

Heiskanen, H., Virkajärvi, I., Viikari, L., 2007. The effect of syngas composition on the growth and product formation of Butyribacterium methylotrophicum. Enzyme Microb. Technol. 41, 362–367. doi:10.1016/j.enzmictec.2007.03.004

Heinzle, E., Biwer, A.P., Cooney, C.L., 2006. Development of Sustainable Bioprocesses. John Wiley & Sons, Ltd, Chichester, UK. doi:10.1002/9780470058916

Henley, E.J., Seader, J.D., 1981. Equilibrium-stage separation operations in chemical engineering. Johh Wiley & Sons, Inc., New York.

Humbird, D., Davis, R., Tao, L., Kinchin, C., Hsu, D., Aden, A., Schoen, P., Lukas, J., Olthof, B., Worley, M., Sexton, D., Dudgeon, D., 2011. Process Design and Economics for Biochemical Conversion of Lignocellulosic Biomass to Ethanol – Dilute-acid pretreatment and enzymatic hydrolysis of corn stover. Report NREL/TP-5100-47764. National Renewable Energy Laboratory (NREL), Golden, Colorado.

Humbird, D., Fei, Q., 2016. Scale-Up Considerations for Biofuels, in: Biotechnology for Biofuel Production and Optimization. pp. 513–537. doi:10.1016/B978-0-444-63475-7.00020-0

Jacques, C., 2016. News and events – Raizen has lowest price as cellulosic ethanol hinges on feedstock cost. http://www.luxresearchinc.com/news-and-events/press-releases/read/raizen-has-lowest-price-cellulosic-ethanol-hinges-feedstock-cost (acessed 08.03.2016).

Kazi, F.K., Fortman, J., Anex, R., Kothandaraman, G., Hsu, D., Aden, A., Dutta, A., 2010. Techno-economic analysis of biochemical scenarios for production of cellulosic ethanol. Report NREL/TP-6A2-46588. National Renewable Energy Laboratory (NREL), Golden, Colorado.

Klasson, K.T., Ackerson, M.D., Clausen, E.C., Gaddy, J.L., 1991. Bioreactor design for synthesis fermentations. Fuel 70, 605–614.

Klasson, K.T., Ackerson, C.M.D., Clausen, E.C., Gaddy, J.L., 1992. Biological conversion of synthesis gas into fuels. Int. J. Hydrogen Energy 17, 281–288. doi:10.1016/0360-3199(92)90003-F

Lane, J., 2015. Steel's Big Dog jumps into low carbon fuels: ArcelorMittal, LanzaTech, Primetals Technologies to construct $96M biofuel production facility. Biofuels Dig. http://www.biofuelsdigest.com/bdigest/2015/07/13/steels-big-dog-jumps-into-low-carbon-fuels-arcelormittal-lanzatech-primetals-technologies-to-construct-96m-biofuel-production-facility/ (accessed 08.03.2016)

Lane, J., 2014. On the Mend: Why INEOS Bio isn't producing ethanol in Florida. Biofuels Dig. http://www.biofuelsdigest.com/bdigest/2014/09/05/on-the-mend-why-ineos-bio-isnt-reporting-much-ethanol-production/ (accessed 08.03.2016)

Lee, M.C., Seo, S. Bin, Yoon, J., Kim, M., Yoon, Y., 2012. Experimental study on the effect of N2, CO2, and steam dilution on the combustion performance of H2 and CO synthetic gas in an industrial gas turbine. Fuel 102, 431–438. doi:10.1016/j.fuel.2012.05.028

Linnhoff, B., Dunford, H., Smith, R., 1983. Heat integration of distillation columns into overall processes. Chem. Eng. Sci. 38, 1175–1188.

Martín, M., Ahmetovic, E., Grossmann, I.E., 2011. Optimization of water consumption in second generation bioethanol plants. Ind. Eng. Chem. Res. 50, 3705–3721. doi:10.1021/ie101175p

Martín, M., Grossmann, I.E., 2011. Energy Optimization of Bioethanol Production via Gasification of Switchgrass. AIChE J. 57, 3408–3428. doi:10.1002/aic.12544

Moulijn, J.A., Makkee, M., Diepen, A.E. van, 2013. Chemical Process Technology. Wiley, Chichester, UK.

Nipattummakul, N., Ahmed, I.I., Gupta, A.K., Kerdsuwan, S., 2011. Hydrogen and syngas yield from residual branches of oil palm tree using steam gasification. Int. J. Hydrogen Energy 36, 3835–3843. doi:10.1016/j.ijhydene.2010.04.102

Palacios-Bereche, R., Ensinas, A. V., Modesto, M., Nebra, S.A., 2015. Double-effect distillation and thermal integration applied to the ethanol production process. Energy 82, 512–523. doi:10.1016/j.energy.2015.01.062

Parikh, J., Channiwala, S.A., Ghosal, G.K., 2005. A correlation for calculating HHV from proximate analysis of solid fuels. Fuel 84, 487–494. doi:10.1016/j.fuel.2004.10.010

Peters, M.S., Timmerhaus, K.D., 1991. Plant design and economics for chemical engineers. McGraw-Hill, New York.

Phillips, J.R., Clausen, E.C., Gaddy, J.L., 1994. Synthesis gas as substrate for the biological production of fuels and chemicals. Appl. Biochem. Biotechnol. 45–46, 145–157. doi:10.1007/BF02941794

Piccolo, C., Bezzo, F., 2007. Ethanol from lignocellulosic biomass: A comparison between conversion technologies. Comput. Aided Chem. Eng. 24, 1277–1282. doi:10.1016/S1570-7946(07)80237-9

Piccolo, C., Bezzo, F., 2009. A techno-economic comparison between two technologies for bioethanol production from lignocellulose. Biomass and Bioenergy 33, 478–491. doi:10.1016/j.biombioe.2008.08.008

Porzio, G.F., Prussi, M., Chiaramonti, D., Pari, L., 2012. Modelling lignocellulosic bioethanol from poplar: estimation of the level of process integration, yield and potential for co-products. J. Clean. Prod. 34, 66–75. doi:10.1016/j.jclepro.2012.01.028

Puig-Arnavat, M., Bruno, J.C., Coronas, A., 2010. Review and analysis of biomass gasification models. Renew. Sustain. Energy Rev. 14, 2841–2851. doi:10.1016/j.rser.2010.07.030

Rajagopalan, S., P. Datar, R., Lewis, R.S., 2002. Formation of ethanol from carbon monoxide via a new microbial catalyst. Biomass and Bioenergy 23, 487–493. doi:10.1016/S0961-9534(02)00071-5

Ramzan, N., Ashraf, A., Naveed, S., Malik, A., 2011. Simulation of hybrid biomass gasification using Aspen plus: A comparative performance analysis for food, municipal solid and poultry waste. Biomass and Bioenergy 35, 3962–3969. doi:10.1016/j.biombioe.2011.06.005

Richter, H., Martin, M.E., Angenent, L.T., 2013. A two-stage continuous fermentation system for conversion of syngas into ethanol. Energies 6, 3987–4000. doi:10.3390/en6083987

Roy, P., Dutta, A., Deen, B., 2015. Greenhouse gas emissions and production cost of ethanol produced from biosyngas fermentation process. Bioresour. Technol. 192, 185–191. doi:10.1016/j.biortech.2015.05.056

Shen, Y., Brown, R., Wen, Z., 2014a. Syngas fermentation of Clostridium carboxidivoran P7 in a hollow fiber membrane biofilm reactor: Evaluating the mass transfer coefficient and ethanol production performance. Biochem. Eng. J. 85, 21–29. doi:10.1016/j.bej.2014.01.010

Shen, Y., Brown, R., Wen, Z., 2014b. Enhancing mass transfer and ethanol production in syngas fermentation of Clostridium carboxidivorans P7 through a monolithic biofilm reactor. Appl. Energy 136, 68–76. doi:10.1016/j.apenergy.2014.08.117

Shen, Y., Jarboe, L., Brown, R., Wen, Z., 2015. A thermochemical-biochemical hybrid processing of lignocellulosic biomass for producing fuels and chemicals. Biotechnol. Adv. 33, 1799–1813. doi:10.1016/j.biotechadv.2015.10.006

Siemens AG, 2009. SGT-300 Industrial Gas Turbine. Brochure. Siemens Energy, Inc. http://www.energy.siemens.com/hq/pool/hq/power-generation/gas-turbines/SGT-

300/Brochure%20Gas%20Turbine%20SGT-300%20for%20Power%20Generation.pdf (acessed 11.26.2016)

Silva, V.B., Rouboa, A., 2014. Predicting the syngas hydrogen composition by using a dual stage equilibrium model. Int. J. Hydrogen Energy 39, 331–338. doi:10.1016/j.ijhydene.2013.10.053

Souza, G.M., Victoria, R.L., Joly, C.A., Verdade, L.M., 2015. Bioenergy and sustainability: Bridging the gaps, SCOPE briefing. doi:10.1017/CBO9781107415324.004

Spath, P.L., Dayton, D.C., 2003. Preliminary Screening -- Technical and Economic Assessment of Synthesis Gas to Fuels and Chemicals with Emphasis on the Potential for Biomass-Derived Syngas, NREL Technical Report NREL/TP-510-34929. National Renewable Energy Laboratory (NREL), Golden, Colorado.

Turton, R., Bailie, R.C., Whiting, W.B., Shaeiwitz, J.A., 2008. Analysis, Synthesis and Design of Chemical Processes, Prentice Hall International Series in the Physical and Chemical Engineering Sciences. Pearson Education, Michigan, USA.

UNICA - Sugarcane Industry Association. Report. http://www.unicadata.com.br (accessed 06.13.2016).

Van der Heijden, H., Ptasinski, K.J., 2012. Exergy analysis of thermochemical ethanol production via biomass gasification and catalytic synthesis. Energy 46, 200–210. doi:10.1016/j.energy.2012.08.036

Vega, J.L., Klasson, K.T., Kimmel, D.E., Clausen, E.C., Gaddy, J.L., 1990. Sulphur gas Tolerance and Toxicity of CO-Utilizing Bacteria. Appl. Biochem. Biotechnol. 24/25, 329–340.

Vega, J.L., Prieto, S., Elmore, B.B., Clausen, E.C., Gaddy, J.L., 1989. The Biological production of ethanol from synthesis gas. Appl. Biochem. Biotechnol. 20-21, 781–797. doi:10.1007/BF02936525

Wagner, H., Kaltschmitt, M., 2012. Biochemical and thermochemical conversion of wood to ethanol—simulation and analysis of different processes. Biomass Convers. Biorefinery 3, 87–102. doi:10.1007/s13399-012-0064-0

Wankat, P.C., 1993. Multieffect distillation processes. Ind. Eng. Chem. Res. 32, 894–905. doi:10.1021/ie00017a017

Wärtsilä, 2016. Gas turbine for power generation: Introduction. http://www.wartsila.com/energy/learning-center/technical-comparisons/gas-turbine-for-power-generation-introduction (accessed 12.01.2016).

Wei, L., Pordesimo, L.O., Igathinathane, C., Batchelor, W.D., 2009. Process engineering evaluation of ethanol production from wood through bioprocessing and chemical catalysis. Biomass and Bioenergy 33, 255–266. doi:10.1016/j.biombioe.2008.05.017

Worley, M., Yale, J., 2012. Biomass Gasification Technology Assessment. Consolidated Report NREL/SR-5100-57085. National Renewable Energy Laboratory (NREL), Golden, Colorado.

Younesi, H., Najafpour, G., & Mohamed, A. R. (2005). Ethanol and acetate production from synthesis gas via fermentation processes using anaerobic bacterium, Clostridium ljungdahlii. Biochemical Engineering Journal, 27(2), 110–119. https://doi.org/10.1016/j.bej.2005.08.01

Chapter 3

Dynamic modeling of syngas fermentation in a continuous stirred-tank reactor: multi-response parameter estimation and process optimization

"The point of making models is to be able to bring a measure of order to our experience and observations, as well as to make specific predictions about certain aspects of the world we experience."

John Casti, Reality Rules

3.1. Introduction

Gas fermentation is a promising biotechnological process that has gained attention due to its potential as a versatile waste-to-fuels route. It employs anaerobic bacteria called acetogens, that are capable of autotrophically metabolizing CO, H_2 and CO_2 into cell mass, acids (e.g. acetate) and solvents (e.g. ethanol and butanediol). The microbial substrate is therefore a gas with various possible origins; it may be, for example: (i) syngas produced via gasification of a wide range of feedstocks, including municipal solid waste and lignocellulosic biomass; (ii) off-gases from steel production and cement industries; (iii) CO_2 captured from power plants blended with H_2 from renewable electricity, generated via electrolysis, and (iv) reformed biogas (Liew et al., 2016). There has been a great expansion of gas fermentation technology over the last years: at least three commercial-scale ethanol plants are currently under construction (LanzaTech, 2018) or have started operation (China News Service, 2018), and many pilot plants have already operated for long periods of time (Liew et al., 2016). Different studies indicate that the process can play an important role in the development of a sustainable bio-economy, being comparable to other lignocellulosic processes in terms of cost, energy efficiency and environmental impact, while also permitting feedstock flexibility (de Medeiros, Posada, Noorman, Osseweijer, & Filho, 2017; Liew et al., 2016; Pardo-Planas, Atiyeh, Phillips, Aichele, & Mohammad, 2017; Roy, Dutta, & Deen, 2015). From the point of view of process systems engineering, however, there is still vast room for improvement, from strain enhancement and efficient product separation, to the integrated optimization of process parameters. With that in mind, in this article we address specifically the syngas fermentation bioreactor, coveting the presentation and analysis of a model that can be useful in optimization frameworks.

Models to describe syngas fermentation are still scarce in the literature, and only a few authors have attempted to adjust kinetic expressions to experimental data. Younesi, Najafpour, and Mohamed (2005) and Mohammadi, Mohamed, Najafpour, Younesi, and Uzir (2014) adjusted logistic curves to the growth of *Clostridium ljungdahlii* on artificial syngas using experimental data from batch fermentation essays in serum bottles. Mohammadi et al. (2014) were also able to fit Gompertz equations to their experimental profiles of product formation, and uptake rate equations for CO, presenting estimations of kinetic parameters that were later

adopted by Chen, Gomez, Höffner, Barton, and Henson (2015) in their dynamic Flux Balance Analysis (dFBA) model of a syngas fermentation bubble column. The latter was the first application of FBA in a dynamic model for syngas fermentation and the first spatiotemporal model of this process, but it was not compared with experimental data. The same group also published an improved version of their model, applied for CO fermentation with *Clostridium autoethanogenum* and considering uptake parameters obtained and protected by Lanzatech (Chen, Daniell, Griffin, Li, & Henson, 2018). Furthermore, Jang, Yasin, Park, Lovitt, and Chang (2017) simulated CO fermentation in a batch culture of *Eubacterium limosum* KIST612 using a dynamic model with kinetic parameters previously estimated by Chang, Kim, Lovitt, and Bang (2001), but this process results in the formation of acetic acid as only product, which has lower a value than ethanol.

In the present study, a dynamic model was constructed for syngas fermentation with ethanol production in a continuous stirred tank reactor (CSTR). The unknown model parameters were estimated with a multi-response minimization framework using experimental culture data from the literature and the significance of parameters was assessed with statistical analysis and generation of confidence intervals. The model was then used to study the effects of different process conditions (i.e. gas composition, dilution rate, gas residence time and cell recycle), as well as the sensitivity of the kinetic parameters, and a multi-objective optimization was conducted for maximization of productivity and conversion. Although similar studies exist for other process, such as ABE fermentation (see for example Buehler and Mesbah, 2006), to our knowledge there are no previous studies contemplating parameter estimation, statistical treatment, sensitivity analysis and multi-objective optimization of syngas fermentation, therefore this work was devised to fill this lacuna.

3.2. Model Description

The dynamic model developed in this study describes a stirred tank with continuous supply of syngas and batch or continuous flow of liquid, with or without cell recycle. It accounts for two phases (G/L) and seven species – CO, H_2, CO_2, ethanol (C_2H_6O or EtOH), acetic acid ($C_2H_4O_2$ or HAc), water, and biomass; therefore comprising 13 state variables which are the concentrations of the six chemical compounds in the gas $C_{G,j}$ [mmol.L^{-1}] and in the liquid $C_{L,j}$ [mmol.L^{-1}] (where j = CO, H_2, CO_2, EtOH, HAc, H_2O), as well as the concentration of biomass in

the liquid C_X [g.L^{-1}]. Two types of input are provided to the modeling framework: (i) kinetic parameters, which define the relations between biochemical reaction rates and concentrations of chemical species and cells – these parameters are estimated in this study; and (ii) operating conditions, such as gas flow rate, dilution rate, agitation rate and syngas composition – these are specified for each of the cases analyzed in this work and their effects are further evaluated.

Fitting the model parameters with literature data turned out to be a challenge due to several reasons: first, the number of experimental papers on syngas fermentation is relatively small compared to other types of fermentation; and an even smaller number provides data without co-production of other chemicals such as butanol and butanediol. Among these, some provide exploratory data of very long cultures in which several accidents or interventions occur, and others fail to provide clear information about the process conditions (e.g. often the gas flow rates are omitted from the text, probably because they were not fixed during the experiment). In the present work the model parameters were estimated for five different case studies from three different papers: (C1) (Phillips, Klasson, Ackerson, Clausen, & Gaddy, 1993); (C2) (Gaddy et al., 2007); (C3-A,B,C) (Maddipati, Atiyeh, Bellmer, & Huhnke, 2011). These case studies have in common the use of continuous supply of syngas mixtures in stirred tanks and the formation of acetic acid and ethanol as only products. Table 3.1 presents the main differences between the five scenarios, apart from the liquid medium composition which is omitted due to space limitations. It is worth noting that C2 actually consists of 35 steady-state points obtained under different conditions of gas composition, flowrates and agitation, while C1 and C3(A,B,C) comprise dynamic data. C3 is one case study subdivided in three, i.e. all of the process conditions are the same, except for the concentration of yeast extract or corn steep liquor.

The next three sub-sections present the modeling approach for the specific production/consumption rates of species due to cell fermentation (Sec 3.2.1); the mass balance equations considering in/out flows, gas-liquid mass transfer, fermentation and cell recycle (Sec. 3.2.2); and the calculation of special terms that appear in the mass balance equations (Sec. 3.2.3).

Table 3.1. Case studies used for the estimation of kinetic parameters.

Case	C1 [†]	C2	C3 (A,B,C) [‡]
Microbe	*C.ljungdahlii*	*C. ljungdahlii*	*Clostridium* strain P11
Number of experiments under different conditions	1	35	3
Number of points per experiment (N_E)	24	1	17
Number of types of responses (N_R)	5	5	3
Type of data	dynamic liquid concentrations and gas conversions	steady-state liquid concentrations and gas conversions	dynamic liquid concentrations
Gas composition [H_2:CO:CO_2:inert]	20:55:10:15	20:65:10:5 16:27:6:51 50:45:0:5	5:20:15:60
Gas residence time [§] (GRT) [min]	33 – 100	4.25 – 30	20
Dilution rate (D_{rate}) [h^{-1}]	0.0035 – 0.012	0.018 – 0.083	0
Agitation [rpm]	300 – 450	750 – 900	150
Cell purge fraction [¶] (XP)	0.1	0.3 – 1	1
Reference	Phillips et al. (1993)	Gaddy et al. (2007)	Maddipati et al. (2011)

[†] The gas and liquid flow rates, and the agitation rate in C1 change with time within the specified ranges as shown in Supp. Mat. (Fig. A2-1).

[‡] Cases C3-A to C3-C differ in the amount of yeast extract (YE) or corn steep liquor (CSE), respectively: 1 g/L YE, 10 g/L CSE, 20 g/L CSE.

[§] Liquid volume divided by inlet gas flow rate.

[¶] Fraction of cells that are not recycled to the reactor vessel (i.e. $XP = 1$ when there is no cell recycle).

3.2.1. Reaction Rates

Clostridium ljungdahlii and other acetogens assimilate CO, H_2 and CO_2 through the Wood-Ljungdahl (WL) pathway to produce acetyl-CoA, which is then used to produce cell biomass and products, as schematized in Fig. 3.1.
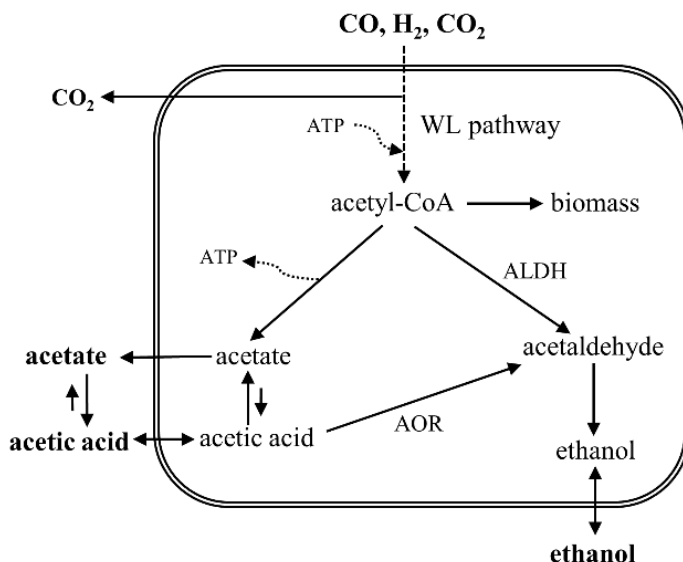
Figure 3.1. Schematic representation of syngas fermentation metabolism in *Clostridium ljungdahlii* under acidic pH, including acetic acid diffusion through the cell membrane. AOR: aldehyde:ferredoxin oxidoreductase. ALDH: aldehyde dehydrogenase. In this study, ethanol formation is considered possible only via the AOR pathway.

In theory, acetyl-CoA reduction towards ethanol is possible with aldehyde dehydrogenase (ALDH), but this route is always thermodynamically less favorable and actually infeasible if H_2 is the electron donor (Bertsch and Muller, 2015). Indeed, Richter et al. (2016) found with proteome analysis of *C. ljungdahlii* that ethanol was produced exclusively through the AOR route. Ethanol production is favored when acetate accumulates inside the cell due to growth limiting conditions (i.e. biomass cannot be produced) or due to low extracellular pH (Richter et al., 2016). In the latter case, undissociated acetic acid, which is prevalent under pH lower than 4.76 (acetic acid pKa), diffuses freely through the cell membrane due to its neutral charge; however it dissociates again in the cytosol where the pH is close to neutrality and it cannot be exported through the cell membrane without active transport processes (i.e. using cellular energy), thus

leading to the accumulation of acetate and protons inside the cell. In *C. ljungdahlii*, Richter et al. (2016) reported that the enzymes needed for the synthesis of ethanol were always available in excess and, as reducing equivalents are constantly being provided by the oxidation of CO and H_2 (see Eqs. (3.1)-(3.2) catalyzed by carbon monoxide dehydrogenase and hydrogenase, respectively), the authors suggest that ethanol is formed as soon as undissociated acetic acid and reducing equivalents reach a threshold concentration required to make the reduction of acetic acid thermodynamically feasible.

$$CO + H_2O \rightarrow CO_2 + 2H^+ + 2e^- \qquad\qquad (3.1)$$

$$H_2 \rightarrow 2H^+ + 2e^- \qquad\qquad (3.2)$$

With that in mind, we propose a kinetic model following the stoichiometry of the reactions presented in Eqs. (3.3)-(3.6), which intend to generally represent the chemical reactions catalyzed by the cell. The model accounts for the following assumptions: (i) the uptake rates of CO and H_2 follow Monod kinetics with inhibition by substrate and product (Eq. (3.7)); (ii) acetic acid and ethanol inhibit substrate uptake with standard inhibition kinetics (Eq. (3.7b)), but ethanol inhibition is only activated after a threshold concentration is achieved; (iii) CO inhibits the uptake of H_2 but not CO (Eq. (3.7c)) – this was decided after preliminary estimation routines showed that a CO inhibition constant for CO uptake could not be estimated with the experimental data used here; (iv) biomass growth is a function of the uptake rates of CO and H_2 (Eq. (3.8)) and cell death (Eq. (3.9)), and its composition is assumed constant; (v) acetic acid is produced from CO (Eq. (3.3)) and H_2/CO_2 (Eq. (3.4)); (vi) ethanol is produced exclusively through reduction of acetic acid (Eqs. (3.5)-(3.6)), with reaction rates that are hyperbolic functions of the acetic acid concentration, also mimicking Michaelis-Menten kinetics (Eq. (3.10)); (vii) the effects of pH are not directly included in the model, but it is assumed that the estimated values of the kinetic parameters associated with acetic acid uptake and reduction will reflect the pH conditions adopted in the experiments used for the parameter estimation. With these assumptions, we may calculate the specific reaction rates v_k^R [mmol.g^{-1}.h^{-1}] (where k indicates the reaction's equation number, i.e. Eqs. (3.3)-(3.6)), and the specific consumption/production rates of species j, V_j [mmol.g^{-1}.h^{-1}] , where a negative

sign in the value of v_j indicates that the species is consumed otherwise it is produced.

$$4CO + 2H_2O \rightarrow C_2H_4O_2 + 2CO_2 \qquad (3.3)$$

$$4H_2 + 2CO_2 \rightarrow C_2H_4O_2 + 2H_2O \qquad (3.4)$$

$$C_2H_4O_2 + 2CO + H_2O \rightarrow C_2H_6O + 2CO_2 \qquad (3.5)$$

$$C_2H_4O_2 + 2H_2 \rightarrow C_2H_6O + H_2O \qquad (3.6)$$

Ethanol inhibition in acetogens is still a research gap in the literature, but there are evidences that it occurs in a similar fashion to what is observed in the ABE fermentation: for example, Ramió-Pujol, Ganigué, Bañeras, and Colprim (2018) observed that ethanol had inhibitory effects on C. ljungdahlii, though much milder than butanol, but the authors were not capable of achieving the critical concentration for full inhibition. The experimental data from case study C1 show an immediate decrease in gas conversion after the ethanol concentration surpasses 35 g.L^{-1}, after which the concentrations of cells and products continue to increase for a while but eventually drop as a result of low substrate conversion. To express this behavior, the standard noncompetitive enzyme inhibition model used for ethanol inhibition is only activated after $C_{L,EtOH}$ reaches this threshold concentration.

$$v_j = -\frac{v_{max,j} \cdot C_{L,j}}{K_{S,j} + C_{L,j}} \cdot I_E \cdot I_A \cdot I_{CO,j} \ , \ \ j = CO, H_2 \qquad (3.7a)$$

$$I_E = \frac{1}{1 + \dfrac{C_{L,EtOH}}{K_{IE}}} \quad , \quad I_A = \frac{1}{1 + \dfrac{C_{L,HAc}}{K_{IA}}} \qquad (3.7b)$$

$$I_{CO,\ j=H_2} = \frac{1}{1 + \dfrac{C_{L,CO}}{K_{I,CO}}} \quad , \quad I_{CO,\ j=CO} = 1 \qquad (3.7c)$$

The specific biomass growth rate μ [h^{-1}] is then calculated from these uptake rates via yield coefficients $Y_{X,j}$ [g.mol^{-1}] for both substrates as shown in Eq. (3.8).

Although H_2 is not a source of carbon, it is coupled with the consumption of CO_2 and it has also been shown to be associated with the growth rate (Mohammadi et al., 2014). The death rate r_d is a function of cell concentration as shown in Eq. (3.9), where k_d is the death constant estimated in this study. It is worth noting that, with this equation, the growth rate is also affected by the concentration of inhibitors (ethanol, acetic acid and CO), and the effects of other nutrients and maintenance issues are expressed in the yield coefficients and the death constant.

$$\mu = -v_{CO} \cdot Y_{X,CO} - v_{H_2} \cdot Y_{X,H_2} \tag{3.8}$$

$$r_d = k_d \cdot X \tag{3.9}$$

The reaction rates of acetic acid reduction (AcR), i.e. v_k^R for k = 5 and 6, are calculated with Eqs. (3.10a-b), where the parameters $v_{max,j}^{AcR}$ and $K_{s,j}^{AcR}$ (j = CO, H_2) are estimated in this study. The condition in Eq. (3.10a) should be read as "for j = CO and k = 5, or for j = H_2 and k = 6". The expressions $F_{AcR,j}$ are only used to make the equations clearer; they are not model parameters. The idea behind this set of equations is that acetic acid is reduced with hyperbolic kinetics limited by its concentration (Eq. (3.10b)), and the consumption rate of CO or H_2 necessary to provide reducing equivalents to these reactions are bounded by the total uptake rates previously calculated from Eq. (3.7); thus it can be easily verified that $v_k^R (k=5,6)$ tends to the expression $F_{AcR,j}$ when the uptake of CO or H_2 is significantly larger than $F_{AcR,j}$, whereas it tends to $-v_j/2$ when $|v_j/2|$ is smaller than $F_{AcR,j}$ (the division by 2 is due to the stoichiometric coefficient of CO and H_2 in Eqs. (3.5)-(3.6)).

$$v_k^R = \left(\frac{1}{2}\right)\left(\frac{2F_{AcR,j}}{2F_{AcR,j} + |v_j|}\right) \cdot |v_j| \quad , \quad (j,k) = (CO,5), (H_2,6) \tag{3.10a}$$

$$F_{AcR,j} = \frac{v_{max,AcR}^j \cdot C_{L,HAc}}{K_{S,AcR}^j + C_{L,HAc}}, \quad j = CO, H_2 \tag{3.10b}$$

The remaining substrate that is consumed can then be assumed to be used in Eqs. (3.3)-(3.4), and the corresponding reaction rates are calculated from Eq. (3.11), where $v_{AcR,j}$ is the reaction rate of acetic acid reduction (Eq. (3.5) or (3.6)) using

substrate j (i.e. CO or H$_2$), for example $v_{AcR,CO}$ in Eq. (3.11) corresponds to v_5^R as calculated from Eq. (3.10). The total consumption/production rates of other components then follow the stoichiometry of Eqs. (3.3)-(3.6) as calculated with Eqs. (3.12)-(3.15).

$$v_k^R = -\frac{\left(v_j + 2v_{AcR,j}\right)}{4} \ , \ (j,k) = (CO,3),(H_2,4) \tag{3.11}$$

$$v_{CO_2} = 2v_3^R - 2v_4^R + 2v_5^R \tag{3.12}$$

$$v_{EtOH} = v_5^R + v_6^R \tag{3.13}$$

$$v_{HAc} = v_3^R + v_4^R - v_5^R - v_6^R \tag{3.14}$$

$$v_{H_2O} = -2v_3^R + 2v_4^R - v_5^R + v_6^R \tag{3.15}$$

3.2.2. Mass Balance Equations

The mass balance equations are presented in the following manner: the concentration fields, excepting biomass concentration, are divided into four categories regarding their phase (gas, G, or liquid, L) and species type (non-condensable, NC, or condensable, C). The governing differential equations, Eqs. (3.16)-(3.20), assume isothermal and isobaric operation, as well as homogeneity and constant liquid and gas volumes in the reactor.

For non-condensable (NC) species j in the gas phase, $j \in \{CO, H_2, CO_2\}$:

$$\frac{dC_{G,j}}{dt} = \left(\frac{1}{V_G}\right) \cdot \left(Q_{G,in} C_{G,j,in} - Q_{G,out} C_{G,j}\right) - k_L a_j \left(\frac{C_{G,j}}{m_{j \in NC}} - C_{L,j}\right)\left(\frac{V_L}{V_G}\right) \tag{3.16}$$

For condensable (C) species j in the gas phase, $j \in \{EtOH, HAc, H_2O\}$:

$$\frac{dC_{G,j}}{dt} = \left(\frac{1}{V_G}\right) \cdot \left(Q_{G,in} C_{G,j,in} - Q_{G,out} C_{G,j}\right) + k_L a_j \left(\frac{C_{L,j}}{m_{j \in C}} - C_{G,j}\right)\left(\frac{V_L}{V_G}\right) \tag{3.17}$$

For non-condensable (NC) species j in the liquid phase, $j \in \{CO, H_2, CO_2\}$:

$$\frac{dC_{L,j}}{dt} = \left(\frac{Q_L}{V_L}\right) \cdot \left(C_{L,j,in} - C_{L,j}\right) + k_L a_j \left(\frac{C_{G,j}}{m_{j \in NC}} - C_{L,j}\right) + v_j C_X \tag{3.18}$$

For condensable (C) species j in the liquid phase $j \in \{EtOH, HAc, H_2O\}$:

$$\frac{dC_{L,j}}{dt} = \left(\frac{Q_L}{V_L}\right) \cdot \left(C_{L,j,in} - C_{L,j}\right) - k_L a_j \left(\frac{C_{L,j}}{m_{j \in C}} - C_{G,j}\right) + v_j C_X \tag{3.19}$$

For the biomass concentration (in the liquid phase):

$$\frac{dC_X}{dt} = \left(\frac{Q_L}{V_L}\right) \cdot \left(-C_X \cdot XP\right) + \mu C_X - r_d \tag{3.20}$$

The gas-liquid equilibrium factors $m_{j \in NC}$, $m_{j \in C}$ in Eqs. (3.16)-(3.20) are described in Eqs. (3.21)-(3.22), where R=8.314 Pa.m³/mol.K is the ideal gas constant; MM_L and ρ_L refer to liquid phase molar mass [kg.mol⁻¹] and density [kg.m⁻³] assumed pure water at 36 °C; and the respective physical parameters – Henry's law constants H_j [Pa], saturation pressures $P_{sat,j}$ [Pa] and infinite-dilution activity coefficients γ_j^∞ – can be found in the Supp. Mat. (Table A2-1). V_L and V_G are the volumes [L] of liquid and gas inside the reactor; $Q_{G,in}$ and $Q_{G,out}$ are the gas volumetric flow rates [L.h⁻¹] in/out the vessel, with the latter calculated as described in Sec. 3.2.3; $k_L a_j$ are mass transfer coefficients calculated as described in Sec. 3.2.3; Q_L is the liquid volumetric flow rate [L.h⁻¹]. The specific rates v_j, μ and r_d were presented in Sec. 3.2.1 and are calculated accordingly at each time point; subscript $_{in}$ refer to inlet gas and liquid concentrations; and XP is the cell purge fraction, i.e. the fraction of cells that are not recycled to the vessel.

$$m_{j \in NC} = \frac{H_j MM_L}{RT \rho_L} \tag{3.21}$$

$$m_{j \in C} = \frac{\rho_L RT}{MM_L \gamma_j P_{sat,j}} \tag{3.22}$$

3.2.3. Calculation of Special Terms

Certain terms that appear in the right-hand side of the ODEs, but which are not state variables, are calculated as explained in the following.

3.2.3.1. Outlet volumetric gas flow rate $Q_{G,out}$

$Q_{G,out}$ is calculated from a mole balance in the gas phase considering isobaric conditions inside the vessel. Taking into account the mass transfer of non-condensable species ($j \in$ NC) from gas to liquid and the mass transfer of condensable species ($j \in$ C) from liquid to gas, the total gas mole flow rate leaving the reactor is calculated at each time with Eq. (3.23). $Q_{G,out}$ is then calculated with the assumption of ideal gas in Eq. (3.24).

$$N_{G,out}\left[\frac{mol}{h}\right] = Q_{G,in}\sum_j C_{G,j,in} - \sum_{j \in NC}\left(k_L a_j\left(\frac{C_{G,j}}{m_{j \in NC}} - C_{L,j}\right)V_L\right) + \sum_{j \in C}\left(k_L a_j\left(\frac{C_{L,j}}{m_{j \in C}} - C_{G,j}\right)V_L\right)$$

(3.23)

$$Q_{G,out}\left[\frac{m^3}{h}\right] = \frac{N_{G,out}RT}{P}$$

(3.24)

3.2.3.2. Mass transfer coefficients

The mass transfer coefficient $k_L a$ for air in water at T = 36 °C is calculated via Eqs. (3.25)-(3.27). It considers a weighted average between the values of $k_L a$ estimated at 20 °C for non-coalescing ($k_L a_0^{(20)}$) and coalescing ($k_L a_1^{(20)}$) broth according to the correlations proposed by Van 't Riet (1979) for air in water (Eq. (3.25c-d)), where P_g/V_L is the impeller power per unit volume, which is estimated from the impeller un-gassed power P_{ug} (Eq. (3.26)) and the correlation for the ratio P_g/P_{ug} in Eqs. (3.27) (Cui, Van der Lans, & Luyben, 1996). The weighting factor f_0 is an unknown parameter which is estimated in this study. In Eqs. (3.25)-(3.27) all variables are in SI units, except for the temperature which is in °C. The ungassed power number is assumed to be N_p = 12.4 for two impellers (cases C1 and C2) or N_p = 16.5 (case C3) for three impellers based on the equation available in the New Brunswick Bioflo manual; N is the agitation rate in s^{-1}; u_s is the gas superficial velocity (volumetric gas flow at the inlet divided by the reactor cross sectional area). In all cases, the reactor is assumed to have a height/diameter ratio of 2 and an impeller diameter of 40% the reactor diameter, as standard in New Brunswick Bioflo bioreactors.

$$\frac{k_L a^{(20)}}{k_L a^{(T)}} = 1.024^{(20-T)} \quad , \quad T = 36$$

(3.25a)

$$k_L a^{(20)} \ [h^{-1}] = f_0 \cdot k_L a_0^{(20)} + (1 - f_0) \cdot k_L a_1^{(20)} \tag{3.25b}$$

$$k_L a_0^{(20)} \left[h^{-1} \right] = 3600 \cdot \left(0.002 \left(\frac{P_g}{V_L} \right)^{0.7} (u_s)^{0.2} \right) \tag{3.25c}$$

$$k_L a_1^{(20)} \left[h^{-1} \right] = 3600 \cdot \left(0.026 \left(\frac{P_g}{V_L} \right)^{0.4} (u_s)^{0.5} \right) \tag{3.25d}$$

$$P_{ug} = N_p \rho_L N^3 d_i^5 \tag{3.26}$$

$$\frac{Q_{G,in} \cdot N^{0.25}}{d_i^2} \leq 0.055 \quad , \quad \left(1 - \frac{P_g}{P_{ug}} \right) = 9.9 \left(\frac{Q_{G,in} \cdot N^{0.25}}{d_i^2} \right) \tag{3.27a}$$

$$\frac{Q_{G,in} \cdot N^{0.25}}{d_i^2} \geq 0.055 \quad , \quad \left(1 - \frac{P_g}{P_{ug}} \right) = 0.52 + 0.62 \left(\frac{Q_{G,in} \cdot N^{0.25}}{d_i^2} \right) \tag{3.27b}$$

The individual $k_L a_j$ for each species is then obtained from the reference air-water $k_L a$ by applying the Penetration Theory as in Eq. (3.28) (Talbot, Gortares, Lencki, & de La Noüe, 1991), where Df_j is the mass diffusivity of species j in water (Supp. Mat., Table A2-1).

$$k_L a_j = k_L a \left(\frac{Df_j}{Df_{air}} \right)^{1/2} \tag{3.28}$$

3.3. Numerical Methods

The dynamic fermentation model described by the ODEs, Eqs. (3.16)-(3.20), and its supplemental algebraic equations in Sec. 3.2, represents a non-linear algebraic-differential system which demands specialized numerical solvers for stiff problems. In the present case, the ode15s variable-order method from MATLAB was used for time integration from a feasible initial condition, given the appropriate value of the vector of model parameters in Eq. (3.29). The $\underline{\beta}$ vector of parameters (N_P x 1,N_P=15) comprises the 14 kinetic parameters explained in Sec. 3.2.1, as well as the $k_L a$ weighting factor f_0.

$$\underline{\beta}^T \equiv \left[V_{max,CO} \ V_{max,H_2} \ K_{S,CO} \ K_{S,H_2} \ K_{IE} \ K_{IA} \ K_{I,CO} \ Y_{X,CO} \ Y_{X,H_2} \ v_{max,CO}^{AcR} \ K_{S,CO}^{AcR} \ v_{max,H_2}^{AcR} \ K_{S,H_2}^{AcR} \ k_d \ f_0 \right]$$

$$(3.29)$$

3.3.1. Estimation of model parameters

The unknown model parameters $\underline{\beta}$ were estimated as $\underline{\hat{\beta}}$ using the Maximum Likelihood Principle - MLP (Himmelblau, 1970) - with the experimental data from the case studies presented in Table 3.1, which are structured into five categories of response (for C1 and C2, j = 1...N_R with N_R = 5) or three categories of response (for C3, j = 1...N_R with N_R = 3): ethanol ($C_{L,EtOH}$), acetic acid ($C_{L,HAc}$) and biomass (C_X) liquid phase concentrations [g.L^{-1}], as well as CO and H$_2$ conversions (X_{CO} and X_{H_2} [%]), which indirectly provide information about the concentrations of these species. For C3(A,B,C) the gas conversions were not available, so only the liquid concentrations were used. The MLP is built with three assumptions: (A1) independency of N_E experiments (i = 1...N_E); (A2) the model is correct; and (A3) experimental responses ($y_{j,i}$) are uncorrelated and follow normal probability density functions (PDF) around unknown correct responses ($\eta_{j,i}$) according to the variance model in Eq. (30), where $r_{j,i}$ are known response-experiment factors and σ_ε^2 is the unknown fundamental variance (Himmelblau, 1970).

$$y_{j,i} \rightarrow N\left(\eta_{j,i}, \sigma_{j,i}^2\right) \ , \ \sigma_{j,i}^2 = r_{j,i}\sigma_\varepsilon^2 \tag{3.30}$$

With Eq. (3.30) and assumptions (A1) and (A3), it can be shown that the identities in Eqs. (3.31) result for $\underline{y}_j$, the N_E x 1 vector of experimental values of response j at all points, where E(.), $\underline{\underline{Cov}}(.), \underline{\underline{w}}_j$ and $\underline{\eta}_j$ represent, respectively, the expectancy operator, the variance-covariance matrix operator, the N_E x N_E diagonal weight matrix for response j and the N_E x 1 vector of correct values for response j.

$$\mathrm{E}(\underline{y}_j) = \underline{\eta}_j \tag{3.31a}$$

$$\underline{\underline{Cov}}(\underline{y}_j) = \sigma_\varepsilon^2 \cdot \underline{\underline{W}}_j^{-1} \tag{3.31b}$$

$$\underline{\underline{W}}_j^{-1} = \underline{\underline{Diag}}(r_{j,1}, r_{j,2}, ..., r_{j,N_E}) \tag{3.31c}$$

It can also be shown (Himmelblau, 1970) with assumptions (A1), (A2) and (A3), and Eqs. (3.30)-(3.31) that the application of the MLP to this multi-response (N_R = 5 or 3) estimation problem results in the minimization of the weighted sums of squares of residuals written in Eq. (3.32), where $\hat{\underline{\beta}}$ is the N_P x 1 vector of estimated parameters and $\hat{\underline{y}}_j\left(\hat{\underline{\beta}}\right)$ is the corresponding N_E x 1 vector of model predicted responses. Due to its high non-linearity and likely multi-modal nature, the objective function was minimized using the meta-heuristic method Genetic Algorithm (ga MATLAB function), but a bounded Simplex Algorithm (fminsearch MATLAB function) was also applied to deepen a candidate optimum when a good estimate of initial point was known. In both cases, sensible lower and upper bounds were stipulated for $\hat{\underline{\beta}}$. These bounds are displayed in Table A2-2 of the Supplementary Materials, jointly with ad hoc variable transformations to convert the original unrestricted Simplex Algorithm into a bounded Simplex Algorithm.

$$\underset{\{\hat{\underline{\beta}}\}}{Min} \sum_{j=1}^{N_R} \psi_j\left(\hat{\underline{\beta}}\right) \quad , \quad \psi_j\left(\hat{\underline{\beta}}\right) = \left(\underline{y}_j - \hat{\underline{y}}_j\right)^T \underline{\underline{W}}_j \left(\underline{y}_j - \hat{\underline{y}}_j\right) \quad , \quad j = 1...N_R \qquad (3.32)$$

The factors $r_{j,i}$ (j=1...N_R, i=1...N_E) of the variance model of experimental responses in Eqs. (3.30) and (3.31), were chosen considering plausible variances of experimental values – e.g. (10% of value)^2 – as well as the interests of the modeling framework, which can privilege more adherence onto some experimental responses (e.g. ethanol concentration) in detriment of others (e.g. acetic acid concentration). The underlying fact is seen in Eq. (3.31c): as $r_{j,i}$ decrease the respective elements of the weight matrix $\underline{\underline{W}}_j$ rise, increasing the "pressure" for adherence of $\hat{\underline{y}}_j$ onto $\underline{y}_j$. In this regard, the following choices were made after multiple estimation test runs: (i) for ethanol liquid concentrations (j=1) $r_{j,i} = (0.025 \cdot y_{j,i})^2$; (ii) for acetic acid liquid concentrations (j=2) $r_{j,i} = (0.05 \cdot y_{j,i})^2$; (iii) for biomass concentrations (j=3) $r_{j,i} = (0.05 \cdot y_{j,i})^2$; (iv) for CO conversions (j=4) $r_{j,i} = (0.1 \cdot y_{j,i})^2$; and (v) for H$_2$ conversions (j=5) $r_{j,i} = (0.1 \cdot y_{j,i})^2$.

The experimental response values were read from the dynamic profiles (C1 and C3) or steady-state outcomes (C2) reported in the case studies considered here (see Table 3.1). For C1 and C3, the predicted responses $\hat{\underline{y}}_j\left(t_i, \hat{\underline{\beta}}\right)$ at each time (with i = 1…N_E) were obtained via ode15s numerical integration starting from the initial conditions of liquid composition reported in the respective papers; for C2, the predicted responses $\hat{\underline{y}}_j\left(i, \hat{\underline{\beta}}\right)$ were obtained with the integration starting from arbitrary initial conditions until sufficient time to reach steady state (as explained further in Sec. 3.3.3 the steady state was found to be non-sensitive to the initial conditions). In all cases, the initial gas-phase concentrations were considered equal to the inlet gas concentrations and the liquid-phase concentrations of non-condensable species were considered equal to gas-liquid equilibrium concentrations.

3.3.2. Significance of parameters

The confidence intervals of the estimated parameters $\hat{\beta}_k$ were calculated with Eq. (3.33), where $t_{1-\alpha/2}$ is the abscissa at $(1-\alpha/2)\cdot100\%$ probability (α=0.05) of the t-Student PDF with $N_R \cdot N_E - N_P$ degrees of freedom (N_P = 15), and the estimated standard deviations $\hat{\sigma}_{\hat{\beta}_k}$ are the kth diagonal elements of the estimated variance-covariance matrix of the parameters. For a detailed explanation the reader is referred to the Supplementary Materials provided with this work. The F-test to reject the null hypothesis (i.e. parameter β$_k$ is significant) with 95% probability is given (Himmelblau, 1970) in Eq. (3.34), where $\phi_{1-\alpha}\left(1, N_R \cdot N_E - N_P\right)$ is the abscissa at $(1-\alpha)\cdot100\%$ probability (α=0.05) of the Fisher PDF with degrees of freedom (1, $N_R \cdot N_E - N_P$).

$$\hat{\beta}_k - t_{1-\alpha/2} \cdot \hat{\sigma}_{\hat{\beta}_k} \leq \beta_k \leq \hat{\beta}_k + t_{1-\alpha/2} \cdot \hat{\sigma}_{\hat{\beta}_k} \quad , \quad \hat{\sigma}_{\hat{\beta}_k} = \sqrt{\left[\hat{\underline{\underline{Cov}}}(\hat{\underline{\beta}})\right]_{kk}} \qquad (3.33)$$

$$R(\hat{\beta}_k) = \frac{\left(\hat{\beta}_k\right)^2}{\left(\hat{\sigma}_{\hat{\beta}_k}\right)^2} > \phi_{1-\alpha}\left(1, N_R \cdot N_E - N_P\right) \Rightarrow \beta_k \neq 0 \qquad (3.34)$$

3.3.3. Steady-state sensitivity and multi-objective optimization

After the estimation of kinetic parameters, the model was used to study the effects of several process conditions on the steady-state productivity of ethanol (i.e. $C_{L,EtOH} \cdot D_{rate}$). The steady states were obtained by integrating the ODE system until all the state variables showed absolute gradients smaller than 10^{-6}. This procedure was found to be faster than solving the system of nonlinear algebraic equations, as this required the initial guesses to be very close to the actual solutions. It can also be shown that, for a wide range of initial conditions, the steady state was stable and independent of such specifications (phase-portraits depicting the dynamic trajectories are presented in the Supp. Mat., Fig. A2-2), therefore an arbitrary set of initial conditions equal to those of case study C1 was used. With this framework, the sensitivity was analyzed with respect to the gas composition (varying the molar fractions of CO and H_2), the gas residence time (GRT), the dilution rate (D_{rate}), and also to the kinetic parameters under different conditions of GRT and D_{rate}. Based on these results, the process was optimized using multi-objective genetic algorithm for the maximization of two conflicting objectives: ethanol productivity and CO conversion. The decision variables were three operating conditions (GRT, D_{rate} and XP – cell purge fraction) and nine kinetic parameters which could possibly be tuned with the design of the nutrient medium, the choice of strain and/or genetic engineering. In a last study, the H_2:CO ratio was also included as a decision variable. For this optimization routine, the bounds were specified based on the ranges of kinetic parameters estimated for the five case studies (see Supp. Mat., Table A2-3).

3.4. Results and Discussion

3.4.1. Parameter estimation and confidence intervals

The full parameter vector $\underline{\beta}$ in Eq. (3.29) was first estimated with the data from C1. Since C2 employed the same strain, the maximum uptake rates (v_{max}), saturation constants (K_s) and inhibition constants (K_I) were fixed and the remaining eight parameters were re-estimated with the steady-state data from C2. It should also be said that the ethanol inhibition term was excluded from this case study since the reported data did not achieve the threshold concentration considered in the model. Similarly, for the three case studies C3(A,B,C) it was considered that the difference in nutritional supplement would affect the cell

yield, product selectivity, death/maintenance and the degree of coalescence of the liquid; therefore β was estimated for C3-A (without ethanol inhibition) and for C3-B and C3-C all parameters were fixed except for $Y_{CO,X}$, $v_{\max,AcR}^{CO}$, $K_{S,AcR}^{CO}$, k_d and f_0, which were re-estimated. The results are presented in Table 3.2 along with their 95% confidence intervals. Results of F-test score for significance of parameters can be found in Supp. Mat., Table A2-4.

The estimated values of the maximum CO and H_2 uptake rates $\hat{v}_{\max,CO}$ and $\hat{v}_{\max,H_2}$ are comparable to CO uptake rates reported by other authors: Chen et al. (2018) obtained CO uptake rates from 41 – 43 mmol.g^{-1}.h^{-1} in continuous cultures of *C. autoethanogenum* in a bubble column; Mohammadi et al. (2014) estimated a maximum rate of 34 mmol.g^{-1}.h^{-1} for *C. ljungdahlii*; and Gaddy et al. (2007) reported a large range of 14 – 100 mmol.g^{-1}.h^{-1} for different operating conditions with *C. ljungdahlii*. The saturation constants K_s, which are inversely related to the microbe's affinity to the substrate, reflect the disparity observed between the conversions of CO and H_2 in cases C1 and C2: $K_{S,CO}$ is around 2% the value of K_{S,H_2} in C1 and C2, and 6% in C3, while the pure component solubility of CO is only about 13% higher that of H_2 at the culture temperature. With regard to the inhibition constants, it can be concluded that the effect of CO on H_2 uptake was higher in cases C1 and C2 given the lower value of $K_{I,CO}$ for these cases, although it should also be noted that cases C3 use a small percentage of only 5% H_2 in the feed gas. Acetic acid inhibition was also found to be statistically significant although its large value in all cases (> 850 mmol.L^{-1}) indicate small inhibitory effects under the conditions of the experiments considered here. For case C2, the uncertainty associated with this parameter is also notably high, reaching around 60% of its nominal value while in the other case studies this percentage is less than 20%. In fact, for most of the estimated parameters, C2 presents the highest uncertainties among the cases, which is also due to the large variety of experimental conditions adopted in this case and relatively small number of samples. It should be noted that as more experiments are performed, new data can be incorporated into the modeling framework presented here and the parameters can be re-estimated with higher accuracy.

Table 3.2. Parameter estimates with their 95% confidence intervals.

Parameter	Unit	C1	C2	C3-A	C3-B	C3-C
$V_{max,CO}$	mmol.g^{-1}.h^{-1}	46.3 ± 5.33	46.3 ± 6.79	37.5 ± 5.28	37.5 ± 6.99	37.5 ± 2.70
V_{max,H_2}	mmol.g^{-1}.h^{-1}	31.6 ± 5.30	31.6 ± 8.47	29.5 ± 3.81	29.5 ± 4.02	29.5 ± 2.27
$K_{S,CO}$	mmol.L^{-1}	0.0115 ± 0.000637	0.0115 ± 0.00631	0.0454 ± 0.00670	0.0454 ± 0.0112	0.0454 ± 0.00525
K_{S,H_2}	mmol.L^{-1}	0.675 ± 0.0853	0.675 ± 0.235	0.718 ± 0.0732	0.718 ± 0.197	0.718 ± 0.0427
$K_{I,EtOH}$	mmol.L^{-1}	217 ± 38.9	-	-	-	-
$K_{I,HAc}$	mmol.L^{-1}	962 ± 127	962 ± 594	869 ± 117	869 ± 85.2	869 ± 183
$K_{I,CO}$	mmol.L^{-1}	0.136 ± 0.0224	0.136 ± 0.110	0.827 ± 0.110	0.827 ± 0.179	0.827 ± 0.110
$Y_{X,CO}$	g.mol^{-1}	0.754 ± 0.133	1.34 ± 0.226	1.69 ± 0.365	1.92 ± 0.463	2.41 ± 0.301
Y_{X,H_2}	g.mol^{-1}	0.201 ± 0.0233	0.156 ± 0.0623	0.248 ± 0.0399	0.248 ± 0.0369	0.248 ± 0.0121
$V_{max,CO}^{AcR}$	mmol.g^{-1}.h^{-1}	24.2 ± 2.85	37.6 ± 17.6	13.0 ± 1.27	20.2 ± 1.98	8.581 ± 0.620
$K_{S,CO}^{AcR}$	mmol.L^{-1}	388 ± 20.3	303 ± 163	223 ± 16.1	557 ± 169	483 ± 57.2
V_{max,H_2}^{AcR}	mmol.g^{-1}.h^{-1}	1.76 ± 0.166	22.2 ± 7.62	15.9 ± 1.73	15.9 ± 3.39	15.9 ± 1.16
K_{S,H_2}^{AcR}	mmol.L^{-1}	464 ± 37.1	586 ± 287	72.7 ± 6.68	72.7 ± 12.6	72.7 ± 7.87
k_d	h^{-1}	0.00697 ± 0.000297	0.00862 ± 0.00453	0.0119 ± 0.00135	0.0112 ± 0.00271	0.00959 ± 0.00163
f_0	-	0.988 ± 0.0464	0.958 ± 0.339	0.700 ± 0.0699	0.973 ± 0.243	0.988 ± 0.123

The cell yields, specifically $Y_{X,CO}$, showed a wide variation among the five case studies, being the highest for C3-C (the experiment with high concentration of corn steep liquor) at 2.41 g.mol^{-1} (nominal value). As expected the value of $Y_{X,CO}$ increases from C3-A to C3-C as a result of increasing concentrations of nutritional supplement. Clearly this parameter is specific to the culture conditions and microbial strain, and this can be verified by looking at the diversified results of cell yield in syngas fermentation reported by different authors, some of which are in good agreement with this study: 0.25 g.mol^{-1} for clostridial bacteria P7 (Rajagopalan, Datar, & Lewis, 2002); 1.4 g.mol^{-1} for *C. ljungdahlii* (Phillips, Clausen, & Gaddy, 1994); 2.1 – 3.2 g.mol^{-1} for *C. ljungdahlii* (Mohammadi, Mohamed, Najafpour, Younesi, & Uzir, 2016); 2 g.mol^{-1} for *Rhodospirillum rubrum* (Kerby, Ludden, & Roberts, 1995); 7.2 g.mol^{-1} for *Eubacterium limosum* KIST612 (Chang, Kim, Lovitt, & Bang, 2001).

The results generated by the model with the different parameter vectors are shown in Figs. 3.2-4 along with the respective experimental points. The model showed overall reasonable predictive power for ethanol, acetic acid and biomass concentrations, although certain dynamic features were only roughly captured. For example, in cases C3 the acetic acid peak around 75 h was flattened and slightly displaced to the right (this was also the tendency of the experimental data going from case C3-A to C). In case C1, the model was able to predict the conversion decrease after 500 h, but the experimental data also suggest a recovery which could not be predicted by the model. In the modeling framework, this decrease is a consequence of joint inhibitory effects of ethanol and CO, the latter which accumulates in the liquid phase due to impaired uptake as a consequence of the former, and acetic acid to a smaller extent. Since this is the only experiment with such high concentrations of ethanol, it is unclear whether this behavior is due to product inhibition or if other external factors could be the cause of this perturbation. Although it is likely that ethanol exhibits inhibitory effects, as demonstrated by Ramió-Pujol et al. (2018) and Férnandez-Naveira, Abubackar, Veiga, and Kennes (2016), a final conclusion cannot be drawn from the current set of experiments with regard to this matter, and further experimental investigation is needed to evaluate critical product concentration and inhibition constants.

Case C2 (steady-state) showed the highest deviations from the experimental data as well as parameter uncertainties, which is probably due to the large range of

process conditions encompassed by the data. It should also be noted that it is unclear whether the medium composition was kept fixed or not during these experiments. Nonetheless, the model was still good at capturing the tendency of the data, especially the concentrations of products and cells. In comparison with C1, which used the same strain, the AcR parameters (acetic acid reduction) were more favorable to ethanol production, i.e. with higher $v_{max,j}^{AcR}(j=CO,H_2)$. The saturation constants $K_{S,j}^{AcR}(j=CO,H_2)$ were similar if we consider the confidence intervals.

The last parameter, f_0, indicates the level of coalescence in the liquid, with higher f_0 (as in cases C1 and C2) meaning the liquid is highly non-coalescing and thus enables higher gas-liquid mass transfer coefficients. It is worth noting that f_0 increased from case C3-A to C3-C and specially from C3-A to C3-B (when 1 g/L yeast extract was replaced with 10 g/L corn steep liquor).
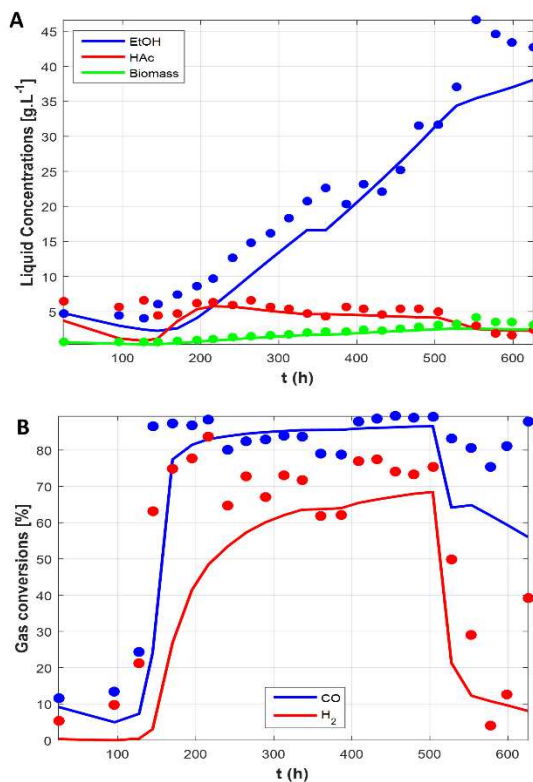
Figure 3.2. Predicted dynamic profiles (solid lines) and experimental points (circles) for case study C1: (A) concentration of products and cells in the liquid; (B) conversions of CO and H$_2$.
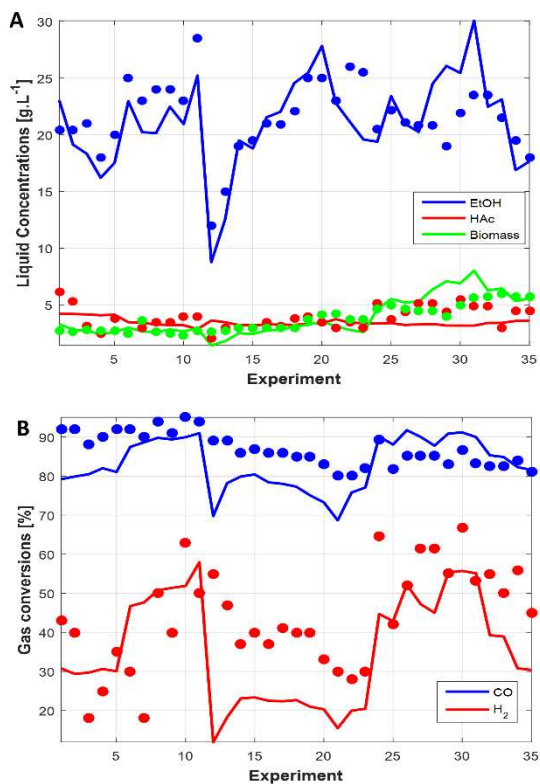
Figure 3.3. Predicted steady-state responses (solid lines) and experimental points for case study C2: (A) concentration of products and cells in the liquid; (B) conversions of CO and H_2.
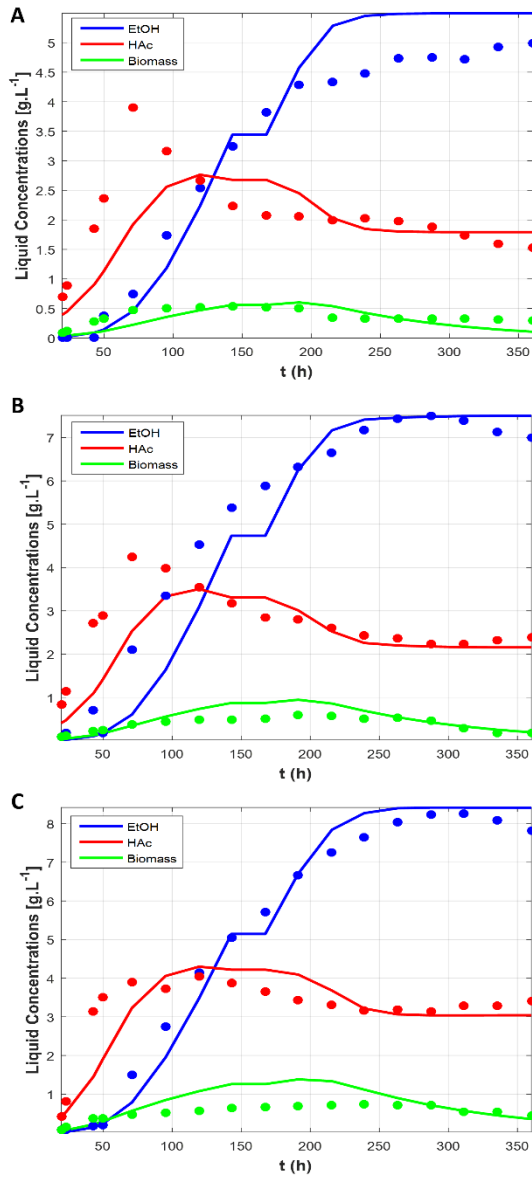
Figure 3.4. Predicted dynamic profiles (solid lines) of products and cells, and experimental points (circles) for case studies C3: (A) case C3-A; (B) case C3-B; (C) case C3-C.

3.4.2. Sensitivity of process conditions and kinetic parameters

With the fitted models, the performance of the bioreactor was evaluated for different conditions of gas composition, dilution rate and gas flow rates. For these sensitivity analyses, the parameter vector estimated in C2 was used as basis. The effects of syngas composition are depicted in Fig. 3.5 for ethanol productivity and CO conversion. It can be seen that both responses are enhanced with the CO content, but there is a maximum outcome at H_2:CO close to 1 and the peak is slightly dislocated to the left (higher H_2:CO) for CO conversion. This result suggests that the syngas composition can be tuned to improve the performance of the bioreactor, but the optimal composition would, of course, depend on the balance between extra productivity/conversion in the bioreactor and extra energy costs in upstream operations (gasification and gas conditioning). It was also observed that cell mass concentration always increased with the fraction of CO, going from near 1 g.L^{-1} at low values up to 11 g.L^{-1} with pure CO (figure shown in Supp. Mat., Fig. A2-5).

Assuming fixed gas composition of a CO-rich gas, the response surfaces shown in Fig. 3.6 were generated to illustrate the effects of dilution rate (D_{rate}) and gas residence time (GRT) with cell recycle (10% purge) and without. Both cases demonstrate how lower values of GRT (i.e. higher gas flow rates) enhance the productivity due to higher supply of substrate as well as higher gas-liquid mass transfer coefficient, although at the expense of the CO conversion. Moreover, as typically observed in chemostat cultures, the productivity is a concave function of the dilution rate with a clear maximum – in this case also dependent on the gas flow rate. From Fig. 3.6, it is also clear that cell recycle enhances the ethanol productivity (the maximum increases from around 1.13 g.L^{-1}.h^{-1} to 1.44 g.L^{-1}.h^{-1}) and broadens the region of operation without cell wash-out. Moreover, the maximum cell mass concentration increases from 4.5 g.L^{-1} to around 16 g.L^{-1} when cell recycle is used (response surfaces shown in Supp. Mat., Fig. A2-6). The effects of agitation are not shown here, but response surfaces with this variable can be found in the Supp. Mat. (Fig. A2-3). Evidently, increasing the agitation rate also enhances the mass transfer of CO and H_2 between the gas and the liquid, which allows for higher conversions and ethanol productivity; however at the price of higher energy consumption.
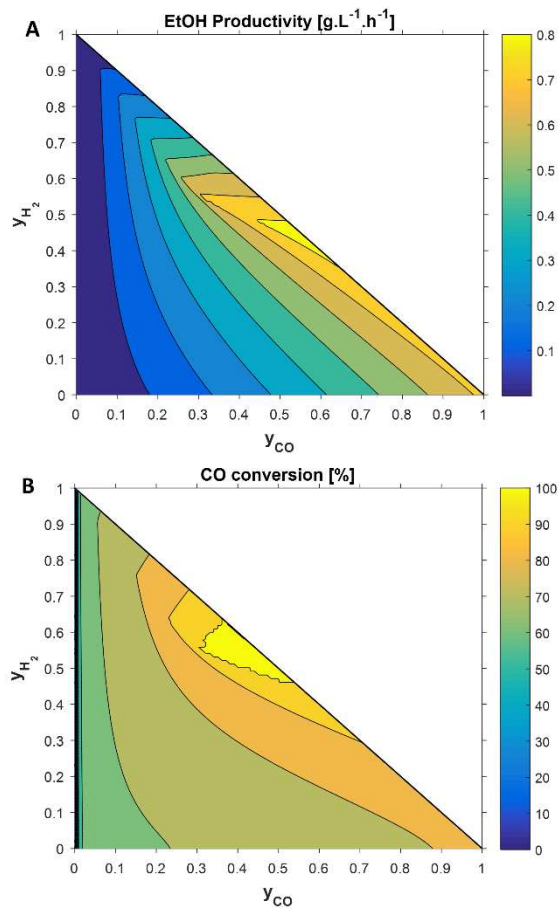
Figure 3.5. Steady-state ethanol productivity achieved with different gas compositions ($y_{CO_2} = 1 - y_{CO} - y_{H_2}$ **) with fixed conditions:** *GRT* **= 20 min,** *D_{rate}* **= 0.025 h⁻¹,** *N* **= 500 rpm, cell recycle = 90%.**

The same response surfaces were constructed for H_2-rich gas (see Supp. Mat., Fig. A2-4), which had overall the same shape and tendencies as Fig. 3.6. In accordance with Fig. 3.5, it was also observed that increasing the content of H_2 by adopting a gas composition of $[H_2:CO:CO_2] = [50:45:5]$ increased the maximum productivity to around 1.6 g.L⁻¹.h⁻¹ when cell recycle was used. However the maximum productivity under no cell recycle actually decreased from 1.13 to 0.93 g.L⁻¹.h⁻¹.
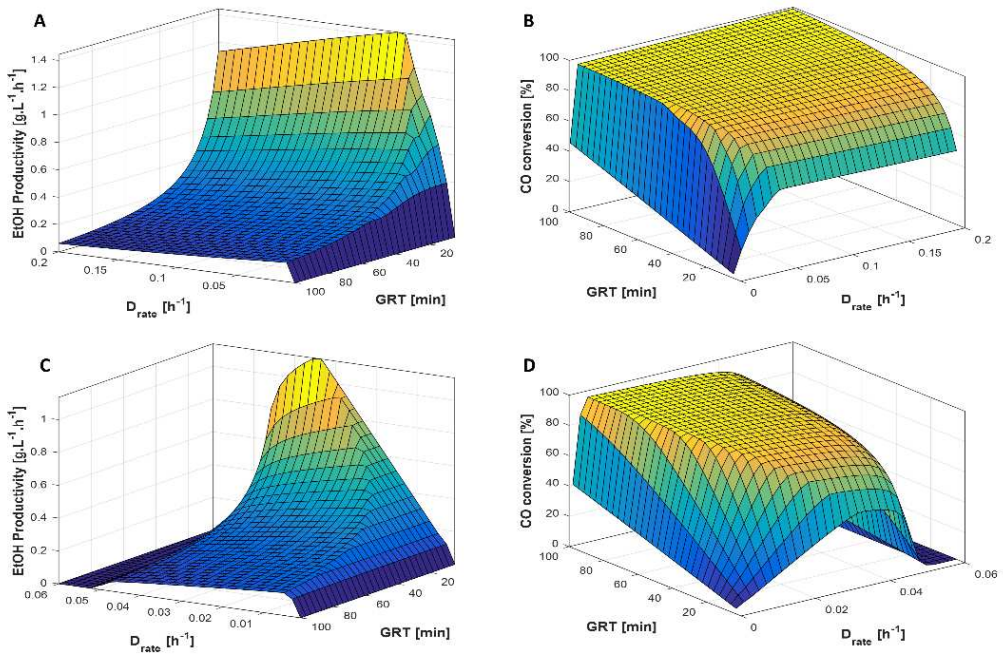
Figure 3.6. Steady-state ethanol productivity and CO conversion as function of gas residence time (*GRT*) and liquid dilution rate (*D*$_{rate}$): (A, B) with 90% cell recycle; (C, D) without cell recycle. Fixed conditions: y_{CO} **= 0.65,** y_{H_2} **= 0.2,** y_{CO_2} **= 0.15,** *N* **= 500 rpm. Note: the axes are rotated in (A) and (C).**

With regard to the effects of kinetic parameters, it was observed that the operating conditions contributed significantly to the sensitivity of this type of variable. Two illustrative examples are given in Fig. 3.7, where the parameters vary from 0.05 to 2 times their nominal value (as obtained in C2), and 6 combinations of low/high gas flow rate and dilution rate are employed. It can be seen that not only do lower values of GRT improve the productivity, but they also enhance the effects of changing the kinetic parameters (see the inclination of solid lines in Fig. 3.7 in comparison with the dashed lines). Fig. 3.7a also suggests that increasing $Y_{X,CO}$ will eventually lead to the same outcome of productivity for different values of D_{rate} under the same GRT (see green and blue lines). Very low values of D_{rate}, however, showcase the opposite trend: the two orange lines (D_{rate} = 0.005 h^{-1}) are coincident until a bifurcation occurs at $\beta_k / \hat{\beta}_k \approx 0.75$. These and other kinetic parameters showed considerable variation between the five estimations as presented in Sec. 3.4.1., indicating that such microbial properties can be customized with the

selection of strain and medium composition, besides of course genetic engineering which would be a natural extrapolation of this conclusion. The performance of the bioreactor can therefore be improved with integrated design considering the simultaneous effects of bio-kinetic parameters and process conditions.
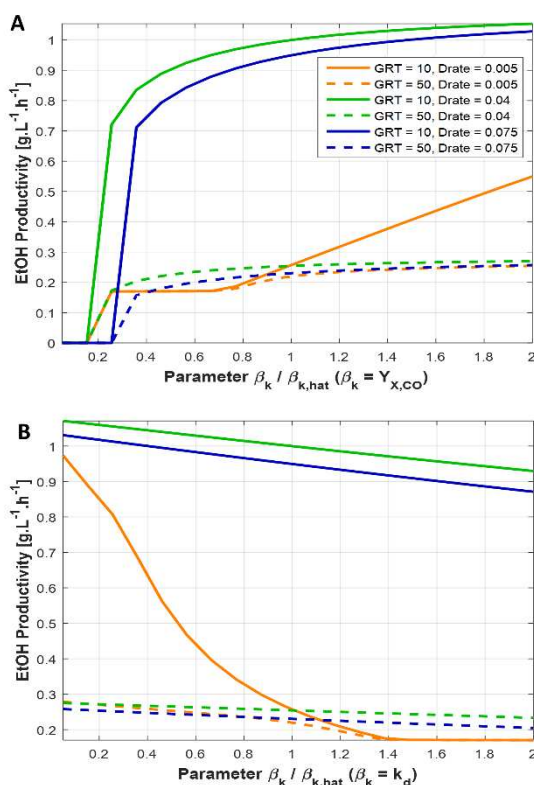
Figure 3.7. Sensitivity of steady-state ethanol productivity to kinetic parameters under different conditions of gas residence time (*GRT*) and liquid dilution rate (*D_rate*): (A) cell yield on CO (*Y_{X,CO}*) ; (B) cell death rate constant (*k_d*). Fixed conditions: y_{CO} = 0.65, y_{H_2} = 0.2, y_{CO_2} = 0.15, *N* = 500 rpm. The corresponding profiles of cell mass concentration are shown in Fig. A2-7 of the Supplementary Material.

3.4.3. Optimization of ethanol productivity and CO conversion

The solutions to three optimization runs are shown in Fig. 3.8. The multi-objective optimization was first solved for three operating conditions (GRT, D_rate and XP) and nine kinetic parameters (all excepting the saturation and inhibition constants, which were fixed at the values obtained for C2). The lower and upper bounds were

chosen based on the intervals of the parameters estimated in Table 3.2 (see Supp. Mat., Table A2-3); for the operating conditions, the GRT was free to vary in the range 5 – 50 min, D_{rate} in the range 0.005 – 0.2 h^{-1} and XP in the range 0.1 – 1 (this meaning no cell recycle). In the first run, the gas composition was fixed for a CO-rich gas , i.e. $[H_2:CO:CO_2]$ = [20:65:15]. For this case, the Pareto-optimal points reflected the classical problem of two conflicting objectives (Fig. 3.8a): higher gas flow rates (lower GRT) can enhance the productivity at the expense of CO conversion, as a higher fraction of the gas is also wasted. The Pareto front in Fig. 3.8a is projected on the x-y axis, with the highest productivity (1.5 g.L^{-1}.h^{-1}) corresponding to 55% CO conversion. These points are the so-called non-dominated solutions, at which none of the objective functions can be improved without harming the other. The decision variables GRT and D_{rate} tied to these points are plotted along the Pareto curve with their normalized values on the z-axis. The other decision variables (including kinetic parameters) are not shown because their variation along the Pareto curve was considerably smaller, but maximum and minimum values of all decision variables from the set of Pareto-optimal points are presented in Table A2-5 (Appendix A2.). In a second run (Fig. 3.8b), the gas composition was changed to a H_2-rich gas, i.e. $[H_2:CO:CO_2]$ = [50:45:5]. Unexpectedly, for this case the CO conversion could be maximized to 100% over a wide range of productivities, therefore instead of depicting a Pareto front, Fig. 3.8b presents the solutions of ethanol productivity obtained under 100% CO conversion, with the corresponding normalized GRT and D_{rate} plotted on the y-axis. It's also worth noting that, with a high content of H_2, even a relatively small GRT of 8.2 min enabled full conversion of CO while also achieving a high productivity of 1.92 g.L.h^{-1} – this point can thus be selected as the optimal solution in terms of both productivity and conversion.

By analyzing the results of the kinetic parameters in both runs, it is clear that employing a H_2-rich gas also boosts the sensitivity of H_2-related parameters, in special the parameter v_{max,H_2}^{AcR} which is related to the reduction of acetic acid – the average value of this parameter in the optimal solutions increased from 1.4 to nearly 20 mmol.g^{-1}.h^{-1} from the CO-rich to the H_2-rich optimization run. Interestingly, the parameter $v_{max,CO}^{AcR}$ was on average 20% smaller in the second case, while the other parameters remained more or less constant. It was also noted that the parameters of cell yield on CO and death constant were close to their specified bounds in both cases, with $Y_{X,CO}$ being close to 2.4 g.mol^{-1} (the value

estimated with the data from C3-C) and k_d being close to 0.007 h^{-1} (the value estimated with the data from C1). While this result demonstrates the efficacy of manipulating kinetic parameters to improve bioreactor performance, it also raises the question as to whether it would be feasible in real operation to use medium formulation and genetic engineering to change the parameters independently from each other.

Finally, a third optimization was conducted adopting the $H_2:CO$ ratio in the feed gas as a new decision variable, which was allowed to vary between 0 (pure CO) and 3 (25% CO and 75% H_2). Also for this case, shown in Fig. 3.8c, the solutions did not form a Pareto front, as 100% CO conversion was attainable for a wide range of productivities. Fig. 3.8c is hence analogous to Fig. 3.8b but $H_2:CO$ is included, although it is basically constant for all solutions at around 0.78 – 0.86. The maximum productivity that can be obtained with 100% CO conversion is just over 2.0 $g.L^{-1}.h^{-1}$, which is achieved with GRT = 8.6 min, D_{rate} = 0.06 h^{-1}, XP = 0.11 and $H_2:CO$ = 0.85 (i.e. 54% CO and 46% H_2). The kinetic parameters at this solution are: $v_{max,CO}$ = 40.3 $mmol.g^{-1}.h^{-1}$, v_{max,H_2} = 34.8 $mmol.g^{-1}.h^{-1}$, $Y_{X,CO}$ = 2.37 $g.mol^{-1}$, Y_{X,H_2} = 0.223 $g.mol^{-1}$, $v_{max,CO}^{AcR}$ = 34.2 $mmol.g^{-1}.h^{-1}$, v_{max,H_2}^{AcR} = 16.6 $mmol.g^{-1}.h^{-1}$, $K_{S,CO}^{AcR}$ = 398 $mmol.L^{-1}$, K_{S,H_2}^{AcR} = 396 $mmol.L^{-1}$, and k_d = 0.00546 h^{-1}. It's noteworthy that all of these parameters, with the exception of the yield coefficients, remain relatively close to the nominal parameters estimated for C2, in fact inside their confidence intervals, which suggests that efforts should be concentrated on enhancing the cell yields and not, for example, the maximum uptake rates (at least for the conditions of gas-liquid mass transfer encompassed by this study). Even though v_{max} is directly associated with the cell's capacity to take up substrate, the uptake rate might just be limited by the mass transfer, such that after a certain point there would be no actual gain with increasing v_{max}.

Another result from the optimization studies is that high productivities would be attained with very large cell concentrations reaching up to 30 $g.L^{-1}$ (results shown in Fig. A2-8 of the Supp. Mat.), although this depends on the gas composition. For example, 1 $g.L^{-1}.h^{-1}$ of ethanol productivity would be attainable with H_2-rich gas with operating conditions and kinetic parameters that result in 10 $g.L^{-1}$ of cell mass, while for CO-rich gas the cell concentration would be a little over 20 $g.L^{-1}$ for the same ethanol productivity.
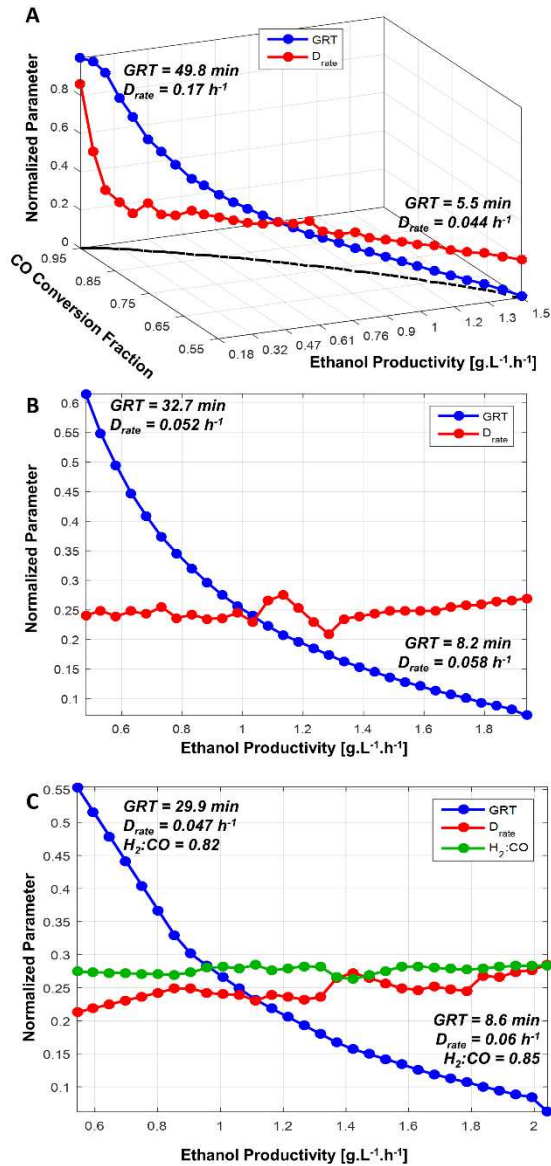
Figure 3.8. Pareto-optimal solutions for maximization of steady-state ethanol productivity and CO conversion: (A) fixed gas composition at 65% CO, 20% H_2 and 15% CO_2 with normalized decision variables *GRT* and D_{rate} plotted in the z-axis; (B) fixed gas composition at 45% CO, 50% H_2 and 5% CO_2, all points correspond to 100% CO conversion; (C) H_2:CO ratio free to vary between 0 and 3, all points correspond to 100% CO conversion. In all cases the decision variables are normalized with respect to their lower and upper bounds, i.e. *GRT* between 5 – 50 min and D_{rate} between 0.005 – 0.2 h^{-1}. The values of the most relevant decision variables at the solutions are shown in the Supp. Mat., Tables (A2-6)-(A2-8).

Agitation rate and gas recycle rate are also important operating variables which were not included in this study, but should be evaluated in the future with the inclusion of power consumption as a third objective function. It is possible, for example, that under certain conditions the gains in productivity and conversion might compensate for any extra spending with electricity. Other reactor designs should also be evaluated, such as bubble column, gas-lift, and membrane reactors. Ultimately, however, the bioreactor should be optimized simultaneously with other unit operations, such as gasification and distillation, since optimal conditions in one unit might lead to worse outcomes in other units with respect to economic and/or environmental issues.

3.5. Conclusions

A dynamic model was presented for the production of ethanol via syngas fermentation in a continuous stirred tank reactor, and unknown kinetic parameters were estimated with literature data employing different conditions of gas flow rate, dilution rate, syngas composition and medium composition. The modeling framework was then used to evaluate the effects of different input variables on the outcomes of ethanol productivity and gas conversion, and it was observed that cell recycle rate, gas flow rate and H_2 content had clear positive effects on the productivity, while the dilution rate gives a different maximum depending on the other variables. Moreover, the kinetic parameters were found to have different sensitivity patterns depending on the process conditions, for example some of them having larger effects on the productivity when higher gas flow rates are used. Since these parameters are specific to the type of strain and composition of the liquid medium, we conducted an optimization of productivity and conversion using operating conditions and kinetic parameters as decision variables, thereby showing the possibility of attaining higher values of both responses at the same time. Implementation of the results predicted in this work would require further studies connecting the kinetic parameters to the exact aspects of the liquid medium and strain capabilities, as well as more experiments investigating the inhibitory effects of products and CO. Therefore, as more experimental data becomes available the modeling framework presented here can be used to re-estimate parameters, generate more accurate results and provide new insights for integrated process optimization.

Acknowledgments

References

Bertsch, J., & Müller, V. (2015). Bioenergetic constraints for conversion of syngas to biofuels in acetogenic bacteria. Biotechnology for Biofuels, 8, 1–12. https://doi.org/10.1186/s13068-015-0393-x

Buehler, E. A., & Mesbah, A. (2016). Kinetic study of acetone-butanol-ethanol fermentation in continuous culture. PLoS ONE, 11(8), 1–21. https://doi.org/10.1371/journal.pone.0158243

Chang, I. S., Kim, B. H., Lovitt, R. W., & Bang, J. S. (2001). Effect of CO partial pressure on cell-recycled continuous CO fermentation by Eubacterium limosum KIST612. Process Biochemistry, 37(4), 411–421. https://doi.org/10.1016/S0032-9592(01)00227-8

Chen, J., Daniell, J., Griffin, D., Li, X., & Henson, M. A. (2018). Experimental testing of a spatiotemporal metabolic model for carbon monoxide fermentation with Clostridium autoethanogenum. Biochemical Engineering Journal, 129, 64–73. https://doi.org/10.1016/j.bej.2017.10.018

Chen, J., Gomez, J. A., Höffner, K., Barton, P. I., & Henson, M. A. (2015). Metabolic modeling of synthesis gas fermentation in bubble column reactors. Biotechnology for Biofuels, 8, 1–12. https://doi.org/10.1186/s13068-015-0272-5

China News Service. (2018). Beijing iron maker to turn waste gas into biofuels. Retrieved from http://www.ecns.cn/business/2018/02-28/293914.shtml

Cui, Y. Q., Van der Lans, R. G. J. M., & Luyben, K. C. A. M. (1996). Local power uptake in gas-liquid systems with single and multiple rushton turbines. Chemical Engineering Science, 51(1), 2631–2636. https://doi.org/10.1016/0009-2509(96)00128-5

de Medeiros, E. M., Posada, J. A., Noorman, H., Osseweijer, P., & Filho, R. M. (2017). Hydrous bioethanol production from sugarcane bagasse via energy self-sufficient gasification-fermentation hybrid route: Simulation and financial analysis. Journal of Cleaner Production, 168, 1625 – 1635. https://doi.org/10.1016/j.jclepro.2017.01.165

Férnandez-Naveira, Á., Abubackar, H. N., Veiga, M. C., & Kennes, C. (2016). Carbon monoxide bioconversion to butanol-ethanol by Clostridium carboxidivorans: kinetics and toxicity of alcohols. Applied Microbiology and Biotechnology, 100, 4321–4240. https://doi.org/10.1007/s00253-016-7389-8

Gaddy, J. L., Arora, D. K., Ko, C.-W., Phillips, J. R., Basu, R., Wikstrom, C. V., & Clausen, E. C. (2007). US 7,285,402 B2.

Himmelblau, D. M. (1970). Process analysis by statistical methods. New York: John Wiley & Sons, Inc.

Kerby, R. L., Ludden, P. W., & Roberts, G. P. (1995). Carbon monoxide-dependent growth of Rhodospirillum rubrum. Journal of Bacteriology, 177(8), 2241–2244.

Jang, N., Yasin, M., Park, S., Lovitt, R. W., & Chang, I. S. (2017). Determination of volumetric gas–liquid mass transfer coefficient of carbon monoxide in a batch cultivation system using kinetic simulations. Bioresource Technology, 239, 387–393. https://doi.org/10.1016/j.biortech.2017.05.023

LanzaTech. (2018). LanzaTech commercial scale facilities. Retrieved April 26, 2018, from http://www.lanzatech.com/facilities/

Liew, F. M., Martin, M. E., Tappel, R. C., Heijstra, B. D., Mihalcea, C., & Köpke, M. (2016). Gas Fermentation-A flexible platform for commercial scale production of low-carbon-fuels and chemicals from waste and renewable feedstocks. Frontiers in Microbiology, 7, 1–28. https://doi.org/10.3389/fmicb.2016.00694

Maddipati, P., Atiyeh, H. K., Bellmer, D. D., & Huhnke, R. L. (2011). Ethanol production from syngas by Clostridium strain P11 using corn steep liquor as a nutrient replacement to yeast extract. Bioresource Technology, 102, 6494–6501. https://doi.org/10.1016/j.biortech.2011.03.047

Mohammadi, M., Mohamed, A. R., Najafpour, G. D., Younesi, H., & Uzir, M. H. (2014). Kinetic studies on fermentative production of biofuel from synthesis gas using Clostridium ljungdahlii. The Scientific World Journal, 2014(1), 1–8. https://doi.org/10.1155/2014/910590

Mohammadi, M., Mohamed, A. R., Najafpour, G., Younesi, H., Uzir, M. H. (2016). Clostridium ljungdahlii for production of biofuel from synthesis gas. Energy Sources, Part A: Recovery, Utilization, and Environmental Effects, 38(3), 427–434. http://dx.doi.org/10.1080/15567036.2012.729254

Pardo-Planas, O., Atiyeh, H. K., Phillips, J. R., Aichele, C. P., & Mohammad, S. (2017). Process simulation of ethanol production from biomass gasification and syngas fermentation.

Bioresource Technology, 245, 925–932. https://doi.org/10.1016/j.biortech.2017.08.193

Phillips, J. R., Klasson, K. T., Clausen, E. C., & Gaddy, J. L. (1993). Biological production of ethanol from coal synthesis gas - Medium development studies. Applied Biochemistry and Biotechnology, 39–40(1), 559–571. https://doi.org/10.1007/BF02919018

Phillips, J. R., Clausen, E. C., Gaddy, J. L. (1994). Synthesis gas as substrate for the biological production of fuels and chemicals. Applied Biochemistry and Biotechnology, 45/46, 145–157. https://doi.org/10.1007/BF02941794

Rajagopalan, S., Datar, R. P., & Lewis, R. S. (2002). Formation of ethanol from carbon monoxide via a new microbial catalyst. Biomass and Bioenergy, 23, 487–493. https://doi.org/10.1016/S0961-9534(02)00071-5

Ramió-Pujol, S., Ganigué, R., Bañeras, L., & Colprim, J. (2018). Effect of ethanol and butanol on autotrophic growth of model homoacetogens. FEMS Microbiology Letters, 365(10), 1--4. https://doi.org/10.1093/femsle/fny084

Richter, H., Molitor, B., Wei, H., Chen, W., Aristilde, L., & Angenent, L. T. (2016). Ethanol production in syngas-fermenting Clostridium ljungdahlii is controlled by thermodynamics rather than by enzyme expression. Energy and Environmental Science, 9(7), 2392–2399. https://doi.org/10.1039/c6ee01108j

Roy, P., Dutta, A., & Deen, B. (2015). Greenhouse gas emissions and production cost of ethanol produced from biosyngas fermentation process. Bioresource Technology, 192, 185–191. https://doi.org/10.1016/j.biortech.2015.05.056

Talbot, P., Gortares, M. P., Lencki, R. W., & de la Nouë, J. (1991). Absorption of CO_2 in algal mass culture systems: A different characterization approach. Biotechnology and Bioengineering, 37, 834–842. https://doi.org/10.1002/bit.260370907

van 't Riet, K. (1979). Review of Measuring Methods and Results in Mass Transfer in Stirred Vessels Nonviscous Gas-Liquid. Ind. Eng. Chem. Process Des. Dev, 18(3), 357–364. https://doi.org/10.1021/i260071a001

Younesi, H., Najafpour, G., & Mohamed, A. R. (2005). Ethanol and acetate production from synthesis gas via fermentation processes using anaerobic bacterium, Clostridium ljungdahlii. Biochemical Engineering Journal, 27(2), 110–119. https://doi.org/10.1016/j.bej.2005.08.015

Chapter 4

Production of ethanol fuel via syngas fermentation: optimization of economic performance and energy efficiency

"Nothing takes place in the world whose meaning is not that of some maximum or minimum."

Leonhard Euler

4.1. Introduction

Biofuels are one of the possible means to reduce CO_2 emissions in transportation, a sector responsible for roughly 25% of global greenhouse gas (GHG) emissions in 2016 (IEA, 2019). However, the rapid expansion of 1st generation biofuels (i.e. those produced from food crops) has also been associated with impacts that were initially neglected or unforeseen, such as deforestation, indirect land use change, and significant GHG emissions during agricultural stages (Goldemberg et al., 2008). Lignocellulosic or 2nd generation biofuels have the potential to minimize these impacts by using waste carbon materials such as agricultural residues, forestry waste and marginal land (energy) crops. Yet, despite large efforts towards commercialization, most of these production pathways face technical challenges that are inherent to emerging technologies. An alternative path to biofuels and the object of this work is syngas fermentation, the microbial conversion of $CO/H_2/CO_2$ to ethanol and potentially other chemicals using facultative autotrophic bacteria called acetogens. Since syngas can be produced via gasification of multiple types of feedstocks – including even municipal solid waste –, this process is considered a promising and flexible alternative to biochemical routes that rely on the liberation of sugars from lignocellulosic biomass. Moreover, it also constitutes a valorization pathway for works arising gases (WAG) from steel production containing large amounts of CO, as demonstrated by the increasing number of commercial projects led by LanzaTech and partners in the past years (ArcelorMittal, 2019; Biofuels Digest, 2019; Renewables Now, 2018).

In order to upgrade the technology readiness level (TRL) and achieve full commercialization, not only scaling-up technical issues need to be resolved, but the process also needs to be boosted at different levels, for example: improving gas-liquid mass transfer through better reactor design; genetically engineering bacteria; adjusting the gasification process to deliver syngas with favorable composition; reducing energy use in the product recovery unit; and tuning the process conditions at all units simultaneously to approach overall optimal operation. Most published research about syngas fermentation has focused on running experiments to test the capabilities of different strains and reactor configurations, and to study the effects of changing nutritional composition of the liquid medium as well as the pH, such as done by Abubackar et al. (2015). Many studies have also tried to elucidate the metabolism of these microbes so that yield

and selectivity of the desired product (usually ethanol) can be improved (Richter et al., 2016). On the other hand, studies about modeling, simulation and optimization are still limited, despite being of paramount importance for the evaluation of feasibility and comprehension of these systems. A few recent works have discussed results obtained with simulations using Aspen plus, such as de Medeiros et al. (2017), Benalcázar et al. (2017), Pardo-Planas et al. (2017) and Roy et al. (2015). Though these studies look at the whole process from feedstock (biomass) to ethanol and provide meaningful estimates of process performance in different domains (technical, economic and environmental), the process conditions were mostly fixed or in some cases changed through univariate sensitivity analysis, and simulation of the bioreactor was based on strong assumptions and simplifications with limited connection to the operating conditions. In a previous study (de Medeiros et al., 2019), we discussed the contributions of more elaborate bioreactor models developed by other authors and presented the model of a dynamic continuous stirred tank (CSTR), demonstrating its application for sensitivity analysis and technical optimization. In the present work, we extended the CSTR model to a bubble column reactor model (BCR) with distribution of key process variables in time and space, and employed it in the optimization of operating (e.g. dilution rate) and design (e.g. reactor size) variables considering different objectives in parallel, both technical and economic. The BCR model was first considered standalone and subsequently integrated with the distillation unit, whose input was concurrently optimized. The contributions of this paper can be summarized as follows:

(i) Development of a spatial dynamic model of a bubble column reactor (BCR) for syngas fermentation considering kinetics of cell growth and death, mixed product formation and acetic acid re-assimilation.

(ii) Application of artificial neural networks as surrogate models for two types of intricate models: BCR model and distillation model (nonlinear system of MESH equations – material-equilibrium-summation-enthalpy – solved in Aspen Plus).

(iii) Development of a multi-objective optimization framework for the integrated process of anhydrous ethanol production from syngas via fermentation and distillation.

(iv) Evaluation of Pareto-optimal solutions for the most important input variables of the system, in terms of economic performance, thermodynamic efficiency and productivity.

4.2. Methodology

4.2.1. Process overview

Fig. 4.1 presents the conceptual process flowsheet to produce anhydrous ethanol from syngas, which consists of three main unit operations: (i) the syngas bioreactor (R-01); ethanol distillation (T-01 and T-02) to achieve azeotropic composition (also called hydrous ethanol); (iii) ethanol dehydration in molecular sieves (T-04 and T-05) to achieve 99.5% ethanol. There is also a vent scrubber (T-03) to recover any ethanol present in CO_2 off-gases. Three main types of stream are recycled to the bioreactor: (i) water from the distillation bottoms and the scrubber; (ii) unconverted syngas; and (iii) microbial cells. Sections 4.2.2 and 4.2.3 lay out the methodology for process design and modeling of the two main blocks of the process: fermentation and product recovery.

4.2.2. Model of syngas fermentation in bubble column reactor (BCR)

The syngas bioreactor consists of a bubble column where syngas enters at the bottom and off-gas leaves from the top, a fraction of it being recycled back to the bottom after compression and cooling. Liquid flows continually in and out of the reactor and a fraction of bacterial cells are recycled after separation from the products in a microfiltration membrane. In the reactor, cells are dispersed in the liquid phase, where they consume CO, H_2 and CO_2 and produce ethanol, acetic acid and CO_2. The latter is both a product from the oxidation of CO and a source of carbon in the reaction with H_2, therefore its consumption or production rate will depend on the availability of the other two molecules.
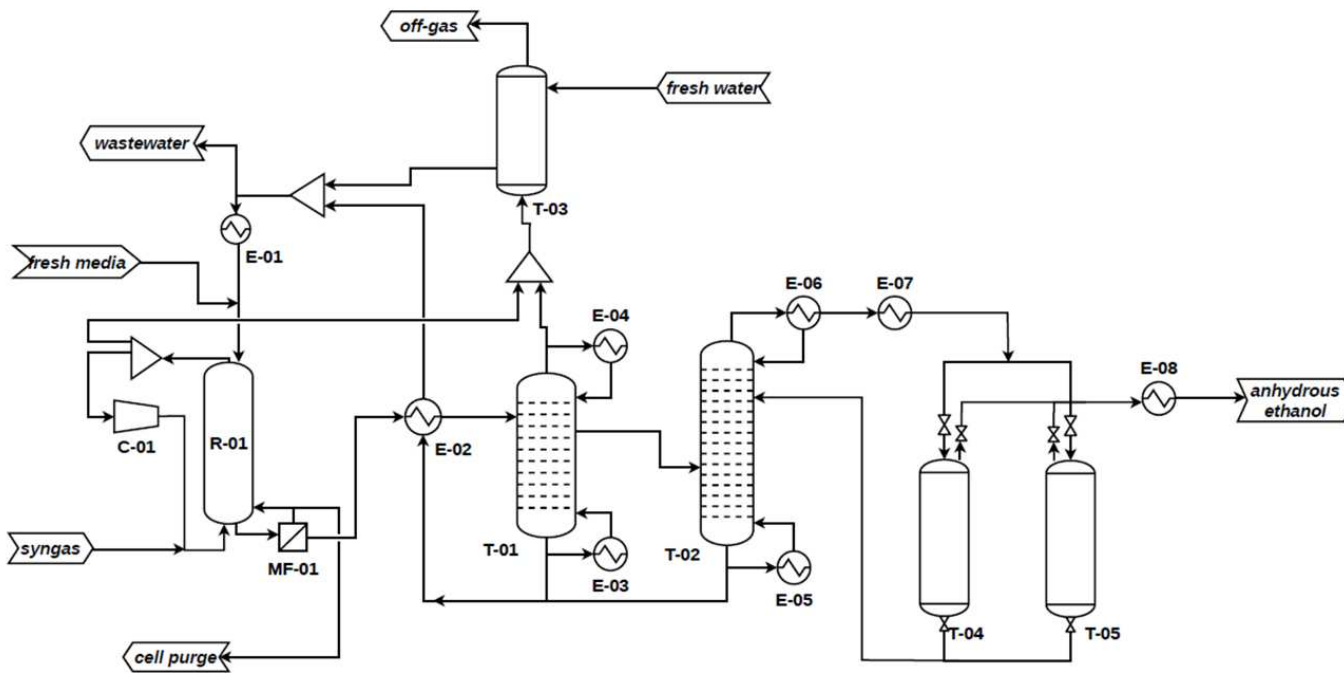
Figure 4.1. PFD of anhydrous ethanol production from syngas. C-01: gas compressor; E-01 to E-08: heat exchangers; R-01: syngas bubble column reactor; T-01 and T-02: distillation columns; T-03: vent scrubber; T-04 and T-05: adsorption and regeneration columns.

Similar models for this process with spatiotemporal distribution have been presented by Chen et al. (2018) and Li et al. (2019), the main difference being the method to calculate the consumption/production rates of components which in their works was done via Flux Balance Analysis (FBA) while in the present study we employ the microbial kinetics developed in our previous work (de Medeiros et al., 2019). Moreover, the procedure to estimate the gas velocity profile and hydrodynamic parameters (assumed constant by Chen et al. [2018]) is different. FBA is a powerful tool for the comprehension of cell metabolism, enabling for example in silico simulations about the effects of gene deletion and knockout; however, it also adds a significant amount of complexity to the model with the inclusion of a linear programming problem that must be solved during the integration of the ODEs. Furthermore, it requires the definition of an objective function (e.g. maximizing the biomass growth rate) and flux bounds which are not always known and might not be constant during the process. The kinetic model used in this work, on the other hand, is based on global reactions for the consumption of gases and formation of products, embedding parameters that were previously estimated with experimental data.

The BCR was described here with the axial dispersion model of Deckwer (1992), considering the following assumptions: (i) isothermal operation at T = 37 °C; (ii) axial dispersion considered in the liquid phase but neglected in the gas phase; (iii) the pressure profile is calculated from the liquid head; (iv) biochemical reactions occur in the liquid phase with rates depending on the concentrations of the components; (v) gas velocity changes along the column as the gas shrinks due to microbial conversion or expands due to pressure reduction; (vi) hydrodynamic parameters are a function of the gas superficial velocity assuming heterogeneous flow in air-water systems. In total 13 state variables are distributed in space: the concentrations [mol.m^{-3}] of six chemical species in the gas and in the liquid, i.e. $C_{G,i}$ and $C_{L,i}$ where i = CO, H_2, CO_2, ethanol (EtOH), acid acid (HAc), and H_2O; and the concentration of cells in the liquid $C_{L,X}$ [g.m^{-3}]. Eqs. (4.1)-(4.3) summarize the governing partial differential equations (PDEs) which are completed by the algebraic equations for the calculation of mass transfer rates (Eq. (4.4)) and cell kinetics. For the latter, the variables ν_i (production/consumption rates), μ (cell growth rate) and k_d (cell death rate) are calculated or specified as explained in de Medeiros et al. (2019), at each discrete point of the system. The physical properties H_i, $P_{sat,i}$ and γ_i can also be found in de Medeiros et al. (2019). In Eqs.

(4.2) and (4.3), a = 1 if the column is operating concurrently and a = -1 otherwise. For the optimizations in the present work, the latter is adopted.

$$\frac{\partial C_{G,i}}{\partial t} = -\frac{u_G}{\varepsilon_G} \cdot \frac{\partial C_{G,i}}{\partial x} - \frac{C_{G,i}}{\varepsilon_G} \cdot \frac{\partial u_G}{\partial x} - \frac{\dot{n}_{MT}}{\varepsilon_G} \qquad (4.1)$$

$$\frac{\partial C_{L,i}}{\partial t} = -\frac{au_L}{(1-\varepsilon_G)} \cdot \frac{\partial C_{L,i}}{\partial x} + D_L \frac{\partial^2 C_{L,i}}{\partial x^2} + \frac{\dot{n}_{MT}}{(1-\varepsilon_G)} + v_i C_{L,X} \qquad (4.2)$$

$$\frac{\partial C_{L,X}}{\partial t} = -\frac{au_L}{(1-\varepsilon_G)} \cdot \frac{\partial C_{L,i}}{\partial x} + D_L \frac{\partial^2 C_{L,i}}{\partial x^2} + (\mu - k_d)C_{L,X} \qquad (4.3)$$

$$\dot{n}_{MT} = k_L a_i (C_{L,i}^* - C_{L,i}) \quad, \ C_{L,i}^* = \frac{C_{G,i}}{m_i} \ , \ m_i = \frac{H_i \cdot MM_L}{R \cdot T \cdot \rho_L}, \ i = CO, H_2, CO_2 \qquad (4.4a)$$

$$\dot{n}_{MT} = -k_L a_i (C_{G,i}^* - C_{G,i}) \quad, \ C_{G,i}^* = \frac{C_{L,i}}{m_i}, \ m_i = \frac{\rho_L \cdot R \cdot T}{MM_L \cdot \gamma_i \cdot P_{sat,i}} \ i = EtOH, HAc, H_2O \qquad (4.4b)$$

The gas hold-up ε_G and the volumetric mass transfer coefficient $k_L a$ [h^{-1}] were calculated from the correlations by Heijnen and van't Riet (1984), adapted in Eqs. (4.5)-(4.6), where u_G [m.h^{-1}] is the gas superficial velocity. In Eq. (4.6), the first term between brackets is the $k_L a$ for air in water at 20°C, which is adjusted to component i using the diffusivity coefficient Df_i, and to the reactor temperature by means of the coefficient $K_T = (1.024)^{(T-20)} = 1.5$ (Heijnen and van't Riet, 1984). The axial dispersion coefficient D_L [m^2.h^{-1}] (Eq. (4.7)) is calculated with the correlation provided by Deckwer et al. (1974).

$$\varepsilon_G = 0.6(u_G / 3600)^{0.7} \qquad (4.5)$$

$$k_L a = \left[(3600) \left(0.32 \cdot (u_G / 3600)^{0.7} \right) \right] \cdot \left(Df_i / Df_{O_2,air} \right)^{1/2} \cdot K_T \qquad (4.6)$$

$$D_L = (0.36) \left(2.7 \cdot (d_C \cdot 100)^{1.4} \cdot (u_G / 36)^{0.3} \right) \qquad (4.7)$$

Finite differences were used to transform the system of partial differential algebraic equations (PDAE) to a system of ordinary differential algebraic equations (DAE). This stiff problem was solved in MATLAB R2015b using ode15s, which is usually the first recommended option before trying other stiff solvers such as ode23s. The state vector contained thus 13·N variables where N = 15 is the number of discretization points. The boundary conditions for both phases at

the bottom (x = 0) and at the top (x = L), considering counter-current operation, are shown in Eqs. (4.8) and (4.9).

$$C_{G,i}\big|_{x=0} - C_{G,i}^{in} = 0 \ , \ \frac{\partial C_{L,i}}{\partial x}\bigg|_{x=0} = 0 \tag{4.8}$$

$$\frac{\partial(C_{G,i} \cdot u_G)}{\partial x}\bigg|_{x=L} = 0 \ , \ C_{L,i}\big|_{x=L} - C_{L,i}^{in} + \frac{(1-\varepsilon_G)D_L}{u_L} \cdot \frac{\partial C_{L,i}}{\partial x}\bigg|_{x=L} = 0 \tag{4.9}$$

The gas velocity u_G was calculated along the reactor by applying a mole balance in the gas phase of each compartment starting from the bottom. If the gas recycle ratio (GRR) is greater than zero (where GRR is the ratio between the gas flow rate recycled to the bottom of the bioreactor and the total gas flow rate at the top), then the flow rate and composition of the inlet are different from those of the fresh syngas. In these cases an iterative procedure was applied to find the correct properties of the inlet stream and the gas velocity profile: first an initial guess is assumed at the bottom and used for the calculation of the velocity along the column, the new properties calculated at the top are then used to re-calculate the properties at the bottom, which replace the initial guess in the next iteration; the velocity profile is calculated again and this procedure is repeated until the differences are negligible between two consecutive iterations. Though this subroutine makes the model more intricate, neglecting the change in gas velocity is an unrealistic assumption (Deckwer, 1976) and substantial differences (>50%) between the velocity at the inlet and outlet have been observed not only with the model developed here but also by Li et al. (2018).

4.2.3. Product recovery unit

Anhydrous ethanol is recovered using distillation and molecular sieve adsorption. In the present work, the design of these operations was based on the flowsheet described by Humbird et al. (2011) for purification of ethanol produced via 2nd-generation biochemical route (dilute-acid pretreatment and enzymatic hydrolysis). First, the dilute broth (1 – 4% w/w ethanol) is fed to a beer column (T-01), from which water is removed at the bottom and CO_2 at the top, while concentrated ethanol is removed as a vapor-side stream and fed to the rectification column (T-02). The design choices adopted by Humbird et al. (2011) were considered as starting point and a preliminary analysis was done to evaluate the effects of different parameters (results not shown here). In the first column it

was observed that the mass ratio of side stream to feed stream (S:F) had significantly stronger effects on the outcome (reboiler duty, ethanol recovery and concentration) than other parameters, therefore this was chosen as the only decision variable in this column. The other parameters were fixed in accordance with the abovementioned design, though with minor modifications: 25 stages, feed stream on the 5th stage from the top, vapor-side stream removed from the 7th stage, top pressure of 2 bar, and molar reflux ratio (RR) of 3:1. Though in the design presented by Humbird et al. (2011) the fermentation broth had a higher ethanol concentration (5.4 % w/w), increasing RR beyond 3:1, even for lower ethanol concentrations, was found to have marginal effects on the separation performance, especially if considering the increased reboiler duty. The mass flow rate of the top stream, which is rich in CO_2, was defined so as to ensure that most of the dissolved CO_2 is removed, therefore it was fixed at 1.1 times the mass flow rate of CO_2 present in the feed stream.

The hot bottom stream from T-01, which contains most of the acetic acid from the feed, is used to pre-heat the latter (in E-02), whereas the CO_2 stream, together with off-gas from the BCR, is fed to the vent scrubber (T-03) to recover any ethanol that is present in these streams. The outlet liquid stream from T-03 is then mixed with bottoms from both distillation columns and part of the resulting stream is recycled to the bioreactor while the rest is sent to wastewater treatment. The concentrated ethanol stream from T-01, which contains between 20 – 40% w/w depending on the case, is sent to the rectification column (T-02) where it is further concentrated to near-azeotropic composition (92.5% w/w). The only fixed parameter in T-02 is the pressure (atmospheric); all the other inputs are decision variables, as explained further in Sec. 4.2.5. The distillate from T-02 is removed as saturated vapor and superheated to 116 ºC before being sent to dehydration with molecular sieves (columns T-04 and T-05). This unit was not modelled but instead the outcomes were fixed considering two output streams: (i) the product (anhydrous ethanol, 99.5% w/w) which is then cooled to 38 ºC (E-08); and (ii) a low-purity ethanol stream (72% w/w) produced during the regeneration step, which is recycled back to the rectifier.

The distillation columns were simulated in Aspen plus using the RadFrac model which solves the system of MESH equations with the Inside-Out algorithm. Four components were considered: water, ethanol, acetic acid and CO_2. The property methods were: for the liquid phase, the activity coefficient model NRTL, due to the

non-ideal ethanol-water mixture; and for the gas phase, Hayden-O'Connell equation-of-state with Henry's law, due to low pressure, presence of acetic acid which may cause vapor phase association, and presence of dissolved gases (CO_2).

4.2.4. Artificial Neural Network (ANN) surrogate models

Surrogate modeling techniques have been applied by many authors in the past years with the goal of reducing the complexity of computationally expensive models. Throughout this paper we refer to the latter as "rigorous" models, although they also incorporate some level of simplification (e.g. equilibrium equations in the calculation of distillation columns).

Recent works, such as Ibrahim et al. (2018) and Ye et al. (2019) have demonstrated the efficacy of this methodology for separation processes, specifically for distillation and adsorption. In the present work, ANNs were trained with input from the two types of models laid out in Sec. 4.2.2 and 4.2.3: (i) the PDAE system describing the BCR; and (ii) the RadFrac models in Aspen plus describing the distillation columns. In both cases, multi-layer feedforward networks were trained with Bayesian regularization backpropagation using the ANN Toolbox in MATLAB R2015b. The networks contained one input layer, one output layer and two hidden layers, with the number of neurons per hidden layer being chosen after a few tests (in all cases between 5 and 25). For some responses, an ensemble of networks was used to reduce the error of a single network by averaging the predictions of the individual networks and removing outliers. For all trained ANNs the correlation coefficient (R value) between network output and original response was higher than 0.99.

4.2.4.1. Bubble column reactor ANNs

Data was generated with the BCR model by varying the input vector and exporting the steady-state responses obtained after integration of the ODE system over a sufficiently long time span. Around 2,000 points were used to train the ANNs. The input vector comprises in total 12 variables which are needed to define the DAE system, though not all of them are used as decision variables in the optimization: (i) dilution rate (D_{rate}), defined as the liquid volumetric flow rate (Q_L) divided by the liquid volume (V_L) in the bioreactor; (ii) the volume of liquid divided by the gas volumetric flowrate at the bottom of the reactor ($V_L/Q_{g,bot}$) which we refer to here as gas residence time (GRT) ; (iii) gas recycle ratio (GRR) defined in Sec. 4.2.2;

(iv) cell purge fraction (XP), which is the fraction of biomass cells that are not recycled to the bioreactor; (v) vessel length (L); (vi) vessel aspect ratio (AR); (vii) and (viii) concentrations of acetic acid and ethanol in the inlet liquid stream; (ix) to (xii) molar fractions of CO, H_2, CO_2 and H_2O in the fresh syngas (note: for the optimization studies the syngas composition was fixed at 50% CO and 50% H_2). It should be noted that although the liquid inlet composition (items vii and viii) is an input of the bioreactor, it is not an input of the integrated process (and even less a decision variable in the optimization), because it depends on the properties of the recycle streams from the distillation unit.

The input matrix was generated using Latin hypercube sampling (LHS) to ensure good coverage of the input domain, which considers realistic ranges of these variables (presented together with optimization results in Tables 4.1 and 4.2). ANNs were trained to predict ten responses that are needed in the calculation of the objective functions or as input for the distillation unit. These responses belong to five categories: (i) concentrations of ethanol, acetic acid, cell biomass and dissolved CO_2 at the liquid outlet; (ii) gas superficial velocities at the bottom and at the top; (iii) gas conversions of CO and H_2; (iv) pressure at the bottom (this response is not straightforward because it depends on the gas hold-up which is not fixed); (v) total cooling duty to keep the reactor isothermal.

4.2.4.2. Distillation columns

Data for the distillation columns was generated using Aspen plus and Aspen Simulation Workbook, which was used to launch the simulations automatically (roughly 2,000 points for each column). The main aspects of the simulations were detailed in Sec. 4.2.3; and the following variables were considered inputs for the ANNs, some of them being outputs of the bioreactor and others being key parameters related to the design and operation of the distillation column: (i) inlet mass fractions of ethanol, acetic acid and CO_2; (ii) number of stages (N_{ST}); (iii) feed stages (F_{ST}); (iv) molar reflux ratio (RR); (v) mass ratio of side to feed stream (S:F), only for T-01; (vi) mass ratio of distillate to feed stream (D:F), only for T-02; (vii) pressure at the top; (viii) feed stream mass flow rate. It should be noted that N_{ST} and F_{ST} are continuous variables when provided to the ANNs and for their training, but they are transformed to integer values before running the Aspen simulations. F_{ST} is written as a fraction of the number of stages, such that $F_{ST} = 0$ when the feed

stage is the first after the reboiler and $F_{ST} = 1$ when it is the last before the condenser.

The following outputs were considered: (i) mass fractions of ethanol and acetic acid at the bottom, at the top, and at the side stream (only for T-01); (ii) same for temperatures; (iii) column diameter; (iv) reboiler and condenser duties.

Multilayer feedforward neural networks were trained for both pattern recognition and function approximation. In the first case, the ANNs were trained to classify the input vector as feasible or infeasible according to the convergence status of the Aspen simulations. The results of the successful simulations were then used to train the ANNs as explained previously in Sec. 4.2.4.

4.2.5. Optimization framework

Multi-objective genetic algorithm (MOGA) was employed to first optimize the standalone BCR and later the integrated process, with regard to the following objectives: (i) in the BCR, maximization of ethanol productivity and minimization of CAPEX; and (ii) in the whole process (shown in Fig. 4.1), minimization of CAPEX per annual production of anhydrous ethanol ($\dot{m}_{AE}$), minimization of minimum ethanol selling price (MESP) and maximization of thermodynamic efficiency (η). MOGA aims at finding a set of non-dominated (i.e. optimal) solutions approaching the true Pareto front of the system, i.e. those feasible points for which one objective function can only be reduced if other objective functions are increased. It's worth noting that MOGA does not use weighted functions to transform multiple objectives into one, therefore it ensures that objectives of different natures are considered fairly. Though other methods exist for multi-objective optimization, MOGA was chosen due to its robustness and easy implementation using the gamultiobj function in MATLAB R2015b, which employs a variant of the NSGA-II method (non-dominated sorting genetic algorithm).

For the standalone BCR, a population of 100 individuals was considered, while for the whole process populations ranging from 250 to 1,000 were tested at multiple runs. The objectives were always defined as minimization functions, hence in the first case (standalone BCR), the two objectives were: $OF_1 = -productivity = -D_{rate} \cdot C_{L,EtOH}$ and $OF_2 = CAPEX_{BCR}$. In the second case (whole process), two pairs of objectives were evaluated: (i) $OF_1 = CAPEX/\dot{m}_{AE}$,

$OF_2 = -\eta$; and (ii) $OF_1 = MESP$, $OF_2 = -\eta$. All the optimizations were performed for two case studies regarding mass transfer capacity: a base case and a high mass transfer case (HMT) in which the k_La calculated with Eq. (4.6) was multiplied by a factor of 3, representing thus a hypothetical case where process intensification methods are employed to increase mass transfer (this is further discussed in Sec. 4.3.3). A summary of the steps required to compute the objective functions is given next, along with the definition of the decision variables (DVs) (note that for the standalone BCR, the procedure stops after the 1st step):

1. DVs related to the BCR (D_{rate}, GRT, GRR, XP, L, V_R) and fixed inputs (e.g. gas composition) are provided to the BCR model, which employs ANNs to calculate multiple responses (broth composition, gas conversions, cooling requirements). The design variables and some of the responses are also used to calculate economic variables (investment, cost of raw materials and utilities), as explained in Sec. 4.2.5.1. Pure water is considered as initial guess for the liquid feed of the bioreactor (this is later adjusted as explained in step 4). Power consumption and cooling requirements associated with the gas compressor (C-01) are also calculated in this step.

2. Applicable responses from step 1 (e.g. broth composition), DVs related to T-01 (S:F) and fixed inputs are provided to the ANNs that calculate the outputs of T-01 (compositions of the streams, reboiler and condenser duties, column diameter). Similarly, some of the outputs (e.g. reboiler duty) and inputs (e.g. number of stages) are used to calculate economic responses.

3. Applicable responses from step 2, DVs related to T-02 (N_{ST}, $F_{ST,V}$, $F_{ST,L}$ and RR) and fixed inputs are provided to the model of T-02. In this step, the distillate to feed ratio (D:F) in T-02 is determined through a minor optimization routine to guarantee an ethanol mass fraction of 0.925 in the distillate. The ANNs are employed again with the complete input vector (including D:F) to generate the relevant responses; other outputs and inputs are used to compute economic results, and heating/cooling requirements are also calculated for the adsorption unit.

4. With the outputs from steps 2 and 3, the composition of the liquid recycle stream is calculated and compared with the initial guess. If required, an iterative procedure is followed to match both streams.

5. If the ethanol mass fraction in the distillate from T-02 is 0.925 and other requirements are met (no negative mass flows, ANN inputs inside their training ranges, equipment capacities inside feasible ranges), then the outputs from steps 1–4 are combined to generate the objective functions, as further explained in Sec. 4.2.5.1 and 4.2.5.2.

4.2.5.1. Computation of economic performance

Economic performance was evaluated in terms of total capital investment (CAPEX) and minimum ethanol selling price (MESP). The total investment was estimated using the module costing technique described by Turton et al. (2009), in which all the costs derive from the individual purchase cost of equipment at base conditions (C_p^0), estimated for each equipment of capacity A using Eq. (4.10). The total module cost (C_{TM}), which considers total direct and indirect costs, as well as contingencies and fees, is calculated as shown in Eq. (4.11). In the present work, CAPEX is considered the same as C_{TM}. The bare module cost of equipment i, $C_{BM,i}$, is calculated from $C_{p,i}^0$ applying bare module cost factors $F_{BM,i}$ which account for pressure, materials and other items such as installation and engineering. The coefficients K_1 and K_2 and the procedures to calculate F_{BM} for each type of equipment can be consulted in Turton et al. (2009).

$$\log_{10} C_p^0 = K_1 + K_2 \log_{10}(A) + K_2 \left[\log_{10}(A) \right]^2 \qquad (4.10)$$

$$C_{TM} = 1.18 \cdot \sum_i C_{BM,i} \quad , \quad C_{BM,i} = C_{p,i}^0 \cdot F_{BM,i} \qquad (4.11)$$

The manufacturing costs COM_d (also called operating expenses or OPEX) comprise direct costs (e.g. raw materials [C_{RM}], utilities [C_{UT}], waste treatment [C_{WT}], maintenance, operating labor [C_{OL}]), fixed costs (e.g. overhead, depreciation, insurance) and general expenses (e.g. administration, R&D). The different components of the manufacturing costs can be estimated using multiplication factors based on historical data; adding up all these costs leads to an expression such as Eq. (4.12), used in the present work, which considers midpoint values from the ranges reported in Turton et al. (2009).

$$COM_d = 0.18 \cdot C_{TM} + 2.73 \cdot C_{OL} + 1.23 \cdot \left(C_{UT} + C_{WT} + C_{RM} \right) \qquad (4.12)$$

The purchase price of syngas was considered 1 US$/kmol for the optimization runs, but its impact on MESP was later evaluated along with other economic parameters. The assumption was based on the ranges estimated with techno-economic modeling studies performed by Yao et al. (2018) and Martinez-Gomez et al. (2017) for syngas production from biomass and shale gas. Fuel for steam generation was considered to be sugarcane bagasse in Brazil, assuming a price of 2 US$/GJ which is inside the reported range from the last years (CanaOnline, 2019). The costs of utilities and waste treatment/disposal were calculated according to the methodology of Ulrich and Vasudevan (2006), also assuming an electricity price in accordance with the Brazilian context, at 0.12 US$/kWh (CPFL Energia, 2019). The cost of operating labor (C_{OL}) was assumed to be 3% of CAPEX.

With CAPEX (C_{TM}) and OPEX, the discounted cash flows can be calculated and the minimum ethanol selling price (MESP) can be found with a subordinate optimization routine to achieve NPV = 0, where NPV (Net Present Value) is the cumulative discounted cash flow at the end of the project. For this calculation a few considerations were made: (i) 15 years of project life and 2 years of construction; (ii) land cost = 7.5% C_{TM}; (iii) taxation rate = 35%; (iv) interest rate = 10%; (v) straight-line depreciation; (vi) project salvage value = 0; (vii) Chemical Engineering Plant Cost Index (CEPCI) = 615.9 as of December 2018 and CEPCI = 397 in base year (2001) (Chemical Engineering Magazine, 2019); and (viii) 350 days of operation per year.

4.2.5.2. Computation of thermodynamic performance

The thermodynamic performance was evaluated with the energy efficiency (η) as calculated in Eq. (4.15). The energy output is given by the lower heating value of ethanol fuel ($LHV_{AE} = 26.5$ MJ.kg^{-1}) multiplied by its production rate, and the total energy input is given by the LHV of syngas containing 50% CO and 50% H_2 ($LHV_{syngas} = 252.4$ MJ.kmol^{-1}) plus heat provided by steam at multiple parts of the process and the equivalent heat associated with the production of electricity consumed in compressors and pumps. For the latter, work-related energy was translated to heat by applying an electric generation efficiency of $\eta_{CC} = 60\%$ for combined cycles operating with natural gas (Siemens AG, 2019).

$$\eta = \frac{LHV_{AE} \cdot \dot{m}_{AE}}{LHV_{syngas} \cdot \dot{m}_{syngas} + \dot{E}_{in}} \ , \ \dot{E}_{in} = \sum \Delta \hat{H}_v \cdot \dot{m}_{steam} + \sum \dot{W}_{in} \big/ \eta_{CC} \qquad (4.15)$$

4.3. Results and Discussion

4.3.1. Techno-economic optimization of the bubble column reactor (BCR)

Fig. 4.2 presents the main results of the optimization conducted for maximization of ethanol productivity and minimization of capital cost considering the standalone BCR. The goal of this study was to analyze the trends in Pareto-optimal points before connecting the BCR to the purification unit. Firstly, there is a clear trade-off between the two objectives, as shown with the Pareto fronts depicted in Fig. 4.2a for both case studies (normal and high mass transfer – HMT), meaning that, as expected, higher productivities can be achieved at the cost of higher investments. The Pareto fronts also seem to comprise at least two convex sub-sets of solutions. For example, for the base case, one subset lies in the region with productivities ≤ 3.15, after which there is a clear change of pattern in the Pareto front, which nonetheless continues to be convex. It's worth recalling that the 1st objective function is the minimization of –productivity, so it is not the objective function itself that is plotted in the x-axis, but its opposite value. For both cases there is a threshold after which the capital costs continue to increase without significant improvement in the productivity (e.g. after 4.5 $g.L^{-1}.h^{-1}$ for the base case, as seen in Fig. 4.2a). These optimal solutions are associated with larger reactor volumes (hence higher capital costs) obtained by decreasing the vessel aspect ratio (the length remains constant, as seen in Fig. 4.2c); but since the gains in productivity are only marginal, these are solutions without interest to the decision-making process. It is also verified that increasing the mass transfer coefficient leads to higher productivities with the same investment, at some points being almost twice the value of the base case.
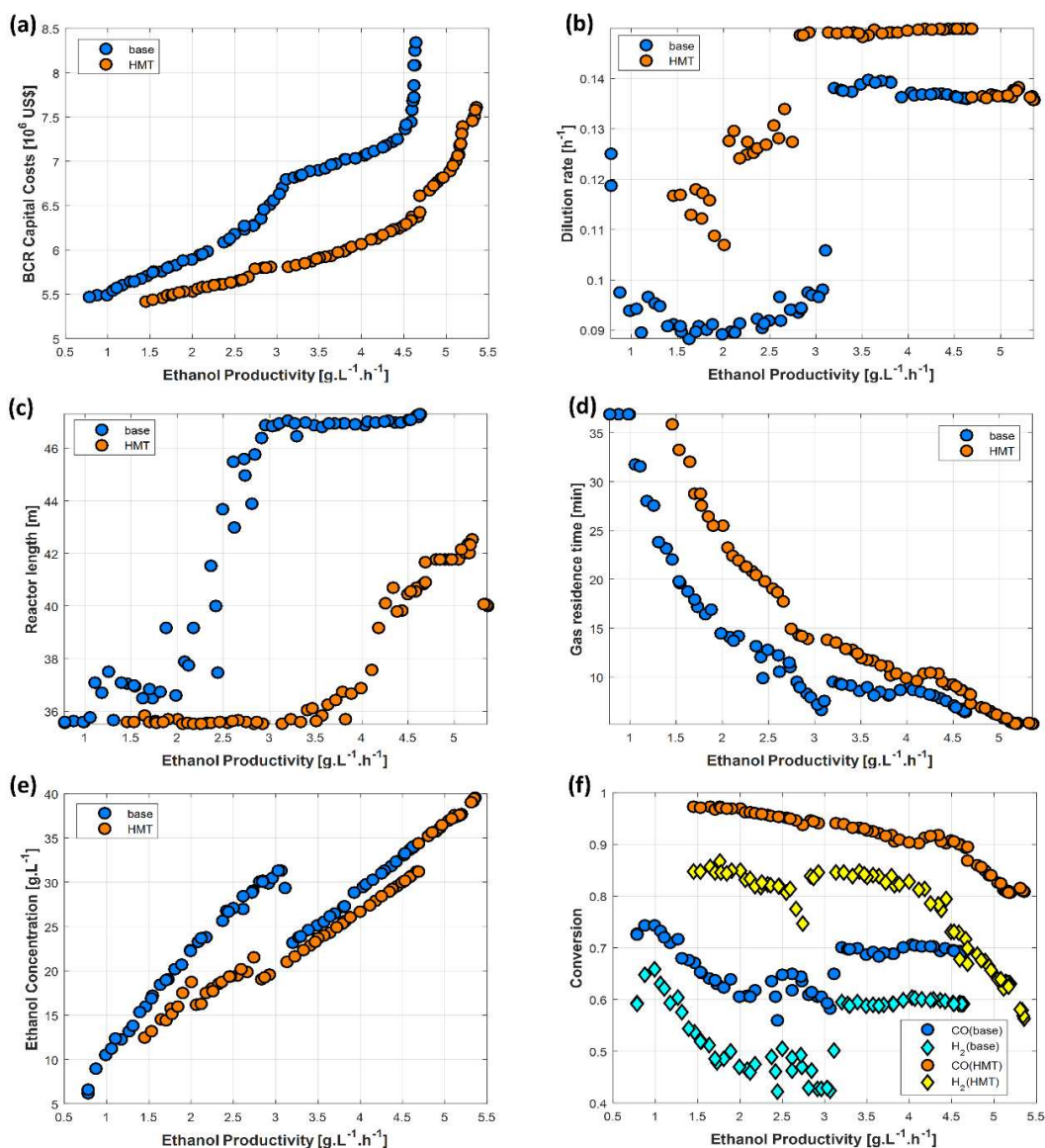
Figure 4.2. Bi-objective optimization of the BCR for maximization of ethanol productivity and minimization of capital costs: Pareto fronts (a); selected decision variables at the Pareto-optimal solutions (dilution rate (b), reactor length (c), and gas residence time (d)); selected process outcomes at the Pareto-optimal solutions (ethanol concentration (e), gas conversions (f)).

The different Pareto subsets are produced by different combinations of the decision variables, as shown in Figs. 4.2b-d. Both case studies show one subset of

solutions characterized by large and nearly constant values of dilution rate and reactor length. In this subset, the productivity continues to increase due to decreasing GRT (Fig. 4.2d) and increasing gas recycle ratio (not shown). In the preceding subset, the increase in productivity is not only due to decreasing GRT but also to increasing reactor length, in combination with changes in D_{rate} and GRR. These variations, of course, also have effects on the capital costs (as seen in Fig. 4..2a): for example, increasing the reactor length has a direct effect on the bioreactor cost; on the other hand, decreasing GRT implies increasing the gas flow rate, which brings higher costs associated with larger gas compressor capacities.

As presented in Table 4.1, the decision variables at the optimal solutions are constrained to similar ranges for both study cases (e.g. optimal vessel volumes are close to the lower bound of the stipulated search space), but the process outcomes are mostly improved when mass transfer is enhanced. Higher conversions are achieved for both CO and H_2 (shown in Fig. 4.2f), as well as higher ethanol concentrations (Fig. 4.2e), though in this case the HMT results also show lower concentrations for a wide range of productivities.

Table 4.1. Multi-objective optimization of the bubble column reactor: ranges of decision variables and process outcomes at the Pareto-optimal solutions.

	Search space	base	HMT
D_{rate} [h^{-1}]	0.01 – 0.15	0.088 – 0.14	0.11 – 0.15
GRT [min]	5 – 50	6.41 – 36.9	5.15 – 35.8
GRR	0 – 0.5	0.032 – 0.43	0.017 – 0.32
XP	0.05 – 0.2	0.035 – 0.049	0.025 – 0.056
L [m]	25 – 50	35.6 – 47.3	35.5 – 42.5
V_R [m^3]	500 – 900	502 – 572	500 – 548
$C_{L,EtOH}$ [g.L^{-1}]	-	6.21 – 34.1	12.5 – 39.5
$C_{L,HAc}$ [g.L^{-1}]	-	1.35 – 2.75	2.17 – 2.98
X_{CO}	-	0.56 – 0.74	0.81 – 0.93
X_{H_2}	-	0.42 – 0.66	0.56 – 0.87

4.3.2. Thermo-economic optimization of the integrated process

Integrating the BCR to the purification unit brought several difficulties due to the high non-linearity of the MESH equations, which often leads to infeasible solutions, and the inclusion of a recycle stream of distillate bottoms containing traces of ethanol and acetic acid. This was observed by the much longer time required to run the optimization (from 5 minutes to over 3 hours), despite the use of reduced (surrogate) models. Another reason for the higher complexity of the integrated model is that the input variables of the distillation columns must be set to guarantee an ethanol mass fraction of 0.925 in the distillate stream of the second column.

The generated Pareto fronts are depicted in Fig. 4.3, where again the opposite of an objective function is shown: for all fronts in Fig. 4.3, the 2nd objective function was to minimize $-\eta$, but η itself is plotted in the y-axis. As explained in Sec. 4.2.5, the optimization was performed for two mass transfer cases (base and HMT) and two pairs of objective functions. The difference between these pairs is the formulation of the 1st objective function, which is either to minimize CAPEX/$\dot{m}_{AE}$ (Fig. 4.3a-b) or MESP (Fig. 4.3c-d). It's worth mentioning that the results presented here are the best found approximations of the Pareto fronts, which were selected after multiple runs of the multi-objective genetic algorithm.
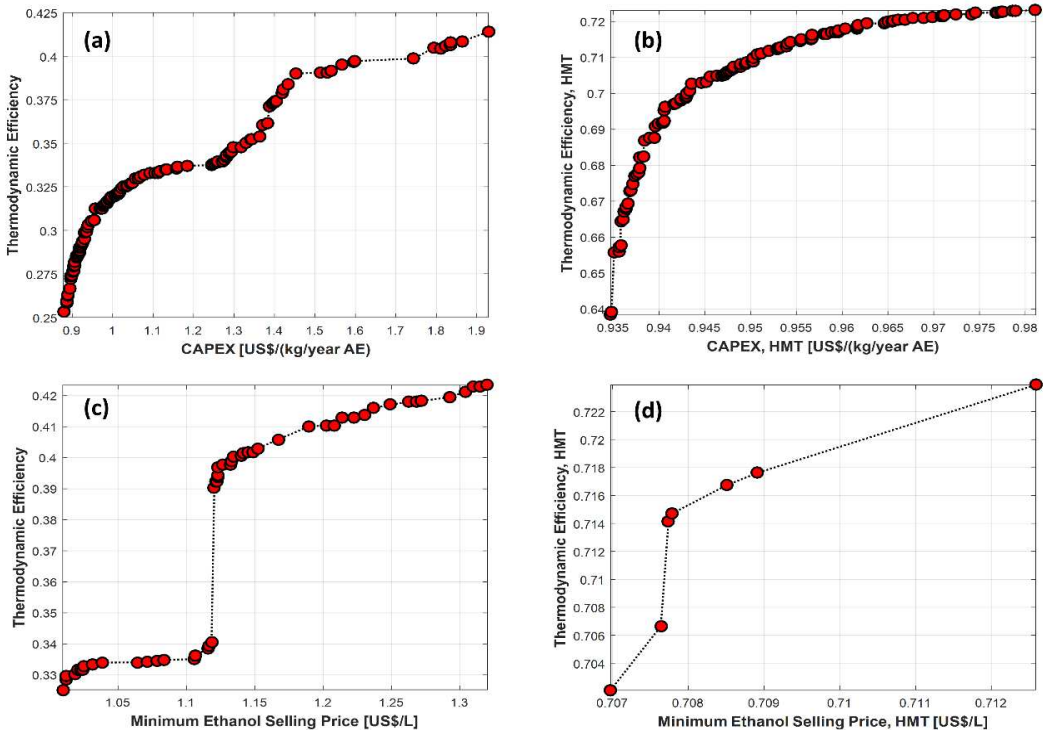
Figure 4.3. Bi-objective optimization of the integrated units: optimization A with base (a) and high mass transfer model (b); optimization B with base (c) and high mass transfer model (d).

The first observation is that the thermodynamic efficiency was bounded to around 0.42 in the base model and 0.72 in the HMT case, also with lower CAPEX and MESP achieved in the latter. The trade-off is visible for all cases, although the optimization of the η-MESP pair with HMT (Fig. 4.3d) led to a small set of non-dominated solutions distributed between $0.707 \leq$ MESP (US\$/L) ≤ 0.713. As explained by Goh and Tan (2009), finding a diverse set of solutions is specially challenging in the presence of multi-modality (i.e. multiple local Pareto fronts), discontinuity and non-uniformity. Moreover, balancing diversity of solutions and proximity to the true Pareto front is a multi-objective problem in itself, since these two qualities are both desirable and conflicting (Bosman and Thierens, 2003). Despite the lack of diversity in the solutions presented in Fig. 4.3d, the results are deemed sufficient for the purposes of the present work, and testing different algorithms to improve this aspect is left as recommendation for a future work.

To support the interpretation of the Pareto fronts, the Pareto-optimal values of two selected decision variables are shown in Fig. 4 along with process outcomes. In this figure, optimization A (Opt$_A$, circles) refers to the objective pair (CAPEX,η) and B (Opt$_B$, diamonds) to the pair (MESP,η). For both mass transfer cases, the increase in η (accompanied by increase in CAPEX and MESP) was associated with a decrease in D$_{rate}$ (Fig. 4a) and increase in GRT (Fig. 4b), though in the HMT case the range spanned by these variables was very narrow. Other DVs (not shown here) that had predominant increasing trends with η were the gas recycle ratio (GRR), the number of stages in T-02 and its reflux ratio. Fig. 4 also suggests that in the base case the Opt$_B$ Pareto front (MESPxη) constitutes a subset of Opt$_A$ (CAPEXxη), with decision variables and process outcomes following similar trends and ranges. This also happens to a lesser extent with HMT.

The minimum and maximum values of the optimal DVs are presented in Table 4.2, where it can be observed that for all case studies and optimization pairs the ranges were significantly reduced from the search space. For comparison, the ranges obtained by minimizing MESP as a single objective are also shown. The minimum values of MESP in this case were 0.958 US$/L (base) and 0.705 US$/L (HMT), but the energy efficiencies at these points were far from their highest values, at 0.31 and 0.50 respectively, indicating that inefficiencies are compensated by low price of resources. An intriguing outcome is that when optimizing a single objective many DVs had optimal values outside the ranges of the Pareto-optimal solutions; in fact, this was observed for all the DVs in the HMT case. For the gas recycle ratio (GRR) specially, the single-objective optimum was close to zero while being almost at the search space upper bound for Pareto-optimal points with higher η.

This illustrates the importance of using multi-objective as opposed to single-objective optimization: as technology progress is driven by multiple values other than economic profit, it is inevitable that industries will seek to optimize conflicting objectives; and not only bi-objective but many-objective problems will need to be tackled. In fact, even if the goals are kept within the economic sphere, it is still challenging to reduce them to a single variable, since different indicators can be used to evaluate the profitability of a process: CAPEX, MESP, OPEX, NPV, payback time, ROI (return on investment), etc.
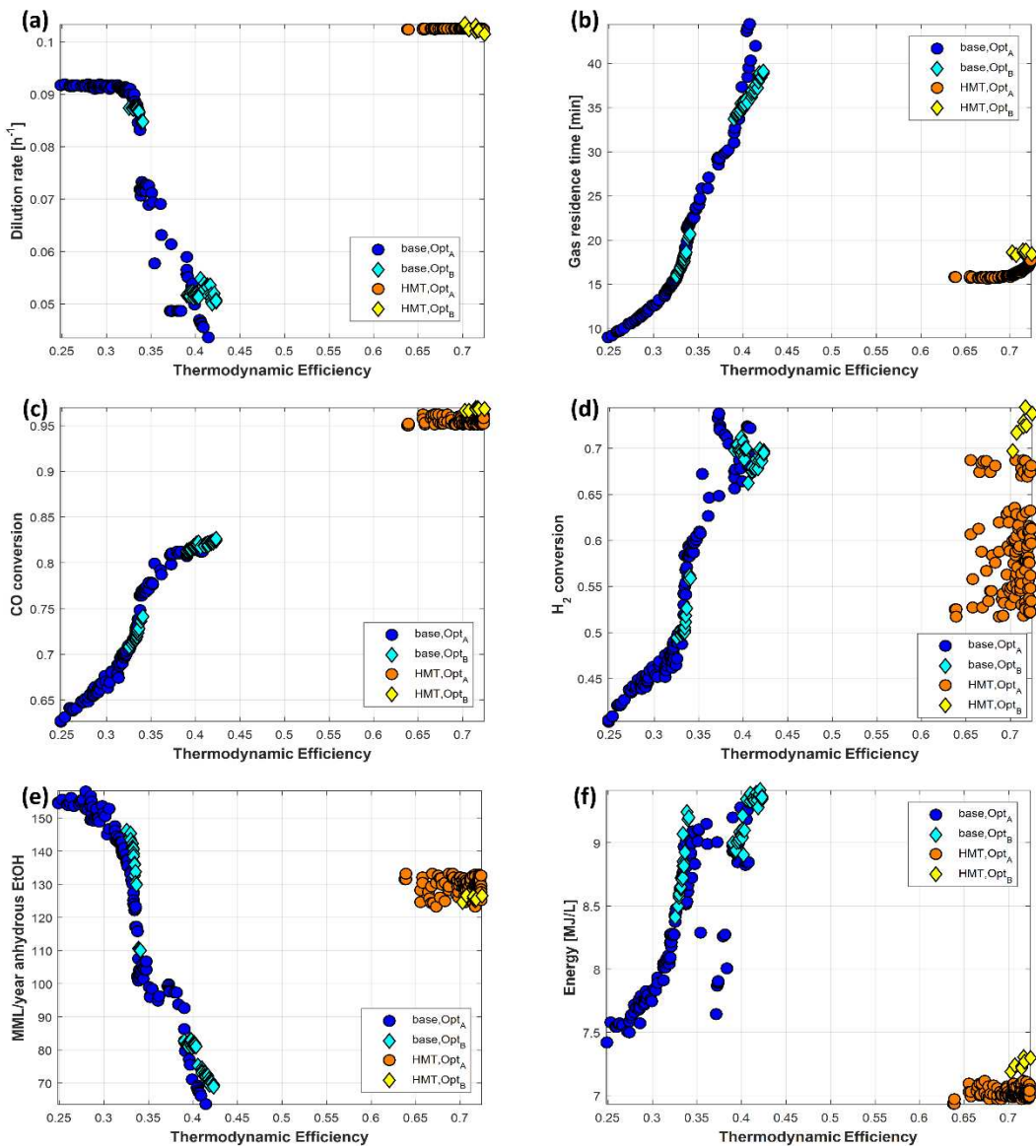
Figure 4.4. Bi-objective optimization of the integrated units: selected decision variables at the Pareto-optimal solutions (dilution rate (a) and gas residence time (b)); selected process outcomes at the Pareto-optimal solutions (CO conversion (c), H_2 conversion (d), production rate (e), and energy consumption (f)).

Table 4.2. Multi-objective and single-objective optimization of the integrated process: ranges of decision variables at the Pareto-optimal or optimal solutions.

	Search space	CAPEX x η	CAPEX x η (HMT)	MESP x η	MESP x η (HMT)	MESP	MESP (HMT)
D_{rate} (BCR) [h^{-1}]	0.01 – 0.15	0.044 – 0.092	0.1022 – 0.1025	0.050 – 0.087	0.101 – 0.103	0.099	0.106
GRT (BCR) [min]	5 – 50	8.95 – 44.4	15.7 – 17.7	15.9 – 39.1	18.3 – 18.9	14.5	21.3
GRR (BCR)	0 – 0.5	0.062 – 0.43	0.489 – 0.493	0.092 – 0.45	0.478 – 0.496	0.0086	0.061
XP (BCR)	0.05 – 0.2	0.084 – 0.19	0.0553 – 0.0639	0.12 – 0.17	0.044 – 0.054	0.198	0.0902
L (BCR) [m]	25 – 50	44.9 – 49.9	41.3 – 43.4	48.3 – 49.9	42.6 – 42.8	49.9	47.2
V_R (BCR) [m^3]	500 – 900	710 – 853	630 – 645	713 – 811	645 – 654	633	595
$S{:}F$ (T-01)	0.04 – 0.3	0.094 – 0.106	0.0796 – 0.0818	0.096 – 0.10	0.079 – 0.080	0.0963	0.0824
N_{ST} (T-02)	40 – 50	40 – 46	43 – 45	43 – 47	44	41	40
$F_{ST,V}$ (T-02)	0.6 – 0.9	0.62 – 0.76	0.755 – 0.773	0.61– 0.80	0.76 – 0.78	0.67	0.724
$F_{ST,L}$ (T-02)	0.2 – 0.5	0.26 – 0.47	0.336 – 0.359	0.297 – 0.496	0.34 – 0.36	0.22	0.456
RR (T-02)	3 – 6	4.4 – 5.80	3.78 – 3.89	5.14 – 5.83	3.95 – 4.02	5.25	4.17

It's worth noting that the optimization of the BCR alone is not enough for meaningful decision-making, since the operating and design variables of the purification unit must be adapted to the outcomes of the bioreactor and optimized accordingly. When analyzing the whole process, the possible choices for the operating conditions and design variables were optimized to give a range of solutions from which a single one can be picked. If both energy efficiency and MESP are considered equally important, an illustrative example for the base case is to take the solution at $\eta \approx 0.4$ following the notably steep increase in Fig. 4.3c, since after this point the gains in efficiency are relatively slow with respect to MESP. This solution gives the following decision variables: D_{rate} = 0.052 h^{-1}, GRT = 34.1 min, GRR = 0.37, XP = 0.13, L = 49.5 m, V_R = 772 m^3, S:F = 0.10, N_{ST} = 45, $F_{ST,V}$ = 0.65, $F_{ST,L}$ = 0.4, and RR = 5.55. For the high mass transfer case, a similar solution can be drawn out at $\eta \approx 0.714$: D_{rate} = 0.10 h^{-1}, GRT = 18.6 min, GRR = 0.49, XP = 0.05, L = 42.7 m, V_R = 652 m^3, S:F = 0.08, N_{ST} = 44, $F_{ST,V}$ = 0.76, $F_{ST,L}$ = 0.34, and RR = 3.95.

Relevant process outcomes are presented in Table 4.3. The average ethanol concentration in the broth was around 29 g.L^{-1} for the base case and 36 g.L^{-1} for the HMT case, with the acetic acid concentration staying under 4 g.L^{-1}. As consequence, lower energy consumption in the distillation unit (roughly 7.2 MJ/L ethanol) could be obtained with HMT, while the base case spans a range from 7.4 to 9.4 MJ/L, mostly increasing with η. The results also show that high CO conversions (Fig. 4.4c) of up to 97% can be achieved with increased mass transfer and 83% for the base case, while the H$_2$ conversions (Fig. 4d) were bounded to lower values (74%) in both cases, due to the CO inhibition as considered in the kinetic model. For comparison purposes, LanzaTech's process is able to achieve high and stable CO conversions above 90% and ethanol selectivity of 95% (LanzaTech, 2018). Though their process configuration might be similar to the one considered here, employing gas-liquid column reactors, distillation to purify ethanol, and water recycle, the exact design and conditions of their process are not reported. Another point worth mentioning is that in the present work the gas composition was fixed at 50% CO and 50% H$_2$, but the proportions of CO/H$_2$/CO$_2$ are also expected to have significant impacts on the gas conversion and ethanol productivity in the bioreactor (de Medeiros et al., 2019). Since the syngas composition is a result of design choices in upstream stages, which in turn also affect prices and energy efficiency, another study is currently under development

for the impact analysis and optimization of the whole process including syngas production via gasification.

The Pareto-optimal solutions of the integrated process span smaller ranges of ethanol productivity in the bioreactor than the BCR optimization, indicating that higher productivities are not necessarily advantageous when taking into account the whole process, due to much higher capital costs (also corroborated by the steep increase in the Pareto fronts from Fig. 4.2a) and losses in gas conversion (thus lower energy efficiency). With regard to the annual production of anhydrous ethanol (Fig. 4.4e), in the base case the trends are opposite to the energy efficiency, but with HMT there doesn't seem to be a correlation between the two, with the optimal production rate in this case being between 121–133 MML/year. However, if MESP is used as single objective both cases lead to similar production rates of around 121–124 MML/year (Table 4.3).

Table 4.3. Multi-objective optimization of the integrated process: ranges of process outcomes at the Pareto-optimal solutions.

	CAPEX x η	CAPEX x η (HMT)	MESP x η	MESP x η (HMT)	MESP	MESP (HMT)
$C_{L,EtOH}$ (BCR) [g.L^{-1}]	26.3 – 34.7	36.6 – 38.3	26.0 – 30.1	35.5 – 36.7	28.4	34.6
$C_{L,HAc}$ (BCR) [g.L^{-1}]	1.61 – 3.74	2.33 – 2.43	1.97 – 3.44	2.33 – 2.46	4.20	3.0
Heat consumption [MJ.L^{-1} AE]	7.42 – 9.35	6.93 – 7.11	8.41 – 9.41	7.18 – 7.30	8.71	7.45
Electricity consumption [kWh.L^{-1} AE]	0.40 – 0.58	0.37 – 0.41	0.40 – 0.53	0.36 – 0.37	0.43	0.25
X_{CO} (BCR)	0.63 – 0.82	0.95 – 0.96	0.71 – 0.83	0.97	0.68	0.97
X_{H_2} (BCR)	0.40 – 0.74	0.52 – 0.69	0.50 – 0.71	0.70 – 0.74	0.40	0.78
$\dot{m}_{AE}$ [MML.year^{-1}]	63.5 – 158	123 – 133	68.8 – 146	125 – 127	124	121
EtOH Productivity (BCR) [g.L^{-1}.h^{-1}]	1.17 – 3.19	3.74 – 3.93	1.33 – 2.63	3.66 – 3.73	2.81	3.67

4.3.3. Effects and prospects of mass transfer enhancement

It can also be observed in Fig. 4.4 and Table 4.2 that the optimal values of the decision variables differ significantly between the base case and the HMT case, demonstrating the importance of accurate $k_L a$ estimations for the effective application of model-based optimization results. Several factors could compel the real $k_L a$ to deviate from the predictions of empirical correlations such as Eq. (4.6),

for example the presence of salts and alcohols in low concentration, which have been shown to increase k_La by factors up to 2 (van de Donk, 1981). Heijnen and van't Riet (1984) have also noted that, in non-coalescing media, fine bubble systems can present a six-fold increase in k_La as compared to coarse bubble systems measured at the same gas superficial velocity, although in strongly coalescing media the difference is modest. Therefore the results presented here suggest that great improvements can be achieved with ingenious tuning of k_La via enhancement techniques. Ultimately, such "mass transfer enhancement" can be included as a factor in the optimization framework in order to find the optimal amount of efforts and costs that should be spent into increasing mass transfer capacity in the bioreactor. Examples of process intensification (PI) strategies for this purpose are given next.

Groen et al. (2005) presented a method to increase the oxygen transfer capacity in aerobic fermentation which consisted of injecting a second gas stream (pure oxygen) via a special nozzle configuration to achieve supersonic velocities and a non-uniform bubble size distribution. With a ratio of 6:1 between the two gas flows (air/pure oxygen) the authors were able to increase the mass transfer rate 3.6 times. Along the lines of reducing bubble size to increase the surface to volume ratio, the generation of micron size (< 1 mm) bubbles is generally considered an efficient way of enhancing gas-liquid mass transfer while requiring low power inputs: Bredwell and Worden (1998), for example, obtained a six-times higher k_La using a spinning-disk microbubble generator as compared to the conventional sparging system in a stirred tank for syngas fermentation. Moreover, while micro-porous diffusers can be used to generate microbubbles in a passing gas stream, several works have demonstrated even further size reduction by oscillating this stream, with the oscillation frequency in this case being a central optimization variable (Brittle et al., 2015). A myriad of other methods have also been reported for the formation of microbubbles, relying on different aspects: with or without accompanying liquid flows, using polymers or with very low power consumption such as microchannel techniques and ultrasonic systems (Parmar et al., 2013).

Finally, nanoparticles have also been shown to improve mass transfer, though only limited work has been developed for syngas fermentation. Kim et al. (2016), for example, observed substantial increase in the dissolved concentrations of CO, H_2 and CO_2 when using functionalized nanoparticles, and they also reported that

adding a magnetic layer to the particles enabled their reuse up to five times, thereby improving their economic feasibility.

4.3.4. Sensitivity of MESP

The Pareto-optimal MESP was in the range 1.0–1.3 US$/L (base) and 0.707–0.713 US$/L (HMT), while in a previous work by our group the estimated MESP for a process including biomass gasification and heat/power generation was in the range 0.63–0.93 US$/L hydrous ethanol (i.e. before dehydration) (de Medeiros et al., 2017). In another study about syngas fermentation, even higher values between 1.58–1.93 US$/L were found (Benalcázar et al., 2017). Not only technical considerations and process modeling methods lead to these disparities, but also economic considerations such as the prices of utilities and raw materials. With that in mind, Fig. 4.5 shows the sensitivity of MESP to several economic parameters, where the midpoint is one of the Pareto-optimal solutions from Figs. 4.3c and 4.3d. In this analysis the parameters were varied each at a time, with the other parameters being fixed at the values used in the optimization. For both cases the highest impacts on MESP (around 15% of its original value) were caused by a 30% change in the capital investment, which might also explain why the optimizations with CAPEX and MESP have similar results. A forthcoming work by our group suggests that in other cases MESP can decrease with higher η, probably because the contributions of raw materials and utilities are more significant than in the present study.
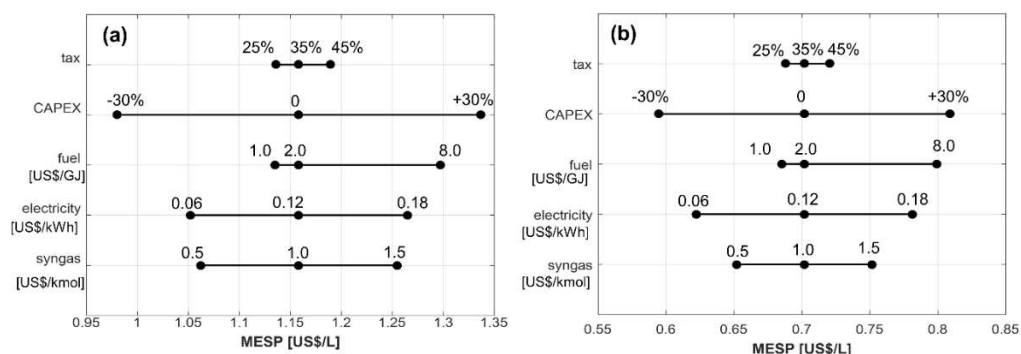
Figure 4.5. Sensitivity of MESP to economic parameters: base (a) and high mass transfer model (b).

4.4. Conclusions

Different process systems engineering (PSE) tools (modeling, simulation, neural networks, genetic algorithm) were applied in this work to develop an optimization framework through which ranges of operating conditions and design variables can be selected for optimal production of ethanol fuel from syngas via fermentation, taking into account objectives of distinct natures. When optimizing a standalone bioreactor (BCR) in terms of ethanol productivity and capital costs, it was observed that Pareto-optimal values of productivity ranged between 0.75 – 4.5 $g.L.h^{-1}$ for the base model and 1.5 – 5.4 $g.L^1.h^{-1}$ for an optimistic case with higher mass transfer capacity (HMT), with the productivity increasing at the cost of higher investment due to larger reactor vessel and gas compressor. In the second part of this work, the BCR model was coupled to the purification unit including water recycle, and the integrated process was optimized in terms of economic variables (CAPEX and MESP) and energy efficiency (η). It was observed that, with the assumptions used here, MESP and CAPEX increase with η, which nonetheless was restricted to maximum values of 0.42 (base case) and 0.72 (HMT). The trends of the decision variables along the Pareto fronts were discussed and it was seen that optimization results are greatly affected by the mass transfer calculations, thus corroborating that k_La enhancement is a promising strategy for global process improvement. The results presented here provide information about key process conditions and design variables, as well as sustainability targets and limitations in syngas fermentation. This work can be further extended to evaluate and optimize the whole process from biomass waste to ethanol or other chemicals, and its reliability can be increased with the development of new models for syngas fermentation.

Acknowledgements

References

Abubackar, H.N., Veiga, M.C., Kennes, C., 2015. Carbon monoxide fermentation to ethanol by Clostridium autoethanogenum in a bioreactor with no accumulation of acetic acid. Bioresour. Technol. 186, 122–127.

ArcelorMittal, 2019. World first: ArcelorMittal Belgium starts construction on two pioneering projects to further reduce carbon emissions. https://belgium.arcelormittal.com/en/two-pioneering-projects-to-further-reduce-carbon-emissions/, accessed 22-07-2019.

Benalcázar, E.A., Deynoot, B.G., Noorman, H., Osseweijer, P., Posada, J.A., 2017. Production of bulk chemicals from lignocellulosic biomass via thermochemical conversion and syngas fermentation: a comparative techno-economic and environmental assessment of different site-specific supply chain configurations. Biofuels, Bioprod. Bioref. 11, 861–886.

Biofuels Digest, 2019. South Africa gives green light to country's first LanzaTech ethanol project. http://www.biofuelsdigest.com/bdigest/2018/10/23/south-africa-gives-green-light-to-countrys-first-lanzatech-ethanol-project/, accessed 22-07-2019.

Bosman, P.A.N., Thierens, D., 2003. The balance between proximity and diversity in multiobjective evolutionary algorithms. IEEE T. Evolut. Comput. 7(2), 174–188.

Bredwell, M.D., Worden, R.M., 1998. Mass-transfer properties of microbubbles. 1. Experimental studies. Biotechnol. Prog. 14, 31–38.

Brittle, S., Desai, P., Ng, W.C., Dunbar, A., Howell, R., Tesař, V., Zimmerman, W.B., 2015. Minimising microbubble size through oscillation frequency control. Chem. Eng. Res. Des. 104, 357–366.

CanaOnline, 2016. Há um ano, bagaço de cana era vendido por R$150,00 a tonelada, agora chega a R$25,00.

http://www.canaonline.com.br/conteudo/ha-um-ano-bagaco-de-cana-era-vendido-por-r15000-a-tonelada-agora-chega-a-r2500.html, accessed 19/03/2019.

Chemical Engineering Magazine, 2019. https://www.chemengonline.com/pci, accessed 20/03/2019.

Chen, J., Daniell, J., Griffin, D., Li, X., Henson, M.A., 2018. Experimental testing of a spatiotemporal metabolic model for carbon monoxide fermentation with Clostridium autoethanogenum. Biochem. Eng. J. 129(2018), 64–73.

CPFL Energia, 2019. https://www.cpflempresas.com.br/institucional/tarifas.aspx?emp=CPFL, accessed 19/03/2019.

de Medeiros, E.M., Posada, J.A., Noorman, H., Osseweijer, P., Filho, R.M., 2017. Hydrous bioethanol production from sugarcane bagasse via energy self-sufficient gasification-fermentation hybrid route: Simulation and financial analysis. J. Clean. Prod. 168, 1625–35.

de Medeiros, E.M., Posada, J.A., Noorman, H., Filho, R.M., 2019. Dynamic modeling of syngas fermentation in a continuous stirred-tank reactor: Multi-response parameter estimation and process optimization. Biotechnol. Bioeng. 2019, 1–15. https://doi.org/10.1002/bit.27108

Deckwer, W.-D, 1976. Non-isobaric bubble columns with variable gas velocity. Chem. Eng. Sci. 31, 309–317.

Deckwer, W.-D., 1992. Bubble Column Reactors (V. Cottrell, Trans.), John Wiley & Sons Ltd, Chichester.

Deckwer, W.-D., Burckhart, R., Zoll, G., 1974. Mixing and mass transfer in tall bubble columns. Chem. Eng. Sci. 29, 2177–88.

Goh, C.-K., Tan, K.C., 2009. Evolutionary Multi-objective Optimization in Uncertain Environments: Issues and Algorithms, first ed. Springer-Verlag Berlin Heidelberg.

Goldemberg, J., Coelho, S.T., Guardabassi, P., 2008. The sustainability of ethanol production from sugarcane. Energ. Policy 36, 2086–2097.

Groen, D.J., Noorman, H.J., Stankiewicz, A., 2005. Improved method for aerobic fermentation intensification, in: Jansens, P.J., Stankiewicz, A., Green, A. (Eds.), Proceedings of Sustainable (Bio)Chemical Process Technology Incorporating 6th Int. Conf. Process Intensification. BHR Group Ltd., Cranfield, pp. 105–112.

Heijnen, J.J., van't Riet, K., 1984. Mass transfer, mixing and heat transfer phenomena in low viscosity bubble column reactors. Chem. Eng. J. 28, B21–B42.

Humbird, D., Davis, R., Tao, L., Kinchin, C., Hsu, D., Aden, A., Schoen, P., Lukas, J., Olthof, B., Worley, M., Sexton, D., Dudgeon, D., 2011. Process design and economics for biochemical conversion of lignocellulosic biomass to ethanol: dilute-acid pretreatment and enzymatic hydrolysis of corn stover. Technical Report, NREL/TP-5100-47764 (May 2011).

Ibrahim, D., Jobson, M., Li, J., Guillén-Gosálbez, G., 2018. Optimization-based design of crude oil distillation units using surrogate column models and a support vector machine. Chem. Eng. Res. Des. 134, 212–225.

IEA, 2019. https://www.iea.org/statistics/co2emissions/, accessed 26/06/2019.

Kim, Y.-K., Lee, H., 2016. Use of magnetic nanoparticles to enhance bioethanol production in syngas fermentation. Bioresour. Technol. 204, 139–144.

LanzaTech, 2018. LanzaTech – No such thing as waste. https://ccnet-nibb.co.uk/wp-content/uploads/2018/04/simpson.pdf, accessed 08/08/2019.

Li, X., Griffin, D., Li, X., Henson, M.A., 2019. Incorporating hydrodynamics into spatiotemporal metabolic models of bubble column gas fermentation. Biotechnol. Bioeng. 116, 28–40.

Martinez-Gomez, J., Nápoles-Rivera, F., Ponce-Ortega, J.M., El-Halwagi, M.M., 2017. Optimization of the production of syngas from shale gas with economic and safety considerations. Appl. Therm. Eng. 110, 678–685.

Pardo-Planas, O., Atiyeh, H.K., Phillips, J.R., Aichele, C.P., Mohammad, S., 2017. Process simulation of ethanol production from biomass gasification and syngas fermentation. Bioresour. Technol. 245, 925–932.

Parmar, R., Majumder, S.K., 2013. Microbubble generation and microbubble-aided transport process intensification – A state-of-the-art report. Chem. Eng. Process. 64, 79–97.

Renewables Now, 2018. LanzaTech, Shougang open sustainable ethanol refinery in China. https://renewablesnow.com/news/lanzatech-shougang-open-sustainable-ethanol-refinery-in-china-615844/, accessed 22-07-2019.

Richter, H., Molitor, B., Wei, H., Chen, W., Aristilde, L., Angenent, L.T., 2016. Ethanol production in syngas-fermenting Clostridium ljungdahlii is controlled by thermodynamics rather than by enzyme expression. Energ. Environ. Sci. 9, 2392–99.

Roy, P., Dutta, A., Deen, B., 2015. Greenhouse gas emissions and production cost of ethanol produced from biosyngas fermentation process. Bioresour. Technol. 192, 185–191.

Siemens AG, 2019. Gas Turbine Portfolio Brochure. https://siemens.com/gasturbines, accessed 17-07-2019.

Turton, R., Bailie, R.C., Whithing, W.B., Shaeiwitz, J.A., 2009. Analysis, Synthesis, and Design of Chemical Processes, third ed. Prentice Hall, New Jersey.

Ulrich, G.D., Vasudevan, P.T., 2006. How to estimate utility costs. Chem. Eng. (April 2006), 66–69.

Van de Donk, J., 1981. Water aeration with plunging jets. PhD thesis, Delft University of Technology.

Yao, Z., You, S., Ge, T., Wang, C.-H., 2018. Biomass gasification for syngas and biochar co-production: Energy application and economic evaluation. Appl. Energ. 209, 43–55.

Ye, F., Ma, S., Tong, L., Xiao, J., Bénard, P., Chahine, R., 2019. Artificial neural network based optimization for hydrogen purification performance of pressure swing adsorption. Int. J. Hydrogen Eneg. 44, 5334–44.

Chapter 5

Multi-objective sustainability optimization of biomass residues to ethanol via gasification and syngas fermentation: trade-offs between profitability, energy efficiency and carbon emissions

"Two roads diverged in a yellow wood,
And sorry I could not travel both
And be one traveler, long I stood
And looked down one as far as I could
To where it bent in the undergrowth;"

Robert Frost, The Road Not Taken

5.1. Introduction

In the last years a lot of progress has been achieved in the field of biobased production, especially with regard to ethanol production from lignocellulosic materials such as sugarcane bagasse, corn stover and wood residues – the so-called 2nd-generation (2G) ethanol. However, 2G ethanol is still hardly competitive with conventional ethanol, and despite the existence of several commercial size plants employing 2G technologies, the actual production remains mostly below the installed capacity (Padella et al., 2019). Most of these technologies employ conversion pathways based on hydrolysis and sugar fermentation, but gasification-based pathways are also considered promising due to the alleged feedstock flexibility and potential to convert all parts of biomass (including lignin).

Gasification has a long history of applications with different purposes (heat, electricity, chemicals or fuels), but most large-scale gasifiers operate with coal, while biomass gasification has been applied in a far more limited scale and mostly for heat and power generation as an alternative to natural gas and biomass combustion (Kirkels and Verbong, 2011). Regarding biomass-to-fuel via gasification, currently only eight facilities with technology readiness level (TRL) above 6 are operational or under construction/commissioning, with five of them targeting ethanol production (two operational) and only one at commercial scale: the Enerkem plant in Alberta, Canada, which converts municipal solid waste (MSW) to syngas, with its further chemical conversion to ethanol and other chemicals (Hrbek, 2019). Syngas produced via gasification can also be converted to ethanol via fermentation (i.e. using microbes instead of chemical catalysts), but, among the abovementioned projects, only one of them (by LanzaTech/Aemetis) is following this route. This plant, which is still expected to begin construction, will first convert agricultural waste to syngas via plasma gasification (Hrbek, 2019), a relatively new technology with the ability to convert nearly any type of material but with high costs and limited process understanding (Munir et al., 2019). Gas fermentation technology is by itself a challenge, despite the significant development in the past years which include the construction and operation of several demonstration plants to convert basic oxygen furnace (BOF) gas, a CO-rich gas generated in steel production, into ethanol.

The integration of these two conversion processes, namely, biomass gasification and syngas fermentation (i.e. thermo-biochemical route), has been advocated as a promising and versatile contribution to the biobased economy, but little research has been conducted to explore the simultaneous effects of process conditions and design choices of different units on the performance of the whole process, or to optimize it in terms of multiple objectives. At the same time, integrated optimization will be indispensable for the commercialization of thermo-biochemical processes. As highlighted by Ramachandriya et al. (2016), different challenges arise when integrating both conversion steps (e.g. low product yield, energy requirements in the gasifier and inhibition caused by syngas impurities), but most studies in this field have focused on the microbial physiology of syngas fermenting bacteria. On the other hand, research on biomass gasification has unveiled a complicated relationship between the performance of different gasifier systems and multiple process conditions (steam to biomass ratio, temperature, air equivalence ratio, feedstock moisture content, etc).

In this context, the main goals of this work are: (i) development of a framework for modeling and optimization of the integrated process for ethanol production from biomass via the thermo-biochemical route, considering two types of feedstock (sugarcane bagasse and wood residues); (ii) holistic impact analysis of operating conditions and design parameters; (iii) analysis of optimal trade-offs between economic, energy and environmental performance; (iv) analysis of Pareto-optimal conditions of multiple units in the process taking into account their interactions.

5.2. Methodology

5.2.1. Modeling framework

The process is divided in five main units as presented in Fig. 5.1. In A100, the biomass feed is dried and gasified, after which the syngas is sent to a reformer. Hot streams from this unit are then cooled in A200 with heat recovery for steam and power generation, after which the cold syngas ($\sim$60 ºC) is passed through a scrubber to remove contaminants. In A300 the syngas is compressed to the pressure at the bottom of the bioreactor, cooled to 37 ºC and mixed with recycled gas before being fed to the bioreactor. Cells are separated in a microfiltration membrane and recycled with a small purge, and the product stream (dilute ethanol with traces of acetic acid) is sent to A400 for ethanol purification using

distillation and molecular sieves. In A500 cooling water and chilled water are produced for the whole plant. This section provides details about areas A100 and A200, while information about A300 and A400 can be found in de Medeiros et al. (2020).

Modeling of syngas fermentation has been described in detail in our previous works (de Medeiros et al., 2019, 2020), the former focusing on microbial kinetics and the latter expanding the stirred tank model to a spatially distributed bubble column model. Previously (de Medeiros et al., 2020) we also demonstrated the application of surrogate modeling and machine learning (specifically, artificial neural networks) as tools to simplify the evaluation of responses originally obtained with rigorous models of the bioreactor and distillation columns. This strategy is repeated in the present work and applied to the gasification model, which is described next.

5.2.1.1. Drying, gasification and tar reformer (A100)

As in de Medeiros et al. (2017), the gasification process consists of a dual fluidized bed gasifier with circulation of char and bed material between the two beds as schematized in Fig. 5.2. Hot flue gas from the combustion zone (CZ) is used in the air pre-heater and biomass dryer. Since char formation is regulated by the temperature in the gasification zone (T_{GZ}), and char is the main fuel in the combustion zone, the system in Fig. 5.2 will reach an equilibrium point for T_{GZ} and T_{CZ} (temperature in the combustion zone), therefore making T_{GZ} an output of the process instead of input. In order to transform T_{GZ} into an independent variable, we propose that other variables (namely, air flow rate and additional fuel fed to CZ) can be tuned to satisfy the energy balance for a desired T_{GZ} that is not necessarily at the equilibrium point aforementioned. Therefore, the gasification model proposed here comprises an optimization routine in which, for a given T_{GZ}, we wish to minimize the square difference of the heat duty between GZ and CZ, named here Q_{diff}, by finding the corresponding values of three variables: AE (air excess fed to CZ), DT (temperature difference, $T_{CZ} - T_{GZ}$), and f (split fraction of biomass that is diverted to CZ instead of GZ). The energy difference Q_{diff} also considers a loss of 2% the lower heating value (LHV) of biomass. Since for the whole process we also wish to minimize resources, the objective function then becomes, for a given T_{GZ}:

$$\min\left[\left(Q_{diff}\right)^2 + (AE) + (f) + (DT)\right] = f\left(T_{GZ}, AE, f, DT\right) \qquad (5.1)$$

The calculation of the energy difference Q_{diff} starts by calculating the outcomes of the gasification zone (syngas and char yields and compositions), for which we use temperature-dependent correlations adopted by NREL (Dutta et al, 2011). These correlations are second-degree polynomial functions of T_{GZ} that predict the yield of syngas (scf/lb maf biomass) and the mass fractions (dry basis) of its main components (i.e. CO, CO_2, H_2, CH_4, C_2H_4, C_2H_6, C_2H_6, C_2H_2, C_6H_6). Although there is a correlation for the char yield, we follow NREL's recommendation of using instead the following algorithm based on elemental balances: (i) for carbon, determine the total amount of C in syngas from the results of the correlations and consider any remaining C to be in the form of char; (ii) for oxygen, assume that at least 4% of biomass O ends up in the char, then if the O balance results in a deficit of this element, water decomposition is assumed to provide for the missing amount; if there is an excess of O then the exceeding amount is assumed to also be present in the char; (iii) for sulfur, assume that at least 8.3% of biomass S is in the char, the remainder is converted to H_2S in syngas; (iv) for nitrogen, assume that at least 6.6% of biomass N goes to char, the remainder is converted to NH_3 in the syngas; (v) for hydrogen, determine the total amount of H in all components of syngas, and consider the remaining H to be present in the char. To be consistent with the correlations, other conditions were assumed fixed and equal to the experiments described by the correlations, i.e. biomass moisture entering the GZ equals 10% and steam to biomass ratio SBR = 0.4 kg/kg dry biomass.
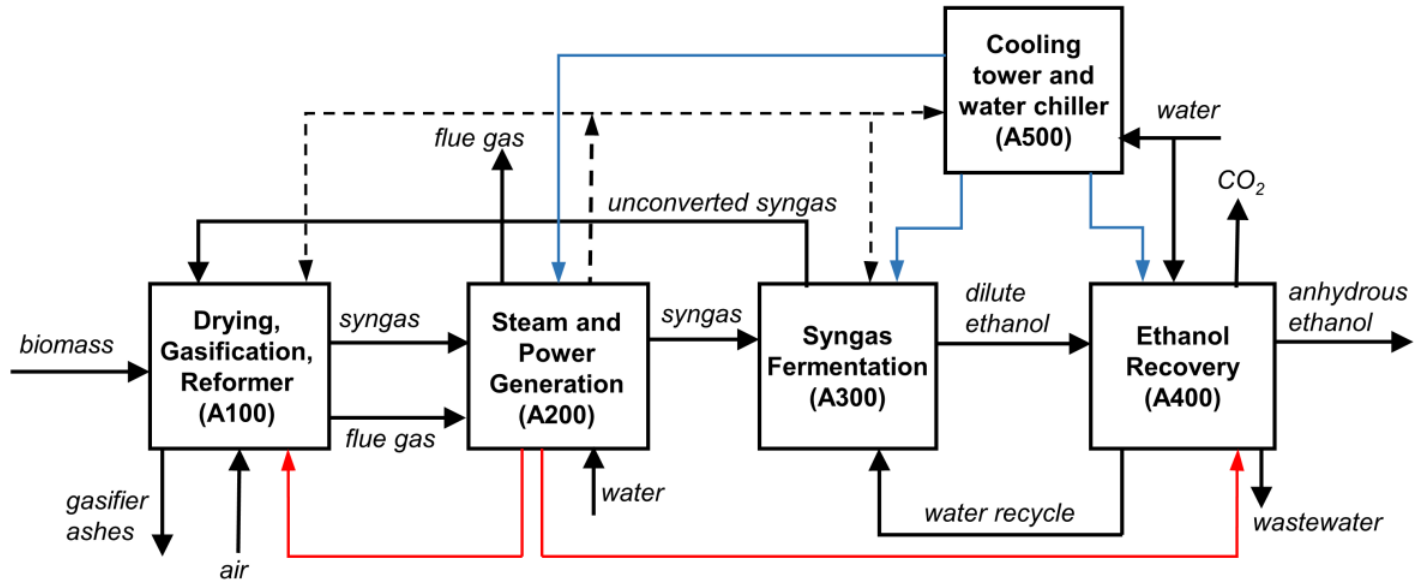
Figure 5.1. Block flow diagram of thermo-biochemical route for ethanol production from biomass. Dashed lines: electricity streams; blue lines: cooling or chilled water; red lines: steam.
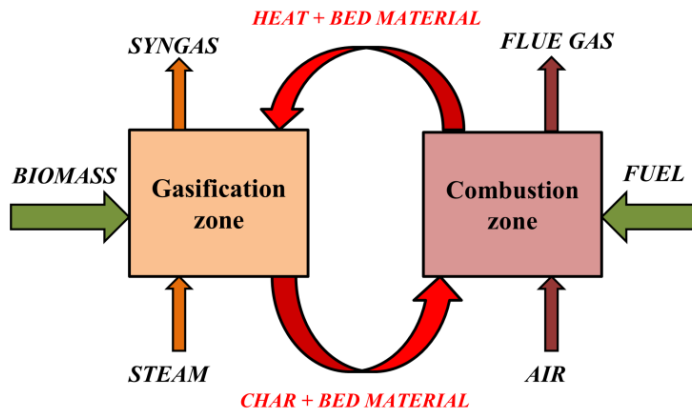
Figure 5.2. Schematic representation of dual fluidized bed reactor in A100.

To calculate Q_{diff}, the gasification unit was simulated in Aspen Plus following the simplified flowsheet presented in Fig. 5.3. The full Aspen flowsheet is presented in Fig. A3-1 of the Appendix. Biomass was specified as a non-conventional component described by its heating value and composition given by proximate and ultimate analyses. These can be found in de Medeiros et al. (2017) and Capaz et al. (2020), for bagasse and wood residues, respectively. For each temperature, results of the GZ algorithm explained above are used as input in the yield reactor that represents the GZ (R-01). The combustion reactor (R-02) is a stoichiometric reactor that is fed with char generated in GZ as well as biomass that might be diverted for this use in the splitter (SP-01). In the simulation, there is also a yield reactor (not depicted in Fig. 5.3) to transform the non-conventional component biomass into conventional components that can participate in combustion reactions. The dryer (D-01) is modelled in Aspen with a stoichiometric reactor and a flash operation: the former converts the non-conventional biomass stream into a stream containing biomass and H_2O, which is later separated in the flash operation. The amount of H_2O generated in this stage is the difference between the initial moisture of the wet biomass and the final desired moisture of 10%. The output Q_{diff} is then the sum of three heat streams related to these operations: the decomposition of nonconventional biomass, the gasification reactions R-01 and the combustion reactions R-02. The tar reformer was simulated as a stoichiometric reactor for the conversion of CH_4, C_2H_6, C_2H_4 and tars into CO and H_2. For this reactor the conversions were assumed the same as adopted by NREL (Dutta et al. 2011), i.e. 80%, 99%, 90% and 99% respectively. The heat duty was

calculated in Aspen and it is assumed to be provided by the combustion of unconverted syngas from A300 as well as a fraction of unreformed syngas from the gasifier. The latter can be adjusted not only to meet the requirements of the tar reformer, but also to increase the amount of energy available for steam/electricity production in A200.

The minimization problem (Eq. 5.1) was solved in MATLAB for a range of T_{GZ}. Since the calculation of Q_{diff} and other outputs requires the Aspen simulation, one possible approach is to link both software programs and run the simulation every time the objective function needs to be evaluated. However, to make the framework more robust and reduce the number of simulation runs, we decided instead to train artificial neural networks (ANN's) with data generated in Aspen for multiple combinations of inputs (T_{GZ}, AE, f, DT). This procedure was previously explained in for a different case (de Medeiros et al., 2020). These surrogate models were then used in the optimization problem, which was solved with fmincon in MATLAB. The ranges used to obtain the data were: T_{GZ} between 700 – 1000 °C; AE between 10 – 150 %; f between 0 – 0.5; DT between 30 – 100 °C.

5.2.1.2. Heat recovery and power generation (A200)

Energy is recovered from three streams of hot gases: syngas from the tar reformer, flue gas from the char combustor, and flue gas from the tar reformer combustor (catalyst regenerator). These hot gases are used as energy source in a Rankine cycle with reheat (Fig. 5.4) to produce electricity. In this cycle there are two expansion stages (ST-01 and ST-02) with an intermediate re-heat operation (E-02) to increase the energy efficiency. In the 2nd stage a slip stream is extracted to provide steam for gasification and process heat (distillation). The specifications of inlet/outlet pressure and temperature at the turbine were considered the same as reported by NREL (Dutta et al., 2011). Since the properties (mass and temperature) of the hot streams are not fixed (i.e. they depend on the conditions of the process), the heat exchanger network (represented in the flowsheet by the exchangers E-01, E-02 and E-05) is designed with an algorithm that roughly maximizes the sensible heat that can be transferred from hot to cold streams. In this unit, the mass flow rate of water/steam circulating in the Rankine cycle is set to meet the plant targets of electricity and steam consumption, but if heat is still available then more water is provided to increase electricity production. This is

done with a short optimization routine to maximize the amount of water while respecting the 1st and 2nd law of thermodynamics.

Electricity generated in this unit is used to supply the gas compressors, air blowers and pumps in the whole plant, as well as the water chiller (which produces chilled water for the bioreactor that must be kept at 37 °C). After heat recovery, the reformed syngas stream is further cooled to 60 °C using cooling water and fed to a scrubbing system following the same specifications as adopted by Dutta et al. (2011), i.e. comprising a venturi scrubber, cyclone separator and a quench water circulation system with a small purge and fresh water makeup.

5.2.2. Evaluation of model outputs and multi-objective optimization

The modeling framework considers 9 decision variables for the optimization: in A100, (i) T_{GZ} (temperature in the gasification zone of the gasifier), and (2) f_s (fraction of unreformed syngas sent to combustion); in A300, (iii) D_{rate} (dilution rate in the bioreactor), (iv) GRT (gas residence time, defined as volume of liquid divided by fresh gas volumetric flow), (v) GRR (gas recycle ratio), (vi) L (column height), (vii) V_R (volume of bioreactor); in A400, (viii) SF_{C1} (mass ratio of side stream to feed stream in the first distillation column) and (ix) RR_{C2} (molar reflux ratio in the second distillation column). The sustainability performance is measured by four types of responses: (i) economic; (ii) energetic; (iii) carbon footprint; and (iv) water footprint. The variable f_s is used to regulate the amount of energy (electricity and heat) that is produced inside the plant: if f_s is too high, the process exports energy and produces less ethanol; if it is too low, energy must be imported which therefore increases the carbon footprint of the process and utility cost. There is of course a point at which the process becomes exactly self-sufficient, but it does not necessarily correspond to the optimum of the process in terms of all sustainability criteria. The optimization was conducted for two feedstocks: sugarcane bagasse and wood (eucalyptus) residues.
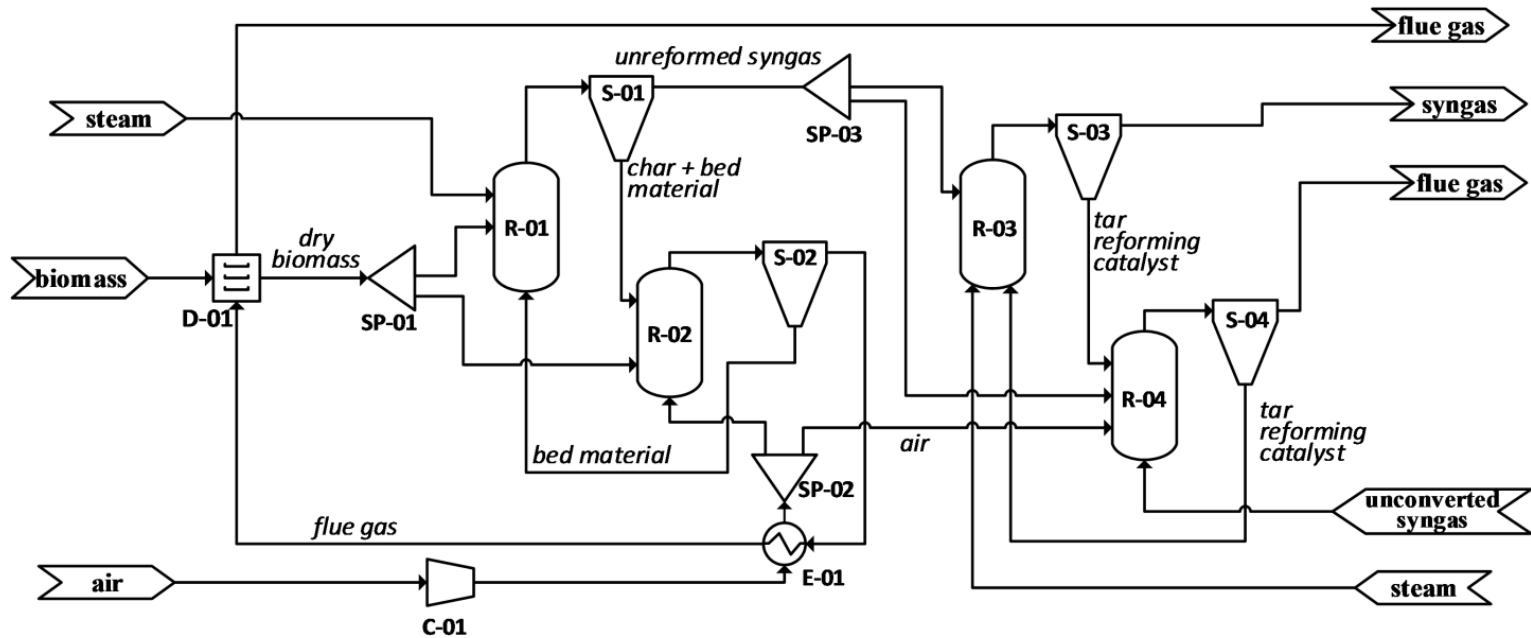
Figure 5.3. Simplified process flow diagram of A100: drying, gasification and tar reformer. D-01: biomass dryer; SP-01 to SP-03: stream splitters; R-01 and R-02: gasification (GZ) and combustion (CZ) zones of dual bed gasifier; S-01 to S-04: cyclones; R-03 and R-04: tar reformer and catalyst regenerator; C-01: air blower; E-01: air pre-heater.
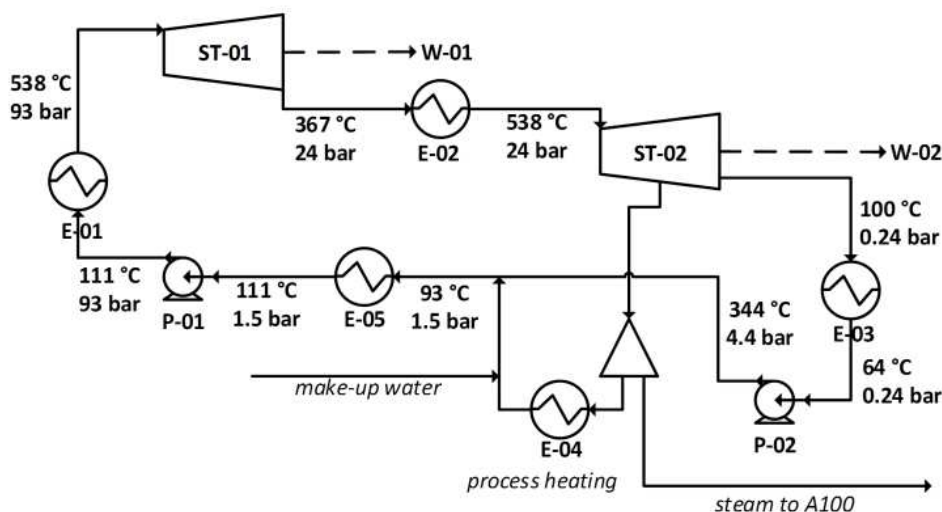
Figure 5.4. Rankine cycle with reheat. E-01 to E-05: heat exchangers (units represent series of exchangers); ST-01 and ST-02: steam turbine, 1st and 2nd stages; P-01 and P-02: water pumps.

Capital costs are calculated following the bare module costing technique detailed in Turton et al. (2009). For the gasification unit and steam turbine, the base costs were taken from NREL (Dutta et al., 2011) and adapted to the year 2019. The capacity was considered the same for both case studies: 2,000 tonnes of dry biomass per day. Costs of heat exchangers, pumps, air blowers and towers were calculated with purchase cost correlations available in Turton et al. (2009). For all types of equipment, capacity ranges are respected by dividing the equipment in more units if that is necessary (for example, if the calculated heat exchanger area is greater than 1000 m^2). The economic performance indicator used for the optimization is the minimum ethanol selling price (MESP), i.e. the price to achieve NPV = 0. Economic assumptions were considered the same as those in de Medeiros et al. (2020).

Table 5.1 presents the considerations of prices and carbon footprint (emission factors) associated with raw materials and utilities used in the process. Costs of other raw materials, such as olivine and tar reformer catalyst, were taken from NREL (Dutta et al., 2011), and were assumed to have negligible carbon footprint contribution. It's worth mentioning that fermentation nutrients were excluded from the analysis since they cannot be calculated with our model, but they are not expected to have a significant impact on either MESP or CO_2 emissions. In a LCA

study using data from LanzaTech, Handler et al. (2016) reported that inputs such as nutrients, water and chemicals amounted together to 9-20% of CO2eqq emissions related to feedstock procurement (corn stover, switchgrass or forest residue). Regarding the carbon footprint of lignocellulosic feedstocks (sugarcane bagasse or eucalyptus residues), these are considered here as co-product instead of waste, i.e. a fraction of the impacts associated with the production of sugarcane/ethanol or eucalyptus are allocated to the residual biomass according to their economic value (Capaz et al., 2020).

The energy efficiency considered here reflects how much of the energy input from biomass and heat/power (if these are not produced inside the plant) is available in the final product (anhydrous ethanol). If there is an excess of electricity production, for example, the carbon footprint of the process will be lower but so will the energy efficiency. Finally, the water footprint is the total water consumed in the process divided by the production rate of ethanol. Cooling water make-up due to losses from evaporation, drift and blowdown are assumed to be 0.4% of the total cooling water consumption.

Table 5.1. Prices and carbon footprint considered in this study

Raw material	Price	Carbon footprint
Sugarcane bagasse	$ 45/t (db) (Bonomi et al., 2016)	0.042 kg CO2eq/kg (db) (Capaz et al., 2020)
Wood residues	$ 11.3/t (db) (SEAB, 2019)	0.0189 kg CO2eq/kg (db) (Capaz et al., 2020)
Electricity	$ 0.14/kWh (CPFL Energia, 2019)	0.17 kg CO2eq/kWh (Capaz et al., 2020)
Steam	variable (Ulrich and Vasudevan, 2006)	70 kg CO2eq/GJ (Ecoinvent)
Natural gas	$ 0.274/kg	2.63 kg CO2eq/kg (Ecoinvent)

Prior to the multi-objective optimization, a sensitivity analysis was conducted to determine the correlations between input and output variables, as well as the correlations between different responses. For the latter, Principal Component Analysis was applied to a set of responses obtained under different combinations of input variables (4,000 points) and the values of the principal component coefficients (also called loadings) were used to interpret correlations between the responses and thus reduce the number of objectives. With the final set of

objectives, the multi-objective optimization was then conducted in MATLAB using genetic algorithm. The search ranges of the decision variables are shown in the Results section together with the ranges of Pareto optimal results in Table 5.2 (Sec. 5.3.4).

5.3. Results and discussion

5.3.1. Gasification

As explained in Sec. 5.2.1.1, the gasification model expands the NREL algorithm (Dutta et al., 2011) by tuning other process conditions in order to maintain a desired temperature in the gasification zone. Main results are presented in Fig. 5.5 and Fig. 5.6. In Fig. 5.5 the compositions are shown for bagasse only, but since the model uses temperature-dependent correlations for the dry molar fractions in the gas phase, there are virtually no differences between the dry composition obtained for the two feedstocks. This is of course a limitation of the model, because it means the feedstock composition has no effects on the dry gas composition; however since the differences are small (e.g. bagasse has lower carbon content, 46.96% against 50.89%, as shown in Table A3-1 in Appendix A3), we can assume that in view of the whole process, and recalling that the moisture at the entrance of the gasifier is the same (i.e. 10%), the main distinctive aspects of the feedstocks will be the initial moisture (50% for bagasse and 12% for wood), price and carbon footprint. It's worth mentioning that the composition correlations were developed for different types of wood, hence it's safe to affirm that the gasifier model is more accurate for eucalyptus residues than for bagasse.

Differences in feedstock composition are compensated in the char yield, which is therefore lower for bagasse (Fig. 5.6a). Another difference is the fraction of biomass that must be diverted to the combustion zone in order to maintain the desired temperature at the gasification zone (Fig. 5.6b): in this case, this fraction is higher for bagasse and begins to be greater than zero at a lower temperature; this is due not only to the feedstock composition but also to the heating value which is lower for bagasse (16.05 MJ/kg against 18.61 MJ/kg, dry basis).
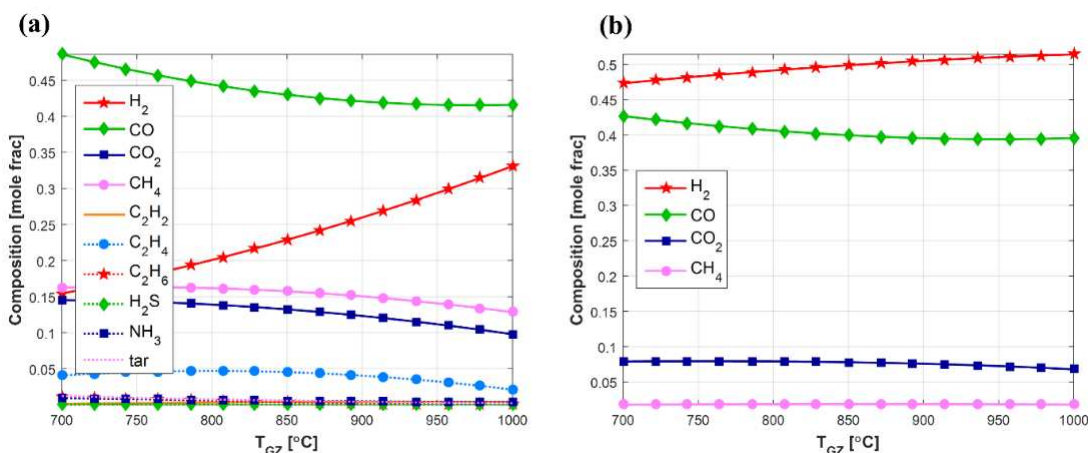
Figure 5.5. Molar composition of syngas (dry basis): (a) after gasifier; (b) after tar reformer (other species are not shown due to negligible concentrations).

Another limitation of the model is the inability to predict the formation of toxic HCN. Although it is produced in much lower amounts than NH_3 (Wilk and Hofbauer, 2013), HCN has been reported to be the main reason behind the shutdown of the INEOS Bio gasification-fermentation plant in Florida (Lane, 2014). On the other hand, recent studies have suggested that the syngas-fermenting microbe *Clostridium ljungdahlii* can adapt to the presence of cyanide and achieve similar growth performance as without the contaminant (Oswald et al, 2018). Moreover, HCN removal from syngas can be accomplished through different cleaning processes, such as absorption into aqueous solution followed by alkaline chlorination or oxidation, or even direct decomposition using heterogeneous catalysts during the gasification process (Kumagai et al., 2017). It can be hypothesized that INEOS Bio underestimated the amount of HCN that would be produced in the gasifier and then, with the plant already constructed, it might have been too problematic to include further cleaning stages.
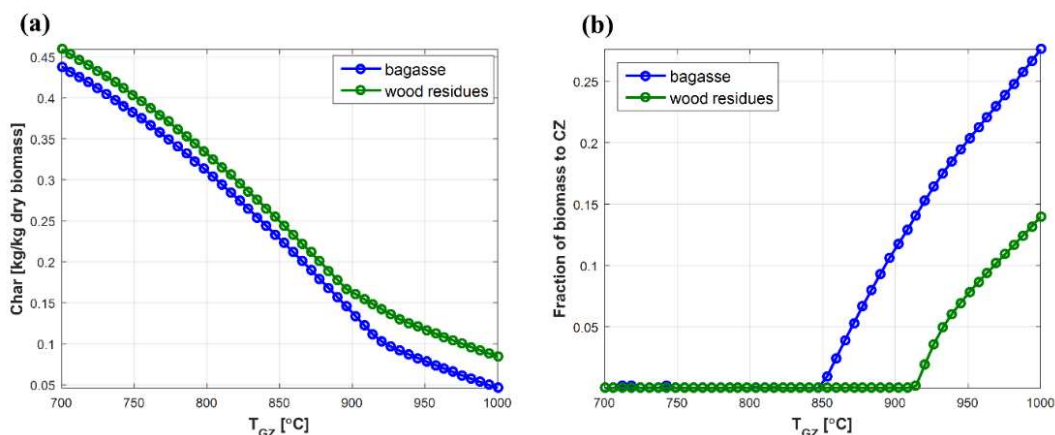
Figure 5.6. Main differences between the predictions of the gasifier model for bagasse and wood residues: (a) char yield; (b) required fraction of biomass sent to the combustion zone.

5.3.2. Bubble column bioreactor

The bubble column bioreactor is affected by several variables. For the optimization study five variables are direct inputs of this unit (D_{rate}, GRT, GRR, L, V_R), but other variables are fixed (e.g. cell recycle ratio, at 0.85) or they are outcomes from other units (e.g. syngas composition). In a previous study (de Medeiros et al., 2019) we showed how the syngas composition affects the gas conversion and ethanol productivity as predicted by the biokinetic model. Fig. 5.7 presents main performance indicators of the bubble column reactor for different values of D_{rate} and GRT, with the syngas molar composition fixed at $[CO:H_2:CO_2]$ = [0.4:0.5:0.1], column height L [m] = 40, volume V_R [m^3] = 500, and no gas recycle (GRR = 0). Clearly the responses presented in Fig. 5.7 are conflicting and cannot be optimized simultaneously: for example, the highest ethanol titers are achieved under very low D_{rate} (< 0.075 h^{-1}) and GRT, while the highest CO conversions are achieved with high GRT. The energy efficiency η_{LHV} is also favored under high GRT (due to higher conversion), but the productivity is favored at low GRT, achieving a maximum close to D_{rate} = 0.1.

5.3.3. Global effects of input variables and correlations between responses

With the framework of the whole process, the model was first used to predict relevant responses for a set of combinations of decision variables. The results were then used to calculate the correlation coefficients between the decision variables and each of the responses, which are presented in Fig. 5.8. Firstly, it's

worth noting that all the decision variables have absolute correlation coefficients greater than 0.1 for at least one of the responses; for this reason, all of them are kept in the optimization problem. Secondly, T_{GZ}, f_s and GRT dominate with the highest correlation coefficients with all the responses. Moreover, a few interpretations can be highlighted:

GRT is a measure of the amount of fresh syngas fed to the bioreactor: for a fixed reactor volume, the higher the value of GRT, the lower the fresh gas volumetric flow rate fed to each vessel, which means that for the same syngas production rate (an outcome of the gasification unit), the number of reactor vessels must be increased, hence the large positive effect on CAPEX. The effect on OPEX is not straightforward, because as seen in Fig. 5.7, increasing GRT increases the gas conversion but also decreases the ethanol titer (which means more resources are used downstream). MESP and η_{LHV} show similar correlation coefficients but with opposite sign, meaning also that lower values of MESP are an indication of higher energy efficiency. The effect on the water use is approximately opposite to the energy efficiency, corroborating that a higher energy use per liter of product also prompts a higher requirement of cooling water and, therefore, make-up water.

The split fraction of unreformed syngas diverted to combustion (f_s) has large negative effects on both OPEX and carbon footprint, since increasing f_s implies decreasing the input of external energy to the plant, hence lower costs and CO_{2eq} emissions. However, as seen in Fig. 5.8c, it turns out to also have a small positive effect on MESP, meaning that the abovementioned gains are overshadowed by the reduced ethanol production.

Although increasing the temperature in the gasification zone (T_{GZ}) means sacrificing more biomass to combustion (Fig. 5.6b), this loss is apparently compensated by the reduced formation of char (Fig. 5.6a), thus higher syngas yield, and by the higher production of H_2 (Fig. 5.5), which favors ethanol production during fermentation. The small increase in CAPEX (probably due to higher gas flow rates) is therefore repaid by these gains, as observed with the correlation coefficients of this variable with other responses.

To conduct the sustainability optimization, MESP was elected as the main economic indicator, and the other responses shown in Fig. 5.8, apart from CAPEX and OPEX, were initially considered as objectives. The results of the correlation analysis described above also indicate existing correlations between the

responses (e.g. between MESP, η_{LHV} and water), and this was verified using Principal Component Analysis (PCA). PCA takes a set of multidimensional data and reduces the dimension by creating new variables (principal components) that are linear combinations of the original variables. The values of these linear coefficients (sometimes called loadings) can then be compared in order to find correlations among the variables. In the present case, two principal components were found to explain more than 90% of the variance in the original data set, therefore the coefficients of the first two components provide an accurate overview of these correlations, as depicted in Fig. 5.9. As expected, MESP, -η and water use are clustered in the same region with similar coordinates. Based on these results, we decided to exclude the water footprint from the multi-objective optimization and proceed with three minimization objectives only: (i) MESP, (ii) –η (because one of the goals is to maximize the energy efficiency), and (iii) carbon footprint.

5.3.4. Multi-objective sustainability optimization

Fig. 5.10 presents the Pareto fronts and their respective interpolant surfaces obtained for the two feedstocks. Significantly lower values of carbon footprint and MESP can be obtained with wood residues (0.93 $/L against 1 $/L, and 3g CO_2eq/MJ against 10 g CO_2eq/MJ), the main reasons behind this being the much lower feedstock price, feedstock-related emissions and initial moisture of the wood residues. The energy efficiency was however bound to 32% in both cases, a result that is lower than a first estimation (η = 38%) given in our previous work (de Medeiros et al., 2017), which considered a much more simplistic bioreactor model. Indeed, as demonstrated in de Medeiros et al. (2020), an optimistic estimation of the gas-liquid mass transfer coefficient (k_La) can lead to substantial improvement in energy efficiency and reduction of MESP. Considering the high values of MESP, even under optimal conditions, and its dependence on the energy efficiency, the results presented here and in de Medeiros et al. (2020) corroborate the need for improvement in the bioreactor, be it with novel reactor designs that facilitate gas-liquid mass transfer while keeping low cost, or with genetic improvement of the microorganisms. These changes must, however, be followed by new optimization studies to re-evaluate the optimal process conditions.
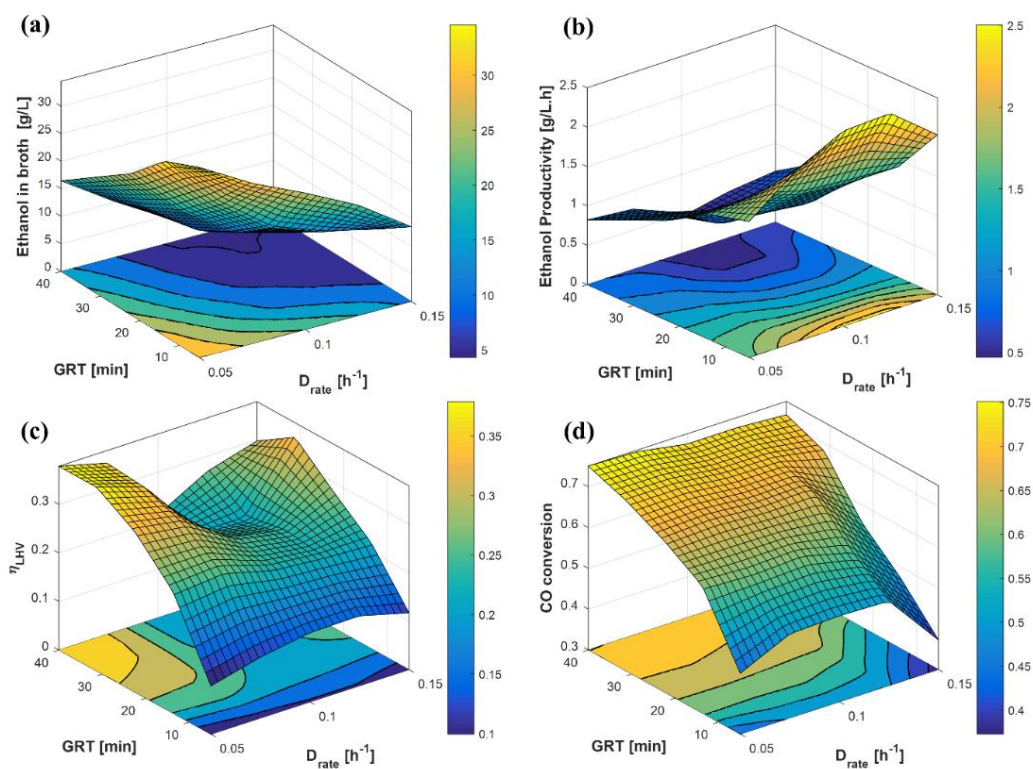
Figure 5.7. Bubble column reactor, sensitivity of D_{rate} and GRT on model outcomes: (a) ethanol concentration [g.L^{-1}] in the liquid phase; (b) ethanol productivity [g.L^{-1}.h^{-1}]; (c) energy efficiency η_{LHV}; (d) CO conversion.
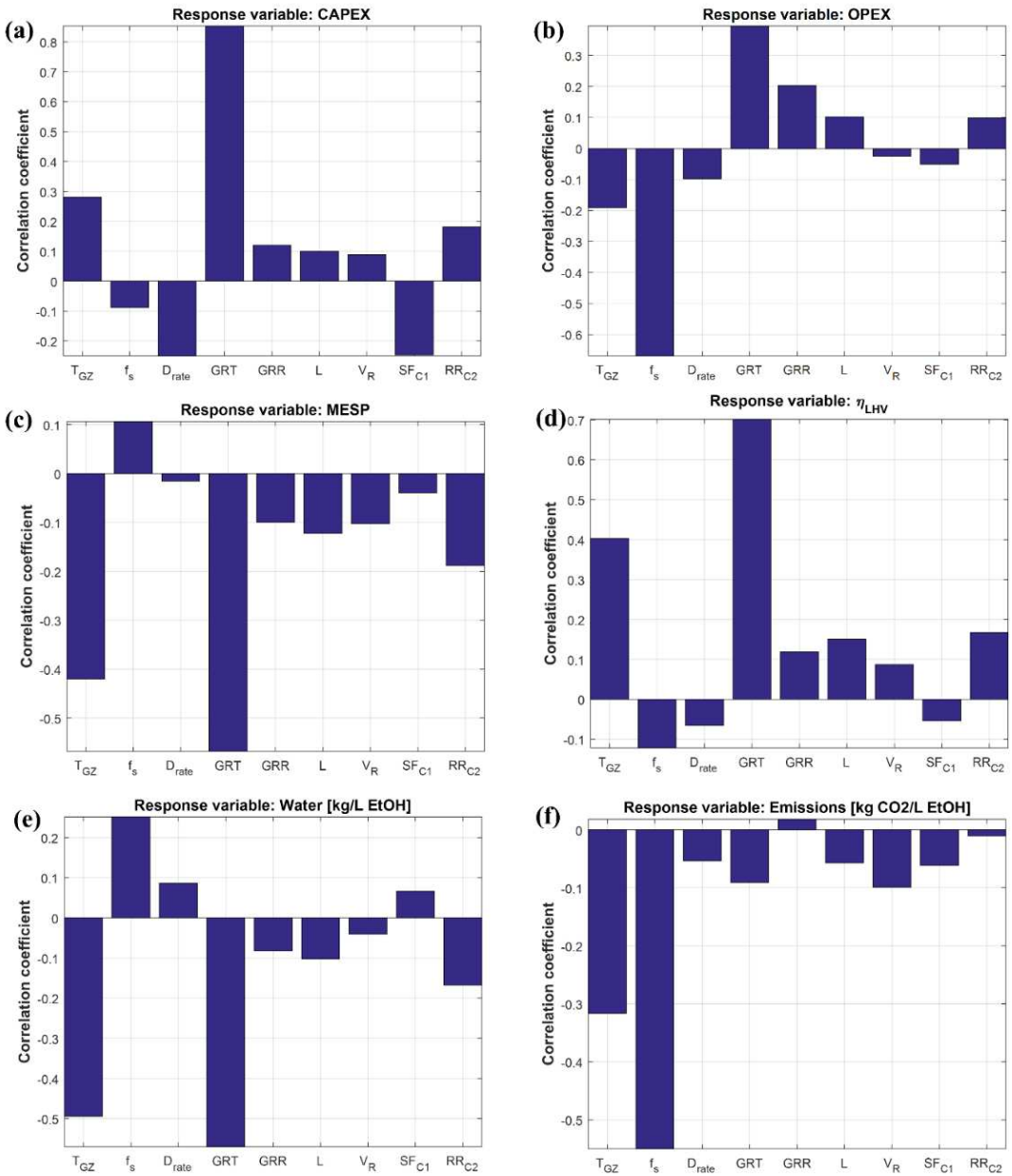
Figure 5.8. Correlation coefficients between decision variables and responses: sugarcane bagasse (results for wood residues are presented in Fig. A3-2 of Appendix A3).
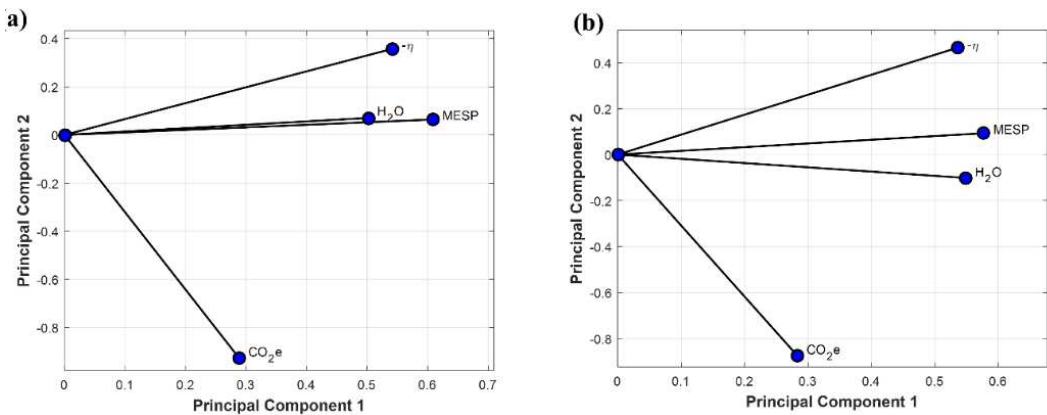
Figure 5.9. PCA of model responses showing the principal component coefficients (loadings) of the first two principal components: (a) sugarcane bagasse; (b) wood residues.

For both feedstocks, the optimal MESP can be decreased at the cost of higher GHG emissions, however, even at the lowest values of MESP, the process still represents a significant emission reduction in comparison with gasoline (94 gCO2eq/MJ) (Elgowainy et al., 2014) and 1st-generation ethanol (38.5 – 44.9 g CO2eq/MJ) (Mekonnen et al., 2018), although it should be mentioned that our calculations do not take into account the emissions related to the distribution of ethanol. The results are comparable to other combinations of 2G technology and feedstock, for example the biochemical route using wheat straw (16 g CO_{2eq}/MJ) (Padella et al., 2019) or sugarcane residues (17.5 gCO_{2eq}/MJ) (Junqueira et al., 2017). Similarly, Handler et al. (2015) reported GHG emissions from gas fermentation to be between 8.0 gCO_{2eq}/MJ for corn stover and 31.4 for basic oxygen furnace gas; but an even better result of 1.5 gCO_{2eq}/MJ was reported for this technology using forest residues.

There are different sources of uncertainty in the framework. Firstly, those associated with the process models: for example, in the correlations used to predict syngas composition as function of temperature; or in the equations and parameters used for the calculation of gas-liquid mass transfer coefficient (k_La) and reaction rates in the bioreactor model. These are uncertainties that can be attenuated with research to deliver more experimental data, either laboratorial or industrial, to validate and improve the models. The other type of uncertainty is related to economic and environmental parameters and assumptions that are unrelated to the process models, such as price of raw materials, capital cost

correlations and emission factors. For example, biomass residues are not traditional materials with established market prices, but they acquire a so-called opportunity price as second-generation technologies or other types of biomass valorization processes gain popularity. Similarly, one can expect that values of CO_{2eq} emissions due to feedstock procurement depend not only on the location and type of biomass, but also on the impact assessment methodology and database used for the calculation of these emission factors. In this context, Fig. 5.11 presents the 2-d projections of the Pareto fronts from Fig. 5.10 along with uncertainty intervals obtained when four economic and environmental assumptions are varied within ± 30% ranges: (i) feedstock price; (ii) CAPEX calculation; (iii) feedstock emission factor; (iv) electricity emission factor. The points A, B, C and D were selected as most desirable candidates as discussed further in this Sec. 5.3.4.
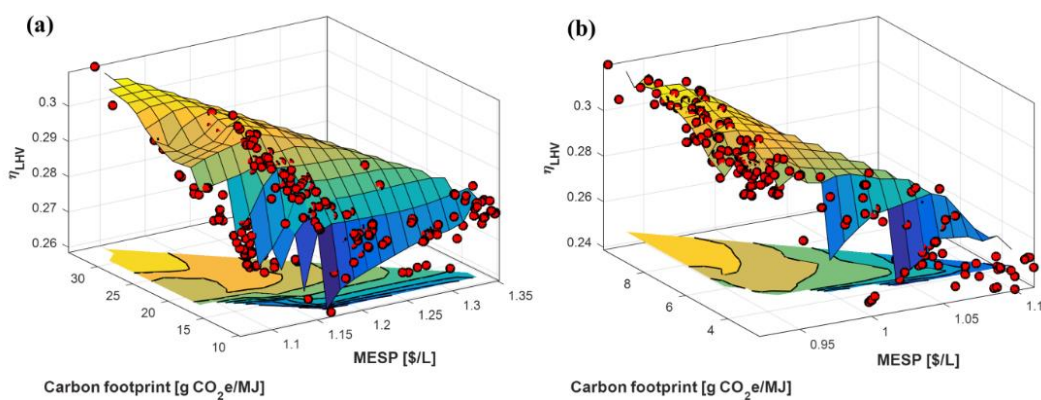
Figure 5.10. Pareto surfaces obtained with 3-objective optimization of thermo-biochemical route (Pareto-optimal solutions represented by red spheres): (a) sugarcane bagasse; (b) wood residues.

The large uncertainty intervals demonstrate the importance of being transparent about the assumptions and limitations of techno-economic-environmental assessment studies. Nevertheless, the main contribution of this paper is not the calculation of MESP, energy efficiency and carbon footprint, but rather the strategies presented for sustainability optimization and the insights about the effects of interconnected input variables and their behavior at the optimal solutions. This is illustrated in Fig. 5.12 for the most relevant variables: T_{GZ}, f_s, D_{rate} and GRT. As seen in Sec. 5.3.3, these variables showed the strongest correlations with the responses, which is why they are also more dispersed along the Pareto

fronts. Other variables, however, were limited to more narrow ranges of optimal values when compared to their original search space. Ranges of Pareto-optimal values obtained for all the decision variables are shown in Table 5.2, together with their original search space.
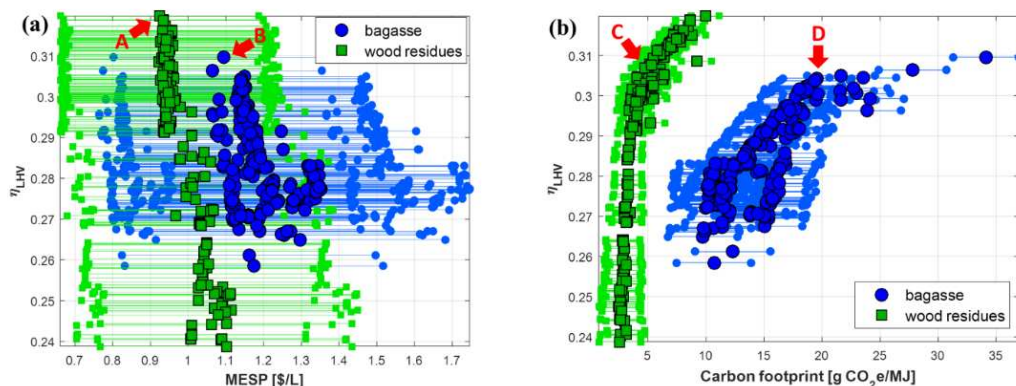
Figure 5.11. Projections of 3-objective Pareto fronts in pairs, including intervals of ± 30% uncertainty in economic and environmental assumptions: (a) MESP; (b) Carbon footprint.

The optimal trends presented in Fig. 5.12 reinforce, to some extent, the correlations discussed in Sec. 5.3.3 (Fig. 5.8). For example, lower MESP (and higher efficiency) can be achieved with higher gasification temperature, while the opposite is observed for the variable f_s (fraction of unreformed syngas that is sent to combustion). The optimal values of D_{rate} are constrained to the range 0.055 – 0.08 h^{-1}, similarly as observed in de Medeiros et al. (2020). Finally, GRT is spread over the range 22 – 32 min, but although its patterns are not as evident as seen for T_{GZ} and f_s, there seems to be a rough tendency of higher GRT leading to higher MESP (and lower η), which is at first sight conflicting with the results presented in Fig. 5.8. However, when considering the whole search space of GRT (see Table 5.2), the optimal values are clearly closer to the upper bound than the lower bound, therefore confirming that higher GRT is better for both MESP and η. It is when the data set is limited to the Pareto fronts that this pattern is not clear anymore, demonstrating that other input variables also exert strong effects on the optimal results.

Although the Pareto-optimal solutions are, by definition, equally optimal, the points A, B, C and D from Fig. 5.11 can be selected as the best candidates according to the following criteria: first, given the current context, in which profitability is still the prevailing standard, points A and B are those for which both profitability

157

and energy efficiency are maximized. It should be noted that it is not always the case that these two targets can be optimized at the same time (for an example, see de Medeiros et al. (2020)). Points C and D take into account the carbon footprint but do not consider it the most crucial target: beyond these points the minor improvements in the energy efficiency are followed by proportionally larger increase of the carbon emissions. Table 5.3 presents the values of the decision variables at these four solutions, along with the corresponding values of the three targets. The main differences between the two types of solutions (A and B against C and D) are related to the gasification temperature (slightly lower in the second case), the bioreactor volume (also lower in the second case), and, more notably, the syngas fraction f_s, which is much higher when carbon footprint is taken into account.
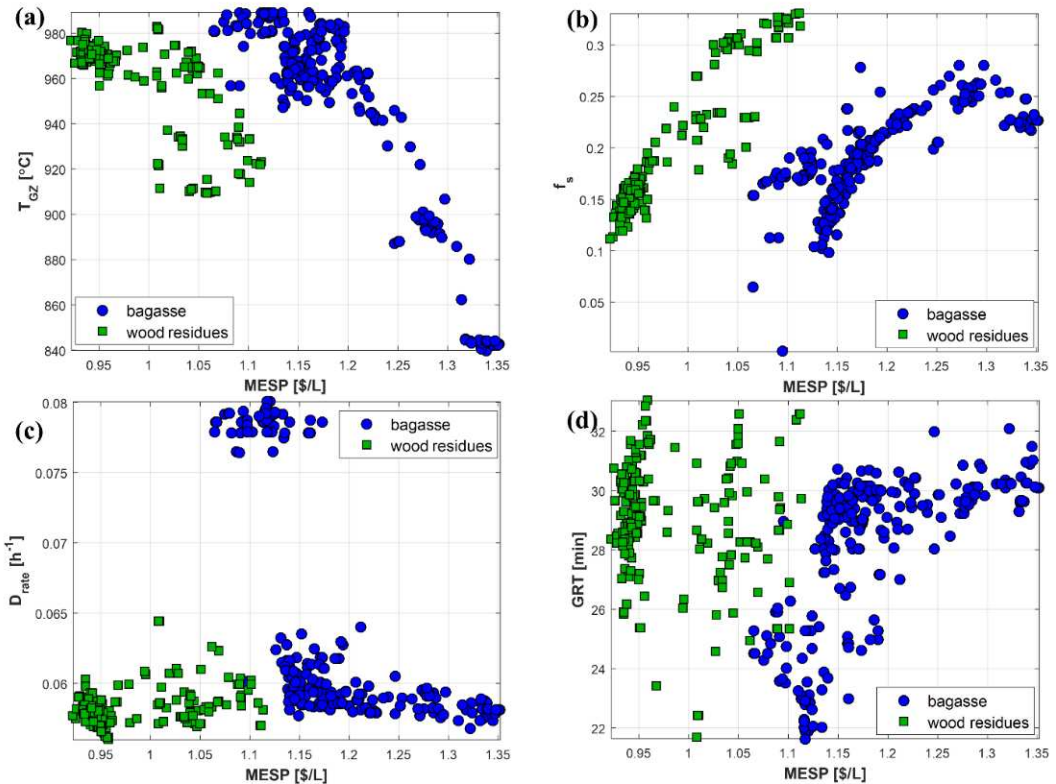
Figure 5.12. Pareto-optimal values of most relevant decision variables: (a) T_{GZ}; (b) f_s; (c) D_{rate}; (d) GRT.

Table 5.2. Multi-objective optimization of thermo-biochemical route: ranges of at the Pareto-optimal solutions.

	search space	bagasse	wood residues
T_{GZ} [ºC]	700 – 1000	839 – 989	909 – 983
f_s	0 – 0.35	0.00182 – 0.280	0.111 – 0.330
D_{rate} [h^{-1}]	0.05 – 0.15	0.0568 – 0.080	0.0560 – 0.0644
GRT [min]	5 – 40	21.6 – 32.1	21.7 – 33.0
GRR	0 – 0.5	0.0990 – 0.293	0.124 – 0.304
L [m]	30 – 50	43.1 – 47.2	40.4 – 48.9
V_R [m^3]	400 – 900	455 – 600	418 – 596
SF_{C1}	0.06 – 0.13	0.0894 – 0.0940	0.0886 – 0.0950
RR_{C2}	3 – 6	4.84 – 5.95	4.75 – 5.87

Table 5.3. Multi-objective optimization of thermo-biochemical route: selected optimal points.

	A (wood)	B (bagasse)	C (wood)	D (bagasse)
MESP [\$.L^{-1}]	0.934	1.09	0.958	1.14
η	0.319	0.310	0.305	0.304
g CO2eq/MJ	8.60	34.1	4.11	19.4
T_{GZ} [ºC]	974	974	961	962
f_s	0.119	0.00182	0.186	0.119
D_{rate} [h^{-1}]	0.0572	0.060	0.058	0.058
GRT [min]	30.3	28.9	31.8	29.8
GRR	0.245	0.248	0.247	0.283
L [m]	45.8	46.0	47.4	45.1
V_R [m^3]	503	554	485	551
SF_{C1}	0.0940	0.0920	0.0930	0.0921
RR_{C2}	5.11	5.13	5.10	5.00

Water footprint was also included in the analysis as a measure of direct water use (i.e. excluding the water footprint to produce the feedstock and raw materials), but as explained in Sec. 5.3.3, it was excluded from the multi-objective optimization due to its high correlation with both MESP and η. In Fig. 5.13a the water footprint of Pareto-optimal points are plotted against the corresponding results of MESP, with minimum values being around 5 kg water per liter of ethanol for bagasse and wood residues. As comparison, Dutta et al. (2011) reported 2.0 kg/L for ethanol production from wood via gasification and mixed alcohol synthesis, but the LanzaTech process is expected to consume around 8.5 kg/L (Handler et al., 2016). Ethanol yields (Fig. 5.13b) are also comparable to other 2G processes found to be in the range 205 – 330 L/ton dry biomass (de Medeiros et al., 2017; Dutta et al., 2011; Wei et al., 2009).
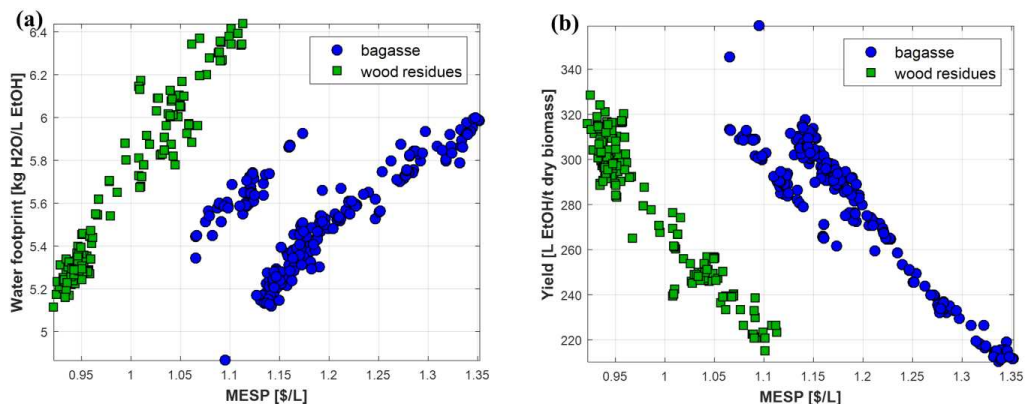
Figure 5.13. Pareto-optimal values of other performance indicators: (a) water footprint; (b) ethanol yield.

At last, Fig. 5.14 illustrates the trade-off between energy efficiency and self-sufficiency. The results indicate that energy self-sufficiency is not necessarily beneficial, as higher values of efficiency can be achieved when energy is purchased (in the form of steam and electricity) instead of produced entirely inside the plant, which sacrifices syngas that could be converted to ethanol. Though this conclusion may seem counterintuitive, it can be clarified by comparing Fig. 5.14 with Fig. 5.13b: as the energy demand increases with η, so does the ethanol yield, with gains that clearly outweigh the extra energy requirement (MESP and η go in different directions, as seen in Figs. 5.10 and 5.11a).
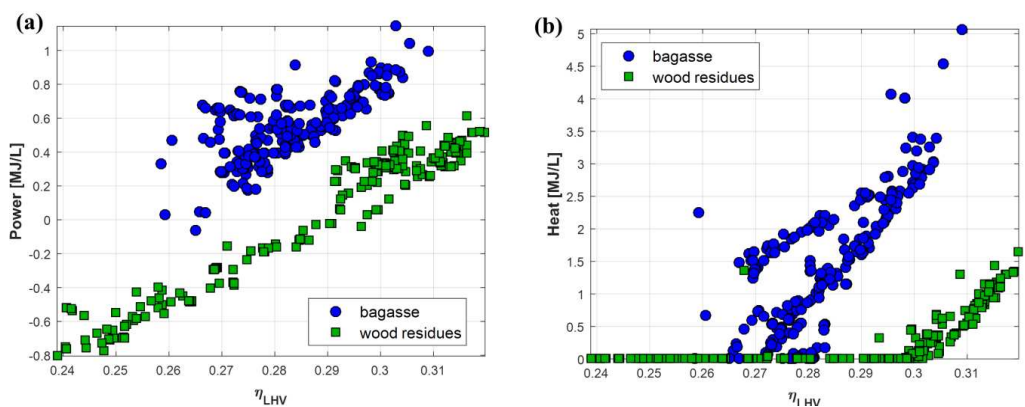
Figure 5.14. Pareto-optimal values of global energy balance (consumed minus produced in the plant): (a) power; and (b) heat (steam).

5.4. Conclusions

In this work we showed how the sustainability of a gasification-fermentation route can be improved (or optimized) by tuning process conditions and design parameters related to different units of the process. We present and discuss the construction of a gasification model and a modeling framework for the whole process from biomass to ethanol fuel, and we show that the input variables have interconnected effects on the outcomes. Multi-objective optimization was then applied as a tool for sustainability optimization that does not rely on assigning weights to goals of different natures (e.g. economic and environmental), but we also discuss the underlined uncertainties in economic-environmental calculations.

References

Bonomi, A., Cavalett, O., da Cunha, M.P., Lima, M.A.P. (Eds.), 2016. Virtual biorefinery, an optimization strategy for renewable carbon valorization. 1st ed., Springer International Publishing.

Capaz, R.S., de Medeiros, E.M., Falco, D.G., Seabra, J.E.A., Osseweijer, P., Posada, J.A., 2020. Environmental trade-offs of renewable jet fuels in Brazil: beyond the carbon footprint. Sci. Total Environ. 714, 136696.

CPFL Energia, 2019. https://www.cpflempresas.com.br/institucional/tarifas.aspx?emp= CPFL, accessed 09/12/2019.

Dutta, A., Talmadge, M., Hensley, J., Worley, M., Dudgeon, D., Barton, D., Groenendijk, P., Ferrari, D., Stears, B., Searcy, E.M., Wright, C.T., Hess, J.R., 2011. Process design and economics for conversion of lignocellulosic biomass to ethanol: thermochemical pathway by indirect gasification and mixed alcohol synthesis. Technical Report NREL/TP-5100-51400.

Elgowainy, A., Han, J., Cai, H., Wang, M., Forman, G.S., DiVita, V.B., 2014. Energy efficiency and greenhouse gas emission intensity of petroleum products at U.S. refineries. Environ. Sci. Technol. 48(13), 7612–7624.

Handler, R.M., Shonnard, D.R., Griffing, E.M., Lai, A., Palou-Rivera, I., 2016. Life cycle assessments of ethanol production via gas fermentation: anticipated greenhouse gas emissions for cellulosic and waste gas feedstocks. Ind. Eng. Chem. Res. 55, 3253–3261.

Hrbek, J., 2019. Status report on thermal gasification of biomass and waste 2019, Annex 3: Gasification facilities for fuel synthesis – operational, under construction, under commissioning. IEA Bioenergy Task 33. http://task33.ieabioenergy.com/content/Task%2033%20Projects (last accessed on 27/01/2020).

Junqueira, T.L., Chagas, M.F., Gouveia, V.L.R., Rezende, M.C.A.F., Watanabe, M.D.B., Jesus, C.D.F., Cavalett, O., Milanez, A.Y., Bonomi, A., 2017. Techno-economic analysis and climate change impacts of sugarcane biorefineries considering different time horizons. Biotechnol. Biofuels 10, 50.

Kirkels, A.F., Verbong, G.P.J., 2011. Biomass gasification: Still promising? A 30-year global overview. Renew. Sust. Energ. Rev. 15, 471–481.

Kumagai, S., Hosaka, T., Kameda, T., Yoshioka, T., 2017. Removal of toxic HCN and recovery of H_2-rich syngas via catalytic reforming of product gas from gasification of polyimide over Ni/Mg/Al catalysts. J. Anal. Appl. Pyrol. 123, 330–339.

Lane, J., 2014. Digest feedback may help explain INEOS Bio's high levels of HCN gas. https://www.biofuelsdigest.com/bdigest/2014/09/08/feedback-may-help-explain-ineos-bios-high-levels-of-hcn-gas/ (last accessed on 27/01/2020).

de Medeiros, E.M., Posada, J.A., Noorman, H., Osseweijer, P., Maciel Filho, R., 2017. Hydrous bioethanol production from sugarcane bagasse via energy self-sufficient gasification-fermentation hybrid route: simulation and financial analysis. J. Clean. Prod. 168, 1625–35.

de Medeiros, E.M., Posada, J.A., Noorman, H., Maciel Filho, R., 2019. Dynamic modeling of syngas fermentation in a continuous stirred-tank reactor: Multi-response parameter estimation and process optimization. Biotechnol. Bioeng. 2019, 2473–2487.

de Medeiros, E.M., Noorman, H., Maciel Filho, R., Posada, J.A., 2020. Production of ethanol fuel via syngas fermentation: optimization of economic performance and energy efficiency. Chemical Engineering Science: X 5, 100056.

Mekonnen, M., Romanelli, T.L., Ray, C., Hoekstra, A.Y., Liska, A.J., Neale, C.M.U., 2018. Water, energy, and carbon footprints of bioethanol from U.S. and Brazil. Environ. Sci. Technol. 52, 14508–14518.

Munir, M.T., Mardon, I., Al-Zuhair, S., Shawabkeh, A., Saqib, N.U., 2019. Plasma gasification of municipal solid waste for waste-to-value processing. Renew. Sust. Energ. Rev. 116, 109461.

Oswald, F., Zwick, M., Omar, O., Hotz, E.N., Neumann, A., 2018. Growth and product formation of Clostridium ljungdahlii in presence of cyanide. Front. Microbiol. 9, 1213.

Padella, M., O'Connell, A., Prussi, M., 2019. What is still limiting the deployment of cellulosic ethanol? Analysis of the current status of the sector. Appl. Sci. 9(21), 4523.

Ramachandriya, K.D., Kundiyana, D.K., Sharma, A.M., Kumar, A., Atiyeh, H.K., Huhnke, R.L., Wilkins, M.R., 2016. Critical factors affecting the integration of biomass gasification and syngas fermentation technology. AIMS Bioeng. 3(2), 188–210.

SEAB, 2019. Preços de produtos florestais. http://www.agricultura.pr.gov.br/Pagina/Precos-de-Produtos-Florestais. Acessed 09-12-2019.

Turton, R., Bailie, R.C., Whithing, W.B., Shaeiwitz, J.A., 2009. Analysis, Synthesis and Design of Chemical Processes, third ed. Prentice Hall, New Jersey.

Ulrich, G.D., Vasudevan, P.T., 2006. How to estimate utility costs. Chem. Eng. (April 2006), 66–69.

Wei, L., Pordesimo, L.O., Igathinathane, C., Batchelor, W.D., 2009. Process engineering evaluation of ethanol production from wood through bioprocessing and chemical catalysis. Biomass Bioenergy 33, 255–266.

Wilk, V., Hofbauer, H., 2013. Conversion of fuel nitrogen in a dual fluidized bed steam gasifier. Fuel 106, 793–801.

Chapter 6

Conclusions and Outlook

"Knowledge is like a sphere: the greater the volume the higher the contact with the unknown."

<div align="right">Blaise Pascal, Pensées</div>

We started this thesis quoting an informal definition of bioeconomy [*the art of bringing value to the valueless*] and after exploring one possible technological route through modeling, simulation and optimization, we are again convinced of its accurateness. Although the second law of thermodynamics naturally limits the reutilization of resources, such that we cannot reuse our waste forever, we are still at a point at which what we call waste contains a significant amount of underutilized resources: it is just a matter of having the right technologies to enable such extraction and conversion of useful resources in an efficient and commercially viable way.

This thesis focused on the thermo-biochemical route, where the process of gasification is used to convert biomass residues to syngas, which is then biochemically converted to ethanol via autotrophic fermentation by acetogenic bacteria. As mentioned in Chapter 1, this route bypasses certain issues encountered in other conversion pathways, such as the complex pretreatment and hydrolysis of biomass prior to sugar fermentation, or the high temperature and pressure conditions needed to convert syngas to ethanol via chemical routes. However, it also faces its own drawbacks and challenges that cannot be ignored. Firstly, there is still a lack of consistent experimental data about yields, conversions and product selectivity for both syngas fermentation and gasification. Although this work did not contribute to filling this gap, we hope that on-going and future research can bring more clarifying information about these two processes, enabling models such as the ones developed in this research to be improved, validated and used in the advancement of this route.

The main goal of this project was laid out in Chapter 1: to find the design and operating conditions that optimize sustainability, therefore a set of targets related to economic performance, environmental impact (carbon footprint) and energy efficiency. The research presented here was fully conducted in dry lab, making use of mathematical models, programming, simulations and numerical methods. A lot of assumptions were made, as needed in every model, and these were disclosed throughout the thesis. We started with a preliminary economic assessment presented in Chapter 2. In this article we developed a simulation of the whole process from feedstock, in this case sugarcane bagasse, to hydrous ethanol, a fuel largely produced from sugarcane in Brazil. For this simulation, the gasification reactor was represented by an equilibrium model, a generic yet effective way of analyzing the thermodynamic limitations of this process. The syngas bioreactor

was initially simulated as a black-box model considering values of conversion and residence time reported in a patent. Ethanol separation, as done in all stages of this research, was simulated rigorously in Aspen with the Inside-Out algorithm to solve the MESH equations. Finally, in this first simulation, some of the process conditions were roughly tuned to achieve energy self-sufficiency by burning unconverted syngas and recovering heat from hot gases. The results of this simulation and preliminary economic assessment revealed a poor economic performance when compared to 1st-generation ethanol, but also demonstrated competitiveness with other 2nd-generation technological routes.

In view of the large research gap in syngas fermentation modeling, the work presented in Chapter 3 followed with the development of a continuous stirred tank model for syngas fermentation considering microbial kinetics and gas-liquid mass transfer. The biokinetic model was conceived to take into account biomass growth and death, product selectivity, acetic acid re-assimilation by the cell, as well as growth inhibition by substrate and product. The unknown parameters used in this model were then estimated using dynamic and steady-state data from five sets of experimental data published in scientific journals. Some of these parameters were assumed to account for specific aspects related to the conditions of the experiments, such as the composition of the nutritional media, and it was observed that fluctuations in these parameters led to different degrees of impact on the results depending on the choice of operating conditions (i.e. dilution rate and gas flow rate). We then discussed how these parameters could potentially be adjusted, along with operating conditions, to improve the results. Finally, the model was used to optimize the input variables with respect to ethanol productivity and gas conversion. We must however reinforce the need for model validation and improvement with more experimental data, especially with regard to expanding the range of input variables and the combinations of variables at different levels.

Continuing the work with modeling of syngas fermentation, the parameters estimated in Chapter 3 were used in the model of a bubble column reactor, which was presented in Chapter 4. The main difference between the two models is the consideration of gradients along the column height, which are neglected in the CSTR model. Because the reactor operates under low pressure (atmospheric), there is a significant pressure drop from the bottom to the top of the column, causing the gas solubility to also decrease. The effects are very nonlinear: the

solubility affects the gas-liquid mass transfer rate and the dissolved concentrations, which in turn affect the reaction kinetics and again the dissolved concentrations. Moreover, the gas expands as the pressure decreases and shrinks due to consumption by the microbial cells, leading to changes in the gas-liquid volumetric mass transfer coefficient (k_La) and the gas hold-up. The model attempts to address all these issues in the system of differential algebraic equations presented in Chapter 4. The other main contribution of this article was the development of an optimization framework for the sub-system consisting of the syngas bioreactor and the separation and purification of anhydrous ethanol, considering also water recycle from the distillation columns to the bioreactor. To enable the large number of objective function evaluations, we applied a technique of surrogate modeling using artificial neural networks (ANNs), where we define and train ANNs with data sets predicted with our models. After validation, these ANNs are then used in the computation of the objective functions considered in the optimization. In this work, multi-objective genetic algorithm was applied to maximize economic performance (measured in terms of the minimum ethanol selling price) simultaneously with the energy efficiency of the process, delivering as result a set of Pareto-optimal solutions representing the optimal trade-offs between these two outcomes. In the article we discussed the behavior of the input (decision) variables along the Pareto fronts and the impact of mass transfer enhancement (increasing k_La), which could be accomplished with process intensification strategies such as microbubble formation methods and the addition of nanoparticles to the reactor. It was also observed that the estimation of k_La has a large impact not only on the outputs of the model but also on the optimal values of the input variables, therefore it is recommended that future works should also contemplate the validation of k_La correlations for the specific cases considered.

Finally, in Chapter 5, the efforts of previous chapters were combined to develop a multi-objective optimization framework for the thermo-biochemical route. The sub-system addressed in Chapter 4 was incorporated in the model of the whole process following a similar arrangement as the flowsheet presented in Chapter 2. We developed a new model for the indirectly-heated dual bed gasifier, thoroughly explained in Chapter 5, which solves the heat balance of the gasification unit by adjusting the amount of air fed to the combustion bed, the temperature difference between the two beds, and the fraction of the inlet biomass that must be burned

instead of gasified, while the temperature of the gasification bed is the independent variable. We included calculations of CAPEX, OPEX, MESP (minimum ethanol selling price), carbon and water footprint, and energy efficiency, and we discussed the simultaneous interactions between these outputs and distinct input variables related to process design choices and operating conditions. For the sustainability optimization, we elected MESP as the main economic indicator, and applied Principal Component Analysis (PCA) to analyze correlations between the responses and reduce the number of objective functions. Energy efficiency and CO_2-equivalent emissions were considered the two other sustainability indicators used as objective functions. This optimization framework was employed for two feedstocks, sugarcane bagasse and wood residues, with the main differences between the two being the composition (e.g. much higher moisture considered for bagasse), the purchase price, and the amount of CO_{2eq} emissions associated with cultivation/transportation stages. The optimization results were displayed as Pareto surfaces representing the optimal trade-offs between the three objectives, as well as 2-D projections with estimated uncertainty intervals related to the uncertainty of various assumptions used in the model, and we also discussed the trends and ranges of the main decision variables along the Pareto-optimal solutions. According to our results, the key variables that define the trade-offs, i.e. those with the widest optimal ranges, would be the temperature in the gasification bed, the fraction of biomass added to the combustion bed of the gasifier, and the ratio between the volumetric flow rate of fresh syngas at the inlet of the bioreactor and the volume of liquid in the bioreactor. Different solutions were obtained for the two feedstocks, although most decision variables spanned similar ranges of optimal values. Due to lower price, moisture and emission factor, wood residues were found to perform better at all sustainability indicators, at least when comparing optimal results. Since economic and environmental predictions involve a number of assumptions, we also addressed the uncertainties of the optimization results with regard to these factors. Eliminating uncertainties at this stage of technology assessment is virtually impossible, nonetheless, the results provide a useful indication of paths towards process improvement/optimization, the relevance of different types of input variables, and the expected performance of the process. Optimization frameworks like the one developed in this research can provide meaningful insights and guidance not only as an early-stage tool, but also during more advanced stages of the development and implementation of a new technology, when concrete data are more readily available and can be fed

back to the models or used to narrow down the search space during the multi-objective optimization.

To wrap up, this thesis has demonstrated that gasification coupled with syngas fermentation can be a competitive technological route for the production of 2nd-generation ethanol. Although our results do not suggest an economic advantage at first, it performs well in terms of energy efficiency and carbon footprint, values which are consistently gaining more weight for the ranking of new technologies. Clearly, the predictions will be more accurate when more data is available to validate the models and make necessary adjustments. Nonetheless, we have demonstrated how different process systems engineering (PSE) concepts and tools can be combined to aid in the design and optimization of sustainable processes, most notably: the use of artificial neural networks as surrogate models to enable the use of predictions from rigorous instead of short-cut models; correlation analysis and Principal Component Analysis to evaluate the relevance of distinct input variables and to reduce the number of objective functions; the use of global optimization methods such as genetic algorithm; and the generation of approximate Pareto fronts for the evaluation of optimal trade-offs among responses. When it comes to biological processes, such as syngas fermentation, we can also add that multi-level optimization frameworks will be a powerful tool for process enhancement, i.e. combining genetic engineering efforts with the simultaneous optimization of design and operating parameters, since we have noticed a different sensitivity of the kinetic parameters depending on the operating conditions in the bioreactor (dilution rate, gas flow rate, gas recycle rate, cell recycle).

Moreover, other reactor designs could bring significant improvement in terms of gas-liquid mass transfer, which was shown to have a great impact on the overall performance of the process. For example, gas-lift, trickle bed and membrane reactors are all candidates that should be tested in future optimization studies. In downstream stages, this thesis focused on distillation as the most feasible technology, but alternative process configurations could include gas stripping in the bioreactor as a way to extract ethanol from the broth via the gas phase, leading to a higher concentration in the feed stream of the first distillation column. However, future research projects should investigate the trade-offs between lower energy requirements in the distillation columns and higher electricity consumption in the recycle gas compressor (due to very large gas flow rates

needed in the stripping process) as well as in the production of chilled water needed to condense the ethanol/water mixture from the overhead vapors. In this case, the energy consumption might be reduced with the use of thermophilic strains (which still need to be engineered for syngas fermentation), thereby allowing the fermentation to occur under higher temperatures (e.g. around 70 °C) and more ethanol to be stripped from the liquid, although this would also lower the solubility of gases in the liquid phase.

A critical issue, which was addressed superficially in this thesis, is the presence of contaminants in the syngas and the actual level of gas cleaning that will be required to avoid complications in real applications of this process. Based on the literature and due to lack of data and time limitations, we have assumed from the beginning that an acceptable amount of contaminants remains in the gas after a mild cleaning step in a water scrubber, but more research is needed to fully comprehend the effects of different components – including tars and even methane – on the microbial metabolism governing the chemical reactions. Though not a contaminant per se, CO_2 can also be removed from syngas for a price that may or may not justify an increased productivity of ethanol, this being a trade-off that should be investigated. Another point that needs further investigation is microbial inhibition caused not only by contaminants, but also by products (i.e. ethanol and acetic acid) and substrate (CO, H_2 and CO_2), which we have tried to address with our syngas fermentation model.

This research project has ended with more questions than answers regarding the thermo-biochemical route, but we hope it also gives a contribution beyond this field, with the collection and presentation of methods and strategies that can be applied to any technology, not only the emerging and "promising" ones, but also consolidated technologies that might need to adapt to pressing sustainability goals. Finally, this thesis illustrates a prevailing aspect of real-world problems: even when focusing on a single technology, we encountered not one, but many (equally optimal) solutions, determined here by different combinations of relevant input variables. In a similar fashion, but on a much larger scale, this is how the solutions to sustainable development will look like: different resource materials, different technologies, different products will be a part of it; and they will interact and affect each other in often unexpected ways.

Appendix A. Supplementary Materials

A1. Supplementary Materials for Chapter 2: Hydrous bioethanol production from sugarcane bagasse via energy self-sufficient gasification-fermentation hybrid route: simulation and financial analysis

A2. Supplementary Materials for Chapter 3: Dynamic modeling of syngas fermentation in a continuous stirred tank reactor: multi-response parameter estimation and process optimization

A3. Supplementary Materials for Chapter 5: Multi-objective sustainability optimization of biomass residues to ethanol via gasification and syngas fermentation: trade-offs between profitability, energy efficiency and carbon emissions

A1. Supplementary Materials for Chapter 2: Hydrous bioethanol production from sugarcane bagasse via energy self-sufficient gasification-fermentation hybrid route: simulation and financial analysis

Financial Model Supplementary Data: Tables A1-1 to A1-7

Aspen Flowsheets: Figures A1-1 to A1-6

Table A1-1. OPEX Estimation Assumptions (adapted from Peters and Timmerhaus, 1991)

OPEX Component	Value
Operating labor (DPC)	10% OPEX
Direct supervisory and clerical labor (DPC)	15% C_{OL}
Maintenance and repair (DPC)	5% FCI_L
Operating supplies (DPC)	0.5% FCI_L
Laboratory charges (DPC)	10% C_{OL}
Patents and royalties (DPC)	1% OPEX
Local taxes and insurance (FPC)	2% FCI_L
Plant overhead (FPC)	10% OPEX
Administrative expenses (GE)	2% OPEX
Distribution and selling (GE)	5% OPEX
Research and Development (GE)	3% OPEX

DPC: Direct production costs; FPC: Fixed production costs; GE: General expenses; C_{OL}: Cost of operating labor; FCI_L: Fixed capital investment excluding land purchase cost. OPEX = DPC + FPC + GE. DPC also includes costs of raw materials, utilities and waste treatment/disposal. Assumptions are based on ranges in agreement with Peters and Timmerhaus (1991).

Table A1-2. Syngas Fermenter Sizing Assumptions

Reactor type	Jacketed agitated vessel
Working volume per vessel	80% of vessel volume
Total working volume (m³)	$V_L = \dfrac{Q_g}{GRT} = \dfrac{Q_l}{LRT}$
Volume per reactor vessel	975 m³
Number of reactor vessels	$N = \dfrac{V_L}{(80\%)975\ m^3}$

V_L: Total working volume of reactor vessels; Q_g: Gas volumetric flow; Q_l: Liquid volumetric flow; GRT: Gas retention time; LRT: Liquid retention time; N: Number of reactor vessels.

Table A1-3. Water Chiller[a,b] Sizing Assumptions

Refrigeration fluid	Propane
$T_{cold\ side}$	10 °C
$T_{hot\ side}$	45 °C
Coefficient of Performance $\left(COP = {Q_{EVAPORATOR}}/{W_{COMPRESSOR}}\right)$	4.5
$U_{Evaporator}$	600 W/m²K
$U_{Air\text{-}Cooled\ Condenser}$	500 W/m²K

[a] Chilled water is sent to the process at 15°C and returns at 25°C.

[b] Chiller is a refrigeration machine comprising a compressor and two heat exchangers (evaporator and condenser), whose capacities can be calculated using the assumptions above.

Table A1-4. Cost Estimation of Installed Gasification Reactor

	Taylor Biomass Energy [b] (Aug 2010)	Present study capacity (Aug 2010)	Present study capacity (Nov 2015)
Capacity (MTPD)[a]	500	624	624
Purchase Cost (US$)	9,700,000	11,080,000	10,940,000
Installation Factor	2.31	2.31	2.31
Total Installed Cost (US$)	22,410,000	25,590,000	25,280,000

[a] Metric tons per day

[b] Retrieved from Dutta et al. (2011)

Table A1-5. Cost Estimation of Installed Microfiltration System

	Han and Cheryan (1996)	Present study capacity (1996)	Present study capacity (Nov 2015)
Membrane module area (m²) [a]	2,513	929.8	929.8
Total Installed Cost ($)	5,402,950 [b]	2,842,923	4,231,345

[a] Membrane module area assumes the same flux rate (m³/m²h); permeate volumetric flow rate is known in both cases.

[b] Calculated using the published value of specific installed cost = $2,150/m²

Table A1-6. Cost Estimation of Installed Tower for Cooling Water (CW)

Base year	1985
Total installed cost (1000US$) [a]	$C = 135 f Q^{0.61}$
$f\ (\Delta t = 10°C)$	1.0
CW volumetric flow rate range	$1 < Q < 60\ kgal/min$

C: Total installed cost; Q: CW volumetric flow rate.

[a] Retrieved from: Walas (1990)

Table A1-7. Assumptions of purchase cost of other raw materials (2015)

	Price (US$/t)	Source for base price
Olivine	238.65	Dutta et al. (2011)
MgO	503.78	Dutta et al. (2011)
Tar reformer catalyst	44.63	Dutta et al. (2011)
CW makeup antifouling chemicals	0.17	Turton et al. (2008)
Fresh water	0.074	Turton et al. (2008)
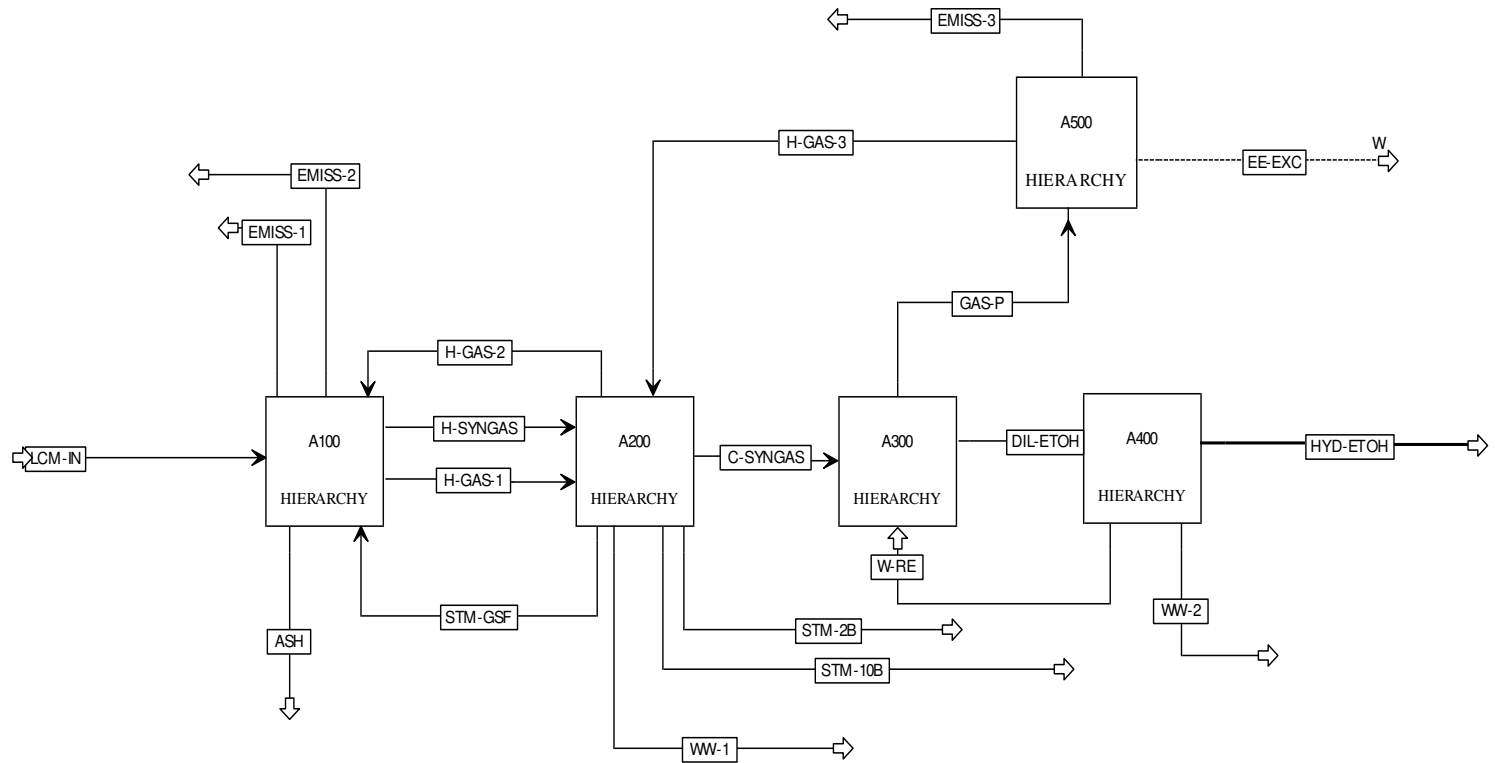
Fig. A1-1. Main Process Flowsheet Diagram

Fig. A1-2. Gasification Unit (A100 in Fig. A1-1). RD: Rotary dryer; RD-CYC: Rotary dryer cyclone; DCMP: Biomass decomposition block; S-1: Carbon splitter; GZ: Gasification zone (bed); CZ: Combustion zone (bed); CYC: Cyclone; E-1: Air preheater; C-1: Air compressor.
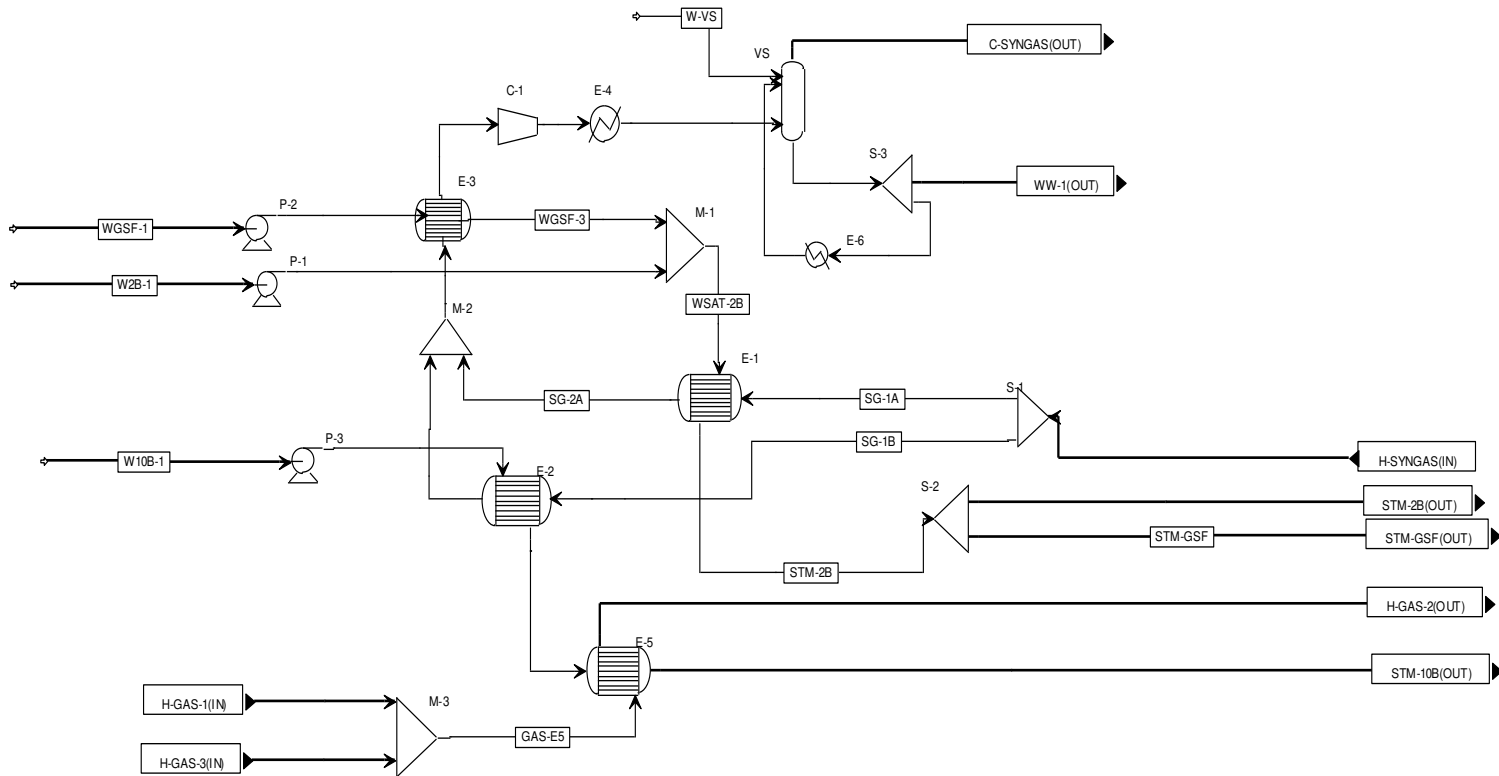
Fig. A1-3. Steam Generation Unit (A200 in Fig. A1-1). VS: Venturi scrubber; E-1 to E-6: Heat exchangers.
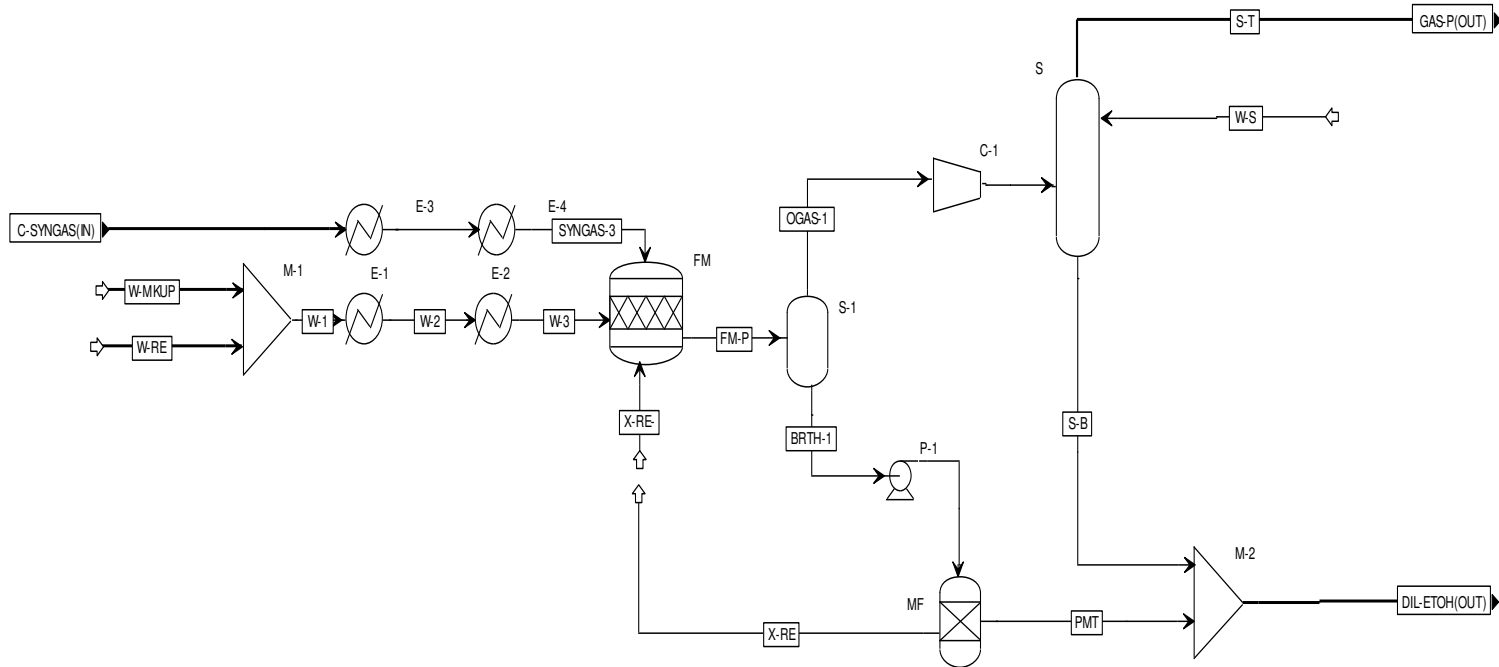
Fig. A1-4. Syngas Fermentation Unit (A300 in Fig. A1-1). FM: Fermenter; S-1: Gas-liquid flash separator; MF: Microfiltration system; S: CO2 scrubber; E-1 and E-3: heat exchanger with cooling water; E-2 and E-4: heat exchangers with chilled water; C-1: Gas compressor.
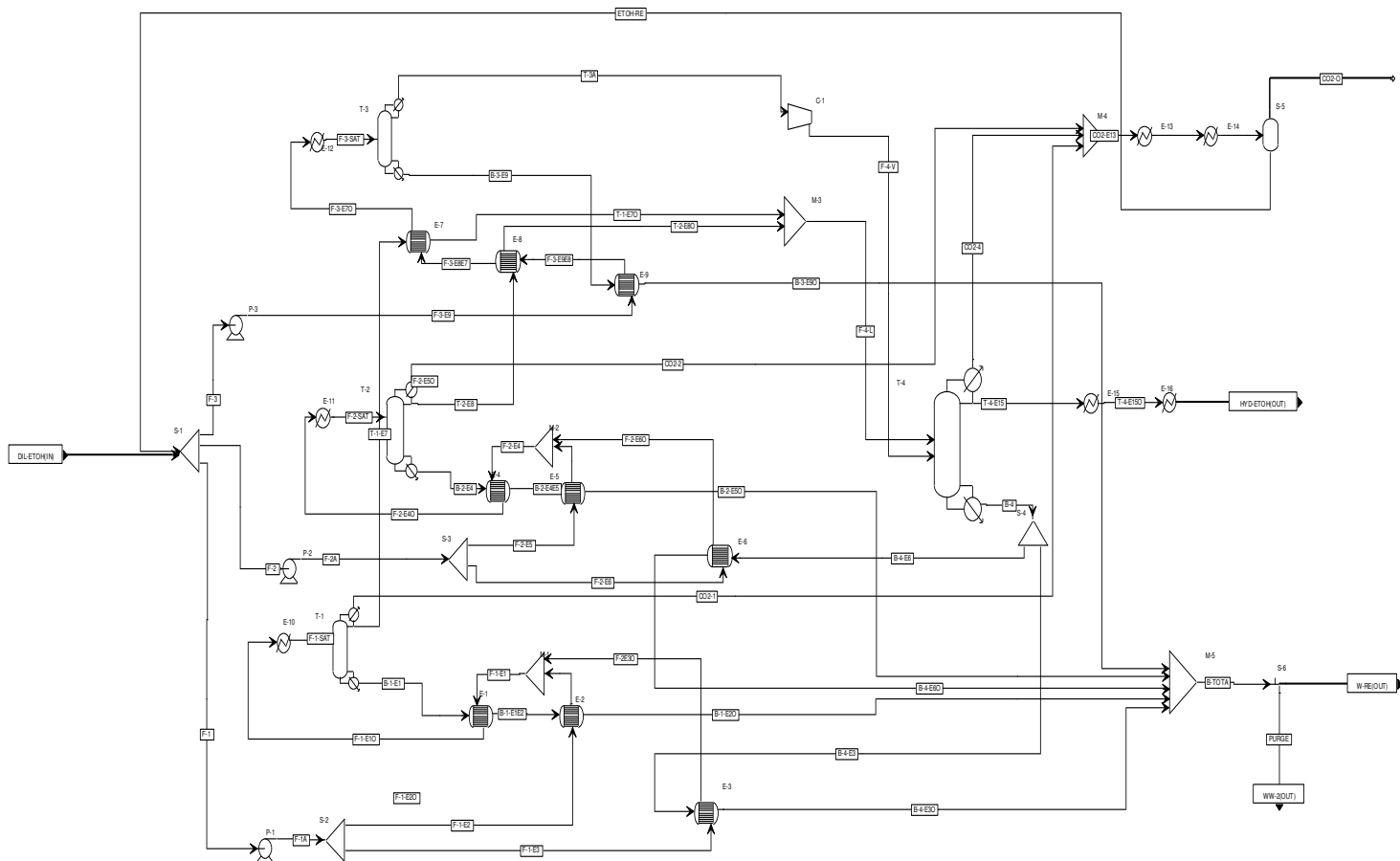
Fig. A1-5. Ethanol Distillation Unit (A400 in Fig. A1-1). T-1 to T-4: Distillation towers; E-1 to E-16: Heat exchangers; S-5: Flash separator.
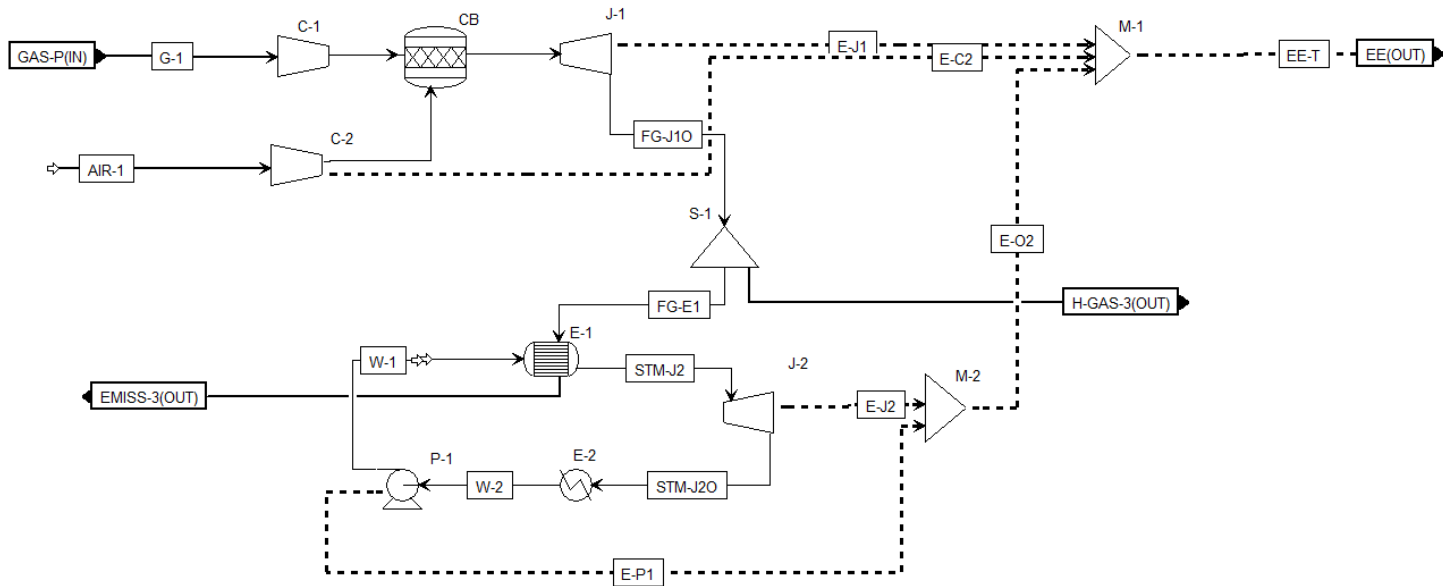
Fig. A1-6. Power Generation Unit (A500 in Fig. A1-1). C-1: fuel gas compression; C-2: air compression; CB: Combustion chamber; J-1: Gas turbine expansion; E-1: steam generation; J-2: Steam turbine expansion; E-2: steam condensation; P-1: water pump

References for Appendix A1

Dutta, A., Talmadge, M., Hensley, J., Worley, M., Dudgeon, D., Barton, D., Groenendijk, P., Ferrari, D., Stears, B., Searcy, E.M., Wright, C.T., Hess, J.R., 2011. Process design and economics for conversion of lignocellulosic biomass to ethanol. Report NREL/TP-5100-51400. National Renewable Energy Laboratory (NREL), Colorado, USA.

Han, I.S., Cheryan, M., 1996. Downstream processing of acetate fermentation broths by nanofiltration. Appl. Biochem. Biotechnol. 57/58, 19–28.

Peters, M.S., Timmerhaus, K.D., 1991. Plant design and economics for chemical engineers. McGraw-Hill, New York.

Turton, R., Bailie, R.C., Whiting, W.B., Shaeiwitz, J.A., 2008. Analysis, Synthesis and Design of Chemical Processes, Prentice Hall International Series in the Physical and Chemical Engineering Sciences. Pearson Education, Michigan, USA.

Walas, S.M., 1990. Chemical Process Equipment: Selection and Design. Butterworth-Heinemann, Boston, USA.

A2. Supplementary Materials for Chapter 3: Dynamic modeling of syngas fermentation in a continuous stirred tank reactor: multi-response parameter estimation and process optimization

Lag-phase

The uptake rates of CO and H_2 were multiplied by a lag-phase term when the experimental data suggested such behavior. This was done only for the dynamic case study C1, in which the uptake rates v_j (j = CO, H_2) were multiplied by I_{lag} as described in Eq. (S1), to simulate lag-phase behavior during the first 150 hours of fermentation.

$$I_{lag} = \left(1 + \exp\left(-0.15 \cdot \left(t - 150\right)\right)\right)^{-1} \tag{A2-1}$$

Table A2-1. Species properties for gas-liquid equilibrium and mass transfer coefficients.

	CO	H_2	CO_2	EtOH	HAc	H_2O
H_j †	4.972×10^9	6.692×10^9	1.205×10^8	-	-	-
$P_{sat,j}$ ‡	-	-	-	1.523×10^4	4.047×10^3	6.260×10^3
γ_j^∞ §	-	-	-	7.6	3.5	-
Df_j ¶	2.03×10^{-5}	4.50×10^{-5}	1.92×10^{-5}	0.84×10^{-5}	0.99×10^{-5}	-

† Henry constants (Pa) in water at 36°C calculated with the correlations reported in Sander (1999).

‡ Vapor pressure (Pa) at 36°C calculated with Antoine equation.

§ Activity coefficients at infinite dilution in water predicted with UNIFAC model using Aspen Plus.

¶ Mass diffusivity ($cm^2.s^{-1}$) in liquid water at 25°C from Cussler (1997). Since for a species i the relationship $Df_i \cdot \mu_{H_2O} / T$ is constant (Perry and Green, 1999), it can be shown that the relationship Df_i / Df_{air} is also constant with temperature. The mass diffusivity of air in water at 25°C is $2 \cdot 10^{-5}$ $cm^2.s^{-1}$.

Table A2-2. Bounds used in parameter estimation.

Parameter β_k	Unit	Lower Bound	Upper Bound
$V_{\max,CO}$	mmol.g^{-1}.h^{-1}	15	60
$V_{\max,H_2}$	mmol.g^{-1}.h^{-1}	15	60
$K_{S,CO}$	mmol.L^{-1}	0.001	0.9
K_{S,H_2}	mmol.L^{-1}	0.001	0.9
$K_{I,EtOH}$	mmol.L^{-1}	100	1000
$K_{I,HAc}$	mmol.L^{-1}	100	1000
$K_{I,CO}$	mmol.L^{-1}	0.1	1
$Y_{CO,X}$	g.mol^{-1}	0.1	3
$Y_{H_2,X}$	g.mol^{-1}	0.1	3
$V_{\max,AcR}^{CO}$	mmol.g^{-1}.h^{-1}	1	50
$K_{S,AcR}^{CO}$	mmol.L^{-1}	20	600
$V_{\max,AcR}^{H_2}$	mmol.g^{-1}.h^{-1}	1	50
$K_{S,AcR}^{H_2}$	mmol.L^{-1}	20	600
k_d	h^{-1}	0.001	0.05
f_0	-	0.1	1

Table A2-3. Bounds used in the optimization of ethanol productivity and CO conversion.

Parameter β_k	Unit	Lower Bound	Upper Bound
GRT	min	5	50
D_{rate}	h^{-1}	0.005	0.2
XP	-	0.1	1
$H_2{:}CO$	-	0	3
$V_{max,CO}$	$mmol.g^{-1}.h^{-1}$	35	50
V_{max,H_2}	$mmol.g^{-1}.h^{-1}$	25	40
$Y_{X,CO}$	$g.mol^{-1}$	0.6	2.5
Y_{X,H_2}	$g.mol^{-1}$	0.1	0.3
$V_{max,AcR}^{CO}$	$mmol.g^{-1}.h^{-1}$	20	50
$K_{S,AcR}^{CO}$	$mmol.L^{-1}$	300	500
$V_{max,AcR}^{H_2}$	$mmol.g^{-1}.h^{-1}$	1	30
$K_{S,AcR}^{H_2}$	$mmol.L^{-1}$	300	600
k_d	h^{-1}	0.005	0.01

Bounded Simplex Algorithm

As explained in the main text (Chapter 3), the estimated parameters presented in this study were obtained using Genetic Algorithm, but the derivative-free method Simplex was also used for deepening . The MATLAB function *fminsearch* applies Simplex Algorithm for unconstrained multi-variable problems, but in the present study the parameters are constrained as shown in Table S2. In order to use this method with constraints on the optimization variables, the vector of constrained parameters being estimated $\hat{\beta}$ must be transformed into a new vector of unconstrained parameters ω, whose individual elements ω_k are computed with Eq. (A2-2) from a given initial estimate $\hat{\underline{\beta}}$, where LB_k and UB_k are the lower and upper bounds pre-established for parameter $\hat{\beta}_k$.

Then, during the Simplex search, the subroutine that receives the unconstrained parameters and generates the responses $\hat{\underline{y}}_j$ in each iteration, receives the new unconstrained vector $\underline{\omega}$ and converts it back to $\underline{LB} \leq \hat{\underline{\beta}} \leq \underline{UB}$ via Eq. (A2-3) so that the right-hand side of the ODE system may be computed with $\hat{\underline{\beta}}$ in the appropriate range of values, allowing to obtain $\hat{\underline{y}}_j$.

$$\omega_k = \left(\frac{\hat{\beta}_k - LB_k}{UB_k - \hat{\beta}_k} \right)^{1/2} \tag{A2-2}$$

$$\frac{\hat{\beta}_k - LB_k}{UB_k - LB_k} = \frac{\omega_k^2}{\omega_k^2 + 1} \quad \Rightarrow \quad \hat{\beta}_k = LB_k + (UB_k - LB_k) \cdot \left(\frac{\omega_k^2}{\omega_k^2 + 1} \right) \qquad -\infty < \omega_k < +\infty \tag{A2-3}$$

Statistical Analysis

With assumptions (A1), (A2), (A3) and Eqs. (3.30)-(3.31) from the main text, as well as the numerically estimated parameters $\hat{\beta}$ from the single-objective minimization (Eq. (3.32) from the main text), several statistical entities were calculated to check the goodness of the estimation and evaluate significance of parameters. The necessary statistical formulas are presented here with limited explanation (see Himmelblau, 1970). The main building block is the N_E x N_P Jacobian matrix $\underline{\underline{X}}_j$ of responses j relative to parameters, from which the N_P x N_P matrix $\left[\underline{\underline{XWX}} \right]$ is constructed as in Eq. (A2-4). Then the variance-covariance matrices of estimated parameters and predicted responses follow, respectively, in Eq. (A2-5).

$$\left[\underline{\underline{XWX}} \right] = \sum_{j=1}^{N_R} \left(\underline{\underline{X}}_j^T \underline{\underline{W}}_j \underline{\underline{X}}_j \right) \tag{A2-4}$$

$$\underline{\underline{Cov}}\left(\hat{\beta} \right) = \sigma_\varepsilon^2 \left[\underline{\underline{XWX}} \right]^{-1} \quad , \quad \underline{\underline{Cov}}\left(\hat{\underline{y}}_j \right) = \sigma_\varepsilon^2 \underline{\underline{X}}_j \left[\underline{\underline{XWX}} \right]^{-1} \underline{\underline{X}}_j^T \tag{A2-5}$$

At the optimal $\hat{\underline{\beta}}$ solution, it can be shown (Himmelblau, 1970) that the statistic S_R^2 – the multi-response weighted sum of squared residuals given in Eq. (A2-6) – has several useful properties: *(i)* it corresponds to the optimum objective value in Eq. (32) (main text) divided by $N_R \cdot N_E - N_P$; *(ii)* it is uncorrelated with $\hat{\underline{\beta}}$; *(iii)* it is the best estimator (unbiased and coherent) of the fundamental variance σ_ε^2 ; and *(iv)* $S_R^2 (N_R \cdot N_E - N_P) / \sigma_\varepsilon^2$ follows a chi-square (χ^2) PDF with $N_R \cdot N_E - N_P$ degrees of freedom. S_R^2 allows to obtain estimators of the variance-covariance matrices in Eq. (A2-5) as given in Eq. (A2-7). From Eq. (A2-7) one can extract estimators of standard deviations of estimated parameter $\hat{\beta}_k$ and estimated response *j* at experiment *i*, $\hat{y}_{j,i}$, as shown in Eq. (A2-8). Confidence intervals at 95% probability for true parameters and responses can be constructed as shown, respectively, in Eqs. (A2-9) and (A2-10), where $t_{1-\alpha/2}$ is the abscissa at $(1-\alpha/2) \cdot 100\%$ probability ($\alpha=0.05$) of the t-Student PDF with $N_R \cdot N_E - N_P$ degrees of freedom.

$$S_R^2 = \left(\frac{1}{N_R \cdot N_E - N_P} \right) \sum_{j=1}^{N_R} \left(\underline{y}_j - \hat{\underline{y}}_j \right)^T \underline{\underline{W}}_j \left(\underline{y}_j - \hat{\underline{y}}_j \right) \tag{A2-6}$$

$$\underline{\underline{C\hat{o}v}}\left(\hat{\beta} \right) = S_R^2 \left[\underline{\underline{XWX}} \right]^{-1} \quad , \quad \underline{\underline{C\hat{o}v}}\left(\hat{\underline{y}}_j \right) = S_R^2 \underline{\underline{X}}_j \left[\underline{\underline{XWX}} \right]^{-1} \underline{\underline{X}}_j^T \tag{A2-7}$$

$$\hat{\sigma}_{\hat{\beta}_k} = \sqrt{\left[\underline{\underline{C\hat{o}v}}(\hat{\beta}) \right]_{kk}} \quad , \quad \hat{\sigma}_{\hat{y}_{j,i}} = \sqrt{\left[\underline{\underline{C\hat{o}v}}(\hat{\underline{y}}_j) \right]_{ii}} \tag{A2-8}$$

$$\hat{\beta}_k - t_{1-\alpha/2} \cdot \hat{\sigma}_{\hat{\beta}_k} \leq \beta_k \leq \hat{\beta}_k + t_{1-\alpha/2} \cdot \hat{\sigma}_{\hat{\beta}_k} \tag{A2-9}$$

$$\hat{y}_{j,i} - t_{1-\alpha/2} \cdot \hat{\sigma}_{\hat{y}_{j,i}} \leq \eta_{j,i} \leq \hat{y}_{j,i} + t_{1-\alpha/2} \cdot \hat{\sigma}_{\hat{y}_{j,i}} \tag{A2-10}$$

The F-test to reject the null hypothesis (i.e. parameter β_k is significant) with 95% probability is given (Himmelblau, 1970) in Eq. (A2-11), where $\phi_{1-\alpha}(1, N_R \cdot N_E - N_P)$ is the abscissa at $(1-\alpha) \cdot 100\%$ probability ($\alpha=0.05$) of the Fisher PDF with degrees of freedom $(1, N_R \cdot N_E - N_P)$.

$$R(\hat{\beta}_k) = \frac{\left(\hat{\beta}_k \right)^2}{\left(\hat{\sigma}_{\hat{\beta}_k} \right)^2} > \phi_{1-\alpha}\left(1, N_R \cdot N_E - N_P \right) \Rightarrow \beta_k \neq 0 \tag{A2-11}$$

Table A2-4. F-test score $R_{\hat{\beta}_k}$ **for the parameter estimates** $\hat{\beta}_k$ **with 95% probability.**

Parameter	C1	C2	C3-A	C3-B	C3-C
$\phi_{1-\alpha}$ †	3.93	3.90	4.10	4.10	4.10
$V_{max,CO}$	297	181	208	118	793
V_{max,H_2}	140	54.3	247	222	696
$K_{S,CO}$	1293	13.0	188	67.8	306
K_{S,H_2}	246	32.3	396	54.1	1163
$K_{I,EtOH}$	123	-	-	-	-
$K_{I,HAc}$	226	10.3	228	427	92.6
$K_{I,CO}$	145	5.98	230	87.4	232
$Y_{X,CO}$	126	137	88.3	70.6	265
Y_{X,H_2}	293	24.5	158	185	1733
$V_{max,CO}^{AcR}$	285	17.7	431	424	788
$K_{S,CO}^{AcR}$	1428	13.5	790	44.3	293
V_{max,H_2}^{AcR}	444	33.2	352	90.8	780
K_{S,H_2}^{AcR}	613	16.3	487	137	351
k_d	2169	14.1	323	69.3	143
f_o	1786	31.1	414	65.5	263

† $R_{\hat{\beta}_k} > \phi_{1-\alpha}$ for parameter significance where $\phi_{1-\alpha}$ is the Fischer abscissa at 95% probability (α = 0.05) for degrees of freedom 1 and $N_R \cdot N_E - N_P$.

Additional variables with time profile

Fig. A2-1 presents the profiles of variables that are model inputs but also change with time, for case study C1. The agitation rate (N), inlet volumetric gas flow rate ($Q_{G,in}$) and volumetric liquid flow rate ($Q_{L,in}$) were obtained assuming linear profiles with time given the information provided in the article used as reference; and the mass transfer coefficient $k_L a_{ref}$ was calculated as explained in the main text. The liquid volume is 1000 mL.
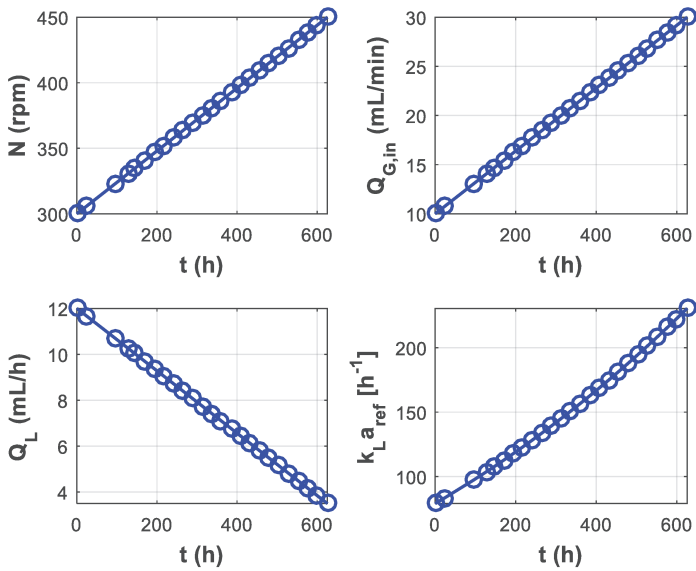
Figure A2-1. Dynamic profiles of agitation rate (N), inlet volumetric gas flow rate ($Q_{G,in}$), volumetric liquid flow rate ($Q_{L,in}$) and calculated $k_L a_{ref}$ in case study C1.

Effects of the initial conditions on the steady-state

(A) (B)
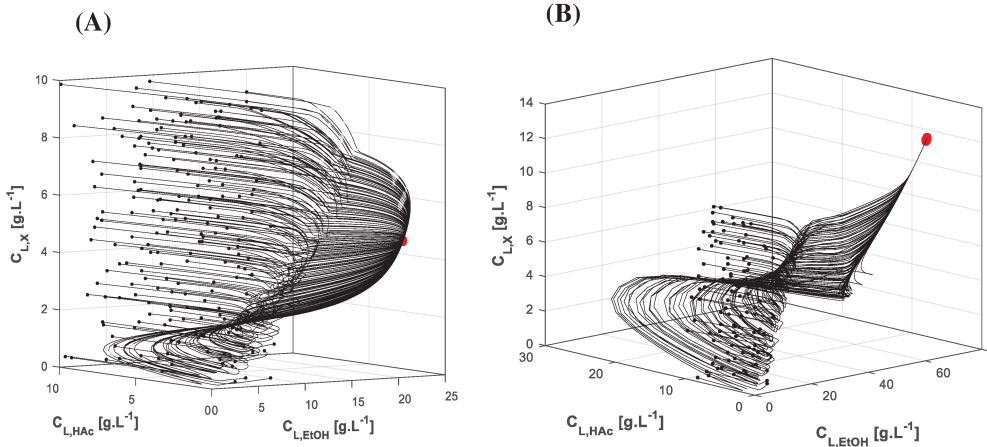
Figure A2-2. Phase portraits of ethanol, acetic acid and biomass concentrations with random perturbations on the initial conditions: dynamic trajectories (black solid lines), initial conditions (black spheres), steady states (red spheres). Operating conditions fixed at: (A) GRT = 50 min and D_{rate} = 0.01 h^{-1}; (B) GRT = 3.33 min and D_{rate} = 0.01 h^{-1}.

Effects of the agitation rate

(A)

(B)

(C)

(D)
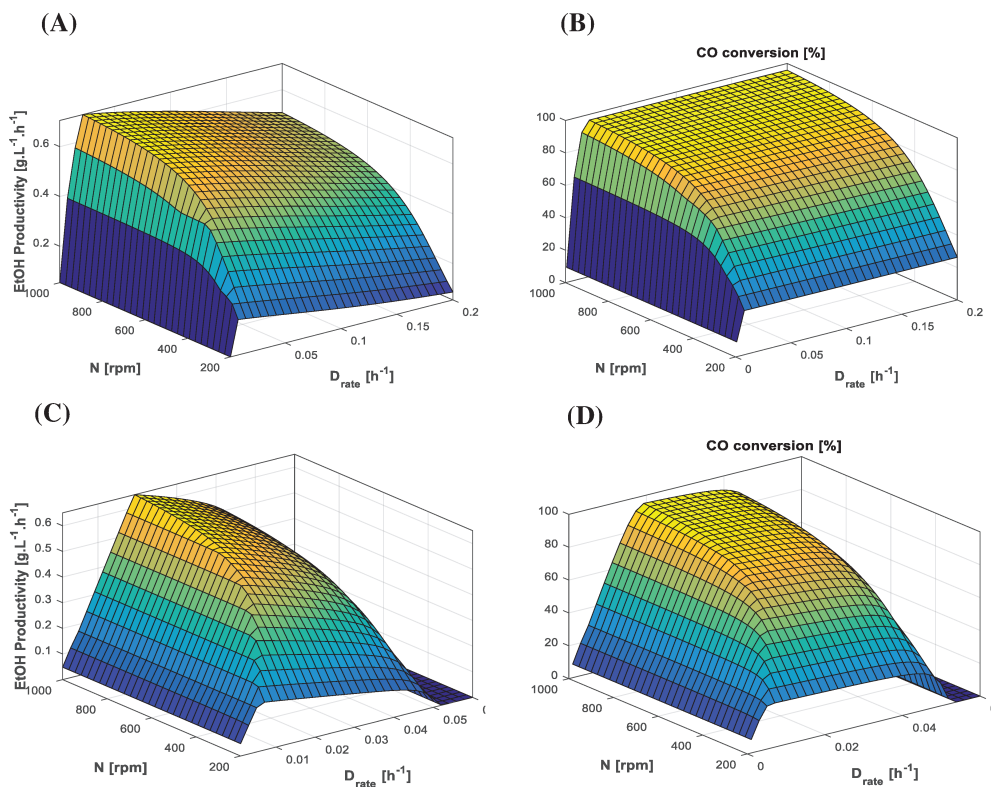
Figure A2-3. Steady-state ethanol productivity and CO conversion as function of agitation rate (N) and liquid dilution rate (D_{rate}): (A, B) with 90% cell recycle; (C, D) without cell recycle. Fixed conditions: y_{CO} = 0.65, y_{H_2} = 0.2, y_{CO_2} = 0.15, GRT = 20 min.

Effects of dilution rate and gas residence time with H_2-rich gas

(A)

(B)

(C)

(D)
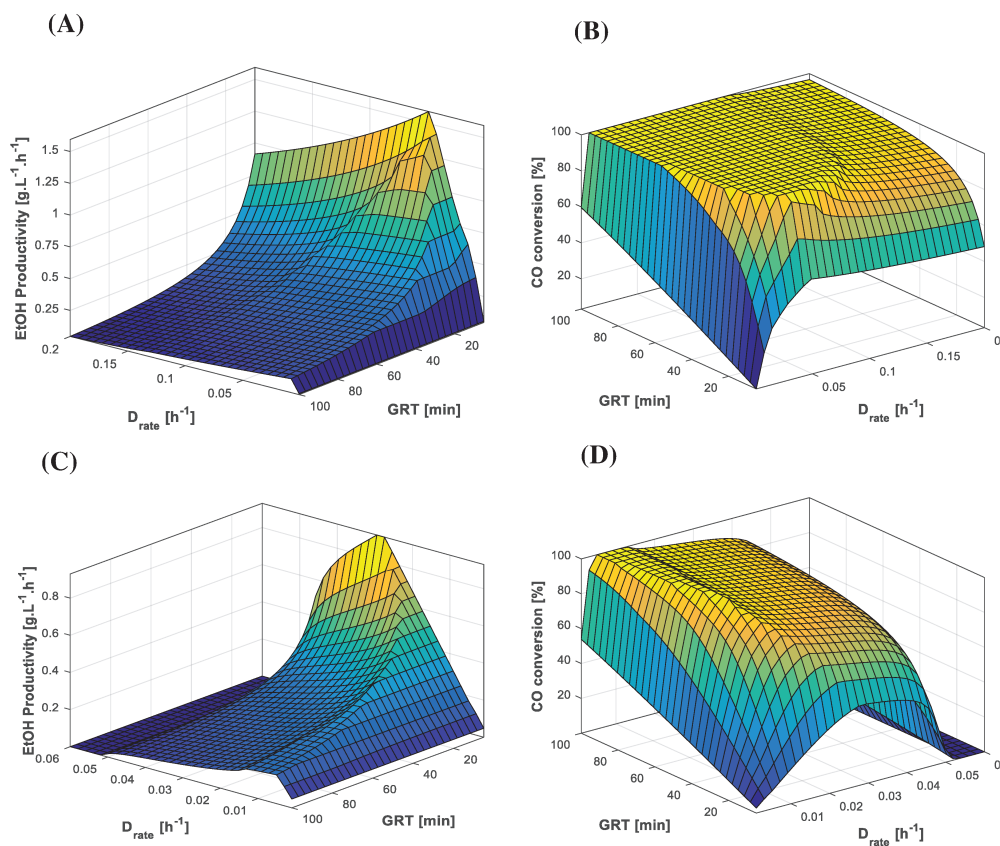
Figure A2-4. Steady-state ethanol productivity and CO conversion as function of gas residence time (GRT) and liquid dilution rate (D_{rate}): (A, B) with 90% cell recycle; (C, D) without cell recycle. Fixed conditions: $y_{CO} = 0.45$, $y_{H_2} = 0.5$, $y_{CO_2} = 0.05$, $N = 500$ **rpm. Note: the axes are rotated in (A) and (C).**

Optimization of process conditions and kinetic parameters

Table A2-5. Minimum and maximum values of the decision variables at the Pareto-optimal solutions

Decision Variable	1st run (65% CO, 20% H₂, 15% CO₂)		2nd run † (45% CO, 50% H₂, 5% CO₂)		3rd run †	
	min	max	min	max	min	max
GRT	5.45	49.8	8.22	32.7	7.79	29.9
D_{rate}	0.0396	0.173	0.0456	0.0607	0.0465	0.0605
XP	0.130	0.150	0.122	0.189	0.105	0.351
$H_2{:}CO$	-	-	-	-	0.778	0.855
$V_{max,CO}$	42.8	45.3	43.7	45.0	38.5	43.2
V_{max,H_2}	34.3	36.6	33.3	36.1	32.4	36.1
$Y_{X,CO}$	2.15	2.49	2.12	2.40	2.02	2.40
Y_{X,H_2}	0.200	0.299	0.209	0.267	0.196	0.289
$V_{max,CO}^{AcR}$	39.0	42.1	31.8	33.3	33.9	35.4
V_{max,H_2}^{AcR}	1.16	2.26	16.2	23.5	12.1	17.5
$K_{S,CO}^{AcR}$	362	365	398	428	397	404
K_{S,H_2}^{AcR}	471	488	403	485	358	449
k_d	0.00637	0.00742	0.00564	0.00870	0.00518	0.00878

† All points achieved 100% CO conversion.

Table A2-6. Selected solutions from the multi-objective optimization: 1st run (CO-rich gas)

GRT	D_{rate}	XP	$V_{max,CO}$	V_{max,H_2}	$Y_{X,CO}$	Y_{X,H_2}	V_{max,H_2}^{AcR}	k_d	EtOH Productivity	CO conversion
49.8	0.173	0.130	45.3	36.6	2.44	0.273	1.54	0.00742	0.180	0.949
45.8	0.0505	0.133	44.4	35.7	2.43	0.259	1.49	0.00722	0.281	0.935
33.6	0.0574	0.133	43.9	35.8	2.42	0.239	1.51	0.00669	0.376	0.912
25.2	0.0407	0.133	43.6	35.9	2.38	0.232	1.45	0.00675	0.506	0.883
20.9	0.0404	0.133	43.6	35.7	2.40	0.258	1.40	0.00644	0.598	0.860
16.5	0.0404	0.137	43.6	35.5	2.41	0.226	1.21	0.00652	0.730	0.824
14.1	0.0438	0.134	43.8	35.0	2.39	0.220	1.20	0.00644	0.821	0.797
11.5	0.0401	0.134	43.4	35.4	2.41	0.219	1.31	0.00642	0.963	0.754
9.75	0.0397	0.134	43.6	35.5	2.40	0.239	1.24	0.00648	1.08	0.716
7.80	0.0417	0.133	43.7	34.4	2.38	0.223	1.82	0.00643	1.23	0.655
6.69	0.0411	0.134	43.4	34.8	2.41	0.211	1.31	0.00644	1.35	0.613
5.71	0.0490	0.134	43.7	35.5	2.30	0.205	1.45	0.00650	1.45	0.564

Table A2-7. Selected solutions from the multi-objective optimization: 2nd run (H₂-rich gas)

GRT	D_{rate}	XP	$V_{max,CO}$	V_{max,H_2}	$Y_{X,CO}$	Y_{X,H_2}	V_{max,H_2}^{AcR}	k_d	EtOH Productivity	CO conversion
32.7	0.0519	0.165	44.4	33.9	2.30	0.236	22.4	0.00770	0.481	1.00
29.6	0.0505	0.149	44.4	33.9	2.29	0.230	21.7	0.00766	0.543	1.00
24.8	0.0535	0.154	44.3	34.0	2.28	0.228	21.4	0.00833	0.639	1.00
22.7	0.0534	0.154	44.3	34.5	2.29	0.227	21.1	0.00823	0.704	1.00
19.0	0.0527	0.153	44.1	34.0	2.30	0.232	21.3	0.00779	0.849	1.00
17.1	0.0537	0.161	44.2	34.0	2.30	0.231	20.3	0.00802	0.948	1.00
14.6	0.0607	0.151	44.2	34.1	2.22	0.231	23.5	0.00734	1.11	1.00
10.1	0.0534	0.125	43.8	34.2	2.26	0.215	19.7	0.00684	1.64	1.00
9.32	0.0566	0.123	44.1	34.6	2.32	0.236	18.2	0.00670	1.77	1.00
9.05	0.0562	0.124	44.4	35.9	2.35	0.249	18.7	0.00670	1.83	1.00
8.75	0.0559	0.123	44.3	35.3	2.39	0.251	17.3	0.00657	1.88	1.00
8.52	0.0570	0.123	44.7	35.8	2.39	0.258	17.1	0.00575	1.93	0.997

Table A2-8. Selected solutions from the multi-objective optimization: 3nd run

GRT	D_{rate}	XP	H$_2$:CO	$v_{max,CO}$	v_{max,H_2}	$Y_{X,CO}$	Y_{X,H_2}	v_{max,H_2}^{AcR}	k_d	EtOH Productivity	CO conversion
29.9	0.0465	0.351	0.822	41.0	34.2	2.02	0.208	17.5	0.00711	0.543	1.00
15.7	0.0517	0.217	0.833	40.8	32.4	2.18	0.210	16.1	0.00668	1.09	1.00
13.2	0.0497	0.218	0.855	39.4	35.8	2.36	0.225	17.3	0.00831	1.31	1.00
10.4	0.0542	0.160	0.842	40.2	34.2	2.11	0.223	17.2	0.00799	1.67	1.00
9.86	0.0528	0.174	0.840	40.0	34.2	2.30	0.210	16.8	0.00692	1.78	1.00
9.54	0.0572	0.136	0.836	40.5	33.8	2.20	0.220	16.5	0.00553	1.83	1.00
9.25	0.0568	0.139	0.844	40.9	34.0	2.20	0.223	16.5	0.00559	1.89	1.00
9.07	0.0580	0.137	0.847	40.4	34.1	2.21	0.221	16.3	0.00529	1.92	1.00
8.92	0.0584	0.127	0.850	40.2	34.6	2.26	0.219	16.4	0.00555	1.95	1.00
8.76	0.0591	0.118	0.849	40.3	35.0	2.36	0.223	16.8	0.00542	2.00	1.00
8.18	0.0603	0.118	0.850	40.4	34.8	2.36	0.246	16.7	0.00546	2.03	0.952
7.79	0.0605	0.116	0.852	40.3	35.5	2.21	0.288	16.6	0.00546	2.04	0.915

Cell mass concentration

Figures (A2-5)-(A2-8) show the ranges of cell mass concentration that correspond to the conditions presented in Figs. 3.5-3.8 from the main text.
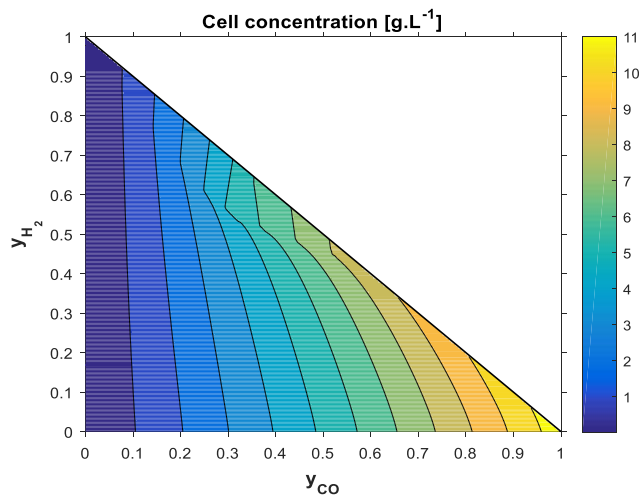
Figure A2-5. Predicted steady-state cell concentration achieved with different gas compositions $\left(y_{CO_2} = 1 - y_{CO} - y_{H_2} \right)$ **, with fixed conditions: *GRT* = 20 min, *D*rate = 0.025 h⁻¹, *N* = 500 rpm, cell recycle = 90%.**
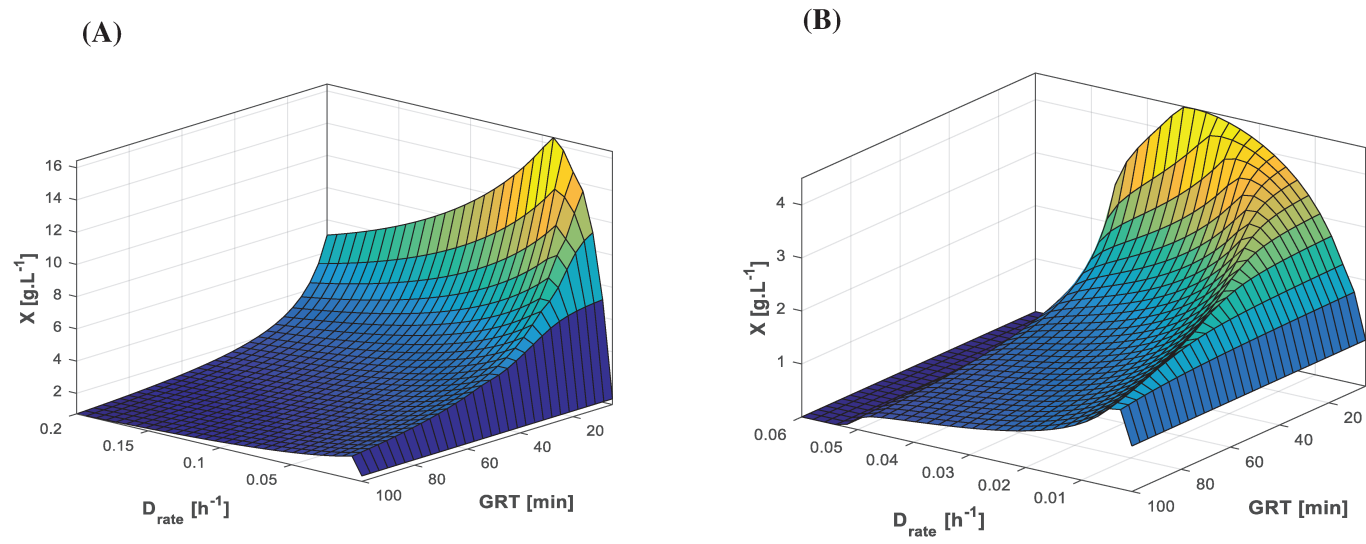
Figure A2-6. Steady-state cell mass concentration as function of gas residence time (*GRT*) and liquid dilution rate (*D_rate*): (A) with 90% cell recycle; (B) without cell recycle. Fixed conditions: $y_{CO} = 0.65$, $y_{H_2} = 0.2$, $y_{CO_2} = 0.15$ **and *N* = 500 rpm.**

(A)

(B)
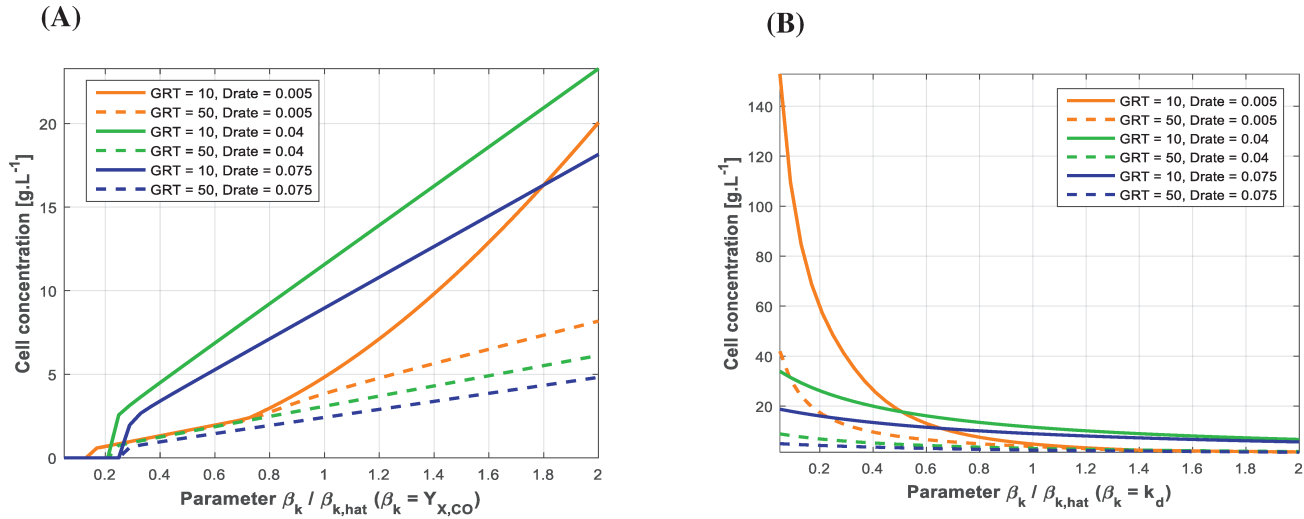
Figure A2-7. Sensitivity of steady-state cell mass concentration to kinetic parameters under different conditions of gas residence time (*GRT*) and liquid dilution rate (*D*$_{rate}$): (A) cell yield on CO (*Y*$_{X/CO}$); (B) cell death rate constant (*k*$_d$). Fixed conditions: $y_{CO} = 0.65$ **,** $y_{H_2} = 0.2$ **,** $y_{CO_2} = 0.15$ **and *N* = 500 rpm.**
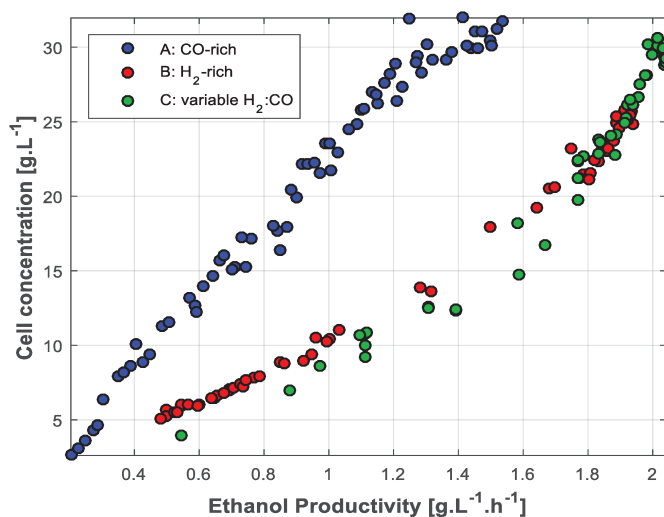
Figure A2-8. Values of cell mass concentration at the Pareto-optimal solutions obtained for maximization of steady-state ethanol productivity and CO conversion (see Fig. 3.8 of the main text). Colors indicate the optimization runs: (A) 1st run, with fixed CO-rich gas composition; (B) 2nd run, with fixed H2-rich gas composition; (C) 3rd run, with variable gas composition.

References for Appendix A2

Cussler, E. L. (1997). *Diffusion: Mass Transfer in Fluid Systems* (2nd ed.). New York: Cambridge University Press.

Himmelblau, D. M. (1970). *Process analysis by statistical methods*. New York: John Wiley & Sons, Inc.

Perry, R. H., Green, D. W. (1999). *Perry's chemical engineers' handbook* (7th ed.). McGraw-Hill.

Sander, R. (1999). *Compilation of Henry's law constants for inorganic and organic species of potential importance in environmental chemistry*.

A3. Supplementary Materials for Chapter 5: Multi-objective sustainability optimization of biomass residues to ethanol via gasification and syngas fermentation: trade-offs between profitability, energy efficiency and carbon emissions

Table A3-1. Elemental analysis (% dry basis) and moisture (%) of sugarcane bagasse and wood residues

	Moisture	C	H	O	N	Cl	S	ash
Bagasse[a]	50	46.96	5.72	44.05	0.28	0.03	0.05	2.94
Wood[b]	11.6	48.55	5.72	45.22	0.26	0.21	0.04	3.52

[a] Bagasse composition is the same as considered in de Medeiros et al. (2017)

[b] Wood residues from eucalyptus are considered the same as in Capaz et al. (2020)
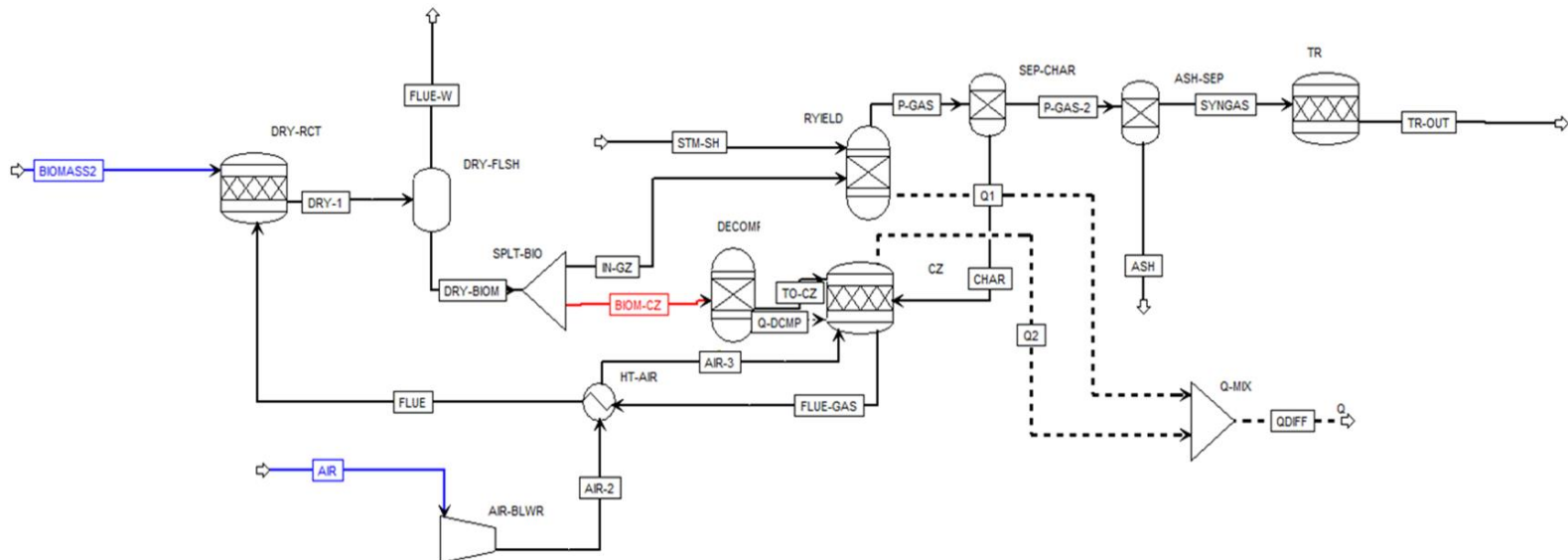
Figure A3-1. Aspen flowsheet of the gasification unit. DRY-RCT and DRY-FLSH: biomass dryer; SPLT-BIO: splitter of biomass between GZ and CZ; DECOMP: RYield reactor to break nonconventional component biomass into conventional components; CZ: combustion zone; RYIELD: gasification zone; SEP-CHAR: gasification bed cyclone to separate char from syngas; ASH-SEP: cyclone to separate ashes; TR: tar reformer; AIR-BLWR: air blower; HT-AIR: air pre-heater; Q-MIX: mixer to sum up heat streams Q1 and Q2 (note: Q-DCMP, heat input of DECOMP reactor, is transferred to CZ, thereby being accounted for in Q2).
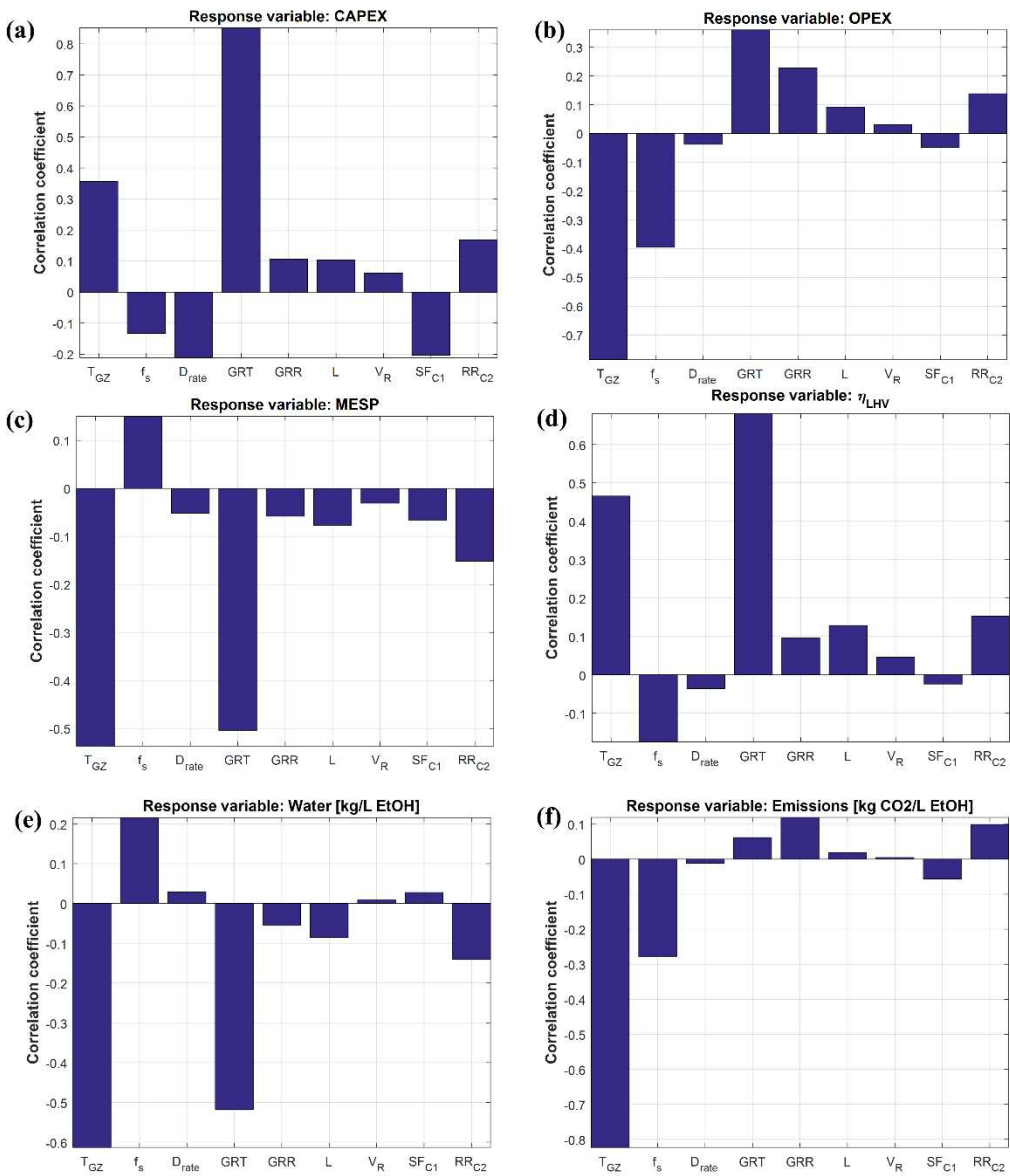
Figure A3-2. Correlation coefficients between decision variables and responses: wood residues.

Appendix B. List of Symbols

Greek Symbols

$\underline{\beta}, \hat{\underline{\beta}}$	vector of parameters: correct, estimated
ε_G	gas hold-up
γ_j^{∞}	activity coefficient at infinite dilution of component j in water at 36 °C
η	thermodynamic efficiency
$\underline{\eta}_j$	vector of correct responses j
μ	biomass specific growth rate [h^{-1}]
ν_j	specific production/consumption rate of component j [mmol.g^{-1}.h^{-1} or mol.g^{-1}.h^{-1}]
ν_k^R	specific rate of reaction number k [mmol.g^{-1}.h^{-1}]
ρ_L	mass density of water or liquid phase at 36 °C [kg/m^3]
σ_ε^2	unknown fundamental variance
$\hat{\sigma}$	estimated standard deviation

Roman Symbols

a	bubble column operation mode (1 for concurrent, -1 countercurrent)
AE	anhydrous ethanol
ANN	artificial neural network
AR	vessel aspect ratio (BCR)
BCR	bubble column reactor
C_{BM}	Bare module cost [$]
$C_{G,i}$, $C_{L,j}$	concentration of component j in the gas (G) or liquid (L) phase [mmol.L^{-1} or g.L^{-1}]
$C^*_{G,i}$, $C^*_{L,i}$	Saturation concentration of component i (gas or liquid phase) [mol.m^{-3}]
$C_{L,X}$ or C_X	Concentration of biomass in the liquid [g.L^{-1}]
C_{OL}	Costs of operating labor [$/year]
C_p^0	Purchase cost of equipment at base conditions [$]
C_{RM}	Costs of raw materials
C_{TM}	Total module cost [$]

C_{UT}	Costs of utilities [\$/year]
C_{WT}	Costs of waste treatment [\$/year]
CAPEX	Capital expenditure [\$]
COM_d	Manufacturing costs excluding depreciation costs [\$/year]
$\underline{\underline{Cov}}$, $\underline{\underline{C\hat{o}v}}$	Variance-covariance matrix: correct, estimated
CW	cooling water
CZ	combustion zone of the gasifier
d	depreciation
d_C	Vessel diameter (BCR) [m]
$D_{f,j}$	Mass diffusivity of component j in water at 25 °C [cm²/s]
d_i	Impeller diameter [m]
D_L	axial dispersion coefficient [m².h⁻¹]
D_{rate}	Dilution rate = Q_L/V_L [h⁻¹]
D:F	Mass ratio of distillate stream to feed stream
DPC	direct production costs
DV	decision variable
E100	hydrous ethanol fuel
EtOH	ethanol
F_{BM}	bare module cost factor
f_0	broth coalescence weighting factor
F_{ST}	feed stage (T-01 or T-02)
FC	fixed carbon
FCI_L	fixed capital investment excluding land purchase cost
FPC	fixed production cost
GE	general expenses
GRR	gas recycle ratio (BCR)
GRT	gas residence time = $V_L/Q_{G,in}$ [min]
GZ	gasification zone
H_j	Henry's law constant of component j dissolved in water at 36 °C [Pa]
HAc	acetic acid
HHV	higher heating value [MJ.kg⁻¹ or MJ.kmol⁻¹]
HMT	high mass transfer (case study)
IRR	Internal Rate of Return
k_d	cell death rate [h⁻¹]
$k_L a_0^{(20)}$, $k_L a_1^{(20)}$	mass transfer coefficient of air in water at 20 °C: non-coalescing and coalescing broth [h⁻¹]
$k_L a_j$	mass transfer coefficient of component j in water at 36 °C [h⁻¹]
K_T	temperature adjustment coefficient for $k_L a$
L	length of vessel (BCR) [m]

LHV	lower heating value [MJ.kg^{-1} or MJ.kmol^{-1}]
LRT	liquid retention time
$\dot{m}$	mass flow rate [kg.h^{-1} or kg.year^{-1}]
MCS	Monte Carlo simulation
MED	multiple-effect distillation
MESP	minimum ethanol selling price [$.L^{-1}]
MM_L	molar mass of water or liquid phase [kg.mol^{-1}]
MML	million liters
MOGA	multi-objective genetic algorithm
N	agitation rate [rpm or s^{-1}]
N_E	number of experimental points
$\dot{n}_{MT}$	mass transfer rate [mol.m^{-3}.h^{-1}]
N_P	number of unknown parameters
N_p	ungassed power number
N_R	number of response variables used for parameter estimation
N_{ST}	number of stages (T-01 or T-02)
NPV	Net Present Value
NRTL	non-random two-liquid model
NRTL-HOC	non-random two-liquid model with Hayden O'Connell equation-of-state
OF	objective function
OPEX	operating expenditures [$/year]
P	pressure inside reactor [Pa]
P_g, P_{ug}	gassed power and ungassed power [W]
$P_{sat,j}$	vapor pressure of component j at 36 °C [Pa]
PCE	purchase cost of equipment [$]
PFD	process flow diagram
Q$_c$	cooling requirement in distillation tower condenser [MW]
Q_G, Q_L	gas and liquid volumetric flowrates [m^3/s, m^3/h, mL/h or mL/min]
Q$_r$	heating requirement in distillation tower reboiler [MW}
R	universal gas constant [J/mol.K]
RKS-EOS	Redlich-Kwong-Soave equation-of-state
RR	molar reflux ratio (T-01 or T-02)
$r_{j,i}$	stipulated response-experiment factors
S:F	mass ratio of side stream to feed stream (distillation column)
STBR	steam to biomass ratio
T	temperature [°C or K]
u$_G$, u$_L$	gas or liquid superficial velocity [m.h^{-1}]
u_s	superficial gas velocity [m/s]

V_G, V_L	volume of gas and volume of liquid inside the reactor [mL, L or m^3]
V_R	volume of reactor vessel (BCR) [m^3]
VM	volatile material
$\underline{\underline{W}}_j$	weight matrix of response j
WGS	water-gas shift reaction
X_i	gas conversion (BCR), i = CO, H$_2$
XP	cell purge fraction (bioreactor)
$\underline{y}_j, \underline{\hat{y}}_j$	vector of responses [g.L^{-1}]: experimental, predicted

Acknowledgements

Curriculum Vitae

Elisa Magalhães de Medeiros was born in Rio de Janeiro, Brazil, on 22/02/1992. In March of 2015 she graduated as a Chemical Engineer from the University of Campinas (Unicamp), in the state of São Paulo, Brazil. During her studies she was involved in teaching activities about MATLAB and Aspen Plus, and conducted a research project about biomass gasification in the Brazilian Bioethanol Science and Technology Laboratory (now called Brazilian Biorenewables National Laboratory), in the Brazilian Research Center for Energy and Materials (CNPEM). In January of 2016 she started a Dual Degree PhD at Unicamp (Chemical Engineering) and TU-Delft (Bioprocess Engineering), under the supervision of Rubens Maciel Filho (FEQ/Unicamp), John A. Posada (BT/TU-Delft) and Henk Noorman (BT/TU-Delft), doing the first 32 months of the project at the Laboratory of Optimization, Project and Advanced Control (LOPCA/FEQ) at Unicamp and the last 16 months at the Department of Biotechnology (BT/TNW) at TU-Delft. In BT she conducted her research at the Biotechnology & Society group (BTS). While at Unicamp, she was a teaching assistant in the School of Chemical Engineering (Introduction to Chemical Engineering; Unit Operations: Separation Processes) and in the Faculty of Food Engineering (Bioprocess Engineering). In February of 2020 she started working as a Process Engineer at the Dow Chemical Company in Terneuzen, Netherlands.

List of Publications

de Medeiros, E.M., Noorman, H., Maciel Filho, R., Posada, J.A., 2020. Production of ethanol fuel via syngas fermentation: optimization of economic performance and energy efficiency. *Chemical Engineering Science*: X 5, 100056.

Capaz, R.S., **de Medeiros, E.M.**, Falco, D.G., Seabra, J.E.A., Osseweijer, P., Posada, J.A., 2020. Environmental trade-offs of renewable jet fuels in Brazil: beyond the carbon footprint. *Science of the Total Environment* 714, 136696.

de Medeiros, E.M., Posada, J.A., Noorman, H., Maciel Filho, R., 2019. Dynamic modeling of syngas fermentation in a continuous stirred-tank reactor: multi-response parameter estimation and process optimization. *Biotechnology and Bioengineering* 116, 2473–2487.

de Medeiros, E.M., Posada, J.A., Noorman, H., Maciel Filho, R., 2019. Modeling and multi-objective optimization of syngas fermentation in a bubble column reactor. In: A.A. Kiss, E. Zondervan, R. Lakerveld, L. Ozkan (Eds.). *Computer Aided Chemical Engineering*, Volume 46: 29th European Symposium on Computer Aided Process Engineering (p.p. 1531-1536).

de Medeiros, E., Posada, J., Noorman, H., Osseweijer, P., Maciel Filho, R., 2017. Conceptual design of a self-sufficient hybrid biorefinery for syngas production and fermentation to ethanol. In: Proceedings of the Biotech France 2017 International Conference. Paris, France, June 28 – 30, 2017.

de Medeiros, E.M., Posada, J.A., Noorman, H., Osseweijer, P., Maciel Filho, R., 2017. Hydrous bioethanol production from sugarcane bagasse via energy self-sufficient gasification-fermentation hybrid route: simulation and financial analysis. *Journal of Cleaner Production* 168, 1625-1635.